Biological Characterisation of a Novel and Naturally Isolated Indole Alkaloid

Vijay Joseph Raja,
B.Sc.(Hons), M.Sc.

Abstract

Natural products play a pivotal role in the treatment of cancer; identification of compounds such as taxanes and the vinca alkaloids were seminal landmarks in natural product drug discovery. Jerantinine A (JA), a novel Aspidosperma alkaloid isolated from plant species *Tabernaemontana corymbosa*, was previously reported to possess cytotoxic activity against vincristine-resistant nasopharyngeal carcinoma cells and is therefore an ideal candidate for biological investigation. Furthermore, *Tabernaemontana corymbosa* has been placed in the endangered list of threatened species by the International Union for Conservation of Nature (IUCN) thus making it a priority to elucidate the biological activity of this alkaloid. Herein, we report detailed biological evaluation of JA on various human-derived carcinoma cell lines. Our preliminary screens showed that significant inhibition of cell growth and colony formation accompanied time- and dose-dependent induction of apoptosis in human cancer cell lines after treatment with JA. Dose-dependent accumulations of cleaved PARP and caspase 3 further confirmed apoptosis. Profound G2/M cell cycle arrest was observed 24 h after treatment in all cell lines. Characteristics of mitotic arrest including inhibition of tubulin polymerisation, microtubule disruption, and aneuploidy were clearly observed. DNA fragmentation was also evident in cells treated

with JA. Indeed, significant increases in phosphorylated-γH2AX were indicative of DNA damage caused by double strand breaks and were relatively similar to levels caused by vincristine. Investigations into JA's ability to overcome vincristine resistance demonstrated that it is not a substrate of Pgp. The role of reactive oxygen species (ROS) in acquired resistance and cell death have also been widely studied. JA induced significant levels of ROS in treated cells, possibly contributing to their apoptotic destiny. Proteomic analyses also corroborated the phenotype of JA-treated cells with increased expression of ROS-neutralising enzymes, aberrant expression of proteins involved in the spindle assembly checkpoint critical to mitosis, and decreased expression in all tubulin proteins detected by LC-MS/MS. A genome-wide RNAi screen revealed several candidate genes involved in mediating sensitivity to JA. The genes corresponding to c-Jun-N-terminal kinases, JNK1/2, were selected for subsequent investigation based on their involvement in multiple pathways that were identified using bioinformatic tools. JNK1/2 were knocked down in MCF-7 and MDA-468 cells and then treated with JA. MTT assays revealed some loss of sensitivity, suggesting that these proteins were indeed involved in mediating cell sensitivity to JA.

Publications

Raja V, Lim KH, Leong C, Kam TS, Bradshaw TB. Novel antitumour indole alkaloid, Jerantinine A, evokes potent G2/M cell cycle arrest targeting microtubules. Investigational New Drugs 2014; 32: 838-50.

Lim KH, **Raja V**, Bradshaw TB, Lim SH, Low YY, and Kam TS. Ibogan, Tacaman, and Cytotoxic Bisindole Alkaloids from Tabernaemontana. Cononusine, and Iboga Alkaloid with Unusual Incorporation of a Pyrrolidone Moiety. Journal of Natural Products 2015; 78: 1129–1138.

Acknowledgements

gratitude to our collaborators **Dr. Chee-Onn Leong** and **Dr. Felecia Chung** for welcoming me into their lab and introducing me to invaluable skills in the fields of genomics and proteomics. I want to acknowledge **Dr. Charles Matthews** for continually challenging me to think outside the box. Heartfelt thanks go out to friends back home who have encouraged me throughout this time. Finally and most importantly, to my parents, **Ashok** and **Mary**, I do not have the words to express my thanks and gratitude to you both. Your love, prayers, and never-ending support have sustained me through my highs and lows. You will forever be a source of inspiration in my life. To my brother, **Sanjay**, your support and advice have always helped me get through some hard situations. My deepest gratitude and appreciation for everything that you have done and continue to do for me. I love you all!

Abbreviations

A549	Adenocarcinomic human alveolar basal epithelial cells
ABCB1	ATP-binding cassette 1
AMPS	Ammonium per-sulfate
APC/C	Anaphase-promoting complex/cyclosome
ATCC	American Type Culture Collection
ATP	Adenosine triphosphate
AURK(s)	Aurora kinase(s)
BCL-2	B-cell lymphoma 2
BRCA1	Breast cancer 1, early onset
BRCA2	Breast cancer 2, early onset
BSA	Bovine serum albumin
BUB1B	Budding-uninhibited-by-benzimidazoles-1-homolog-beta
CASP	Caspase
CDK	Cyclin-dependent kinases
CIN	Chromosomal instability
CML	Chronic Myelogenous leukaemia
COX2	Cycloxygenase 2
CTLs	Cytotoxic T lymphocytes
DAOY	Desmoplastic cerebellar medulloblastoma

DAVID	Database for Annotation, Visualisation, and Integrated Discovery
DHFR	Dihydrofolate reductase
DMSO	Dimethyl sulfoxide
DNA	Deoxyribonucleic acid
DSB(s)	Double strand break(s)
DTT	DL-dithiothreitol
ECM	Extracellular matrix
EGFR	Epidermal growth factor receptor
EMT	Epithelial-mesenchymal transition
ERK	Extracellular signal-regulated kinase
FACS	Fluoresence-activated cell sorting
FAP	Familial adenomatous polyposis
FBS	Foetal bovine serum
FDA	US fod and drug administration
FGF	Fibroblast growth factor
FSC	Forward scatter
G1 phase	Gap 1 phase
G2/M phase	Gap2/Mitosis phase
GAPDH	Glyceraldehyde 3-phosphate dehydrogenase
GDP	Guanosine diphosphate
GI50	Concentration inhbiting growth of cells by 50%
GIST	Gastrointestinal stromal tumours
GLUT1	Glucose transporter 1

GO	Gene ontology
GST	Glutathione S-transferase
GTP	Guanosine triphosphate
h	Hour
HCT-116	Colorectal carcinoma wildtype
Her2	Human epidermal growth factor receptor 2
HIF1	Hypoxia inducible factor
HMEC-1	Microvascular endothelial cells
HPLC	High performance liquid chromatography
HT-29	Colon adenocarcinoma
HTS	High throughput screening
IAA	Iodoacetamide
IGF1/2	Insulin-like growth factor 1/2
JA	Jerantinine A
JAA	Jerantinine A acetate
JA-R HCT-116	Jerantinine A-resistant colorectal carcinoma
JB	Jerantinine B
JBA	Jerantinine B acetate
JE	Jerantinine E
KB	Nasopharyngeal carcinoma
MAPK	Mitogen-activated protein kinase
MCC	Mitotic checkpoint complex
MCF-7	Breast ductal carcinoma
MCL-1	Myeloid cell leukemia 1

MDA(s)	Microtubule-disrupting agents
MDA-468	Metastatic breast adenocarcinoma
Mdm2/Hdm2	Mouse double minute 2/ Human double minute 2
MDSCs	Myeloid-deprived supressor cells
MED1	Primitive neuroectodermal tumour medulloblastoma
MEK	Mitogen-activated protein kinase kinase
MEM	Minimum essential medium
mg	Milligram
MGMT	*O(6)*-Methylguanine-DNA-methyltransferase
MIA PaCa-2	Pancreas adenocarcinoma
ml	Millilitre
MMPs	Matrix metalloproteinases
MPS1	Monopolar spindle 1
MRC-5	Normal lung tissue
MRP(s)	Multidrug resistance protein(s)
MSI	Microsatellite instability
MT(s)	Microtubule(s)
MTT	(3-(4,5-dimethylthiazol-2-yl)-2,5-diphenyltetrazolium bromide)
MudPIT	Multidimensional Protein Identification Technology
Myc	Myelocytomatosis oncogene
NCI	National Cancer Institute
NK	Natural Killer Cells
NNMC	Nottingham Nanotechnology and Nanoscience Centre

NOXA	Phorbol-12-myristate-13-acetate-induced protein 1
NSAIDs	Non-steroidal anti-inflammatory drugs
NSCLC	Non-small cell lung cancer
p53/TP53	Tumor protein 53
PARP	Poly ADP ribose polymerase
PBS	Phosphate-buffered saline
PDGF	Platelet-derived growth factor
PDL1	Programmed-cell death ligand 1
Pgp	Permeability-glycoprotein
PI	Propidium iodide
PI3K	Phosphoinositide 3-kinase
PI6INK4A	Cyclin-dependent kinase inhibitor 2A
PK	Protein kinase
PLK1	Polo-like kinase
PPAR-γ	Peroxisome proliferator-activated receptor gamma
PTEN	Phosphatase and tensin homolog
PUMA	p53 upregulated modulator of apoptosis
Rb/pRb	Retinoblastoma protein
RNA	Ribonucleic acid
RNAi	RNA interference
ROS	Reactive oxygen species
rpm	Revolutions per minute
RPMI-1640	Roswell Park Memorial Institute
S phase	Synthesis phase

SAC	Spindle assembly checkpoint
SCF	Stem-cell factors
SEM	Scanning electron microscope
shRNA	Short hairpin RNA
SSC	Side scatter
TBA(s)	Tubulin-binding agent(s)
TGF-β	Transforming growth factor beta
TKIs	Tyrosine kinase inhibitors
TM	Transmembrane
TSP-1	Thrombospondin-1
TUBB	β-tubulin
TXNRD1	Thioredoxin reductase 1
U373 M	Glioblastoma astrocytoma (high MGMT)
U373 V	Glioblastoma astrocytoma (low MGMT)
UW228-3	Posterior fossa medulloblastomas
VEGF	Vascular endothelial growth factor
V-R HCT-116	Vincristine-resistant colorectal carcinoma
γH2AX	Phosphorylated histone 2A, member X
μl	Microlitre
μM	Micromolar

Contents

Appendices   **206**

A   **206**

B   **211**

C   **214**

List of Figures

List of Tables

Chapter 1

Introduction

1.1 Cancer and Incidence

Cancer may be defined as one of many diseases characterised by the development of abnormal cells that divide uncontrollably whilst having the ability to metastasise and/or infiltrate and destroy normal body tissue [1]. According to Cancer Research UK, 14.1 million new cases of cancer occurred in 2012 with a projected increase of 23.6 million new cases each year by 2030 [2]. Lung, breast, and colorectal carcinomas accounted for the majority of categorical cancers in 2012 as seen in Fig. 1.1. Approximately 8.2 million deaths in 2012 were attributable to cancer making it one of the major causes of death worldwide [2].
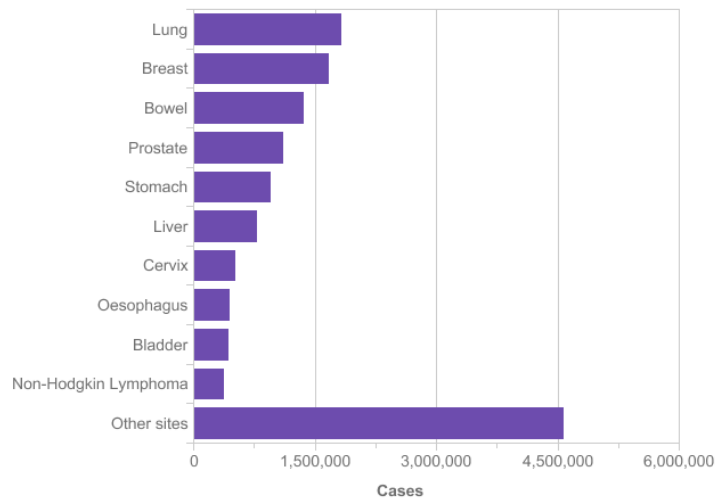
Figure 1.1: The 10 most commonly diagnosed cancers in 2012. Obtained from http://www.cancerresearchuk.org/cancer-info/cancerstats/world/incidence/

1.2 The Nature of Cancer

The ability of the cell to proliferate is crucial to maintaining tissue throughout an organism's lifespan. Normal processes such as repair of wounds and replacement of cells that have been subjected to the external or internal environment of the organism are examples of said maintenance [3]. However, normal genes called proto-oncogenes that control such processes are not immune to mutations that may arise from physical (e.g. ionising and ultraviolet radiation), chemical (e.g. asbestos and alcohol), biological factors (e.g. viruses and bacteria), certain hormones, age and diet [4, 5].

Products of these activated oncogenes can be broadly classified into six groups: chromatin remodellers, transcription factors, growth factors, growth factor receptors, signal transducers and apoptosis regulators [6]. Activation of oncogenes *via* mutations or translocations can occur as initiating events or during tumour progression and maintenance depending
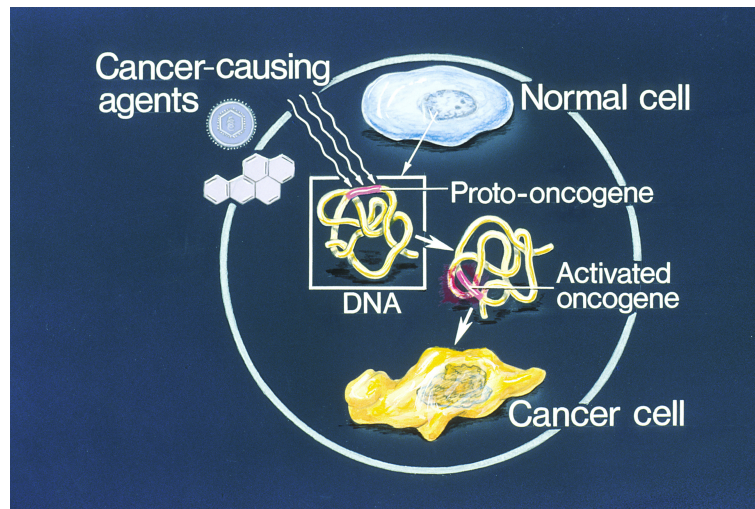
Figure 1.2: Illustration of how an oncogene becomes activated when a normal cell becomes a cancer cell after introduction of a possible risk factor. Obtained from the NCI, AV Number: AV-8808-3615.

on the type of cancer [6, 7, 8, 9]. The NCI classifies cancer into six major categories: carcinoma, sarcoma, myeloma, leukaemia, lymphoma, and mixed types which may involve cancers in one or more different categories [5]. These malignancies share common genetic alterations that lead to uncontrolled growth, consequently exhibiting certain hallmarks of cancer.

1.3 Hallmarks of Cancer

Investigating molecular mechanisms underlying cancer cells and how they differ from normal cells is key for selective and targeted treatment. Douglas Hanahan and Robert A. Weinberg initially conceptualised six distinctive hallmarks characteristic of cancer cells [10]. They include: self-sufficiency in growth signals, insensitivity to antigrowth signals, evading apoptosis, limitless replicative potential, sustained angiogenesis, tissue invasion and metastasis (fig. 1.3) [11, 10].

Four additional hallmarks were added in 2011 [11]. They include two
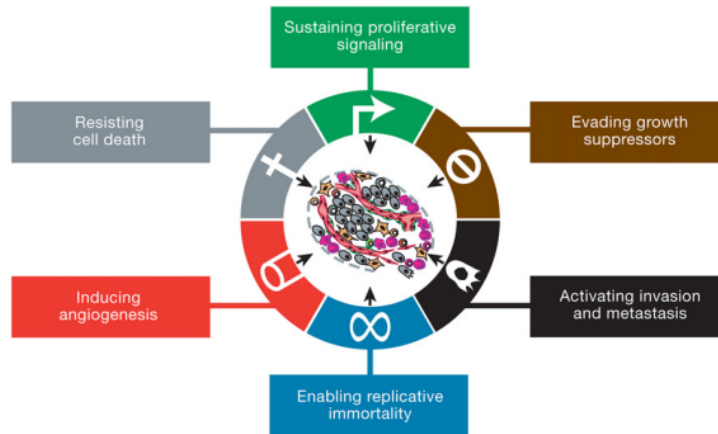
Figure 1.3: Six hallmarks of cancer originally proposed by Hanahan and Weinberg.
[11, 10]

enabling hallmarks: tumour-promoting inflammation and genome instability and mutation. These hallmarks mediate other hallmarks. The other two new hallmarks of cancer include abnormal metabolism and their ability to avoid immune destruction [11]. Although cancers do not require the manifestation of all these hallmarks, no cancer can develop without any of these hallmarks [11, 10].

1.3.1 Self-sufficiency in growth signals

The most fundamental trait of cancer cells is arguably their ability to sustain chronic proliferation [11]. They have the ability to increase or produce their own growth factor ligands, which may correspond to expression of certain specific surface receptors, resulting in autocrine proliferative stimulation [11]. Alternatively, cancer cells can resort to paracrine signalling where they send signals to normal cells within the tumour-associated stroma to supply them with additional growth factors [12, 13]. Furthermore, they can increase the number of growth factor receptors if there are limited amounts

of growth factors available, resulting in hypersensitivity, or structurally modify receptors to facilitate ligand-independent firing [11]. These receptors are capable of activating proteins in downstream signalling cascades or may disrupt negative feedback loops to fuel cellular proliferation and survival [14]. For instance, recent research has shown that most cancers have a disruption in the mitogen-activated protein kinase (MAPK) pathway [11, 14, 15]. Normally, this pathway is activated when growth factors bind to receptors on the surface of the cell which send signals *via* the RAS-BRAF-MEK-ERK (also known as MAPK) pathway until they reach the nucleus where transcription factors attach to specific regions of the DNA that code for cell proliferation and survival and is switched off *via* a negative feedback loop using RAS GTPase [11, 14]. However, the RAS protein is mutated in tumour cells and is continually activated in some cancers. RAS mutations manifest in various isoforms such as K-RAS, N-RAS and H-RAS. Studies show that K-RAS is the most frequently mutated isoform in many cancers with an extreme example of pancreatic cancer where 90% of tumours harbour K-RAS mutations [16]. K-RAS has been shown to play an important role in promoting colorectal adenocarcinoma in addition to promoting proliferation of endodermal stem cells. This is significant because many cancers of the lung, pancreas, colon, and rectum are of endodermal origin [16]. In approximately 66% of metastatic melanomas, mutated BRAF protein remains locked into a constantly active state causing uncontrolled cell division and increased survival/resistance to apoptosis [11, 14, 16]. Some cancer cells may adapt to high levels of oncogenic sig-

nalling by disabling senescence or apoptosis-inducing pathways that are otherwise present in normal cells to prevent excessive proliferation [17].

1.3.2   Insensitivity to antigrowth signals

Cancer cells need to successfully override growth suppressors in order to achieve their proliferative capacity. Specifically, they would need to bypass normal restrictions placed by tumour suppressors in the cell cycle in order to continue to proliferate. Two well-documented tumour suppressors include retinoblastoma (Rb/pRB) and p53 proteins [11]. Both these proteins are integral in determining if the cell can proceed to proliferate or alternatively activate senescence or apoptotic pathways to deter cell division (see Fig.1.4) [18, 19].

Hypophosphorylation of pRB *via* stops cells from progressing through to the S phase of the cell cycle. pRB in association with the E2F transcription factor prevents damaged DNA from replicating and progressing through cell division, specifically from Gap 1 (G1) into the DNA synthesis (S) phase, and is mutated in approximately 40% of all cancers [20]. Consequently, cancer cells with mutated Rb are incapable of binding to E2F allowing for uncontrolled progression past the restriction point into the S phase.

The p53 protein is often referred to as the "guardian of the genome" and is important in determining the fate of a DNA-damaged cell i.e. DNA repair or apoptosis [21]. It is reported to be mutated in roughly 50% of all cancers [20, 21]. Normally, p53 is negatively regulated by MDM2 and hence concentrations of the protein remain low, but various stresses includ-

ing DNA damage and oncogene activation can actuate p53 by disrupting its association with MDM2. If the p53 protein is mutated or inactivated however, it cannot perform its usual functions which include initiation of apoptosis, DNA repair, or cell cycle arrest in the presence of DNA damage, leading to carcinogenesis [11, 18, 21, 22].
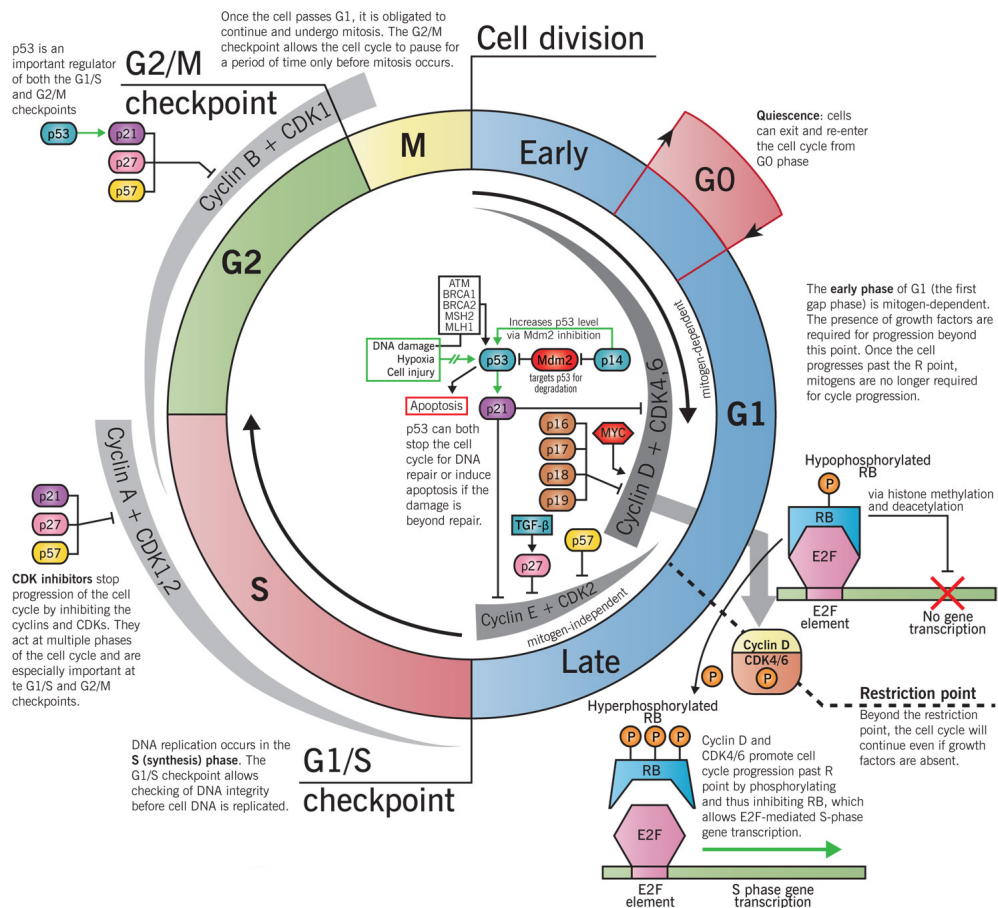
Figure 1.4: Cell cycle and implications in cancer.
[19]

1.3.3 Evading apoptosis

Apoptosis normally serves as a natural barrier to cancer progression, but research has shown that highly malignant cancers can overcome this barrier [23, 24]. Almost all cancer cells have the ability to dysregulate intrinsic

7

and extrinsic pathways of apoptosis (see fig. 1.5 [11, 25, 26]. The intrinsic pathway is prevalent under severe cellular stress that can influence cellular development, whereas the extrinsic pathway is activated in response to multiple extracellular apoptotic signals such as Apo2L/TRAIL and Fas ligand/Fas receptor [11, 25]. Each of these pathways culminate in the activation of proteases (caspase 8 and caspase 9 respectively) leading to a cascade of events that are responsible for executing the apoptotic phase where the cell is then disassembled and consumed by phagocytic cells. Current research alludes to the intrinsic pathway as being the barrier to cancer pathogenesis [11]. Tumour cells can evade cell death through the upregulation of anti-apoptotic proteins such as Bcl-2 and Mcl-1 and survival signals such as Igf1/2 [11, 23]. Loss of p53 tumour suppressor function renders the protein unable to sense DNA damage and initiate apoptosis by activating pro-apoptotic proteins like Noxa and Puma [12, 13, 27].
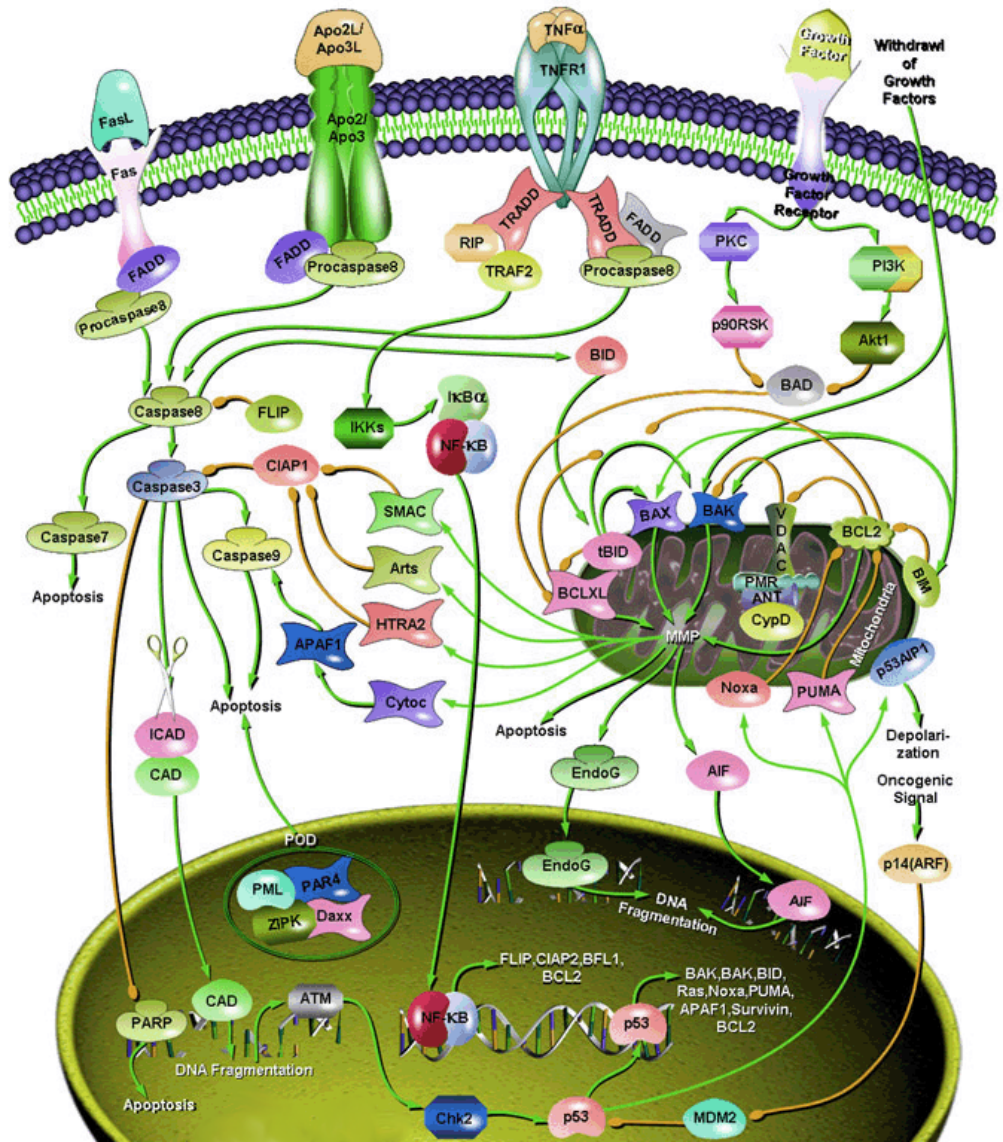
Figure 1.5: Extrinsic and intrinsic pathways of apoptosis.
[26]

Despite advances in chemotherapy and molecular-targeted therapies, insufficient levels of apoptosis as a result of drug resistance remain a barrier to successful treatment of patients with metastatic cancer as 90% of them succumb to their disease [28].

1.3.4   Limitless replicative potential

Well-established research has illustrated that cancer cells require the ability to proliferate in an unlimited capacity in order to form tumours. Normal cells on the other hand, face two barriers to continuous proliferation: senescence, where cells remain viable but are unable to proliferate and crisis, where they undergo cell death [11, 29]. There are instances where cells circumvent the crisis phase and enter a state of immortalisation which is termed as a trait that most established cell lines possess by way of their ability to proliferate indefinitely without evidence of senescence or crisis [11, 29]. A large body of evidence indicates that maintenance of telomeres (multiple tandem hexanucleotide repeats) which protect the ends of chromosomes enable limitless proliferation [11, 29, 30, 31]. Normally, with each cell division there is a loss of telomeric DNA conferring limited lifespan in cells. However in virtually all cancer cells, there is an upregulation in telomerase, a DNA polymerase enzyme that synthesises telomeres and hinders the loss of DNA from the ends of chromosomes after cell division, thereby bestowing these cells with unlimited proliferative capacity [32]. This process is partly aided by the loss of tumour suppressor genes such as p53 (see fig. 1.6) [11, 33].
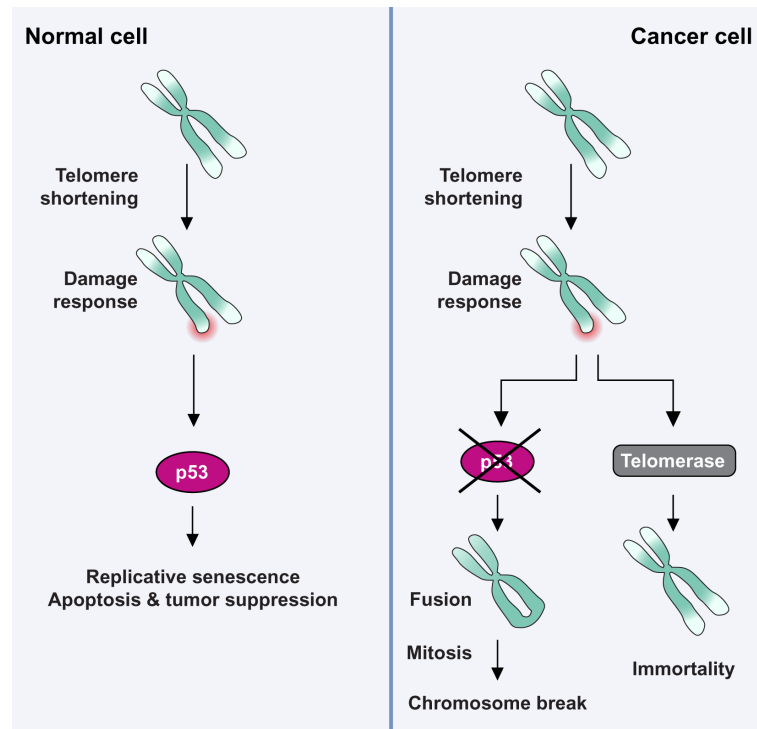
Figure 1.6: The telomere balance in normal and cancer cells.
[33]

1.3.5 Sustained angiogenesis

Angiogenesis is defined as the process of forming new blood vessels from pre-existing vessels. Like normal cells, tumours require nutrition in the form of oxygen and essential nutrients used to fuel and sustain their growth and export of waste products. Angiogenesis is usually initiated and temporarily remains active in adults during physiological processes such as wound healing and the female reproductive cycle [34]. However, during tumourigenesis, an "angiogenic switch" is continually activated resulting in the sprouting of new vessels from normally quiescent vasculature to support neoplastic growth [35]. The "angiogenic switch" is governed by factors that promote and oppose the process of angiogenesis such as vascular endothelial growth factor A (VEGF-A) and thrombospondin -1 (TSP-1), respectively.

VEGF is thought to be one of the most important factors in the angiogenic process and it binds to specific receptors located on endothelial cells lining nearby blood vessels. More specifically, it binds to the extracellular portion of the VEGF receptor promoting receptor dimerisation resulting in activation of the intracellular tyrosine kinase domain that triggers a signaling cascade responsible for the formation of new blood vessels towards the tumour. Blood vessels formed in the tumour environment are usually aberrant in structure resulting in leakiness, microhemorrhaging, endothelial cell proliferation and apoptosis [36, 37]. Oncogenic signals (RAS and Myc proteins) in addition to growth factors like fibroblast growth factor (FGF) have been shown to up-regulate the expression of VEGF and other angiogenic signals implicated in tumour angiogenesis (see fig. 1.7) [38, 39, 24].
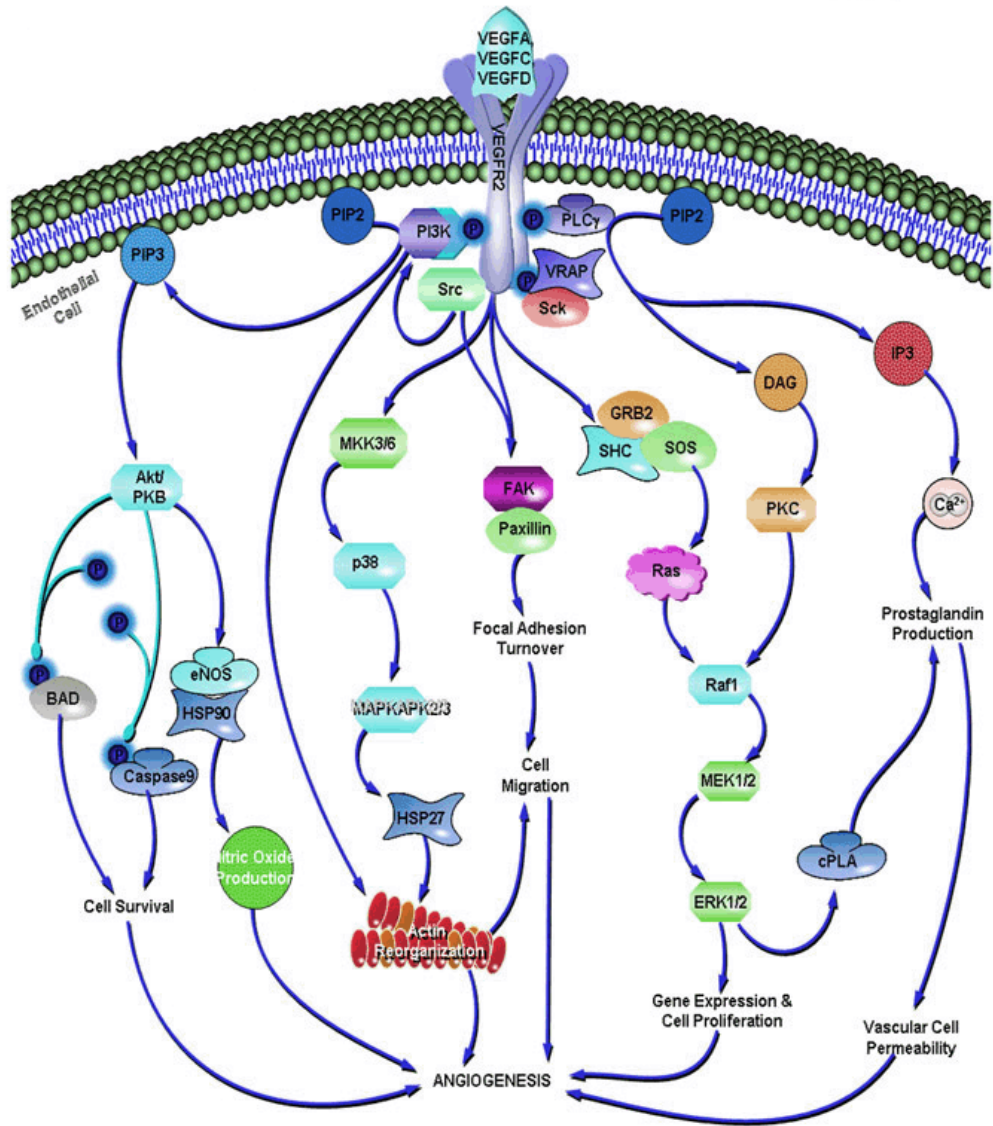
Figure 1.7: Intrinsic components of the VEGF Pathway involved in angiogenesis.

[40]

1.3.6 Tissue invasion and metastasis

Alterations in the shape of cancer cells and their ability to attach to other cells are reflected in the invasive and metastatic characteristics of most carcinomas [11]. One such alteration is the loss of E-cadherin in cancer cells, which is an important cell adhesion molecule. Upregulation of E-cadherin has been shown to be an important antagonist to invasion and

metastasis, while reduction of this molecule potentiates these characteristics [11, 41, 42]. This widely-studied process is termed as the "epithelial-mesenchymal transition" (EMT) where transformed epithelial cells take on invasive and anti-apoptotic characteristics [11, 43]. Essentially, the invasion-metastasis cascade begins with local invasion followed by intravasation of cancer cells into blood and lymphatic vessels in the nearby vicinity, after which cells travel through the lymphatic and cardiovascular systems and escape through vessels *via* extravasation forming small cancerous nodules that finally grow to form macroscopic tumours [11]. Recent studies have identified matrix metalloproteinases (MMPs) as key players in mechanisms of tumour invasion and metastasis [44, 45]. MMPs have the ability to degrade extracellular matrix (ECM) proteins and are thought to promote tumour development *via* proteolytic breakdown of tissue barriers, invasion, and the associated facilitation of circulating tumour cell extravasation [44] (see fig. 1.8) [46].
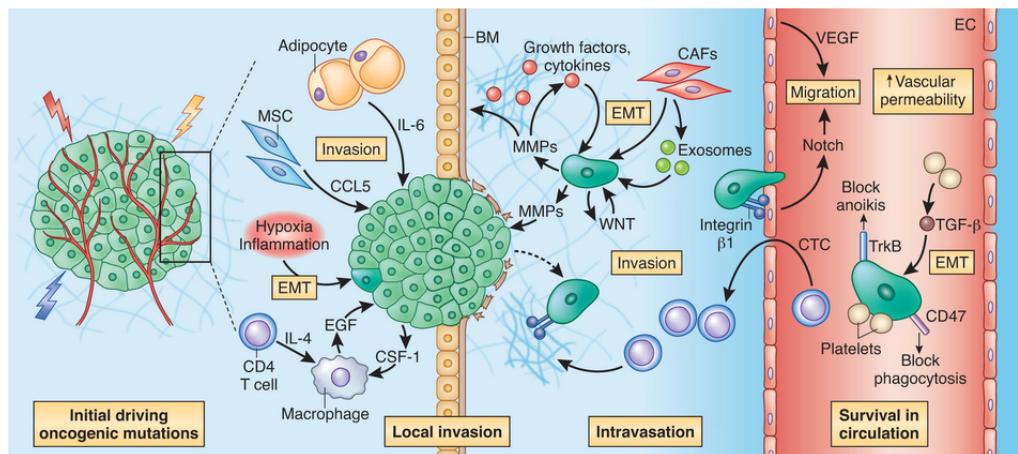
Figure 1.8: The early steps of metastasis: tumor invasion, dissemination and survival in the circulation.

[46]

14

However, there is increasing evidence that MMPs do not play a crucial role in the extravasation process, but rather appear to promote intravasation (invasion of cancer cells into the circulation of blood vessels) [44]. The current view emphasises two types of communications that take place following tissue invasion: cell-cell interactions with host tissue cells and cell-matrix interactions with components of the ECM [44]. The subsequent release of growth factors and cytokines as a result of these interactions can directly or indirectly stimulate tumour growth and generate signals that promote tumour cell survival [44]. The ability of tumour cells to adapt to different tissues stems from the remodelling of host tissue ECM involving the secretion of a variety of proteases (serine-, threonine-, cysteine-, aspartic-, and metalloproteinases) [44].

1.4 Enabling Hallmarks of Cancer

1.4.1 Tumour-promoting inflammation

The association between cancer and inflammation was first conceptualised by Rudolf Virchow in 1863 [47]. He hypothesised that the origin of cancer was at sites of chronic inflammation caused by some classes of irritants and tissue injuries leading to inflammation and subsequently inducing cell proliferation. Although cell proliferation is not the sole cause of cancer, an environment rich in growth factors, inflammatory cells, and activated stroma can certainly potentiate and/or promote neoplastic risk [47]. The link between cancer and inflammation is further demonstrated by the use

of non-steroidal anti-inflammatory drugs (NSAIDs) in preventing tumour formation in people with familial adenomatous polyposis (FAP) [48, 49].

In normal wound-healing, cell proliferation is enhanced concurrently with tissue regeneration. After removal of the assaulting agent that caused the injury, inflammation and cell proliferation subside. However, cells that sustain DNA damage and/or mutagenic assault (e.g. cancer cells) continue to proliferate in microenvironments rich in growth factors and inflammatory cells that support growth. Essentially, tumours can be thought of as wounds that fail to heal and are able to recruit inflammatory immune cells in an effort to survive [50, 47]. These cells then provide the tumour with growth factors and access to blood supply and nutrients thereby sustaining growth [50].

Another scientist by the name of Peyton Rous was the first to discover that tumours can arise from exposure to viral or chemical carcinogens that induce somatic changes [47]. These states are now termed "initiation" which comprises irreversible DNA alterations that can persist in otherwise normal tissue indefinitely until the occurrence of a second type of stimulation called "promotion" [47]. Promotion can result from chronic inflammation or factors released at wound sites. Promoters are also known to directly or indirectly induce cell proliferation, recruit inflammatory cells, increase production of reactive oxygen species leading to oxidative DNA damage, and reduce DNA repair [47].

Recent studies have shown that reactive oxygen and nitrogen species (ROS and RNS respectively), NF-κB, Wnt-β catenin signalling, angio-

genic components, interleukins, interferons, cytokines, and chemokines are
all integral to the connection between inflammation and tumour promo-
tion/progression [47, 51, 52, 53, 54, 55, 56].
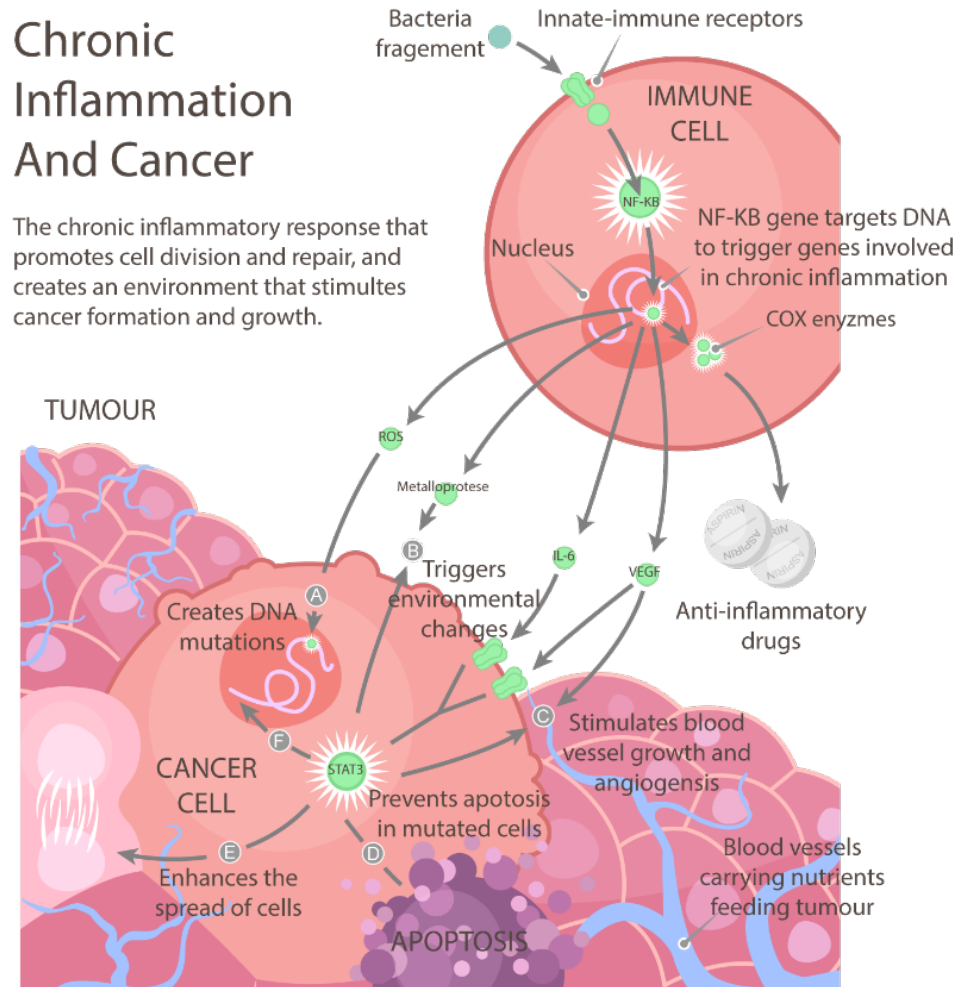
Figure 1.9: The connection between inflammation and cancer.
[56]

1.4.2   Genome instability and mutation

The presence of genome instability contributes to tumour progression.
There are various forms of genomic instability namely chromosomal insta-
bility (CIN) and microsatellite instability (MSI) [57]. CIN refers to the high
rate by which chromosome number and structure changes in cancer cells

over time compared with normal cells. MSI refers to changes in the number of repeats in microsatellite sequences compared to the number of repeats present in DNA when it was inherited and is a consequence of increased frequencies of base-pair mutations [57]. High-throughput sequencing studies suggest that only a handful of genes are mutated, deleted, and/or amplified at high frequencies in sporadic cancers [57]. These include: p53, epidermal growth factor receptor (EGFR), RAS, PTEN, and P16INK4A [57]. Genome instability manifests differently in hereditary and sporadic cancers (see fig. 1.10) [57, 10, 11]. From a hereditary point of view, mutations in DNA repair genes like BRCA1, BRCA2, etc. are quite common thus leading to genomic instability. However, sequencing studies in sporadic cancers reveal that caretaker genes might not frequently be inactivated in the early stages of cancer development, instead activation in growth signalling as a result of mutations in oncogenes or anti-oncogenes appears to be acquired first [57]. The resulting DNA replication stress associated with this activation can lead to genomic instability and selection for TP53 mutations that ultimately allow cells to evade death and senescence, which is another hallmark of cancer [57, 10, 11]. Hereditary and non-hereditary cancers aside, genomic instability arising from the process of cell division remains to be one of the major driving of forces of tumourigenesis [58]. Four main mechanisms are involved in maintaining the integrity of the genome during cell division: fidelity of DNA replication (S-phase), accurate segregation of chromosomes (M-phase), precise repair of DNA damage (throughout the cell cycle), and cell cycle checkpoints [58]. Sustained errors and/or muta-

tions in components belonging to any of the aforementioned mechanisms can result in cancer.
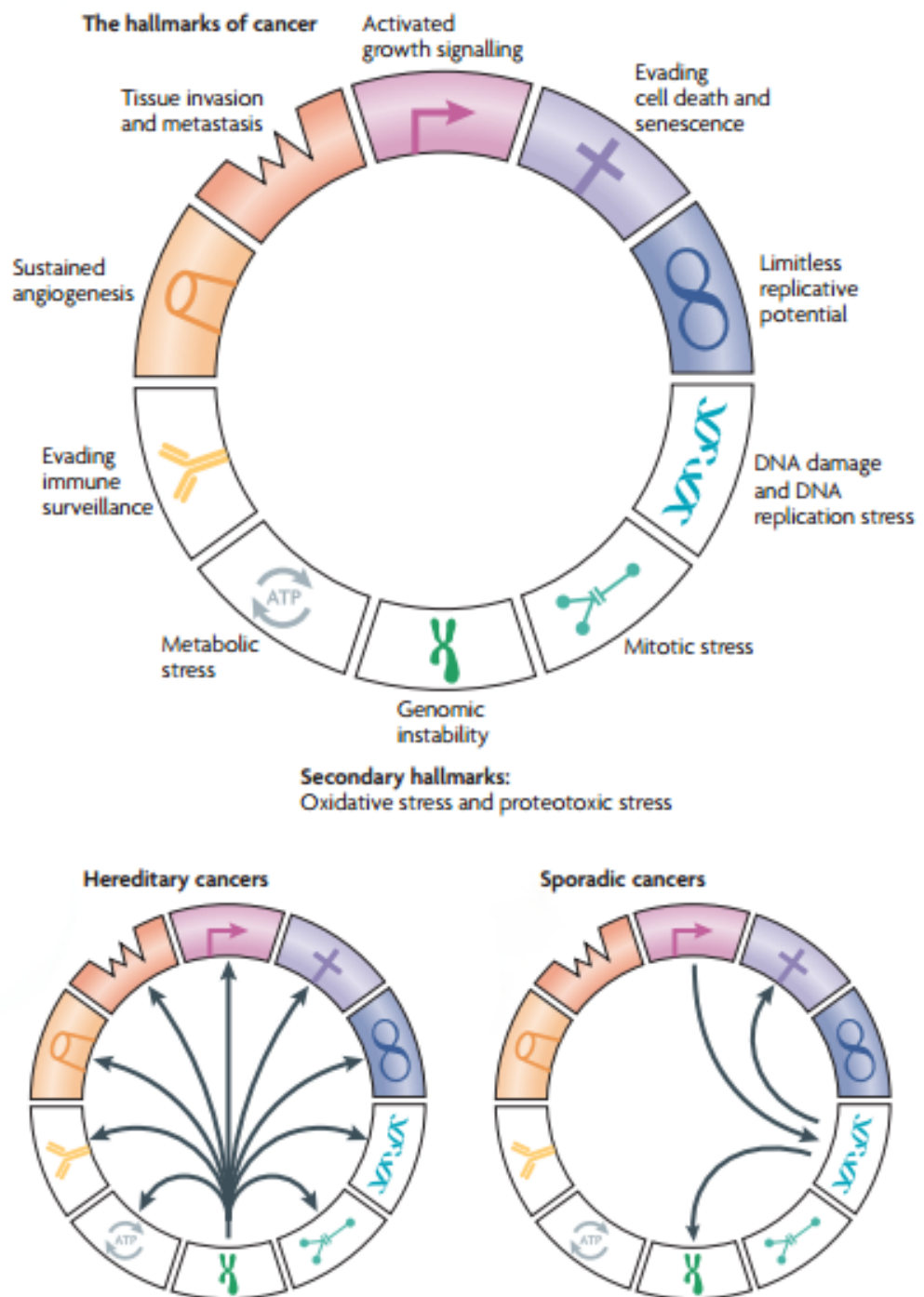
Figure 1.10: The hallmarks of cancer relative to the nature of genomic instability in hereditary and sporadic cancers.

[57]

1.5 Emerging Hallmarks of Cancer

1.5.1 Reprogramming energy metabolism

Cancer cells need to reprogramme cellular metabolism in order to meet the demands of sustained growth and proliferation. The idea of altered metabolism in cancer cells was first conceptualised by Otto Warburg in the early twentieth century [59]. He observed that cancer cells in contrast to normal cells were able to limit their glucose metabolism for energy generation largely to the glycolytic pathway without further mitochondrial oxidative phosphorylation which was termed "aerobic glycolysis" [59, 60]. Essentially, cancer cells are able to convert incoming glucose to lactate instead of metabolising it in mitochondria *via* oxidative phosphorylation [61]. The approach seems paradoxical considering that this process produces far less (18-fold) ATP production per molecule of glucose [60]. One way that cancer cells are able to overcome this is by upregulating glucose transporters like GLUT1 to increase glucose transport into the cytoplasm [59, 60, 61]. Indeed, several studies have shown that cancer cells have significantly higher expression of GLUT proteins than corresponding normal epithelial cells at both the mRNA and protein levels [62, 63]. Many pathways and transcriptional effectors have been implicated in upregulating glucose and glutamine transporters, namely: Hypoxia-inducible factor 1(HIF1), Myc, p53, Phosphoinositide 3-kinase (PI3K) pathway etc. [60, 64, 65]. Arguably one of the most important aspects of cancer metabolism is the role of reactive oxygen species (ROS) in modulating metabolic signalling pathways [66]. ROS

increase cell proliferation and survival *via* post-translational modification of kinases and phosphatases at low levels [60]. At moderate levels, ROS induce expression of stress-responsive genes like HIF1α, which in turn can trigger expression of proteins such as glucose transporters (GLUT1) and VEGF that promote survival. However, when ROS levels are at their highest, damage to macromolecules such as DNA induces activation of protein kinase Cδ leading to senescence and/or apoptosis [67].
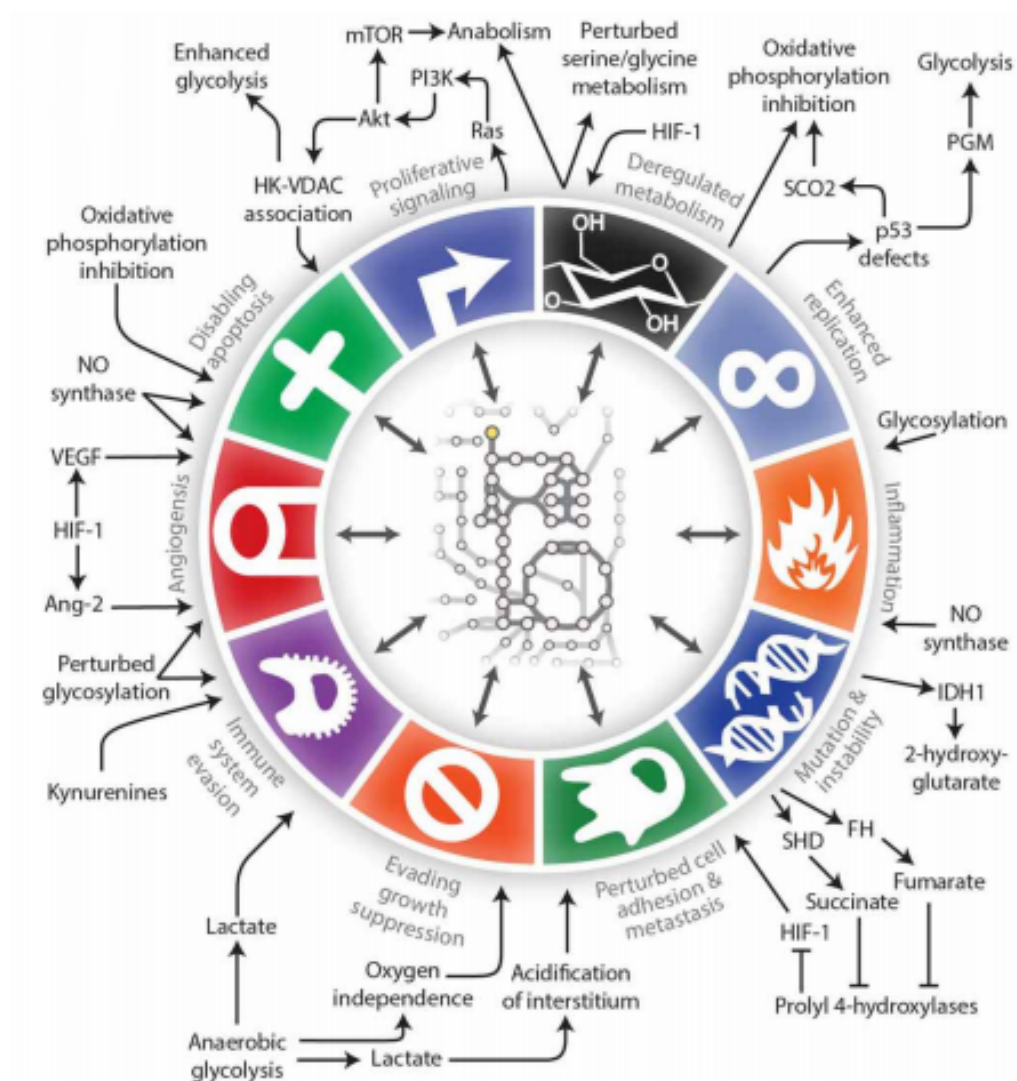
Figure 1.11: The various hallmarks of cancer and their effects on metabolism or how they can be modulated by metabolic changes.
[61]

1.5.2 Evading immune destruction

The role of the immune system in resisting or eradicating formation and progression of tumours remains an unresolved and intensely researched issue [10, 11]. The immune system holds the greatest potential for cancer treatment with no toxicity to normal tissue in addition to long-term memory to prevent recurrent cancers [68]. There is increasing evidence supporting the idea of immunosurveillance whereby tumours are recognised by the immune system *via* tumour-specific antigens [11, 68]. For instance, promising antitumoural immune responses were observed in patients with colon and ovarian tumours that were infiltrated with cytotoxic T lymphocytes (CTLs) and natural killer (NK) cells [69]. Studies have also found that immunocompromised mice are more susceptible to cancer than those with competent immune systems [10, 11]. Figure 1.12 illustrates how the immune system targets cancer cells [70].

Studies have shown that the tumour microenvironment can inhibit immune responses by upregulating inhibitory and immunosuppressive molecules such as programmed-cell death ligand 1 (PDL1) and TGF-β [11, 71]. Tumours can also recruit inflammatory cells such as regulatory T cells (Tregs) and myeloid-derived suppressor cells (MDSCs) that are actively immunosuppressive [72, 73]. The concept of antitumour immunity is yet to be strongly recognised as a hallmark of cancer, but is potentially a promising target for new anticancer therapies.
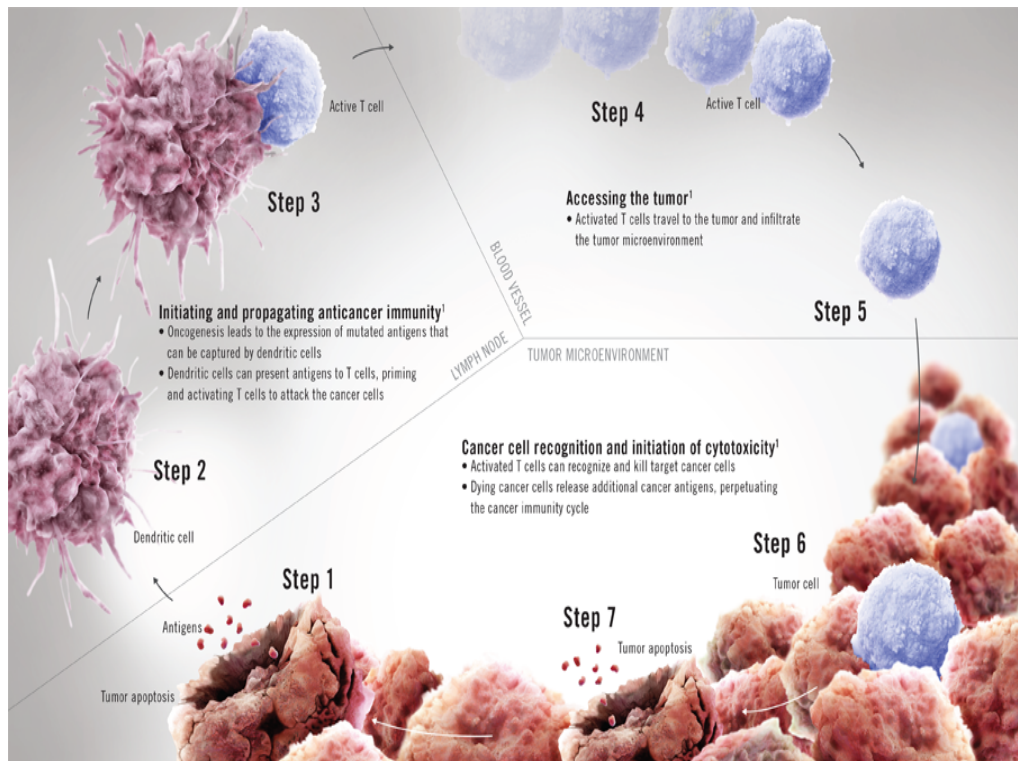
Figure 1.12: The cancer immunity cycle illustrating the ability of the immune system to target cancer cells selectively.
[70]

1.6 Treatment of Cancer

The main modes of cancer treatment include surgery, radiotherapy, and chemotherapy. Other types of treatments such as hormone therapy and bone marrow, stem cell transplants, and immune therapy are also employed. These treatments may be used in combination depending on stage, grade, and location of the tumour. Radiation and surgery are mostly limited to solid tumours (local or local-regional disease). Chemotherapy on the other hand is intended to treat systemic disease. Early diagnosis and developments in such therapies have dramatically increased cancer survival rates with an estimated two-thirds of cases that will eventually be cured; however, striking differences among tumours still pose a challenge to treat-

ment [74].

1.6.1 Surgery

Surgery is the oldest modality of cancer treatment and remains the most effective treatment of localised primary tumours and associated regional lymphatic disease. More patients are cured by surgery when it is used as a single treatment in comparison with any other individual form of cancer therapy [75]. This may be attributed to the fact that surgery operates by zero-order kinetics, in which 100% of excised cells are killed as opposed to radiotherapy and chemotherapy which operate by first-order kinetics where only a fraction of cells are killed by each treatment [74, 75]. During the past two decades, major strides in both operative techniques and combined modality therapy have significantly decreased morbidity and mortality rates associated with surgical resection of solid neoplasms [74]. Surgery is now increasingly being used in specific clinical situations such as treating colorectal-liver metastases [74]. Complete surgical resection of metastases when selected with standard clinical criteria have yielded 30-40% 5-year survival rates, however, this therapeutic option is limited to confined metastases which only represent 10-15% of cases [76, 77].

1.6.2 Radiotherapy

Radiation therapy employs the use of high-energy radiation such as X-rays, gamma rays, and charged particles to shrink tumours and kill cancer cells. Like surgery, it is usually used for localised tumours confined to a specific

region [78]. Approximately 45% of new cancer cases will receive radiotherapy with this proportion increasing over the next few years [79]. Radiation therapy kills cancer cells by either damaging DNA directly or creating free radicals within cells that in turn damage DNA [78]. Radiation also affects normal tissue, but the premise behind it is that it usually kills cells that are actively dividing and does not work very quickly on cells that divide more slowly. Furthermore, normal cells have the added advantage of having uncompromised DNA repair mechanisms (e.g.p53), whereas components of these mechanisms are dysfunctional in many tumours. p53 for instance, is mutated in most cancers which inhibits both DNA repair and apoptosis. Indeed, research has shown that there is very little apoptosis that occurs in mutant p53 cell lines after exposure to radiation suggesting that p53 may be closely linked with radiosensitivity [80, 81, 82].

1.6.3 Chemotherapy

Chemotherapy utilises chemical agents to kill or control the growth of cancer cells. These chemical agents are natural products, natural product-derived or inspired (semi-synthetic), or purely synthetic. The first major stride in chemotherapy emerged from an accidental spill of sulfur mustards on troops from a bombed ship in the second world war and experience from the first world war [83]. This led to the observation that the men exposed to these gases had markedly depleted bone marrow and lymph nodes. Subsequently, an initial study utilising nitrogen mustard on lymphoma patients was carried out in 1943 and results showed marked regression [83].

Unfortunately, the regression observed in these studies was short-lived and incomplete. However, the failure stimulated the development of a new class of compounds known as antifolates which included aminopterin and amethopterin, now known as methotrexate. These compounds were tested in children with leukaemia in 1948 and showed unquestionable remissions [84]. The use of nitrogen mustard and methotrexate in treating cancer spurred an arduous search and development of novel anticancer agents that virtually propelled the field of cancer drug discovery into the industry it has become today. The following table is an adaptation from Goodman and Gilman (2005) and illustrates the current classification system of anticancer agents available today [85]. However, it is worthy of note that this classification scheme is not rigid as many of these agents may fall into more than one category. For instance, some compounds like mitomycins are natural products and alkylating agents as well.

Table 1.1: Classification of anticancer agents currently used in clinics.

Class		Example	Origin/Nature
Alkylating Agents	Nitrogen mustard	Chlorambucil	Synthetic
	Ethyleneimines	Thiotepa	
	Alkyl sulfonates	Buslfan	
	Nitrosoureas	Carmustine	
	Triazenes & hydrazines	Dacrbazine, procarbazine	
	Platinum compounds	Cisplatin	
Antimetabolites	Antifolates	Methotrexate	Synthetic
	Pyrimidine analogues	Fluorouracil	
	Purine analogues	Fludarabine	
Natural Products	Antibiotics	Doxorubicin	*Streptomyces peucetius*
	Camptothecins	Topotecan	*Camptotheca acuminate*
	Epipodophyllotoxins	Etoposide	*Podophyllum platatum*
	Taxanes	Paclitaxel	*Taxus brevifolia*
	Vinca alkaloids	Vincristine	*Catharanthus roseus*
Hormones	Adrenal suppressant	Mitotane	Synthetic
	Corticosteroids	Prednisone	Natural
	ER antagonists	Tamoxifen	Synthetic
	Aromatase inhibitor	Anastrozole	Synthetic
	Antiandrogens	Flutamide	Synthetic
Targeted agents	Proteasome inhibitors	Bortezomib	Dipeptide boronic acid
	Immunomodulators	Thalidomide	Synthetic small molecule
	Protein Kinase inhibitors	Imatinib	Synthetic small molecule
	Antibodies	Rituximab	Monoclonal antibody

1.6.3.1 Alkylating agents

Alkylating agents are the earliest classes of drugs used to treat cancer. Nitrogen mustards are in fact alkylating agents whose mode of action is to inflict cytotoxic DNA damage in addition to collateral mutagenic damage [86]. These agents are strong electrophilic compounds that attach to the alkyl group located at the N7 position of the guanine base in DNA [87]. The end effect of these agents is to inhibit DNA replication. Most alkylating

agents are bifunctional, containing two groups capable of interacting with DNA [88]. Hence, they are able to form bridges between a single strand or two separate strands of DNA, which interfere with enzymes involved in DNA replication ultimately leading to growth inhibition or apoptosis [88]. G2/M arrests are quite commonly observed with most of the damage occurring in the S-phase of the cell cycle as cells are unable to remove damaged fragments. Unfortunately, these agents do not discriminate between normal and tumour cell DNA, but are still used to exploit the fact that cancer cells divide rapidly and are more susceptible to DNA damage as their repair mechanisms are already compromised.

1.6.3.2 Anti-metabolite agents

Anti-metabolites share a long history with alkylating agents as these compounds were also among the first to be used in treating cancer. They are analogues of essential metabolites required for DNA synthesis [89]. They target DNA by either inhibiting its synthesis or production of its precursors *i.e.* nucleotides [89]. Their effects are usually marked by a G1 or S-phase arrest in the cell cycle [88]. As seen in Table.1.1, antimetabolites are classified under three subcategories: folate (e.g. methotrexate), pyrimidine (e.g. fluorouracil), and purine (e.g. pentostatin) analogues. Folate analogues specifically target dihydrofolate reductase (DHFR) and/or thymidylate synthase (pemetrexed). Both these enzymes are required for metabolism of folic acid, a vitamin with an important role in nucleic acid metabolism. Pyrimidine analogues like fluorouracil, on the other hand, po-

tently inhibit thymidylate synthase and therefore inhibit thymidine synthesis [89, 90]. Pentostatin, a purine analogue, inhibits adenosine deaminase, an enzyme involved in the metabolism of adenosine [91]. Resistance to antimetabolites has also been observed in the clinic [92]. Various mechanisms of resistance to antimetabolites have been identified and include mutations in metabolic enzymes, altered drug transport, nucleobase salvage pathways, DNA-damage and cell cycle control pathways [92].

1.6.3.3   Hormones

Hormonal therapeutics plays an important role in the treatment of breast, prostate, ovarian, and kidney cancer [85]. Cancers originating from hormone-producing glands use hormones to grow, hence utilising hormone therapy to block the effects of such hormones or even stop them from being produced is an effective way to treat these cancers. This kind of treatment is prescribed for patients who have tumours that are hormone sensitive or dependent. Hormonal cancer chemotherapy primarily employs the use of anti-oestrogen therapeutics (e.g. tamoxifen), aromatase inhibitors (e.g. anastrozole), anti-androgenic therapeutics (e.g. flutamide), and corticosteroids (e.g. prednisone) [85]. Tamoxifen and flutamide are antagonists of the oestrogen and androgen receptors respectively. Anastrozole inhibits aromatase causing oestrogen deprivation [85, 93].

1.6.3.4   Targeted agents

Most cytotoxic chemotherapeutic drugs were developed and administered to cancer patients at a time when limited knowledge of molecular mecha-

nisms underlying cancer was available. With advancements in technology, researchers have now begun to unearth distinct molecular mechanisms underpinning this group of diseases. Douglas Hanahan and Robert Weinberg's assessment detailing the hallmarks of cancer is a testament to the progress made over decades worth of research [10, 11]. These achievements in understanding the molecular basis of cancer have led to a revolution in cancer chemotherapeutics where the development of rationally and molecularly targeted drugs is considered more desirable than generic intravenous cytotoxic chemotherapy [94]. Targeted therapy exploits the differences between cancer cells and normal cells with high potency and reduced toxicity (side effects) compared to conventional chemotherapy. However, because targeted therapies are aimed at specific molecules that interfere with cancer cell proliferation, resistance can be observed if mutations occur in the target resulting in weak interactions that can reduce the efficacy of the agent. This is why targeted therapy is commonly used in conjunction with more traditional chemotherapy drugs.

The concept of 'the druggable genome' is the foundational basis for rational and targeted drug design and is currently an intense area of research. The druggable genome comprises a subset of the 21,000 genes in the human genome that express proteins able to bind drug-like molecules (see fig.1.13) [95]. Most drugs that are available today mainly target cancer signalling pathways especially those triggered by tyrosine kinases and G protein-coupled receptors [96].

In 2002, only about 120 proteins were reportedly targeted by drugs
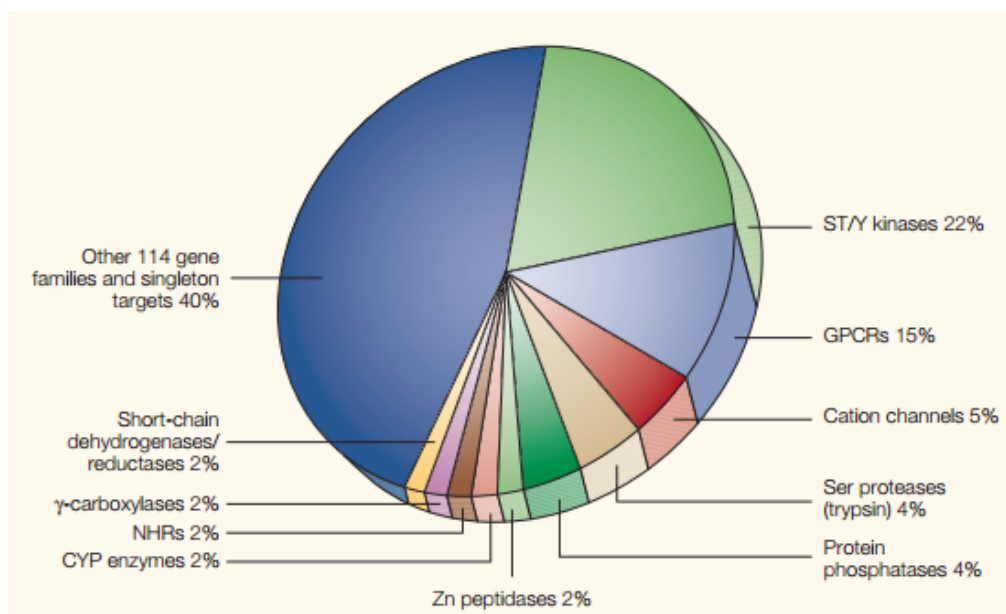
Figure 1.13: The "druggable" genome in target-directed drug discovery.
[95]

marketed at the time with a large number of druggable gene families still underexploited [95]. With vast improvements in high-throughput screening technologies in the future, chemical leads will be available for most potentially druggable targets, the challenge then would be to discover and assess the therapeutic utility of leads and targets [95]. However, current efforts in targeted cancer chemotherapy have focused on protein kinase (PK) inhibitors and monoclonal antibodies as they have undoubtedly been front runners in this field over the past two decades.

Targeting protein kinases

As seen in fig.1.13, PKs occupy the largest portion of the druggable genome. To date, they are the most actively pursued drug targets with 30 distinct kinase targets being developed to the level of a phase 1 clinical trial [97]. PKs are enzymes that catalyse transfer of phosphate to their substrates [98]. Even though PKs account for only 2% of the genome, they are responsible

for phosphorylating at least 30% of all cellular proteins [98]. Phosphorylation plays crucial roles in controlling a wide range of cellular processes that include cell division, metabolism, survival, and apoptosis [99]. Deregulation of PKs contributes to the development of many diseases such as cancer. For instance, constitutive activation of PKs has been found in many cancers such as chronic myelogenous leukaemia (CML), gastrointestinal stromal tumours (GIST), and various other sarcomas and carcinomas [98, 99]. The increasing body of evidence illustrating the importance of phosphorylation in cellular function in cancer has made this family of proteins desirable targets for drug design. Some of the major approaches in modulating kinase activity include: inhibiting phosphorylation activity by blocking ATP binding, disrupting protein-protein interactions, and downregulating kinase gene expression *via* interference RNA (RNAi) [96]. The following briefly outlines some of the major kinase inhibitors used in the clinic today.

One of the most successful tyrosine kinase inhibitor molecules developed to date is Imatinib. It is used to treat CML and GIST. It works by inhibiting elevated kinase activities of oncogenic proteins bcr-abl and c-kit that are inherently overexpressed in these cancers [100]. The bcr-abl fusion protein is a result of reciprocal translocation between chromosome 9 and 22, which was seen in 95% of CML patients [101]; i.e. part of the bcr gene from chromosome 22 is fused with part of the abl gene on chromosome 9. The product of this fusion is a mutant tyrosine kinase protein bcr-abl. Normal functioning tyrosine kinases require activation by other cellular messaging proteins before initiating cell division, however, the fused bcr-

abl protein is constitutively active and consequently stimulates a number of cell cycle proteins and enzymes resulting in rapid and sustained cell proliferation [102]. Imatinib specifically binds to the ATP binding site of bcr-abl thus competitively inhibiting enzyme activity of the protein and hindering proliferative signals [102]. Unfortunately, drug resistance was observed in patients treated with Imatinib over time and this was due to a number of reasons that include: drug efflux, mutations in the ATP binding pocket, and drug metabolism etc. [103]. In response to observed resistance, newer agents such as Nilotinib and Desatinib were developed to treat Imatinib-resistant tumours [104]. A main mechanism of resistance to the old generation of tyrosine kinase inhibitors (TKIs) that emerged was the expression of drug efflux pumps. Fig. 1.14 illustrates a new generation of small-molecule TKIs that modify and overcome problems caused by drug efflux transporters resulting in an increased intracellular accumulation of anticancer drugs.
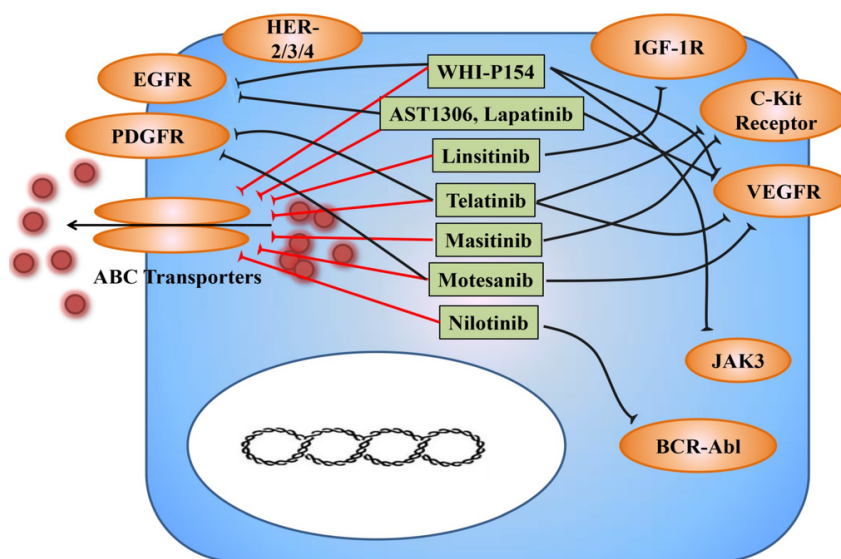
Figure 1.14: Efflux transporter modifications by small-molecule tyrosine kinase molecules and their targets
[105]

Receptor tyrosine kinase inhibitors targeting epidermal growth factor receptors (EGFR) have also seen major successes in the clinic.

EGFR is a cell-surface receptor that plays a vital role in cell proliferation, survival, and differentiation [106]. Mutations in EGFR can result in overexpression and ligand-independent activation as is the case in some cancers, specifically non-small cell lung cancer (NSCLC) which is prevalent in 85-90% of all lung cancers. It is estimated that more than 60% of all NSCLCs show EGFR overexpression [107]. Increased EGFR signalling promotes tumour growth through activation of pathways crucial to invasion, angiogenesis, metastasis, and inhibition of cell death. Drugs like Gefitinib and Erlotinib are competitive inhibitors of the intracellular tyrosine kinase domain of EGFR preventing ATP from binding and inhibiting receptor auto-phosphorylation [108]. This leads to blocking of downstream pathways that promote tumour progression.

Multi-targeted receptor tyrosine kinases as chemotherapeutic agents have also been explored in the treatment of cancer. One such example is Sunitinib, which is approved for treating renal cell carcinoma and imatinib-resistant GIST. *In vitro*, sunitinib has been shown to inhibit angiogenesis and growth of cell lines driven by VEGF, stem-cell factors (SCF), and platelet-derived growth factors (PDGF) [109].

Monoclonal antibodies such as Erbitux and Herceptin target the extracellular domain of the EGFR receptor preventing the normal ligand from binding. This in turn blocks activation of downstream pathways that promote tumour growth and survival [108]. Erbitux is used in the treatment

of squamous cell carcinoma and head/neck cancers [110]. Herceptin was developed as a HER2 (member of the EGFR family) blocker in the treatment of a subset of aggressive breast cancers that comprise 30% of cases [111]. Overexpression of this receptor has been linked to cell proliferation, cell cycle perturbation, and suppression of apoptosis due to increased activation of mitogen-activated protein kinase (MAPK) and PI3K pathways [108].

Targeting cyclin-dependent kinases

Cyclin-dependent kinases are important molecular targets that represent a major area of research involving development of potentially active CDK inhibitors. CDKs play vital roles in cell growth and division as well as protein transcription [112]. However, CDK/Cyclins are dysregulated in several cancers resulting in uncontrolled cell proliferation. Hyperactivation of CDKs has also been reported to confer selective growth advantage to cancer cells [112]. There have been 20 CDKs and 29 cyclins identified to date making this family of proteins highly sought after as potential chemotherapeutic targets [113].

In February, 2015, the US food and drug administration (FDA) approved the first groundbreaking cyclin-dependent kinase (CDK) inhibitor, palbociclib, for the treatment of ER+/HER2- breast cancer. It selectively targets CDK 4,6 and causes G1 arrest in ER+ breast cancer cell lines [114]. Clinical trials demonstrated that the drug improved progression free survival in patients to 20 months when used in combination with letrozole (aromatase inhibitor for treatment of hormonally-dependent breast cancer)

compared to only 10 months with letrozole treatment alone [115].

Despite this breakthrough, CDK inhibitors have faced disappointing results in clinical trials. This can be attributed to three reasons in particular: firstly, there is a lack of understanding as to which CDKs are actually being inhibited *in vivo* contributing to multiple therapeutic effects [114]. Secondly, there has been a lack of stratified patient cohorts concerning CDK inhibitors with low specificity. Palbociclib is a perfect example of how stratifying patient cohorts can improve on currently used chemotherapeutics. Lastly, there is a lack of a therapeutic window as many of these CDKs inherently target several other proteins that are critical to survival and proliferation of normal cells, making it hard to differentiate between healthy and cancerous tissue [114]. However, the approval of palbociclib is encouraging as it provides key insights into designing next-generation CDK inhibitors and how they can be used in the clinic.

The future of targeted therapeutics lies in the success and efficiency of stratified medicine. This field of treatment primarily identifies patient cohorts that are likely to respond to a particular treatment due in part to the genetic makeup of their disease. It is precisely for this reason that there is a need to incorporate predictive and pharmacodynamic biomarkers in drug development as they can be used as powerful tools to guide treatment strategies [116].

Other molecular targets of interest

Research continues to reveal several other molecular targets that are overexpressed in various cancers and are currently under investigation: heat

shock protein 90 (HSP90), matrix metalloproteinases, cyclooxygenase 2 (COX2), the proteasome, histone deactylases, aurora kinases, polo-like kinases and telomerase among others. Agents targeting these molecules are being designed and are at various stages of clinical development with some approved as drugs for certain forms of cancers [117].

1.6.3.5 Natural Product Drug Discovery

Compounds that possess biological activities and derived from natural resources such as plants, animals, and microorganisms, are defined as natural products [118]. The use of natural products in cancer has been prevalent for the past 30 years and continues to serve as the basis for many of the lead structures that are used as templates for synthesising novel compounds with enhanced biological properties [119]. However, large pharmaceutical companies have de-emphasised natural products in drug discovery programmes due to a lack of reproducibility of extracts, inaccessibility of collection sites, laborious procedures to isolate and purify bioactive chemical compounds that often lead to very low yields, and rediscovery of compounds [120]. The emergence of targeted therapies further steered pharmaceutical companies away from natural product drug discovery. The development of natural products is often erratic as it heavily relies on the skill of pharmacologists to elucidate the mechanism of action and clinicians to identify optimal indication in the clinic [121]. This is in contrast to targeted therapeutics, which are designed for a specific target and/or type of cancer. One advantage that natural products may have over synthetic compounds is the fact that they

are natural metabolites: successful molecules that are clinically active have been suggested to possess properties akin to "metabolite likeness", meaning that natural products are not only biologically active, but are likely to be substrates for transporter systems involved in delivering compounds to their intracellular site of action [122]. Furthermore, natural products have had millenia of evolutionary time to optimise structure-activity and are often potent and able to resist metabolic deactivation.

While certain tumours with specific oncongenic addictions have benefited from targeted therapeutics, it is clear that a vast majority of tumours are not dependent on single "targetable" oncogenic activations. For instance, EGFR mutations account for less than 10-15% of lung adenocarcinomas and using EGFR-targeted therapy would primarily be beneficial to this cohort of patients [121, 123]. In these tumours, chemotherapy remains to be a cornerstone of treatment and this is where natural products come to the fore. From the 1940s up until 2008, approximately 175 anticancer drugs were developed and are commercially available in the United States, Europe, and Japan; 65% of these were inspired from natural products, i.e. pure natural products (14% of total), semisynthetic natural products, mimics, or synthetic molecules with pharmacophores from natural products [124]. These numbers are a testimony to the role of natural products in cancer chemotherapy. With the approval of rapamycin in 2007, 12 new natural products have been brought to the market and are illustrated in table 1.2 [121].

Table 1.2: Novel anticancer medicines based on natural products

Name (trade name), structure	Year of approval, company	Therapeutic indication, mode of action
Temsirolimus (Torisel®): R=R¹ Everolimus (Afinitor®), R=R² $R^1 = C(O)C(CH_2OH)_2CH_3$ $R^2 = (CH_2)_2OH$	2007, Wyeth 2009, Novartis	Treatment of renal cell carcinoma (RCC), inhibition of mTOR Treatment of advanced kidney cancer, inhibition of mTOR
Ixabepilone (Ixempra®) 	2007, Bristol-Myers Squibb	Treatment of aggressive metastatic or locally advanced breast cancer no longer responding to currently available chemotherapies, stabilization of microtubules
Vinflunine (Javlor®) 	2009, Pierre Fabre	Treatment of bladder cancer, inhibition of tubulin polymerization
Romidepsin (Istodax®) 	2009, Celgene	Treatment of cutaneous T-cell lymphoma (CTCL), inhibition of the isoforms 1 and 2 of histone deacetylases
Trabectedin = ecteinascidin 743 (Yondelis®) 	2009, Zeltia and Johnson and Johnson	Treatment of advanced soft tissue sarcoma and ovarian cancer, induction of DNA damage
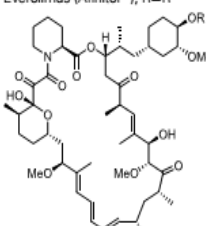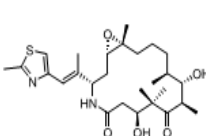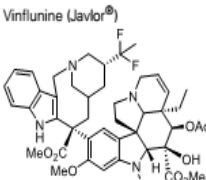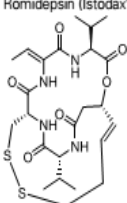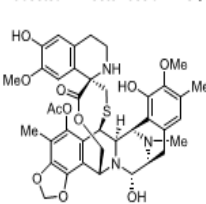
(Continued)

39

Name (trade name), structure	Year of approval, company	Therapeutic indication, mode of action
Cabazitaxel (Jevtana®)	2010, Sanofi-Aventis	Treatment of hormone-refractory metastatic prostate cancer, microtubule stabilization
Eribulin mesylate (Halaven®)	2011, Eisai Co.	Treatment of metastatic breast cancer, inhibition of microtubule dynamics
Homoharringtonine, Omacetaxine mepesuccinate (Synribo®)	2012, Teva	Chronic myelogenous leukemia (CML), inhibition of protein synthesis
Carfilzomib (Kyprolis®)	2012, Onyx	Treatment of multiple myeloma, inhibition of proteasome
Ingenol mebutate (Picato®)	2012, LEO Pharma	Actinic keratosis, activation of PKCδ
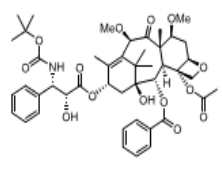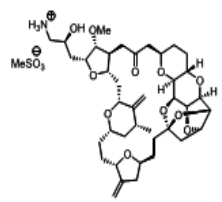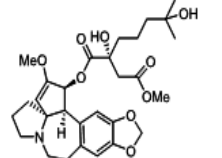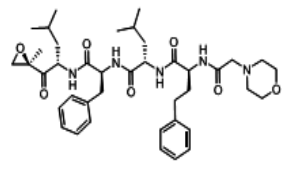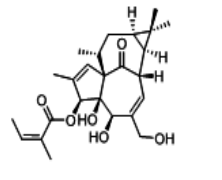
[121]

Furthermore, from the 250,000-300,000 plants around the world, only 10% have been systematically investigated for the presence of bioactive phytochemicals [125]. These numbers are a gross underestimation of the diversity of natural products present therein, as crude extracts from a single plant may yield more than 700 compounds [126]. Traditionally, bioassays were used to screen concentrated extract samples containing complicated mixtures in a process known as bioassay-guided fractionation. This is a common procedure for studying crude extracts where fractions are screened for biological activity and if found to be active, are then further isolated and purified [127]. Advances in high-throughput screening (HTS) technology have greatly improved pre-fractionation strategies that are capable of simplifying extracts by removing artefacts such as polyphenolic tannins, thus making them more suitable for use in bioassays [122]. The use of high-throughput antiproliferative screening has become an invaluable tool in modern day drug discovery. The US NCI is widely considered to be a pioneer in initiating drug screening programmes that have helped in identifying potential candidates for clinical evaluation. The development of the NCI 60 human tumour cell line anticancer drug screen in the late 1980s was a first step towards narrowing the myriad of compounds being developed at the time. The programme was initially intended to supplant the use of transplantable animal tumours in anticancer drug screening [128]. Detailed mechanistic studies are then carried out in sensitive cancer lines and are used as potential models for future *in vivo* efficacy and toxicity studies.

The following sections provide a brief overview of classical examples

of natural products that play an important role in cancer chemotherapy today:

Antibiotics

Actinomycin was the first natural product approved for cancer treatment in 1964. It was isolated from a culture broth of a species of *Streptomyces* where a series of actinomycins were discovered. Actinomycins generally work by binding to DNA and inhibiting transcription by RNA polymerase. More specifically, they intercalate between adjacent pairs of guanine-cytosine base pairs of DNA, while their polypeptide chains extend along the minor groove of the DNA helix [85]. Actinomycin D is currently used to treat solid tumours in children and choriocarcinoma [129].

Perhaps the most important class of antibiotics used in the clinic are anthracyclines. They are derived from a bacterium called *Streptococcus peucetius* var. *caesius*. This class of antibiotics comprises of daunorubicin, doxorubicin, epirubicin, and idarubicin. Idarubicin and epirubicin are analogues of the naturally produced anthracyclines [85]. Daunorubicin and idarubicin have primarily been used to treat acute leukaemias, while doxorubicin and epirubicin have been approved for treatment of solid tumours. These agents however, do have the potential to generate fee radicals that cause cardiotoxicity when used in high doses. Much like the actinomycins, anthracyclines intercalate with DNA directly affecting transcription and replication. Anthracyclines are able to form a tripartite complex with topoisomerase II and DNA, which hinders relaxing of super-coiled DNA and re-ligation of broken DNA strands ultimately leading to apopto-

sis [85]. As mentioned earlier, these agents are able to generate free radicals in solution and do so in both normal and malignant tissues [130]. These radicals attack DNA by oxidising DNA bases leading to strand breaks and apoptosis. Overexpression of DNA strand break repair mechanisms, drug efflux transporters like Pgp), and glutathione peroxidase prevent oxidative damage to the cell [85].

Camptothecins

Camptothecin was a well-known natural compound that had remarkable anticancer properties, but had to be dropped in preliminary clinical trials due to severe bladder toxicity [119]. Chemical manipulation of the compound lead to the synthesis of two new analogues named topotecan and irinotecan, which are both approved for colorectal, ovarian, and small cell lung cancer. Their mechanism of action involves the inhibition of topoisomerase I, an enzyme intimately involved in DNA unwinding, transcription, and replication [119]. Camptothecins bind to and stablise the DNA-topoisomerase I cleavable complex affecting religation which results in an accumulation of DNA single strand breaks [85]. These breaks alone are not lethal to the cell, however, collision of a DNA replication fork with the cleaved position can lead to DNA double strand breaks and apoptosis [85]. At a cellular level, camptothecins target the S-phase of the cell cycle as ongoing DNA synthesis is necessary for cytotoxicity. Experimental models in mammalian cell cultures elude to three mechanisms of camptothecin resistance: (i) reduced cellular accumulation of drugs caused by drug efflux transporters belonging to the ATP-binding cassette (ABCB1)

family which include Pgp and multidrug resistance proteins (MRPs) [131] (ii) alteration of the structure and expression of topoisomerase I. Interestingly, this is the first example of self-resistance to endogenous toxic compounds exploited by plants [131] (iii) modifications in cellular response to camptothecin-DNA-ternary complex that include activation of downstream DNA damage checkpoint, repair, and apoptotic cell death pathways [131].

Epipodophyllotoxins

The American Indians were among the first to treat skin cancers with extracts originating from the roots of mayapple, *Podyphyllum peltatum* [119]. Currently, podophyllin derivatives such as etoposide and teniposide are used to treat various cancers such as paediatric leukaemia, small cell carcinomas of the lung, testicular tumours, Hodgkin's disease, and large cell lymphomas [132, 85]. Both these compounds have been shown to exert cytotoxicity by causing DNA strand breaks as a result of being permanently bound to DNA topoisomerase II in the G2 phase of the cell cycle [133]. Interestingly, podophyllotoxin itself binds to microtubules and inhibits tubulin polymerisation unlike its two analogues [134]. However, like the anthracyclines, etoposide and tenoposide form a ternary complex with topoisomerase II and DNA preventing religation of a strand break which normally follows topoisomerase binding to DNA [85]. Drug efflux *via* upregualtion of Pgp, mutations in topoisomerase II, and/or p53 mutations have all been reported in resistant cells [85].

Antimitotics: Taxanes and the Vinca Alkaloids

Paclitaxel (Taxol) is arguably one of the most successful microtubule disrupting agents to date. It is widely considered to be the highest grossing anticancer agent ever produced and is currently approved to treat ovarian, breast, NSCLC, and head and neck cancers [85]. It was first isolated in the mid 1960s as part of an initiative carried out by a U.S. national institute screening programme. The compound was isolated from the bark of *Taxus brevifolia* (northwest Pacific Yew Tree). It was later discovered that taxol was actually produced by a fungal endophyte that was isolated from the Pacific Yew Tree [135]. After its purification and isolation from biologically active crude extracts, paclitaxel was confirmed to have potent antitumour activity against a mouse melanoma B16 model [136]. A more potent semisynthetic form of paclitaxel called docetaxel was approved by the FDA in the mid 1990s [137]. Paclitaxel and docetaxel bind to β-tubulin subunits and stabilise microtubules (MTs) thus preventing disassembly [136, 135]. Its mechanism of action contrasts with that of another microtubule targeting family of compounds called the vinca alkaloids.

The vinca alkaloids were isolated from the plant *Catharanthus roseus* in 1958, but extracts were generally used as a hypoglycaemic agent in many parts of Asia prior to its isolation. Vincristine and vinblastine have since been used to treat many cancers successfully, specifically childhood leukaemia, testicular teratoma, and Hodgkin's disease among many other cancers [119, 138]. Unlike taxol, the vinca alkloids act by binding to tubulin dimers (α-β tubulin) thus inhibiting the assembly of microtubules (MTs)

[139]. However, cancers have developed an effective way of dealing with antimitotics by overexpressing drug efflux pumps such as Pgp which is encoded by the *MDR1* gene [140]. Other compounds such as colchicine and eribulin also inhibit tubulin polymerisation and bind to different sites on MTs [141].

Tubulin-binding agents (TBAs) have certainly withstood the test of time and continue to be used actively in modern day combinatorial chemotherapy. Given the rapid progression of cancer cells through mitosis, the degree to which they are rendered sensitive to TBAs remains an intensive area of research. One such area that needs to be addressed is the "proliferation rate paradox" in antimitotic chemotherapy [142]. The fact that these cytotoxic drugs are able to kill any dividing cell while promoting tumour regression even in slow growing tumours is indeed "paradoxical" in nature [142, 143]. However, drawing upon the successes of TBAs in comparison to relatively unsuccessful mitosis-specific agents, there is evidence that TBAs not only interfere with mitosis, but disrupt essential interphase cellular mechanisms cascading to subsequent phases as well [143]. An additional characteristic of most TBAs is that they are able to inhibit cancer cell proliferation without causing extensive stabilisation or depolymerisation of the MT network whilst suppressing MT dynamic instability and simultaneously maintaining tubulin polymer mass [144]. Increasing evidence suggests that these agents may exert their effect by inhibiting spindle dynamics resulting in slowing down of metaphase-anaphase transitions, aberrant chromosomal segregation, followed by subsequent induction of mitochondrial-mediated apopto-

sis [144]. Like other classes of anticancer agents, TBAs are not immune to resistance that stem from alterations of the tubulin/MT binding system which include tubulin isotype expression, posttranslational modifications of tubulin, acquisition of tubulin mutations, and changes in expression levels of MT-related proteins [144]. Alterations in actin and tubulin cytoskeletons have also been implicated in resistance to TBAs using proteomics that show overlap in protein expression between these two entities [144]. Recent studies have identified γ-actin as playing a major role in resistance to TBAs. Distinct mutations in γ-actin were found in TBA-resistant cell lines [145]. Exogenous expression of mutant and/or silencing of γ-actin expression induced significant resistance to TBAs [145].

The quest for better targeted therapeutics are a mainstay for the future of cancer chemotherapy, however nature has undeniably played and will continue to play a pivotal role in humanity's fight against cancer.

1.7   Aims and Objectives

The principle aim of this investigation is to investigate antitumour activity and elucidate the mechanism(s) of action of a naturally isolated indole alkaloid called jerantinine A (JA). JA belongs to a family of compounds isolated from the leaf ethanolic extract of the Malayan *Tabernaemontana Corymbosa.* Very little was known about the compound upon commencement of this study. Previous literature demonstrated JA's potent antitumour activity against a nasopharyngeal carcinoma cell line (KB) and vincristine-resistant (V-R) KB cells [146]. However, activity against a broader spectrum of human carcinoma cell lines derived from distinct organ sites had not been investigated. Therefore, assays to determine growth inhibitory and cytotoxic activity of JA in two colorectal (HCT-116 and HT-29), two breast (MCF-7 and MDA468), and one lung (A549) cancer cell lines were conducted. In addition, the mechanism(s) of action underlying JA's activity against KB cells remained unknown. In order to identify mechanisms of action and putative molecular targets of JA within the cell, a number of functional assays measuring aspects cell viability, sensitivity, and cell cycle disruption were undertaken. An additional goal of the study was to successfully generate vincristine- and JA-resistant HCT-116 cell lines to examine cross-resistance. Determination of mechanisms of resistance can often help elucidation of mechanisms of action. In addition, drug efflux pumps contribute to the resistance of many chemotherapeutic agents. It is therefore necessary to assess how JA bypasses vincristine-resistance as

previously reported by Lim et al. (2008) [146]. Investigating processes underlying cell death in response to the agent is also a crucial part of the study, thus efforts to discover the mechanism(s) of action of this exciting new compound included interrogation of signal transduction pathways and protein perturbation in cells following exposure to JA and adopting proteomic and genomic techniques such as Multidimensional Protein Identification Technology (MudPIT) and genome-wide RNAi screens followed by Western blots and shRNA knockdown studies for data validation.

Chapter 2

Antiproliferative Screening of Jerantinine A

2.1 Introduction

It is widely reported that plants of the genus *Tabernaemontana* comprises at least 110 species that have a widespread distribution in pantropical regions that are rich in alkaloids [146]. The IUCN has placed *Tabernaemontana corymbosa* in the red list of endangered species and is therefore a priority for compound characterisation. Lim et al. (2008) isolated seven new alkaloids from a leaf ethanolic extract of the Malayan *Tabernaemontana corymbosa* Roxb. ex Wall. (see fig. 2.1) [146]. JA was among the seven and it constituted the major alkaloid of the leaf extract. Figure 2.2 below illustrates the chemical structures of these alkaloids in addition to acetate derivatives. The acetate derivatives possess greater stability than the parent compounds. Furthermore, converting the 10-OH group to 10-OCOCH$_3$, reduces the overall polarity of the alkaloids enhancing lipophilicity and diffusion across the cell membrane which is hydrophobic in nature. This could mean a higher concentration of the alkaloids can be achieved

within treated cells to act on the target(s), leading to slightly increased potency as demonstrated in a preliminary cytotoxicity screen conducted by Lim et al. (2008) [146]. Esterification is indeed very common among prodrugs used as it is estimated that approximately 49% of all marketed drugs are activated by enzymatic hydrolysis [147].

Figure 2.1: Jerantinine A is isolated from the leaf of *Tabernaemontana corymbosa* which belongs to the Apocynaceae family.
[146]
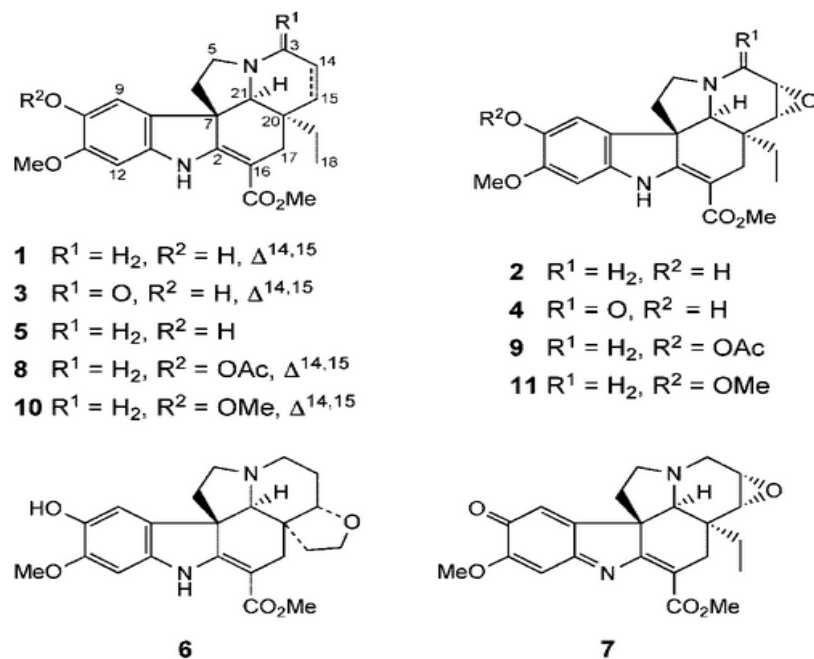
Figure 2.2: Jerantinine family of compounds isolated from the Malayan *Tabernaemontana corymbosa*.

Jerantinine A (1), Jerantinine B (2), Jerantinine C (3), Jerantinine D (4), Jerantinine E (5), Jerantinine F (6), Jerantinine G (7), Jerantinine A acetate (8), Jerantinine B acetate (9), 10-O-methyljerantinine A (10), 10-O-methyljerantinine B (11) [146].

Based on previous literature, JA was shown to have antiproliferative activity against only one cell line, hence it was important to screen the compound against several other cell lines at various concentrations [146]. We used the MTT (3-(4,5-dimethylthiazol-2-yl)-2,5-diphenyltetrazolium bromide) assay to examine antitumour activity (refer to 6.2.3). MTT is a yellow water soluble tetrazolium-based dye that can be metabolised by mitochondrial dehydrogenases of viable cells to form insoluble purple crystal formazan, the concentration of which is directly proportional to the number of viable cells. The concentration of the test agent that inhibits the growth of cells by 50% (GI$_{50}$) is then derived from dose-response curves and

subsequently used to guide treatments in further experiments conducted throughout the study. In addition to measuring growth inhibition, cell sensitivity using the clonogenic assay was adopted to determine whether single cells are able to survive challenge and form colonies after a brief exposure to the test agent.

Markers of apoptosis using flow cytometry and Western blots were also investigated in order to confirm the nature of apoptosis in cells. This phase of the study serves to provide a thorough understanding of the antiproliferative profile of JA.

2.2 Results and Discussion

2.2.1 Jerantinine A, jerantinine B, and acetate derivatives potently inhibit growth of cancer cells

The growth inhibitory properties of jerantinine A, B, and their acetate derivatives against HCT-116, HT-29, MCF-7, MDA-468, and A549 were initially investigated using the MTT assay as discussed previously. The MTT assay was preferred over other cytotoxicity assays such as the sulforhodamine B assay and trypan blue staining primarily because of its capabilities to generate consistently reproducible data quickly and efficiently, which allows for testing of compounds on several cell lines simultaneously.

All cell lines displayed sensitivity to JA; GI_{50} values of ≤ 4 μM were consistently obtained (table.2.1, see fig. 2.3). JA most potently inhibited the growth of breast (MCF-7 and MDA-468) and HCT-116 colon cancer cells with GI_{50} values of <1 μM. A549 lung and HT-29 colon cancer cells were less sensitive to JA with GI_{50} values of 3.74 and 2.52 μM respectively. JA was also screened against MRC-5 (normal lung fibroblasts) which exhibited sensitivity with a GI_{50} value of 1.72 μM. GI_{50} values of <1 μM were observed for jerantinine B (JB) in all cell lines. JB differs from JA by replacement of the double bond in the piperidine ring in JA with an epoxide function in JB (see fig. 2.2). The acetate derivatives of jerantinines A and B (JAA and JBA respectively) were slightly more potent in most of the cell lines tested compared to parent compounds, which is consistent with

the idea that the acetate derivatives may be more permeable across the cell membrane. JBA revealed GI_{50} values <1 μM in all carcinoma cell lines examined. JAA and JBA showed the greatest potency enhancement (>4-fold) when tested against A549. DMSO vehicle had no effect on cancer cell growth (see fig.A.1). Other cell lines were screened throughout the course of the study and also found to be sensitive against JA and JAA (see table 2.2).

Table 2.1: Anti-proliferative activity of jerantinine analogues against human tumour cell lines and a normal fibroblastic cell line

Human cell line			72 h MTT GI_{50} (μM)			
Origin	Designation	JA	Representative GI_{50} concentrations used[a]	JAA	JB	JBA
Breast carcinoma	MDA-468	0.803 ± 0.07	0.9	0.384 ± 0.02	0.392 ± 0.04	0.259 ± 0.02
	MCF-7	0.853 ± 0.09	0.9	0.857 ± 0.01	0.919 ± 0.003	0.480 ± 0.03
Colon carcinoma	HCT-116	0.762 ± 0.13	0.8	0.691 ± 0.36	0.711 ± 0.03	0.358 ± 0.02
	HT-29	2.520 ± 0.28	2.5	2.743 ± 0.17	0.628 ± 0.03	0.649 ± 0.02
Lung carcinoma	A549	3.741 ± 0.65	4.0	0.789 ± 0.01	0.578 ± 0.03	0.887 ± 0.01
Human foetal lung fibroblast	MRC-5	1.723 ± 0.67				

GI_{50} values were determined by MTT assays following 72 h exposure of cells to test agents (n=4) and expressed as a mean and standard deviation of 3 independent trials. Refer to 6.2.3 for experimental methodology.
[a] JA concentrations used as GI_{50} values in subsequent experiments.

Table 2.2: Antiproliferative activity of JA and JAA against other tumour cell lines and a normal microvascular endothelial cell line

Human cell line		72 h MTT GI$_{50}$ (μM)	
Origin	Designation	JA	JAA
Glioblastoma	U373 V	0.530 ± 0.08	0.693 ± 0.20
astrocytoma	U373 M	0.385 ± 0.04	0.611 ± 0.23
Pancreas adenocarcinoma	MIA PaCa-2*	0.251 ± 0.01	0.242 ± 0.02
Microvascular endothelial cells	HMEC-1	0.317 ± 0.06	-

*See appendix A (fig.A.2) for more details
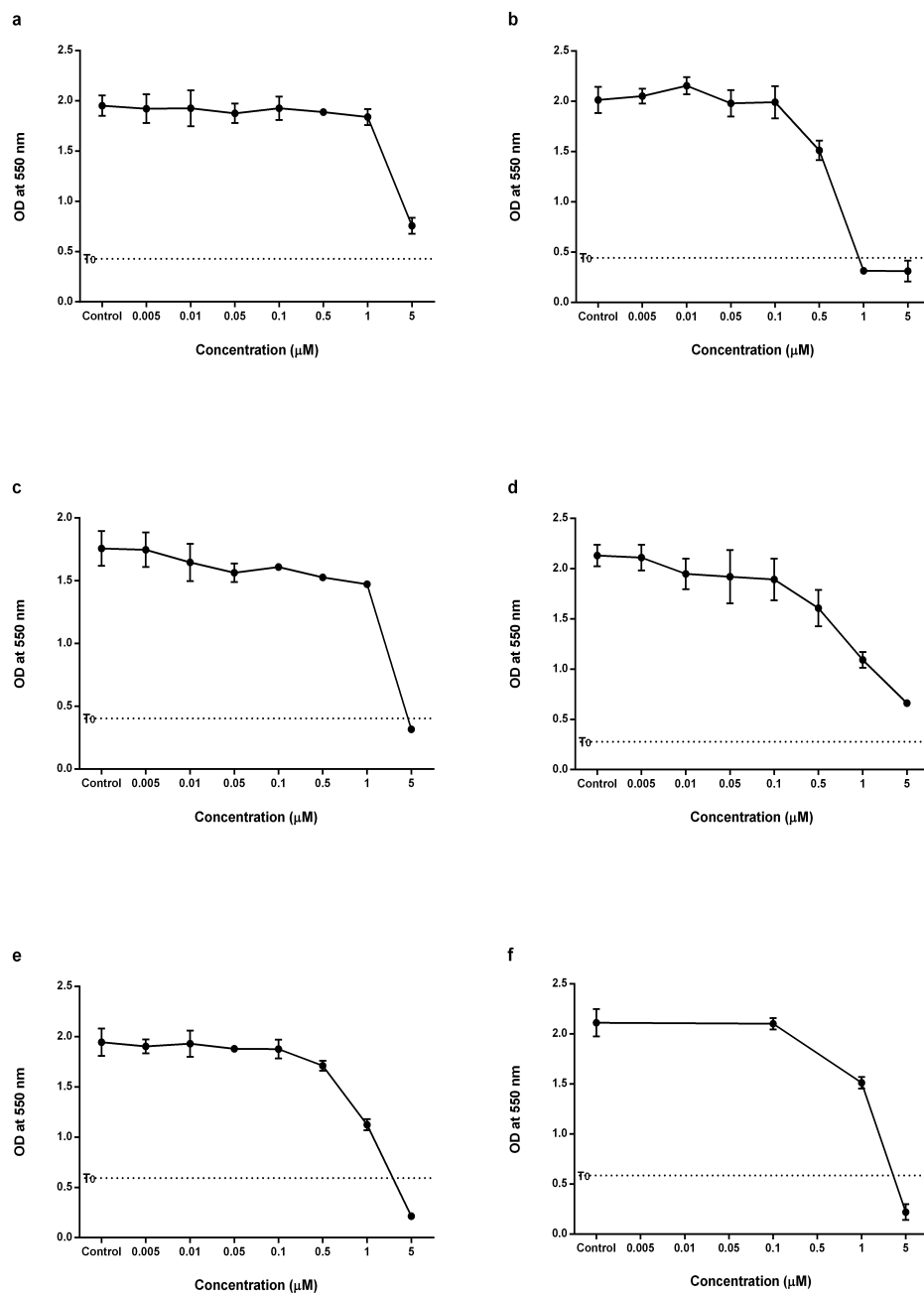
Figure 2.3: Representative MTT graphs from a single trial displaying the growth inhibitory properties of JA.

Growth inhibitory effects of JA from one independent trial in A549 (a), HCT-116 (b), HT-29 (c), MCF-7 (d), MDA-468 (e), MRC-5 (f) cells. Cells were seeded in 96-well plates at a density of 3 x 10^3 cells/well. After allowing to adhere (24 h), cells were treated with JA (n=4) and incubated for 72 h. MTT assays were repeated $\geq$3 times. Refer to 6.2.3 for experimental methodology.

JA and JAA both displayed similar potencies in U373 V compared to the counterpart cell line U373 M. U373 V is a vector control cell line that has low expression of *O(6)*-Methylguanine-DNA-methyltransferase (MGMT) in contrast to U373 M. MGMT is a unique protein that repairs *O(6)*-alkylguanine lesions in DNA [148]. Alkylating agents like temozolomide have been known to work best in cells expressing low levels of MGMT, which is correlated with success in the clinic, as opposed to high levels which are associated with resistance to such agents [148]. As observed in table 2.2, U373 V and U373 M are similarly sensitive to JA and JAA, which means that MGMT status is unlikely to affect the activity of either of these compounds.

2.2.1.1 Investigating cross-resistance between jerantinine A and vincristine

As mentioned previously, JA has been shown to have growth inhibitory activity against a vincristine-resistant KB cell line [146]. In order to confirm and study mechanisms that overcome vincristine-resistance, two cell lines were developed from HCT-116 wild-type CRC cells: HCT-116 cells cultured and maintained in 2 μM of JA (JA-HCT-116) and vincristine-resistant HCT-116 (V-R HCT-116) cells (see fig. 2.4; refer to 6.2.4 for experimental methodology). V-R HCT-116 cells were made resistant to 2 μM of vincristine, nearly 400 times the GI_{50} (5 nM) of vincristine against HCT-116 (see fig. 2.5). HCT-116 cells were unable to develop fold resistance to 2 μM of JA (see fig. 2.6).
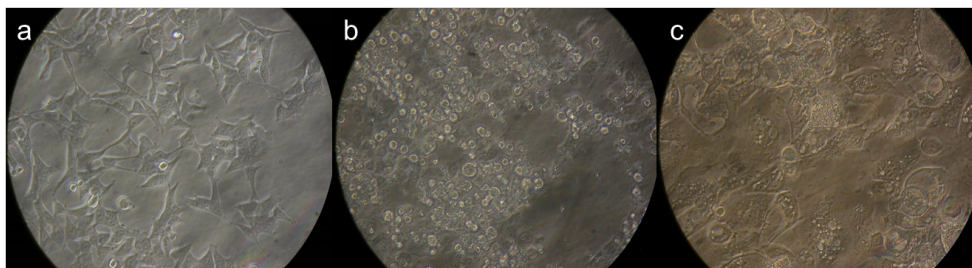
Figure 2.4: Morphological differences between HCT-116 (a), V-R HCT-116 (b), and JA-HCT-116 (c) cells at 40X objective magnification.

Both V-R and JA-HCT-116 cells were maintained in 2 μM of vincristine and JA respectively. V-R HCT-116 cells were smaller and more rounded in appearance compared to JA-HCT-116 cells which contained large vacuoles and were much bigger in size.

Table 2.3: Antiproliferative activity of JA and vincristine against JA-HCT-116 and V-R HCT-116 cells

Human Cell Line		72 h MTT cytotoxicity GI$_{50}$ (μM)	
Origin	Designation	JA	Vincristine
Vincristine-resistant colorectal carcinoma	V-R HCT-116	0.438 ± 0.10	1.64 ± 0.45
Jerantinine A-HCT-116 colorectal carcinoma	JA-HCT-116	0.580 ± 0.008	0.004 ± 0.001
Colorectal carcinoma	HCT-116	0.762 ± 0.13	0.005 ± 0.001

GI$_{50}$ values were determined by MTT assays following 72 h exposure of cells (5000/well) to test agents (n=4) and expressed as a mean and standard deviation of 3 independent trials. Refer to 6.2.3 for experimental methodology.

As seen in table 2.3, vincristine retains activity in JA-HCT-116 cells, however, JA achieves more activity against V-R HCT-116 when compared to naïve HCT-116 cells (approximately 800 nM; see table 2.3). Studies probing possible mechanisms of overcoming vincristine resistance will be discussed in chapter 3.
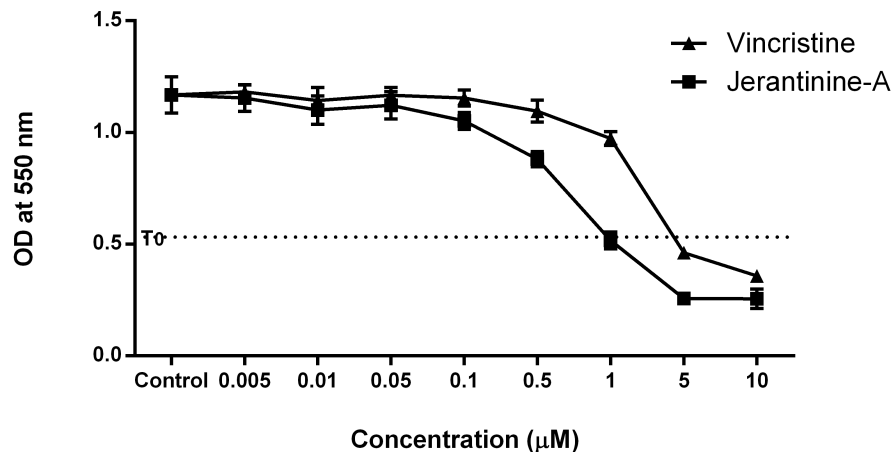
Figure 2.5: Growth inhibitory effects of vincristine and JA from one independent trial in V-R HCT-116.

Cells were seeded in 96-well plates at a density of 3 x 10^3 cells/well. Cells were treated with JA (n=4) and incubated for 72 h after allowing to adhere for 24h. MTT assays repeated $\geq$3 times. HCT-116 was made resistant to 2 μM of vincristine, nearly 400x the GI_{50} value (5 nM) against naïve HCT-116 cells. Last known GI_{50} value for vincristine on this cell line was 1.96 μM.
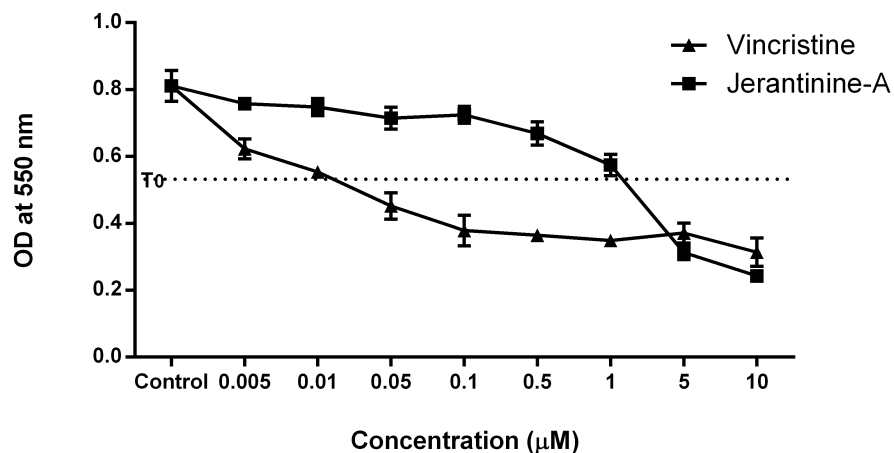
Figure 2.6: Growth inhibitory effects of vincristine and JA from one independent trial in JA-HCT-116.

Cells were seeded in 96-well plates at a density of 3 x 10^3 cells/well. Cells were treated with JA (n=4) and incubated for 72 h after allowing to adhere for 24h. MTT assays repeated $\geq$3 times. V-R HCT-116 were treated with subsequently increasing concentrations of JA starting at 800 nM (GI_{50}) up to 2 μM. Even though cells were maintained in 2 μM of JA, cells were consistently sensitive to concentrations <1μM.

2.2.1.2 Jerantinine A acetate has potent growth inhibitory activities against the NCI60 cell line panel

JAA effectively inhibited growth in all 60 cells lines tested by the NCI yielding GI_{50} values of less than 2 μM (fig.2.7). JAA is considerably more stable than JA and hence was used in the NCI60 cell line screen. A brief review about procedures and analyses pertinent to the NCI60 cell line screen is covered by Robert Shoemaker [149]. The NCI also employs the use of MTT assays to determine patterns of growth inhibition in all these cell lines after treatment with a particular agent [149]. Leukaemic cell lines were most sensitive to JAA with GI_{50} values less than 0.5 μM, followed by prostate cancer, central nervous system (CNS), and ovarian cancer cell lines. HT-29 was the least sensitive in comparison to HCT-116 being the most sensitive colon cancer cell line to JAA, which concurs with results obtained in table 2.1 (2.74 $\pm$ 0.17 μM and 0.69 $\pm$ 0.36 μM respectively). Single-dose data of JAA at 1 μM also showed consistently potent growth inhibition in all leukaemic cell lines. Interestingly, vincristine has also been shown to have potent growth inhibition against leukaemic cell lines.
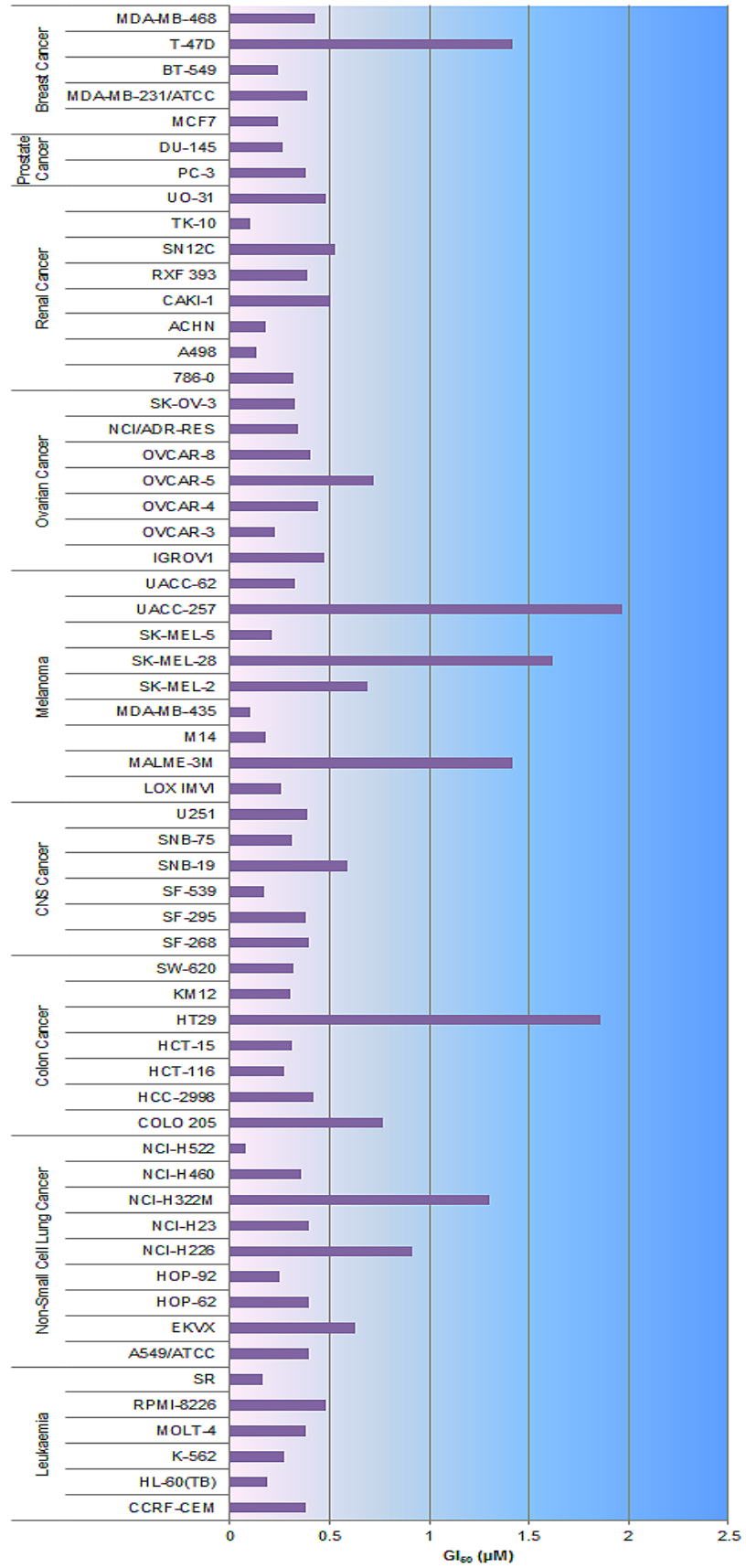
Figure 2.7: Growth inhibitory activity of JAA against the NCI60-cell line panel.

2.2.1.3 Jerantinine A inhibits the ability of cancer cells to form colonies

To determine whether growth inhibitory concentrations of JA were able to inhibit colony formation, clonogenic assays were performed in all cell lines except MDA-468 cells which were unable to grow from low seeding densities required for this assay, and were therefore excluded from this test. Briefly, cells were seeded in 6-well plates and allowed to attach for 24 h. They were then treated with the test agent for an additional 24 h. After removal of treatment media, fresh media was added and cells were incubated until they grew to ≥ 50 cells per colony in control wells. Colonies were then stained and counted (refer to 6.2.5).

JA potently inhibited colony formation in cell lines tested (fig. 2.8; see fig. 2.9); dose-dependent prevention of colony formation was observed in A549 cells: at 1 x and 2 x GI_{50} values, JA inhibited colony formation by 35 and 90% respectively. Intriguingly, in colorectal carcinoma (CRC) cell lines, GI_{50} and 2 x GI_{50}, JA concentrations almost abolished the ability of HCT-116 and HT-29 cells to generate colonies: HCT-116 (fig. 2.8; $GI_{50}=$ 97%; 2 x $GI_{50}=$ 99.6% inhibition), and HT-29 ($GI_{50}=$ 97.7%; 2 x $GI_{50}=$ 97.4% inhibition). In contrast, MCF-7 colony formation (dose-dependently inhibited) was only significantly reduced at 2 x GI_{50} (1.8 μM; 63% inhibition). MCF-7 cells were able to survive after a brief exposure to the test agents and recover proliferative capacity at GI_{50} (900 nM). JA and JAA also significantly inhibited colony formation in MIA PaCa-2 at GI_{50} (250 nM; 21.8% and 31.4% respectively) and 2 x GI_{50} (500 nM; 88% and 75%

respectively) (refer to A.3).
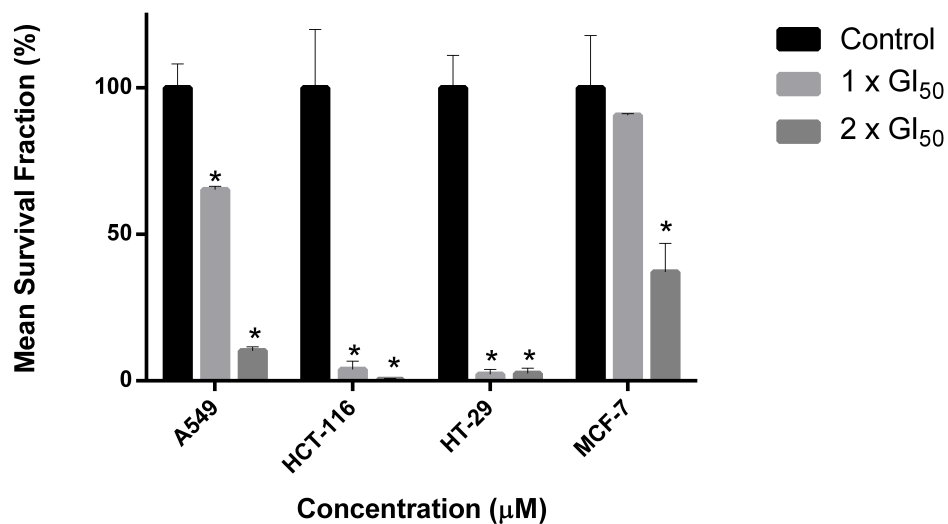
Figure 2.8: Effect of JA on colony formation in A549, HCT-116, HT-29 and MCF-7 cells.

Mean survival fraction as a % of control represented as the mean and SEM of four independent samples. Asterisk indicates significant reduction ($p<0.05$) in colony formation. Mean plating efficiencies from at least two individual experiments were calculated and are as follows: A549 (93.67%), HCT-116 (68.75%), HT-29 (78.63%), and MCF-7 (75.84%). Refer to 6.2.5 for experimental methodology.

Cell line	Jerantinine-A		
A549			
HCT-116			
HT-29			
MCF-7			
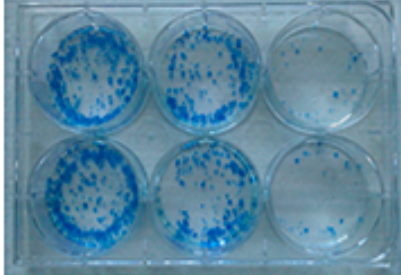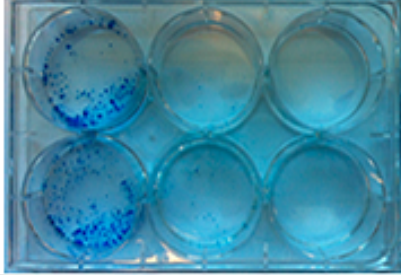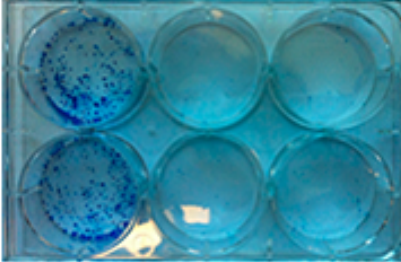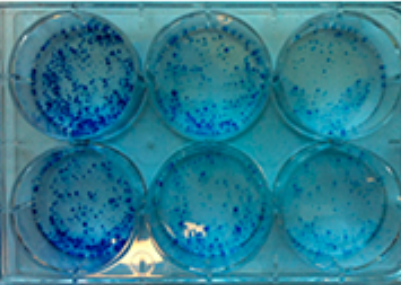
Figure 2.9: Effect of JA on colony formation.

Representative photographs from one of the trials demonstrating potent inhibition of A549, HCT-116, HT-29, and MCF-7 colonies at 1 x and 2 x GI$_{50}$.

2.2.1.4 Jerantinine A induces apoptosis

Results obtained from the MTT and clonogenic assays suggest that cancer cell growth and viability have been compromised by JA. Annexin V assays were conducted to study whether JA induced apoptosis.

During early stages of apoptosis, membrane symmetry is lost resulting in translocation of phosphatidylserine from the inner to the outer membrane of the cell making it accessible for binding to a fluorescein-labelled protein known as annexin V (annexin V-Fluorescein isothiocyanate (FITC)). Propidium Iodide (PI) is used concurrently with the annexin V-FITC antibody in order to discriminate between early stage apoptosis and late stage apoptosis/necrosis [150, 151]. Fluorescence intensity is then measured using a flow cytometer. Refer to 6.2.6.2 for experimental methodology.

We investigated the effects of JA (1 x and 2 x GI_{50} concentrations) on HCT-116 (most sensitive in MTT assays), MCF-7, and A549 (least sensitive in MTT assays) cellular apoptosis after 24 h, 48 h, and 72 h exposure periods. Figures 2.10 and 2.11 show that JA induced significant ($p < 0.05$) dose- and time-dependent apoptosis when compared to controls. Incremental progression from early stage apoptosis (A+/PI−) to late stage apoptosis (A+/PI+) was clearly evident. The highest percentage of apoptosis (annexin V-positive) was present in the A549 cell line at 2 x GI_{50} after 72 h treatment (60 ± 5.97%), compared to 34 ± 1.67% seen in HCT-116 cells. However, MCF-7 cells were resistant to 0.9 μM (GI_{50}) of JA and were able to slightly recover after a 72 h exposure (approximately a 4% decrease in

66

apoptotic events relative to 24 h). The data corroborates well with those

obtained in the clonogenic assay which also showed that MCF-7 cells were

able to recover proliferative capacity and form colonies at GI_{50}.
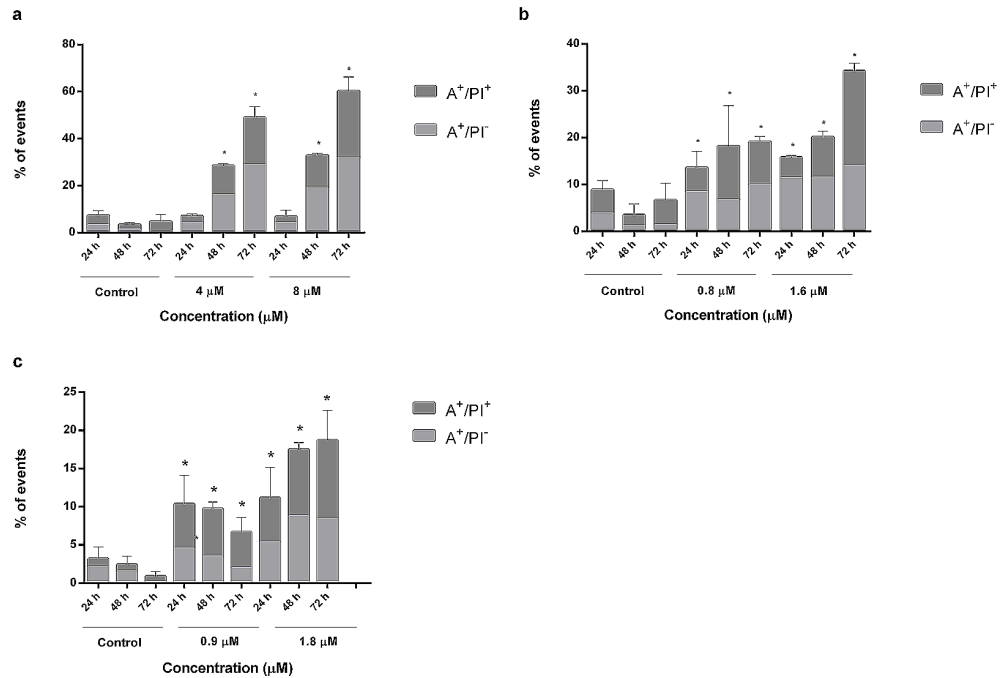
Figure 2.10: Apoptotic effects of JA on A549 (a), HCT-116 (b), MCF-7 (c) cells at GI_{50} and 2 x GI_{50}.

JA induced dose- and time-dependent apoptosis (with the exception of MCF-7 at GI_{50}. The percentage of cells undergoing apoptosis was defined as the sum of early apoptotic cells (annexin V-positive) and late apoptotic cells (annexin V-positive and PI-positive). Data are representative of at least four independent samples. *Asterisk* indicates significant (p<0.05) increase in annexin V-positive events with respect to the control. SD bars represent variation of total % of annexin V + cells within treatments. Refer to 6.2.6.2 for experimental methodology.
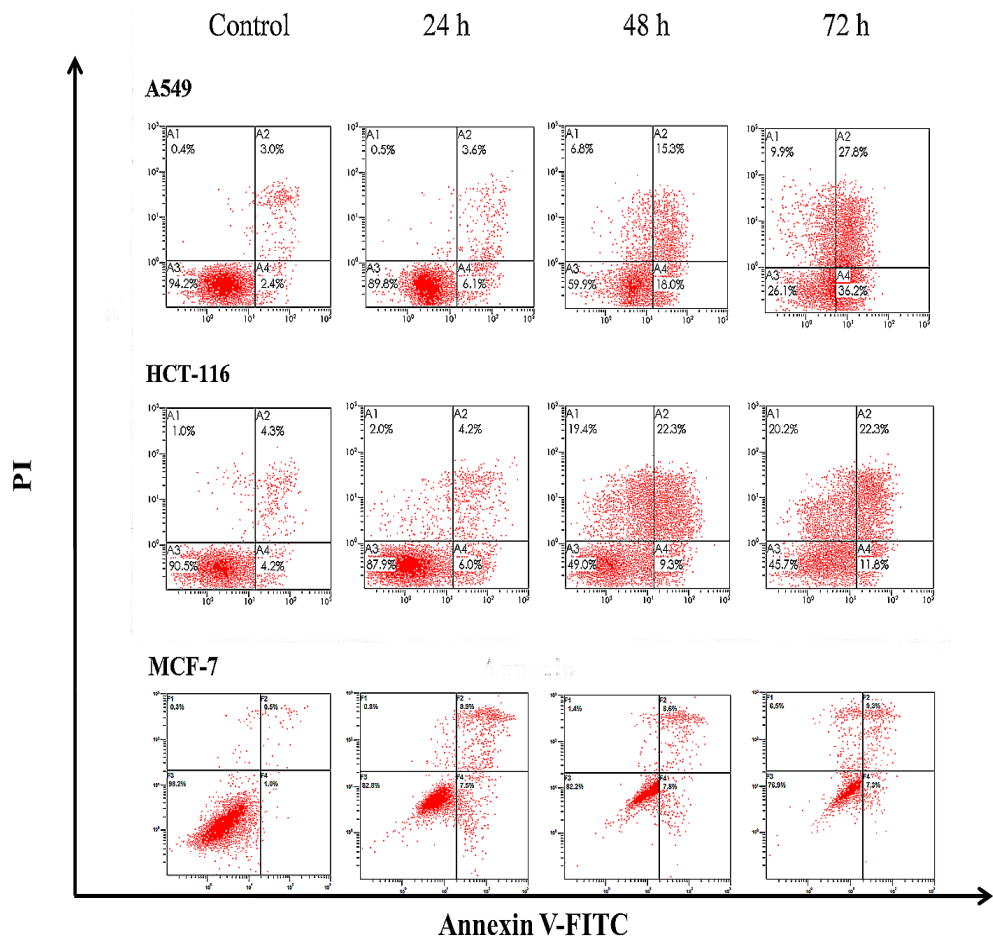
Figure 2.11: Representative dot plots illustrating apoptotic effects of JA (2 x GI_{50}) on A549, HCT-116, and MCF-7 after 24 h, 48 h, and 72 h exposure.

Dose- and time-dependent induction of apoptosis were prevalent in all cell lines. MCF-7 had the least percentage of total A+ cells (approximately 19%) compared to 60% in A549, and 34% in HCT-116 cells at 2 x GI_{50}.

2.2.1.5 Biomarkers of apoptosis

The presence of apoptosis in JA-treated cells was additionally confirmed by results obtained from Western blots (refer to 6.2.10). Figure 2.12 shows increased and decreased expression of pro- and anti-apoptotic proteins respectively. Interactions between p53 and Hdm2 have been widely studied in various tenets of cancer that include apoptosis. The interplay between p53 and Hdm2 are integral to cell cycle arrest, DNA repair, and apoptosis which ultimately govern cell fate by activating downstream effector proteins such as p21 (cell cycle arrest) and/or cleaved PARP (apoptosis) and/or nucleotide/base excision repair pathways (DNA repair) [152, 153, 154]. Antiapoptotic proteins such as Bcl-2 and Mcl-1 can act as key determinants of cell proliferation, differentiation, and tumourigenesis [155]. Caspase 3 and PARP are both enzymes that play important roles in apoptosis and the DNA damage response respectively. PARP plays a key role in repairing DNA single strand breaks and works through the base excision repair pathway (BER). It binds directly to the site of DNA damage and recruits other repair enzymes such as DNA ligase III [156]. Several forms of cancer rely on PARP more so than normal cells and is therefore used as a marker for apoptosis induced by potential anticancer agents [157]. Degradation of cyclin B is necessary for cells to exit mitosis. This process is usually mediated by the anaphase-promoting complex/cyclosome (APC/C), an ubiquitin-protein ligase E3 [158]. Interestingly, some studies have shown that decreased levels of cyclin B results in expression of functional p53 which concurs with blots shown below [159].
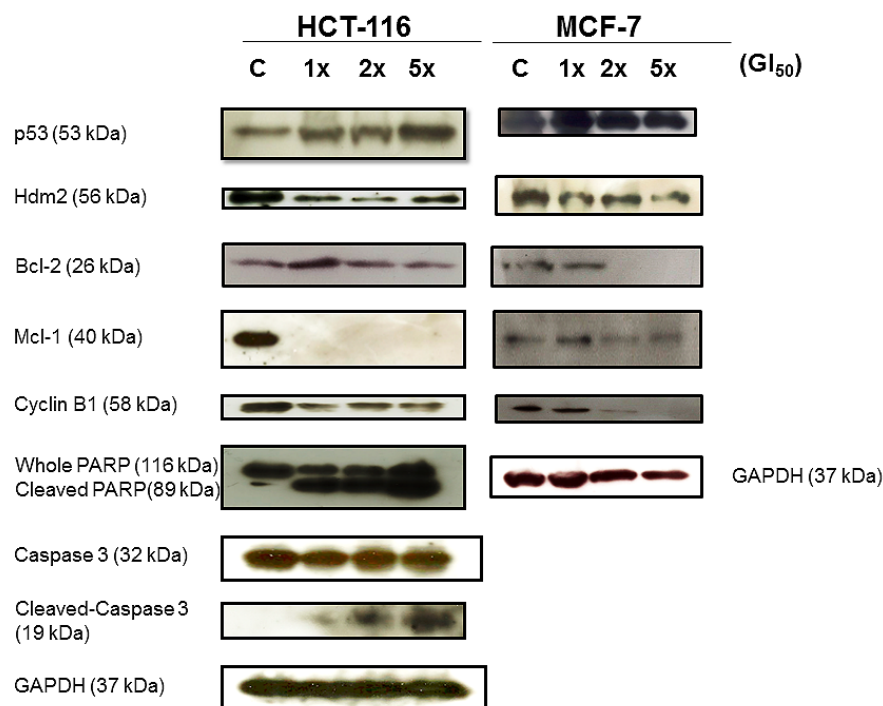
Figure 2.12: Upregulation and downregulation of pro- and anti-apoptotic proteins confirm JA-induced cell death.

Protein expression in HCT-116 and MCF-7 lysates following 72 h exposure of cells to JA. Western blots were performed using antibodies to detect whole and cleaved PARP, whole and cleaved caspase 3, Mcl-1, Bcl-2, cyclin B1, Hdm2 and housekeeping gene GAPDH. HCT-116 cells were treated at 1 x GI$_{50}$ (0.8 μM), 2 x GI$_{50}$ (1.6 μM), and 5 x GI$_{50}$ (4 μM) JA. PARP cleavage was observed $\geq$0.8 μM and was accompanied by a dose-dependent increase in cleaved caspase-3 and complete down-regulation of Mcl-1. Bcl-2 and Mcl-1 down-regulation was also seen in MCF-7 cells (1 x GI$_{50}$ (0.9 μM), 2 x GI$_{50}$ (1.8 μM), and 5 x GI$_{50}$ (4.5 μM)). GAPDH was used as an internal loading control. Refer to 6.2.10 for experimental methodology.

As mentioned in 1.3.3, the apoptotic pathway can be activated extrinsically or intrinsically depending on the stimulus (see Fig.2.13 below). The extrinsic pathway is receptor-mediated whereas the intrinsic pathway is mediated by the mitochondria.

Extrinsic Pathway

Intrinsic Pathway

radiation, toxins, hypoxia, etc.

Perforin/Granzyme Pathway

Cytotoxic T cells

death ligand
death receptor

perforin

adaptors

disc formation

caspase 8 activation

mitochondrial changes (MPT)

apoptosome forms

caspase 9 activation

granzyme B   granzyme A

caspase 10
activation

SET complex

DNA cleavage

caspase 3 activation
(Execution Pathway)

endonuclease activation → degradation of chromosomal DNA
protease activation → degradation of nuclear and cytoskeletal proteins → cytoskeletal reorganization

cytomorphological changes:
chromatin and cytoplasmic condensation, nuclear fragmentation, etc.

formation of apoptotic bodies

Figure 2.13: Schematic representation of apoptotic events.

[160]

In response to diverse upstream stress stimuli originating intrinsically and/or extrinsically, p53 exerts its effects on several downstream genes that regulate important biological processes such as the cell cycle and apoptosis. These stress signals are detected by enzymes such as Hdm2 that regulate p53 activity. When cells are not under stress, low levels of p53 are maintained through interactions with E-3 ligase Hdm2 enzyme, which represses p53 transcriptional activity [161]. However, stress-induced cells have disrupted p53-Hdm2 interactions resulting in Hdm2 degradation (p53 eventually restores Hdm2 levels *via* transcriptional activation of the *Hdm2* gene) [161]. Consequently, p53 is activated and accumulates as a result of an increase in its half-life.

As seen in fig.2.12, p53 levels were indeed upregulated in HCT-116 cells with respect to controls in response to JA treatment. However, based on results from MTT assays, JA potently inhibited growth in cell lines with

varying p53 statuses (refer to 6.1.1). For instance, MCF-7 and MDA-468 have wildtype and mutant p53 respectively, but display the same sensitivity to JA (approximately 0.9 μM). Therefore, it is likely that apoptosis induced by JA is not p53-dependent. Corresponding decreases in Hdm2 levels accompanied increases in p53 levels in both cell lines. Furthermore, the NCI60 cell panel screen showed that JAA also had no preference for cell lines with a particular p53 status.

Anti-apoptotic proteins such as Bcl-2 and Mcl-1 were downregulated in MCF-7, whereas complete suppression of Mcl-1 was observed in HCT-116 $\geq$ GI$_{50}$ value. Mcl-1 is interestingly regulated at the transcriptional, post-transcriptional, and post-translational levels [162]. It has been reported that Mcl-1 reduction can be attributed to caspase (CASP)-dependent cleavage during apoptosis [162, 163].

Caspases are among the most essential players in both initiation and execution of apoptosis. They are a family of cysteine proteases that are divided into two groups: initiator caspases (e.g. CASP2, CASP8, CASP9, and CASP10) and effector caspases (e.g. CASP3, CASP6, and CASP7). In order to trigger apoptosis, initiator caspases cleave inactive pro-forms of effector caspases turning them into active protease complexes capable of cleaving cytosolic proteins and nuclear lamins which maintains structural integrity of the nucleus, thereby triggering apoptosis. As seen in figures 2.12 and 2.14, JA convincingly induces activation of caspase 3 in HCT-116, V-R HCT-116 and MIA PaCa-2 cells.
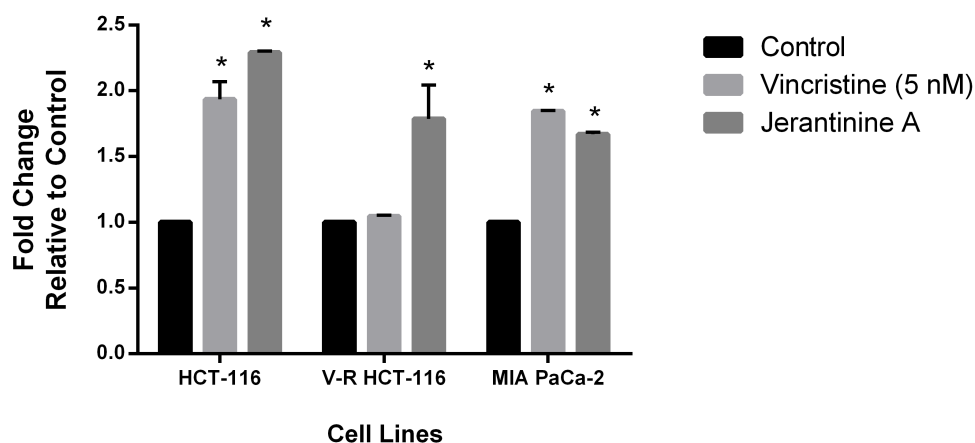
Figure 2.14: Jerantinine A induces significant activation of caspase 3/7 in HCT-116, V-R HCT-116 and MIA PaCa-2 cells after a 48 h exposure.

All cell lines were treated with vincristine (5 nM) which served as a positive control. GI_{50} concentrations of JA were used to treat HCT-116 (0.8 μM), V-R HCT-116 (0.6 μM), and MIA PaCa-2 (0.3 μM). JA induced significant (p<0.05) caspase 3/7 activation in all cell lines. As expected, vincristine (5 nM) did not induce caspase 3/7 activation in V-R HCT-116 cells. Experiments are represented as a mean of at least 2 trials (n=4). Refer to 6.2.11 for experimental methodology.

MCF-7 cells have been reported to be deficient in caspase 3 [164]. According to literature, apoptosis in MCF-7 cells is triggered by downregulation in Bcl-2, increased levels of Bax, release of cytochrome c, and sequential activation of caspase 9, 7, and 6, which bypasses the need for activated caspase 3 in these cells [164]. However, despite Bcl-2 downregulation (fig.2.12), JA-treated (1 μM) MCF-7 cells failed to show significant activation in caspases 3, 7, 8, and 9 at 6 h, 12 h, 24 h, and 48 h (fig.2.15). Interestingly, MDA-468 cells also did not show significant activation in these caspases after the aforementioned time exposures suggesting that other mechanisms of cell death may be at play in these cell lines.
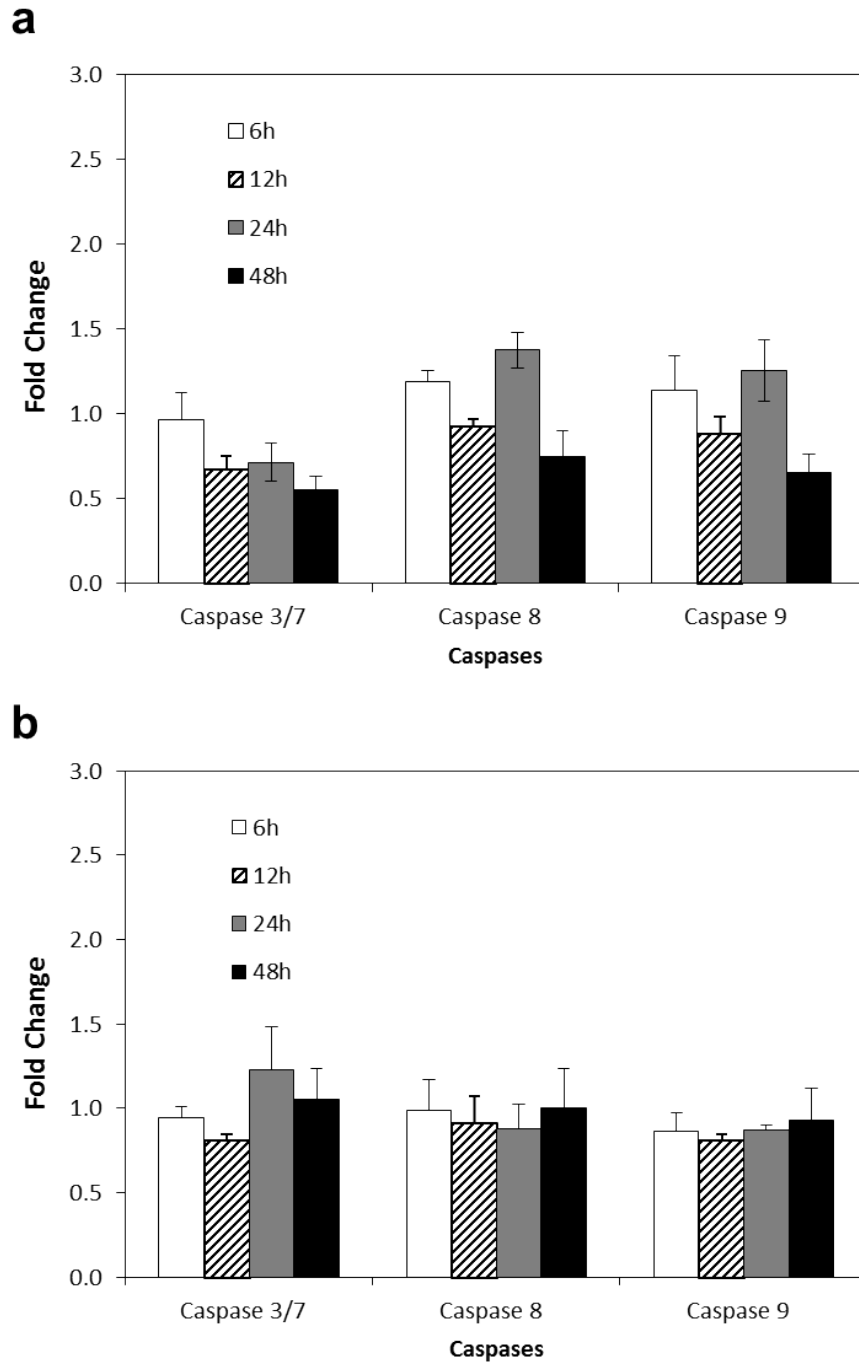
Figure 2.15: JA did not induce activation of caspases 3/7, 8, and 9 in MCF-7 and MDA-468 cells at GI_{50}.

MCF-7 (a) and MDA-468 (b) cells did not exhibit significant caspase activation when treated with 1 μM of JA for 6 h, 12 h, 24 h, and 48 h. Cells were seeded at a density of 3 x 10^3 per well. Experiments shown here are represented as the mean and SD of three trials (n=1). Experiments were kindly performed and data provided by Dr. Chee-Onn Leong (International Medical University, Malaysia).

2.3   Conclusion

In this chapter, a thorough understanding of the antiproliferative activities of JA was established. Preliminary MTT and clonogenic assays revealed potent growth inhibitory activities of JA on A549, HCT-116, HT-29, MCF-7, and MDA-468. MTT screens were also conducted on V-R HCT-116 and JA-HCT-116 cell lines to test for the presence of cross-resistance. V-R HCT-116 cells were more sensitive to JA than naïve HCT-116 cells. Initial MTT screens also showed potent growth inhibition in all cell lines in response to JAA. The NCI60 cell line panel screen against JAA yielded GI_{50} values less than 2 μM for all cell lines.

After establishing the activity of JA in the aforementioned cell lines, further assays were carried out to elucidate the nature of cell death in response to JA. Annexin V assays demonstrated dose- and time-dependent increases in apoptosis in treated cells. Upregulation and downregulation of pro- and anti-apoptotic proteins respectively, confer an apoptotic destiny. Furthermore, induction of caspases 3/7 in HCT-116, V-R HCT-116 and MIA PaCa-2 confirmed involvement of this execution pathway in the cascade of events leading up to apoptosis.

Chapter 3

Cellular Mechanism of Jerantinine A

3.1   Introduction

The previous chapter clearly exhibited potent antitumour activities and the nature of apoptosis of JA. This chapter aims to elucidate JA's cellular mechanism of action and possible molecular target(s). A crucial part of the screening protocol employed in this study entails investigating the effect of this compound on the cell cycle using flow cytometry. Virtually all cytotoxic agents affect the cell cycle to some extent and it is therefore necessary to identify if JA perturbs a specific phase of the cell cycle. From a structural point of view, JA resembles the lower half of the bisindole alkaloid, vincristine, as seen in fig. 3.1. It was therefore hypothesised that JA may target microtubules based on this structural similarity. Vincristine is known for causing significant accumulations in the G2/M phase. If cell cycle analyses revealed potent G2/M arrests, more targeted assays like the tubulin polymerisation assay would be used to identify tubulin as a putative target of JA. Morphological abnormalities in cells treated with JA were

observed by way of confocal microscopy. Furthermore, these observations may shed light on how DNA integrity (i.e. presence of fragmentation or aneuploidy) is compromised if at all. Investigating mechanisms that pertain to vincristine resistance would also help elucidate the mechanism(s) of action of JA. As seen from the above studies, vincristine-resistant cell lines are sensitive to JA, therefore, it was necessary to identify possible mechanisms by which JA overcomes vincristine resistance.
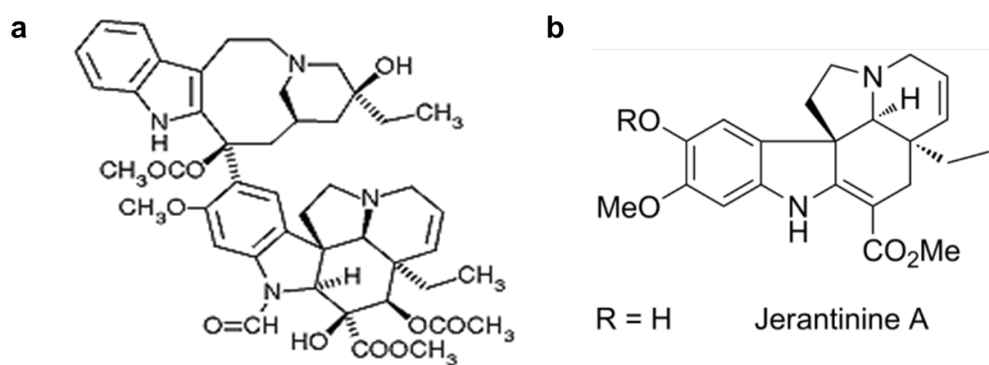
Figure 3.1: Structural similarities between vincristine (a) and JA (b).

3.2 Results and Discussion

3.2.1 Jerantinine A causes severe perturbations in cell cycle progression

Cell cycle analyses were carried out in the manner described in 6.2.6.1. Briefly, cells were seeded at appropriate densities depending on treatment exposure, harvested, and re-suspended in hypotonic fluorochrome solution containing PI, which is an intercalating dye that fluoresces strongly when bound to DNA. The DNA content of an individual cell is proportional to the fluorescence intensity of excited PI (excited by a blue laser at 488 nm). A histogram of DNA content of cells in a population can be used to derive the percentage of cells in each phase of the cell cycle and any perturbations caused by the test agent. PI is normally excluded by intact cells that need to be permeabilised via the use of a gentle detergent/hypotonic solution to allow PI entry into these cells.

Cell cycle analyses were carried out in A549, HCT-116, HT-29, MCF-7, and MDA-468 cells treated with JA (GI_{50} and 2 x GI_{50}; 24 h, 48 h, 72 h; see fig. 3.2; fig. 3.4). Following 24 h exposure, JA induced profoundly significant G2/M accumulation ($p < 0.05$) at both 1 x GI_{50} and 2 x GI_{50} concentrations across all cell lines. Time- and dose-dependent increases in pre-G1 events were also observed in all cell lines with the exception of HT-29. HT-29 seemed to show trends of recovery following JA treatment despite statistically significant accumulations in the G2/M phase at 72 h.

Subdiploid DNA is indicative of apoptosis. Pre-G1 events in A549, MCF-7, and HCT-116 corroborated well with data obtained from the annexin V assay in that A549 had the highest percentage of annexin V-positive cells (refer to 2.10). The least sensitive cell line (indicated by MTT assays; refer to table 2.1), A549, revealed the highest percentage of accumulated events in G2/M (24 h treatment; $88\% \pm 1.25\%$ at 8 μM) and pre-G1 (72 h treatment; $48\% \pm 5.43\%$ at 8 μM) cell cycle phases. Significant accumulation of HCT-116 (the most sensitive cell line in MTT assays) events in G2/M cell cycle phases were detected (fig. 3.2a; 24 h treatment; $86\% \pm 0.65\%$ at 1.6 μM). The presence of aneuploidy (DNA >4 N) was also observed and is shown in fig. 3.3.
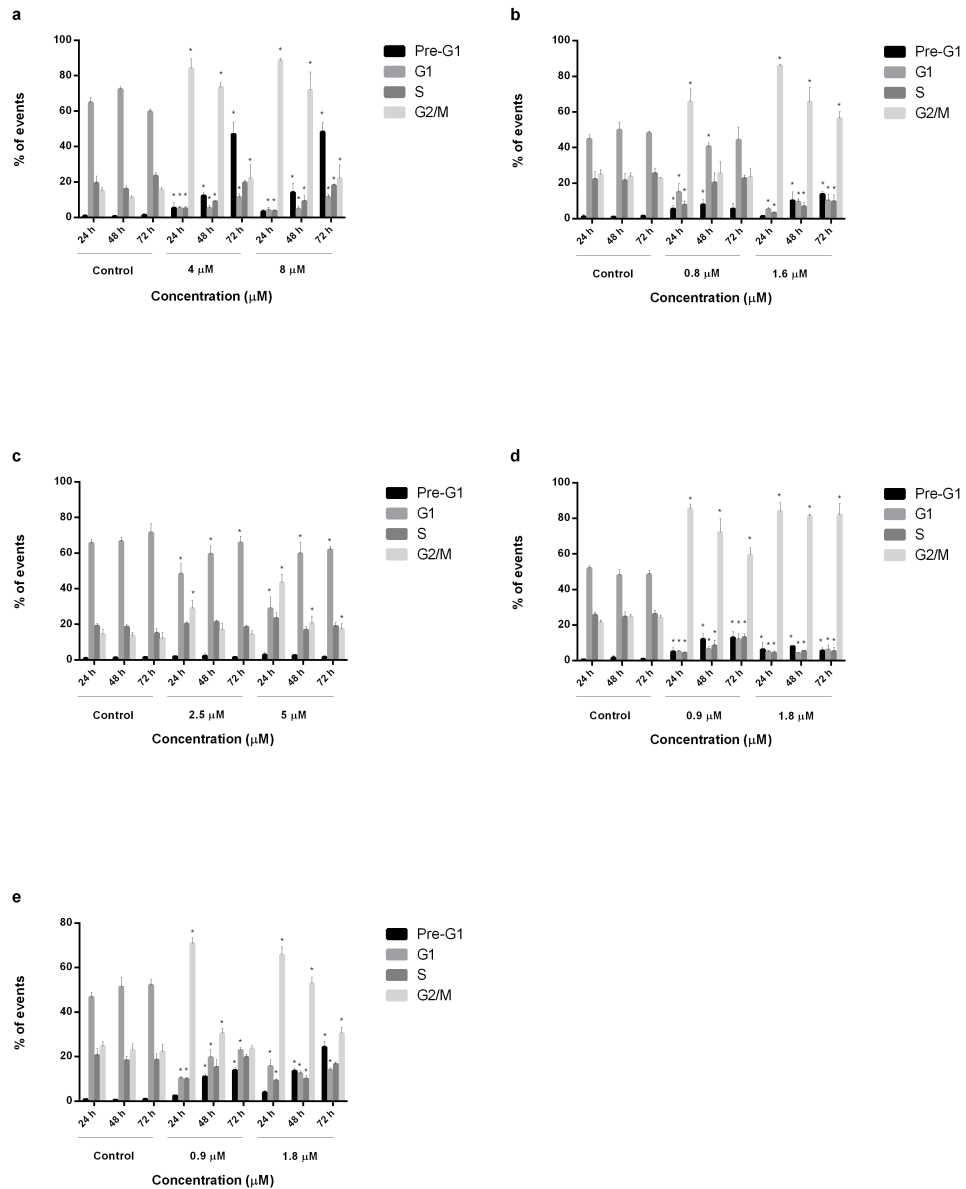
Figure 3.2: Effect of JA on the cell cycle in A549 (a), HCT-116 (b), HT-29 (c), MCF-7 (d), MDA-468 (e).

Cells were treated at 1 x GI_{50} and 2 x GI_{50} after 24, 48, and 72 h exposures. Asterisk indicates significant ($p<0.05$) increase or decrease in events with respect to control. A minimum of 10,000 events were recorded per sample where n=2 ($\geq$6 independent samples). Experiments were repeated $\geq$3 times. All cell lines succumbed to significant ($p<0.05$) accumulations in G2/M after 24 h treatment (A549–88%; HCT-116– 85%; HT-29–43%; MCF-7–83%; MDA-468–65%; % G2/M events at 2 x GI_{50}). Refer to 6.2.6.1 for experimental methodology.
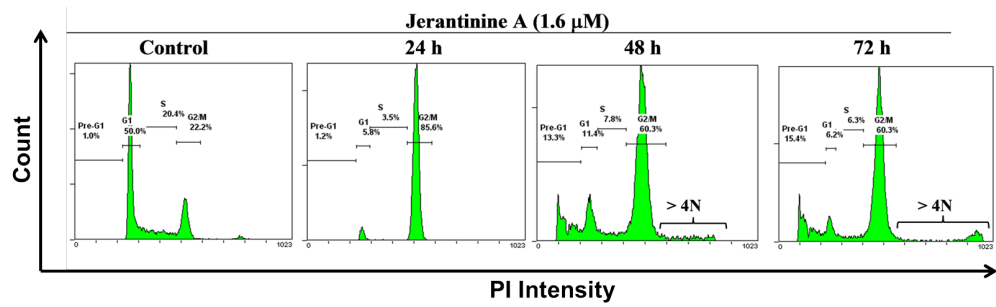
Figure 3.3: Representative cell cycle histogram of JA on HCT-116 cells 24 h, 48 h, and 72 h post-treatment from a single trial.

Significant (p<0.05) G2/M accumulation was observed in addition to the presence of aneuploidy (indicated by brackets) at 2 x GI_{50} (1.6 μM) and appearance of subdiploid DNA.

This cell cycle profile shares similarities to those exhibited by cells treated with taxanes, vinca alkaloids, nocodazole, and colchicine [165]. Microtubule-disrupting agents (MDAs) are thought to cause a G2/M arrest *via* triggering the mitotic checkpoint, a series of biochemical reactions that ensure proper attachment of the microtubule assembly to the chromosomes before progression into anaphase [165]. Following prolonged exposure to MDAs, cells enter an abnormal tetraploid G1-like phase resulting in p53-mediated upregulation of the cyclin-dependent kinase (Cdk) inhibitor p21 $^{Waf1/Cip1}$ which in turn inhibits Cdc2-cyclin B complexes resulting in a G2 arrest [165].
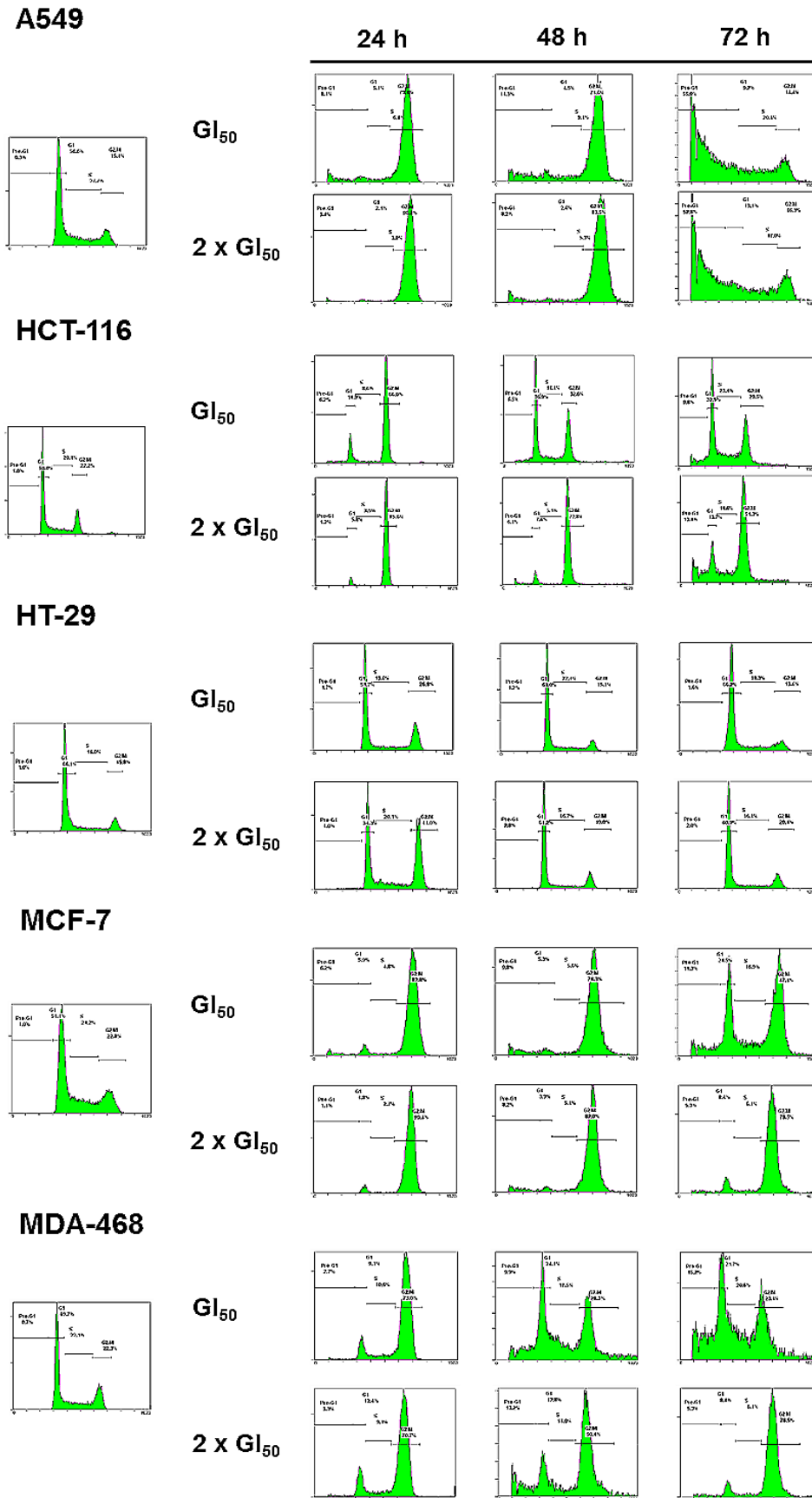
Figure 3.4: Representative cell cycle histograms from a single trial of A549, HCT-116, HT-29, MCF-7, and MDA-468 cells treated with JA at respective GI_{50} and 2 x GI_{50} concentrations for 24 h, 48 h, and 72 h.

3.2.2   Jerantinine A inhibits tubulin polymerisation

Guided by observations of stark G2/M cell cycle arrest, an activity assay was conducted to illustrate possible effects of JA on tubulin polymerisation in comparison to the tubulin-stabilising and destabilising effects of paclitaxel and nocodazole respectively. As shown in fig. 3.5 a and b, paclitaxel (5 and 10 μM) promoted rapid tubulin polymerisation. In contrast, nocodazole (5 and 10 μM) retarded tubulin polymerisation. JA (5 and 10 μM) unambiguously inhibited tubulin polymerisation, being as potent as nocodazole in that respect. These results confirm that tubulin is a viable target for JA and possibly the main mechanism of action and growth inhibition *in vitro*.
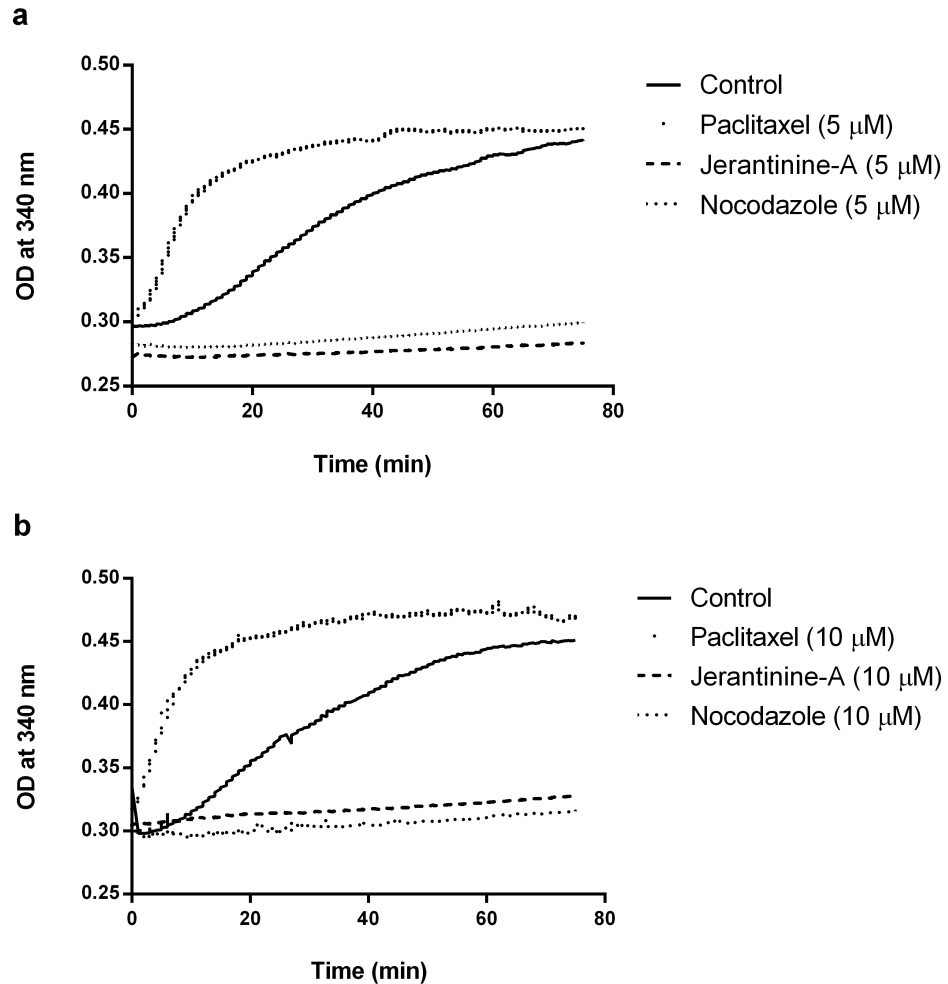
Figure 3.5: Effect of JA on tubulin polymerisation.

All agents were used at 5 μM (a) and 10 μM (b). JA suppressed tubulin polymerisation. Microtubule-stabilising agent paclitaxel, and nocodazole which promotes depolymerisation, were included as controls. End-point means and SDs were calculated at 75 min for all treatment groups and are as follows: controls (5 μM: 0.442 $\pm$ 0.09; 10 μM: 0.451 $\pm$ 0.07), paclitaxel (5 μM: 0.450 $\pm$ 0.09; 10 μM: 0.470 $\pm$ 0.03), nocodazole (5 μM: 0.299 $\pm$0.01; 10 μM: 0.315 $\pm$ 0.02), and JA (5 μM: 0.284 $\pm$ 0.01; 10 μM: 0.329 $\pm$ 0.02). Refer to 6.2.7 for experimental methodology.

Microtubules are composed of α/β heterodimers and are assembled in a head-to-tail fashion to form protofilaments which then associate from side to side forming a tube [166]. They are anchored by their minus ends (less dynamic end) at the microtubule-organising center, disposing their plus ends (more dynamic end) to the cell periphery [166]. The figure below details the assembly of microtubules [167].
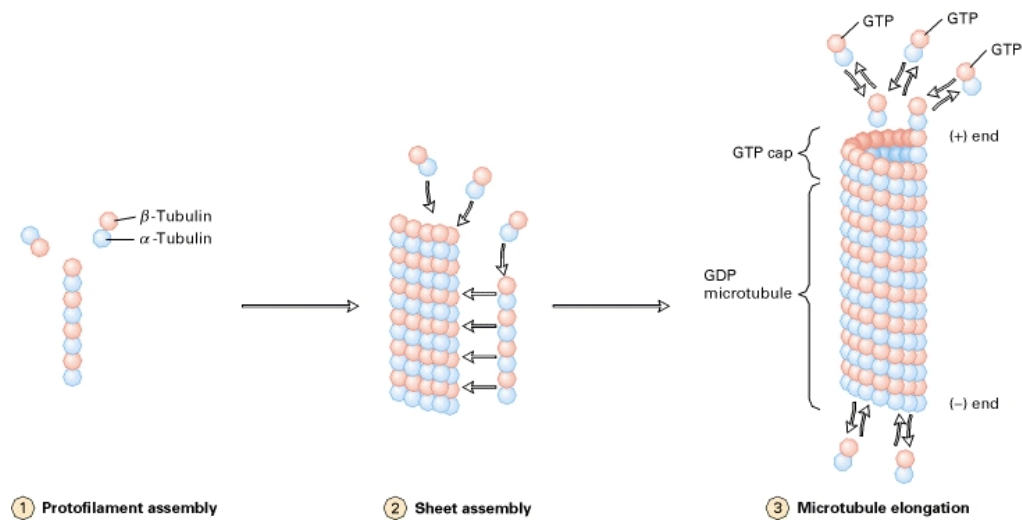
Figure 3.6: Assembly of microtubules.

α/β heterodimers associate longitudinally to form short protofilaments (step 1). Due to probable instability, these dimers quickly associate laterally to form curved sheets which are stable (step 2). Eventually a full sheet consisting of 13 protofilaments wraps around into a microtubule. The microtubule then grows by addition of subunits to the ends of the protofilaments that form the microtubule wall (step 3). The free tubulin dimers have GTP bound to the nucleotide-binding site on the β-tubulin monomer. The GTP on the β-tubulin (not α-tubulin) is subsequently hydrolysed to GDP after incorporation of a heterodimeric subunit into a microtubule. If the rate of GTP hydrolysis is slower than the rate of polymerisation, then a cap comprising of GTP-bound subunits is generated at the plus (+) end, although the bulk of β-tubulin in a given microtubule will contain GDP. The rate of polymerisation is twice as fast at the (+) end when compared to the (−) end [167].

It has been reported that low concentrations of taxotere (chemical derivative of taxol) and vinblastine (vinca alkaloids) stabilise microtubules

by inhibiting microtubule dynamics; i.e. the lengthening and shortening of microtubules. However, at high concentrations, vinblastine promotes depolymerisation of microtubules and inhibits assembly of tubulin dimers [167]. The figure below is a general illustration of different classes of antimitotics and their known binding site on MTs.
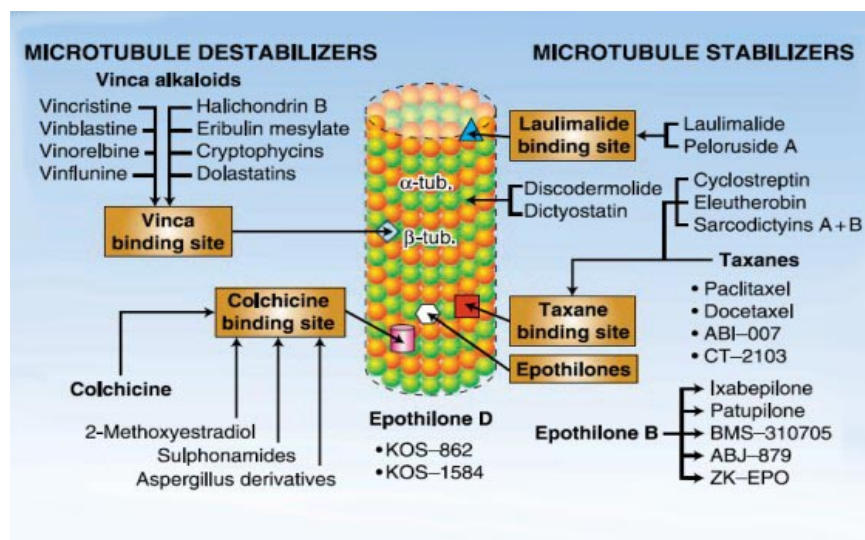
Figure 3.7: Microtubule destabilisers and stabilisers and their binding sites on tubulin.

[168]

3.2.3 Jerantinine A causes severe disruption in cytoskeletal architecture

After successfully identifying tubulin as a target of JA, visual validation was needed to confirm microtubule disruption *in vitro* using confocal microscopy. Following desired treatments, HCT-116 cells were prepared for confocal microscopy. Images were captured to visualise the effects of JA on tubulin, DNA and cell morphology compared to vehicle alone and vincristine, 24 h post-treatment. Figures 3.8 a-d represent HCT-116 cells

treated with vehicle alone. Vincristine treatment rendered cells unable to complete mitosis due to improper chromosomal separation (fig. 3.8 g). Formation of shortened, multipolar astral microtubules was also observed (fig. 3.8 f, h). Images of tubulin networks extending into neighbouring cells were also captured (fig. 3.8 h). Severe membrane blebbing was detected on cells treated with JA, a characteristic most commonly associated with apoptosis (fig. 3.8 n→3, p→3). Similar to cells treated with vincristine, tubulin network disruption led to improper segregation of chromosomes in cells exposed to JA (fig. 3.8 j). Aneuploidy and multinucleation were also detected in HCT-116 cells exposed to JA (fig. 3.8 k, m). Aberrant mitoses where one daughter cell completely lacked DNA content also featured as a common characteristic following JA treatment (fig. 3.8 k). This may serve as a possible explanation to the population of cells with aneuploidy ($>4N$; fig. 3.3) previously detected in cell cycle analyses.
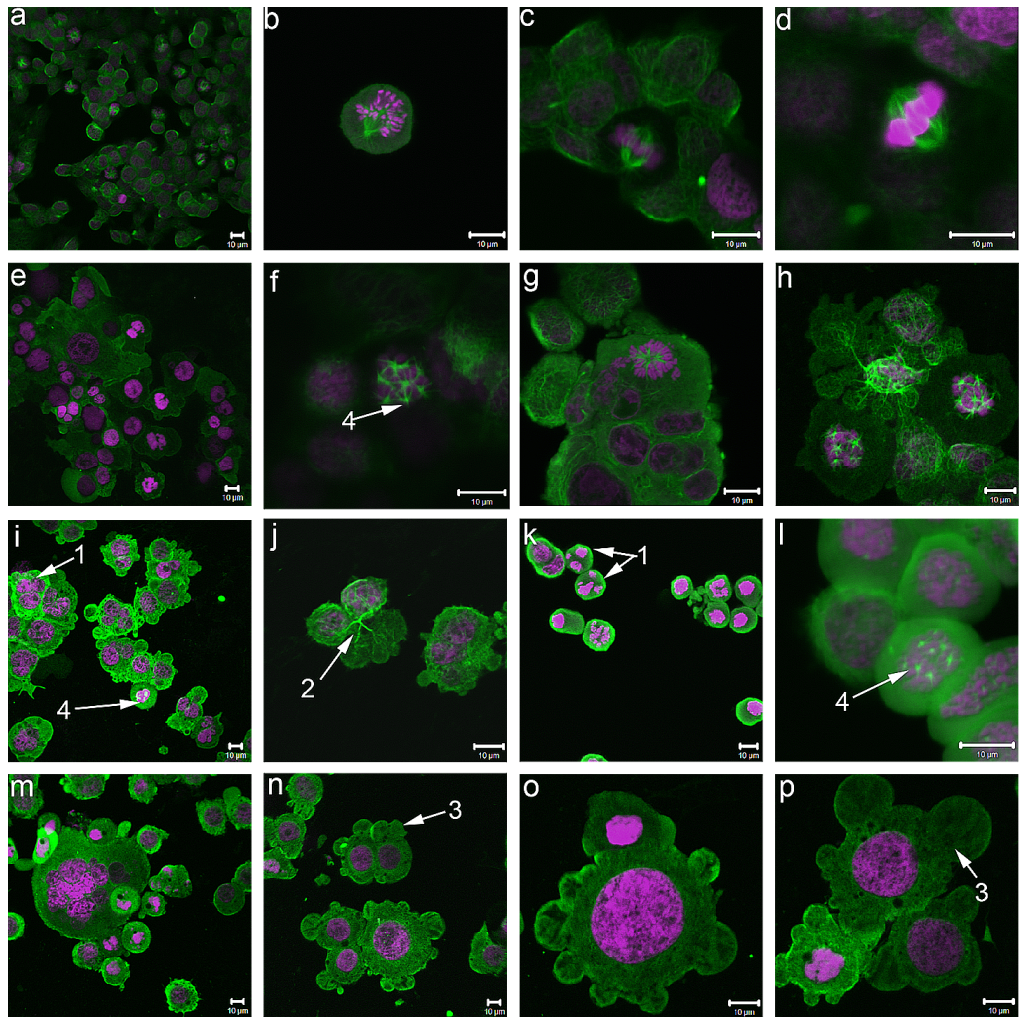
Figure 3.8: Effects of JA and vincristine on HCT-116 cells after 24 h exposure.

a–d Controls with vehicle (medium) only; **e–f** Vincristine (GI_{50}= 5 nM); **g** Vincristine (10 nM); **h** Vincristine (25 nM); **i–j** JA (0.8 μM); **k–l** JA (1.6 μM); **m–p** JA (4 μM). JA causes multinucleation (1) and improper chromosomal segregation due to tubulin disruption (2) and blebbing (3). Multipolar spindles were also evident in samples treated with JA and vincristine (4). Experiments were repeated 3 times. Refer to 6.2.8 for experimental methodology.

As seen in SEM images (fig. 3.9) membrane blebbing is a distinguishing feature of JA treated cells. Membrane blebbing is a phenomenon that has been shown to be present during the execution phase of apoptosis and is identical to those occurring in filament-deficient cells or during cytokinesis in dividing cells [169]. However, the role of blebs during apoptosis remains
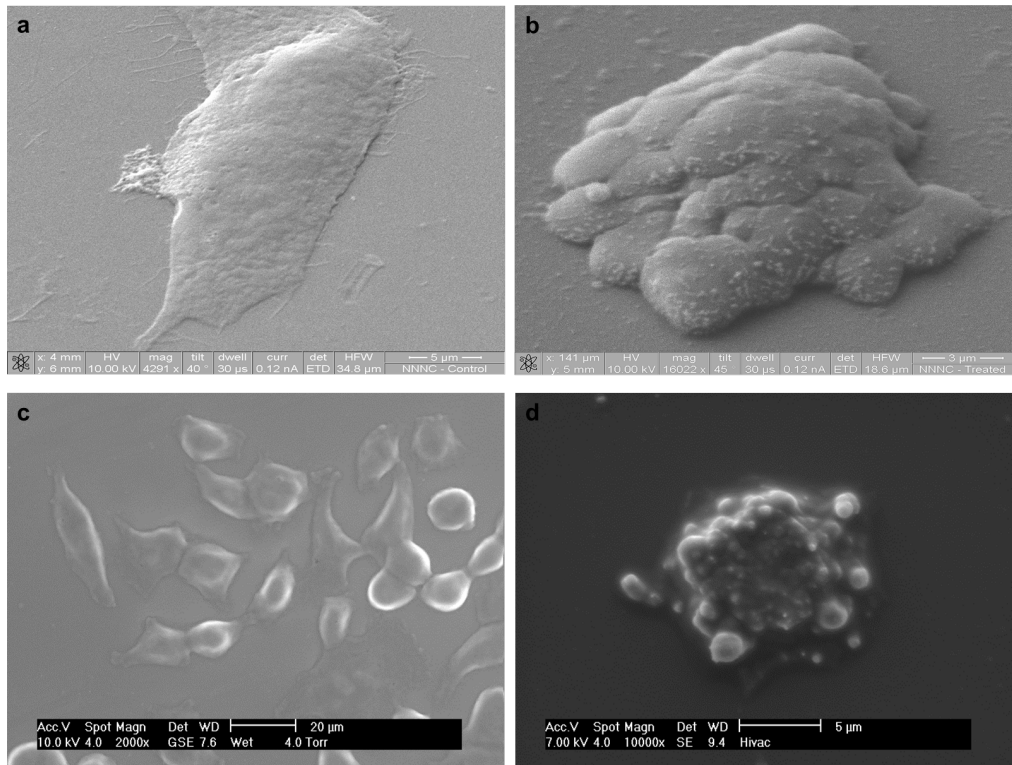
Figure 3.9: Scanning Electron Microscope (SEM) images illustrating the extent of cell blebbing caused by JA.

a-b Taken using a cryo-SEM. (a) HCT-116 control cells and (b) JA-treated HCT-116 (0.8 μM); **c-d** Taken using an environmental SEM (ESEM) (c) HCT-116 control cells and (d) JA-treated HCT-116 cells at (0.8 μM). Images were provided by the Nottingham Nanotechnology and Nanoscience Centre (NNMC) and the Nottingham Advanced Materials research Group.

unclear. It is suggested that connective flows of cytosol that give rise to blebs serve to fragment the nucleus and organelles in the apoptosing cell [169]. This corroborates well with the images obtained from the confocal microscopy studies illustrated above. Furthermore, the development of multipolar spindles has been reported in vincristine-induced apoptosis [170]. It is possible that the formation of multipolar spindles also seen with JA treatment may contribute to apoptosis.

3.2.4   Jerantinine A inhibits activity of kinases involved in mitosis

Taken together, cell cycle analyses, tubulin polymerisation assays, and confocal images have evidently illustrated that JA interferes with growth in cells going through the G2/M transition. Consequently, we were interested in identifying if JA had an affinity to polo-like kinase 1 (PLK1) and aurora kinases (AURKs; AURKA, AURKB, and AURKC), all of which have direct roles in mitosis. JA was sent to Merck Millipore to be screened against purified kinases, PLK1 and AURKS. As seen in fig. 3.10, JA significantly inhibited PLK1 activity in a dose-dependent manner. AURKB activity was slightly but significantly inhibited at lower concentrations (1 and 5 μM).
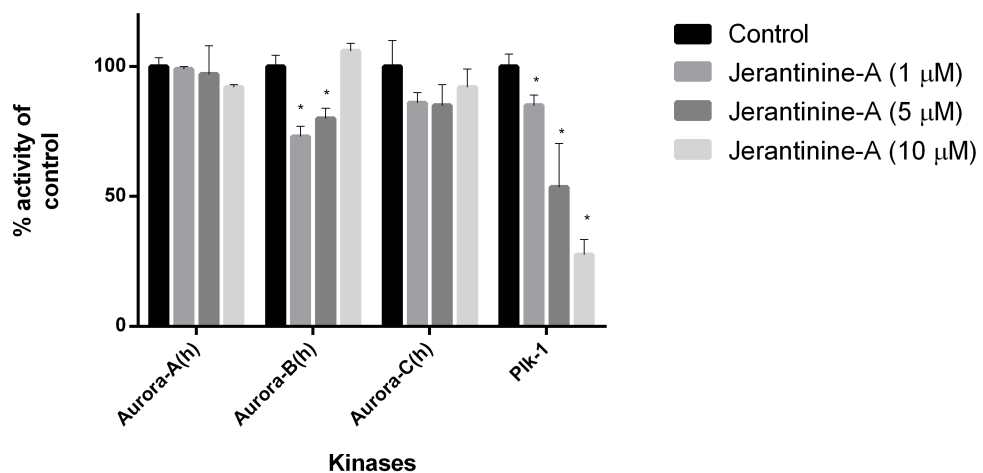
Figure 3.10: Effect of JA on the activity of aurora A, B, C and PLK1

AURKB was slightly but significantly inhibited (27%, 20% inhibition at 1 and 5 μM respectively; $p < 0.05$). Inhibition of PLK1 was significant (22%, 32%, and 67% inhibition at 1, 5, and 10 μM respectively; $p < 0.05$) at all three concentrations tested. Experiments were carried out once where n = 2. A one-way ANOVA was used to determine significance at the 95% confidence interval.

PLK1 belongs to a family of serine/threonine kinases and is an essential enzyme involved in cell cycle progression through M phase in addition to playing an important role in genomic stability [171]. It has been shown to recruit γ-tubulin ring complexes to centromeres to promote maturation [171, 172]. Another important role of PLK1 is to prevent premature entry into mitosis *via* phosphorylation of cyclin B1 leading to cytoplasmic retention, thus preventing nuclear translocation of cyclin B1-Cdk1 complex [173]. PLK1 has been reported to be overexpressed in several haematological malignancies in comparison to normal tissue and may be used as a prognostic factor [171, 174]. PLK1 was recently shown to be a significant prognostic factor in medulloblastoma with high expression correlating with poor prognosis in patients [175]. Inhibition of PLK1 prevented proliferation in medulloblastoma cell lines that expressed high levels of PLK1 by causing microtubule instability and inducing apoptosis. It was also shown that B12536, a potent PLK1 inhibitor, was not able to inhibit growth of human astrocytes, cerebellar tissue, and neural stem cells, due to low levels of PLK1 [175]. However, medulloblastoma cell lines with high PLK1 expression were sensitive to B12536.

Collaborative studies with Dr. Beth Coyle (personal communication) have shown a correlation between growth inhibition and PLK1 expression in paediatric MB cell lines. Three medulloblastoma cell lines were used for this particular study: DAOY (high PLK1 expression), MED1 (intermediate PLK1 expression), and UW228-3 (low PLK1 expression). Vincristine was used as a positive control alongside JA treatments in MTT and clonogenic

assays (refer to fig. A.4). Results showed significant growth inhibition in DAOY cells after treatment with JA in both MTT and clonogenic assays compared to MED1 and UW228-3 cell lines (table A.1).

Like the PLKs , the Aurora kinase family are a collection of highly conserved serine/threonine kinases that regulate mitosis and multiple signaling pathways. Alterations in aurora kinase activity has been associated with chromosomal aneuploidy and mitotic errors in cancer cells. Several studies have shown that certain haematologic malignancies and solid tumours overexpress AURKA and AURKB. Results from the activity assays shown above indicate that JA may have an affinity to AURKB and therefore inhibit its activity at lower concentrations (i.e. 1 and 5 μM). Interestingly, AURKB is a chromosomal passenger protein critical for accurate chromosomal segregation, cytokinesis, protein localisation to the centromere and kinetochore, correct microtubule-kinetochore attachments, and regulation of the mitotic checkpoint [176]. Abnormalities in some of these features such as chromosomal segregation and aneuploidy were clearly evident in images obtained from confocal microscopy of HCT-116 cells treated with JA, hence our rationale for testing possible inhibitory activity of these kinases (see fig. 3.8).

3.2.5 Monitoring DNA double strand breaks by observing phosphorylated γH2AX

Confocal microscopy studies also revealed some DNA fragmentation as a consequence of JA treatment. We were therefore interested in identifying

if JA caused DNA double strand breaks (DSBs) in cells. A flow cytometry based method was adapted to test for the presence of DSBs inherent within samples (refer to 6.2.6.3 for more details). DSBs are paradoxical in nature in that they may lead to cancer by initiating genomic instability, but can also be used to kill cancer cells. One of the key components of DNA repair is the histone protein H2AX, which becomes rapidly phosphorylated on a serine (c-4) to form γH2AX at nascent DSB sites [177]. Large numbers of γH2AX molecules form in the chromatin around the DSB site, creating foci and accumulation of proteins involved in DNA repair and chromatic remodelling making it possible to detect individual DSBs using an antibody targeted to γH2AX. Results obtained from this assay revealed that JA did induce significant ($p < 0.05$) DNA DSBs after a 24 h exposure. Cell cycle analyses were also carried out concurrently and revealed a vast majority of DNA damage occurred in the G2/M phase (see figs. 3.12, 3.11). Vincristine also caused relatively similar levels of phosphorylated γH2AX compared to JA. A very recent study convincingly demonstrated that microtubule targeting agents (MTAs) are able to prolong DNA damage by interfering with the trafficking of DNA repair proteins that associate with dynein and interphase microtubules [178]. It was further suggested that this may be a reason as to why MTAs work well in combinatorial chemotherapy with other DNA damaging agents. Indeed, it was shown that cells treated with vincristine along with a DNA damaging agent exhibited higher and sustained levels of phosphorylated γH2AX [178].
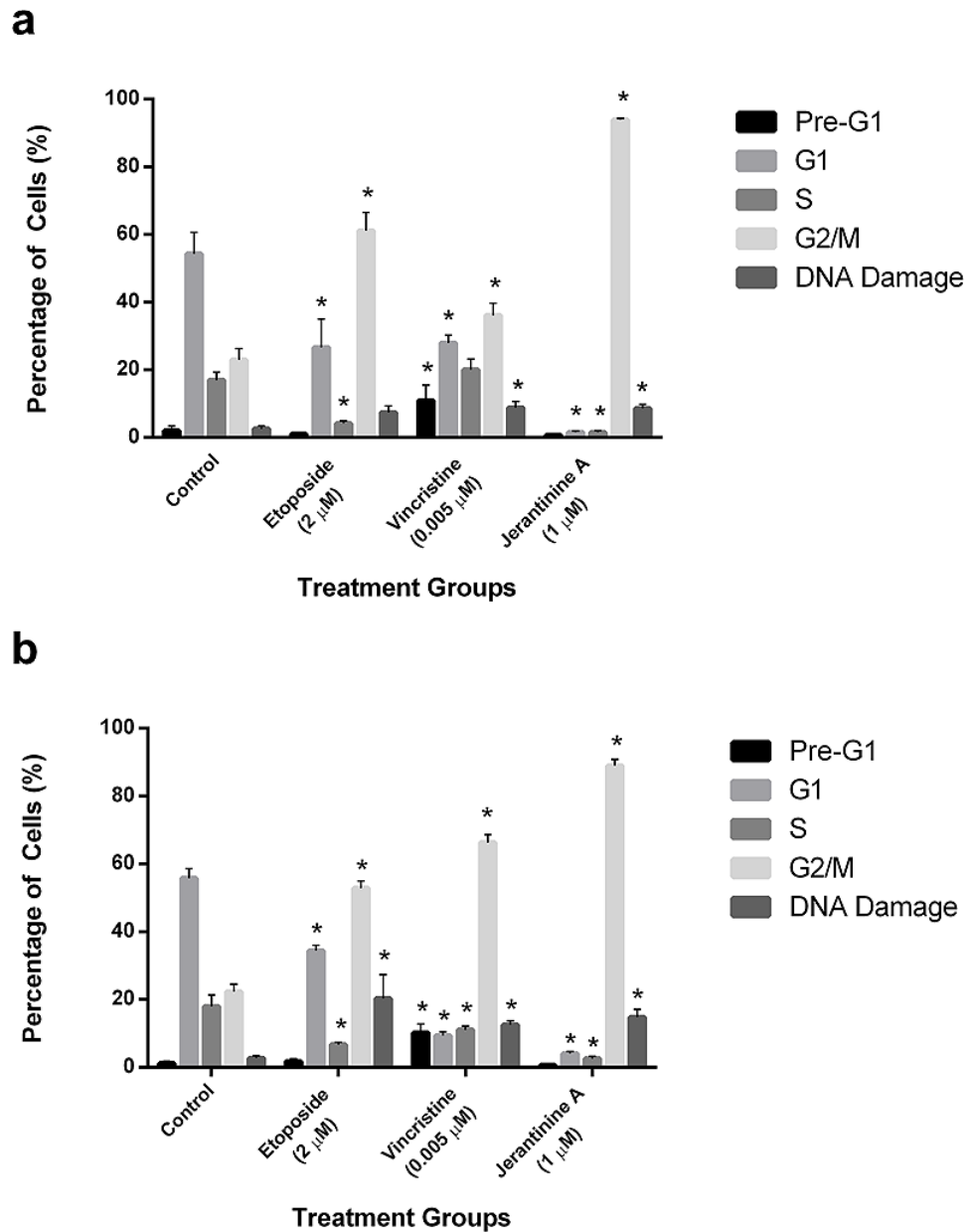
Figure 3.11: JA induces DNA DSBs in HCT-116 and MCF-7 cell after a 24 h exposure.

Both HCT-116 (a) and MCF-7 (b) cells were treated with 1 μM of JA for 24 h. Etoposide was used as a positive control as it is a known DNA damaging agent. Vincristine was used as a comparator control as it is a known microtubule depolymerising agent. Experiments were repeated at least 3 times (n=2). Refer to 6.2.6.3 for experimental methodology.
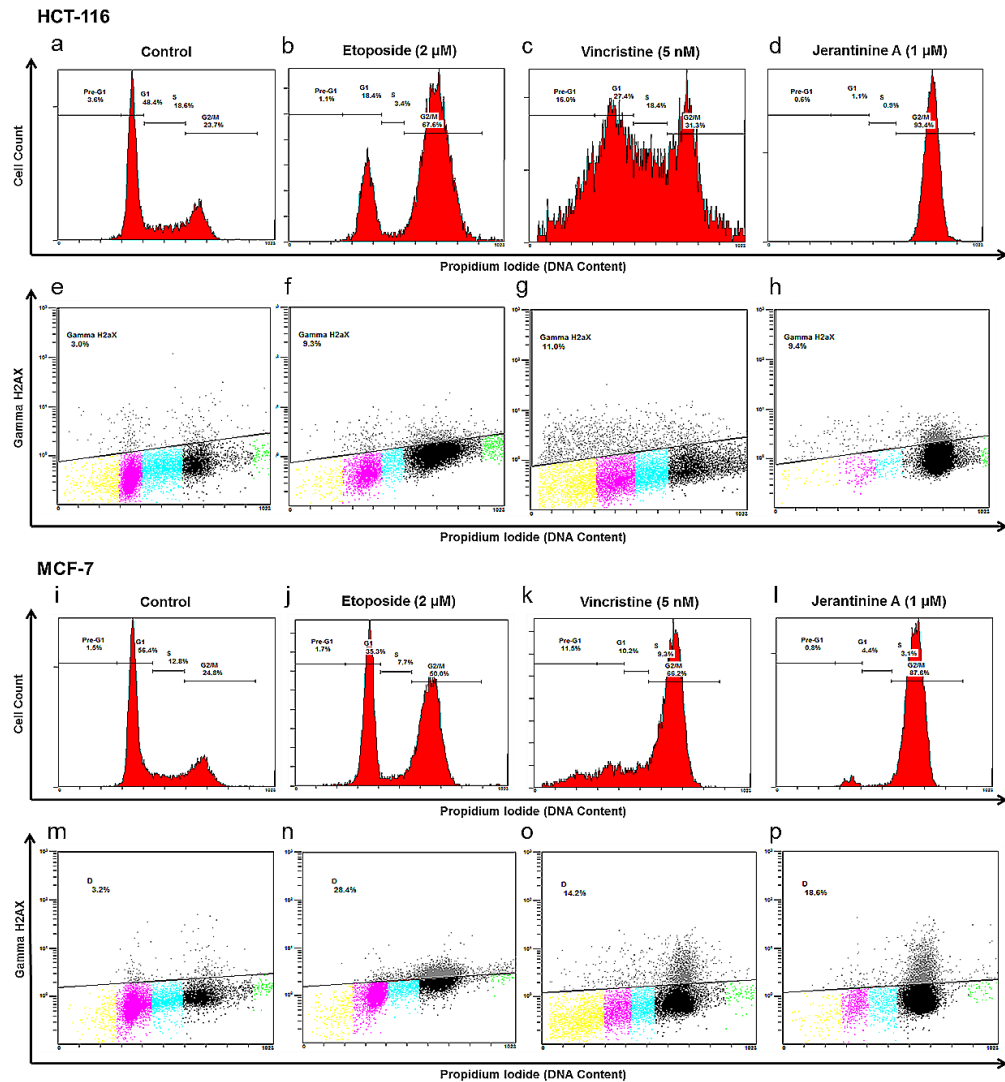
Figure 3.12: Representative cell cycle histograms and γH2AX dot plots from an independent trial illustrating induction of DNA DSBs in HCT-116 and MCF-7 cells after 24 h of JA treatment.

HCT-116 (a, e) and MCF-7 (i, m) controls. Etoposide [2μM; HCT-116 (b, f) and MCF-7 (j, n)] was used on both cell lines as a positive control as it is a known DNA damaging agent. Being a depolymerising agent, vincristine [5 nM; HCT-116 (c, g) and MCF-7 (k, o)] was used as a comparison to JA [1 μM; HCT-116 (d, h) and MCF-7 (l, p)]. Cell cycle and γH2AX were run concurrently which made it possible for simultaneous gating (yellow= Pre-G1 phase; pink= G1 phase; teal= S phase; black= G2/M phase). Experiments were repeated at least 3 times where n=2.

3.2.6 Investigating possible mechanisms by which jerantinine A overcomes vincristine resistance

The use of vincristine in the clinic has been plagued with various forms of resistance in patients, many of which have been reported [179]. One of the earliest forms of resistance identified in association with vincristine, was the increased expression of the Pgp also known as multidrug resistance protein 1 (MDR1) or ATP-binding cassette sub-family B member 1 (ABCB1). Pgp, encoded by the *MDR1* gene, is a member of the ABC transporter family and is implicated in facilitating the efflux of various anticancer drugs, including anthracyclines, epipophyllotoxins, kinase inhibitors, taxanes, and vinca alkaloids, from the cell [180]. It is expressed in only a limited number of tissues with barrier function which include epithelia of the kidney, liver, small and large intestine and capillary endothelial cells in brain, ovary, and the testis [181]. The proposed structure of human Pgp is thought to comprise of two transmembrane (TM) domains, each consisting of six TM segments along with two nucleotide-binding domains (fig. 3.13). Polymorphisms in the *MDR1* gene may affect pharmacokinetics of many commonly used drugs, including anticancer agents [181]. Substrate recognition of drugs takes place at the multiple overlapping binding sites in TM domains. Transferring these substrates from binding sites on Pgp to the extracellular environment is energised by the hydrolysis of two ATP molecules for every molecule of drug transported.

An important part of this investigative study is to identify if Pgp ex-

pression affects the sensitivity of cancer cells in response to JA treatment. Our studies confirm that cells do indeed retain sensitivity to JA regardless of Pgp expression and hence JA is not a substrate of Pgp as shown in fig. 3.14. Results corroborate with those obtained in the MTT assay in Chapter 2 (refer to 2.3). Pgp was clearly not expressed in HCT-116 and MCF-7 cells treated with vehicle alone or JA for all time exposures. In support of these results, there is some evidence suggesting that wildtype p53 usually represses the expression of Pgp, whereas mutant p53 has been shown to activate the Pgp gene promoter [182].
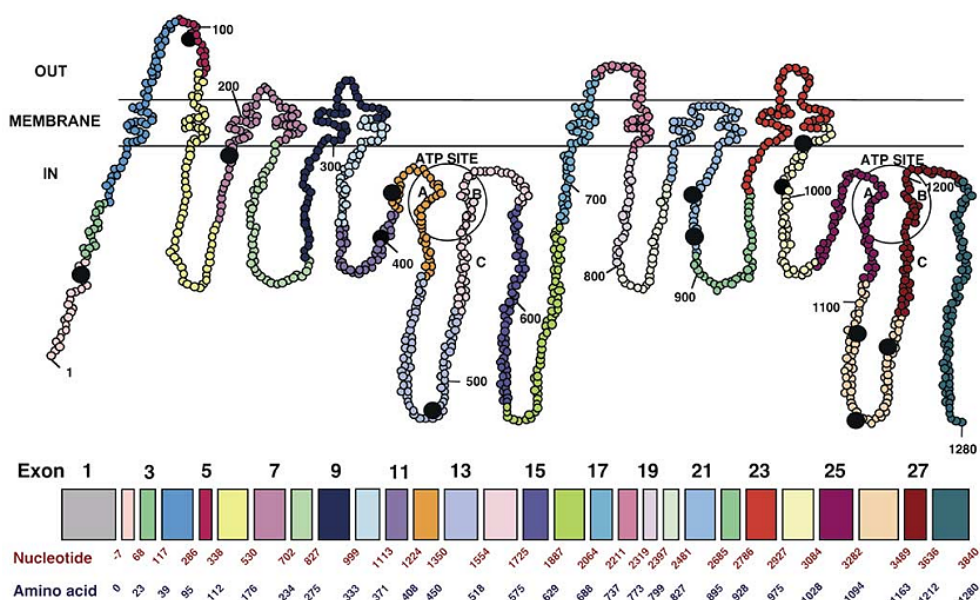
Figure 3.13: Predicted 2-D structural model of Pgp with a schematic representation showing the distribution of single nucleotide polymorphisms of the MDR1 gene.

[181]
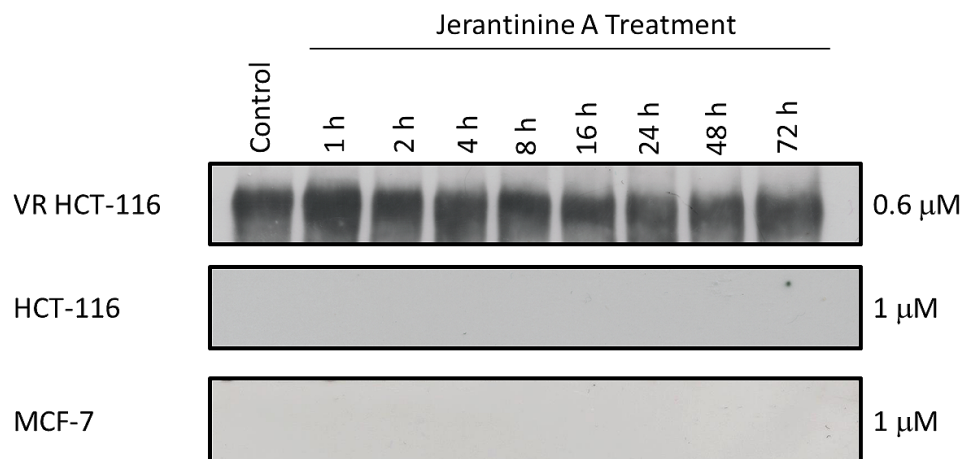
Figure 3.14: V-R HCT-116 cells retain sensitivity to JA despite expressing high levels of Pgp.

V-R HCT-116 that were resistant to 2 μM of vincristine were treated with 0.6 μM of JA for 1, 2, 4, 8, 16, 24, 48, and 72 h. Protein lysates were collected and subsequently used for Western blots to detect expression levels of Pgp. Lysates from HCT-116 and MCF-7 cells were also obtained from samples treated for the aforementioned time exposures. Experiments were repeated at least 3 times on two separate batches of lysates.

Furthermore, our collaborative studies with Dr. Beth Coyle (personal communication) have also shown that the activity of JA in MB cells is not related to Pgp expression using verapamil, an ABCB1 inhibitor, which potentiated vincristine and not JA activity (refer to B.1). Verapamil is a calcium channel blocker developed for the treatment of hypertension. However, ABCB1 inhibitors like verapamil exhibit higher toxicities than chemotherapy alone leading to severe myelosuppression, due to high expression of ABCB1 in bone marrow cells [183]. Additionally, verapamil alone results in cardiac toxicity which prevents its concurrent use with vincristine in the clinic. Therefore, it may be more efficient to find drugs that circumvent ABCB1 rather than inhibiting its function for the treatment of cancer. In this study, medulloblastoma cell lines (DAOY, MED1, and

UW228-3) were treated with vincristine and JA alongside verapamil. As seen in fig. B.1, there was no difference between survival percentages in clonogenic assays between cells treated with JA alone or with both JA and verapamil. Vincristine and verapamil on the other hand did exhibit a synergistic effect resulting in a significant decrease in colony formation.

3.2.6.1 Overcoming resistance *via* production of Reactive Oxygen Species

A few anticancer agents generate Reactive Oxygen Species (ROS) that result in cell death *via* apoptosis. However, prolonged treatment with the same drug has been shown to reduce ROS levels that contribute to the development of drug-resistant cancer cells [184]. Exogenous ROS in conjunction with the same drug resensitises these drug-resistant cells. There is increasing evidence illustrating that apoptosis caused by elevated ROS levels and drug resistance by lack of ROS may very well be one of the principle mechanisms underlying drug resistance and drug sensitivity in cancer cells [184]. Interestingly, ROS levels have also been closely linked to Pgp expression [185]. It was found that both chronic and transient ROS stress upregulated Pgp expression at the RNA, protein, and functional levels, which could be counteracted by antioxidants [186, 187]. In contrast, low levels of ROS downregulated Pgp expression [188]. ROS have also been implicated as mediators of apoptosis by activating different caspases and signalling pathways such as mitogen activated protein kinase (MAPK) pathway, extracellular signal-regulated kinase (ERK) pathway, and phos-

phoinositide 3-kinase(PI3K) signaling pathways among others [185].

Our investigations demonstrated that JA produced significantly higher levels of ROS in V-R HCT-116 cells compared to vincristine treatment (refer to 6.2.12 for methodological details). Vincristine did not generate significant ROS in V-R HCT-116 which corroborates the aforementioned literature (see fig. 3.15). It can be argued that V-R HCT-116 cells do not efficiently retain vincristine within the cell due to expression of Pgp. However, JA still produced higher levels of ROS in comparison to vincristine in naïve HCT-116 cells. JA also evoked significant ROS production in JA-R HCT-116 cells further providing credence to the fact that these cells were not able to develop resistance even though they were maintained and cultured in 2 μM of JA. Interestingly, JA-HCT-116 inherently possessed approximately 2.09 times the ROS levels than V-R HCT-116 cells which may be attributed to possibly different processes involved in metabolism of JA and vincristine within these cells.
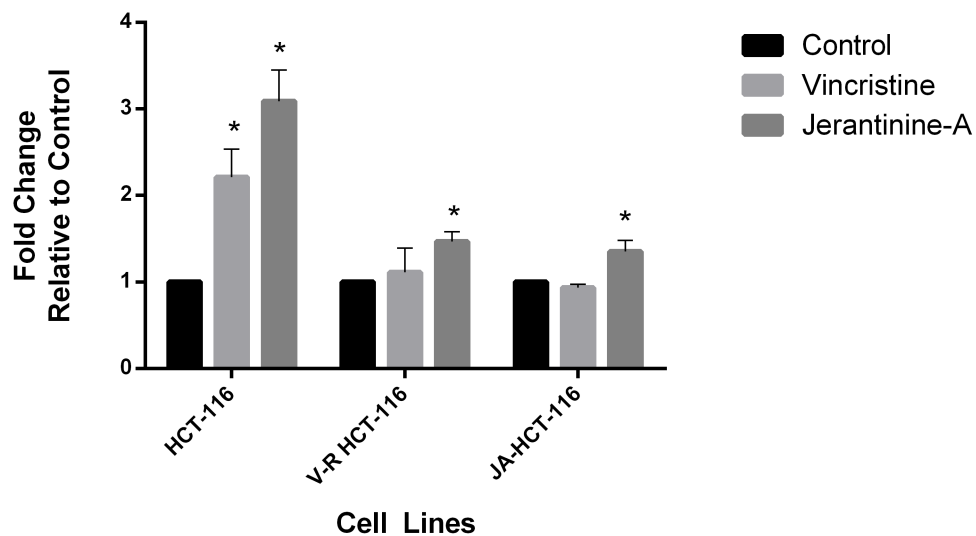
Figure 3.15: JA generated significantly higher ROS levels in V-R HCT-116 cells compared to vincristine.

Vincristine treatment (5 nM) did not generate significant ROS in V-R HCT-116 cells compared to the same treatment in naïve HCT-116 cells. Interestingly, JA generated more ROS than vincristine in naïve HCT-116 cells (1 μM), V-R HCT-116 (0.6 μM), and JA-R HCT-116 cells (1 μM). Experiments were repeated $\geq$2 times where n=2. Two-way ANOVAs were used to compute significance (p<0.05). Refer to 6.2.12 for experimental methodology.

3.2.6.2 Differences in binding sites on microtubules can account for the lack of cross-resistance

As seen below in fig. 3.16, microtubule disrupting agents (MDAs) are capable of binding on multiple sites on microtubules, thus altering their dynamics during mitosis. It is possible that JA binds to a completely different site on microtubules than vincristine despite structural similarities, which may account for the lack of cross-resistance in addition to its enhanced activity in V-R HCT-116 cells.
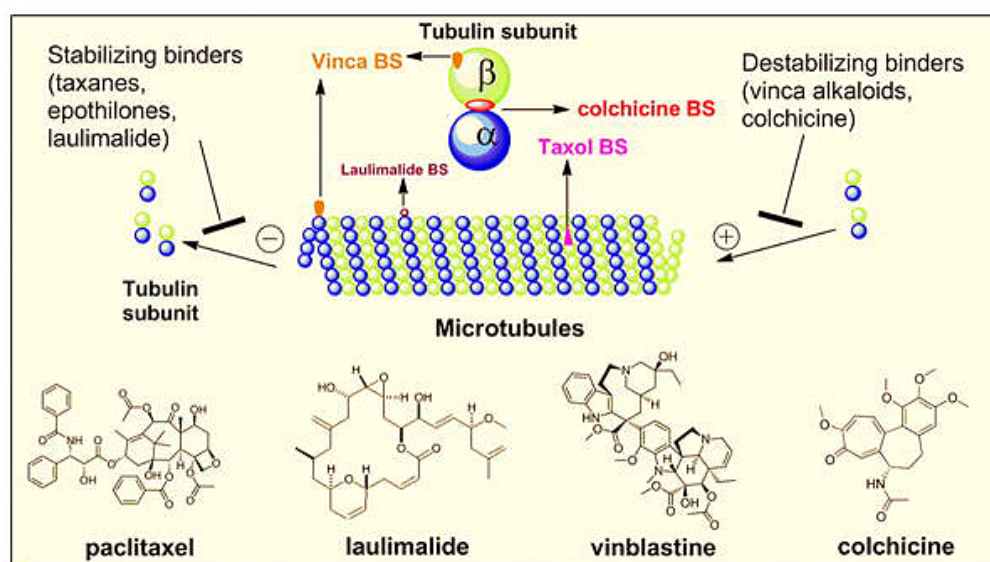
Figure 3.16: Tubulin binding sites of various MDAs.
[189]

Indeed, one of the most important findings to arise towards the end of this investigative study was the identification of the binding site of JBA. With the help of our collaborators at the Paul Scherrer Institute (PSI; Switzerland), we were able to obtain high resolution crystal structures showing that JBA binds to the colchicine site on microtubules as illustrated below in fig. 3.17. Refer to fig. B.2 for more details.
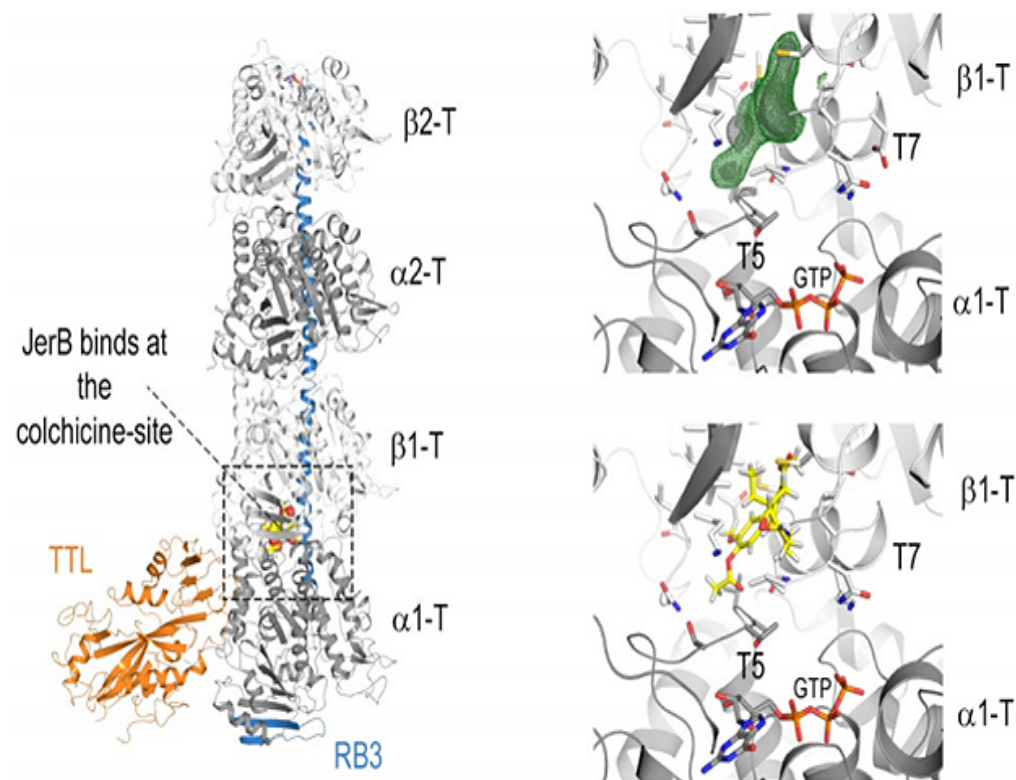
Figure 3.17: 2.4Å crystal structures illustrating that JBA binds to the colchicine site on microtubules. Images were provided by Dr. Michel O. Steinmetz et al. (PSI, Switzerland). Refer to B.2.

Colchicine was initially extracted from the poisonous meadow saffron *Colchicum autumnale L.* and was the first tubulin destabilising agent [189]. Colchicine like vincristine can effectively inhibit mitosis and is thus investigated as an anticancer agent. Unfortunately, due to its low therapeutic window, colchicine is not clinically approved to treat cancer. However, there have been multiple efforts to clinically develop colchicine binding site agents primarily because of their ability to inhibit tumour vasculature and overcome MDR resistance which includes Pgp expression [189]. This is consistent with results showing that Pgp expression and blocking Pgp does not affect activity of JA. It was also reported that colchicine binding site agents are not affected by expression patterns of β-tubulin and still

maintain potent activity against cancer cells.

Interestingly, a recent study involving the total synthesis and biological evaluation of jerantinine E (JE) also matched colchicine as the closest neighbour of JE based on impedance profiling that comprised of 27 other MDAs [190]. The study additionally confirmed JE as a potent inhibitor of tubulin polymerisation [190].

3.3   Conclusion

Cell cycle analyses revealed potent G2/M arrests in A549, HCT-116, HT-29, MCF-7, and MDA-468 cells. These cell cycle profiles were similar to those associated with other MDAs like the taxanes or the vinca alkaloids leading to the hypothesis that JA may target microtubules. Tubulin polymerisation assays were carried out with JA, paclitaxel (microtubule stabilising agent) and nocodazole (microtubule destabilising agent) as controls. Results revealed that JA did indeed inhibit tubulin polymerisation and is thus similar to destabilising agents such as the vinca alkaloids. Visualising microtubule disruption as a consequence of JA treatment using confocal microscopy revealed striking changes in cell morphology with regards to cytoskeletal architecture, membrane blebbing associated with apoptosis, multipolar spindle formation, DNA fragmentation, and aneuploidy, all of which are consistent with data obtained from cell cycle analyses and annexin V apoptosis assays. The integrity of DNA in JA-treated cells was also investigated by carrying out flow cytometric assessments of phosphorylated γH2AX levels in HCT-116 and MCF-7 cells. Results revealed significant increases in phosphorylated-γH2AX indicative of DNA DSBs. This corroborates confocal images that show some DNA fragmentation. PLKs and AURKs (A, B, C) are both integral to the mitotic process and inhibition of these kinases have been reported to result in many of the characteristics observed in the above studies. Furthermore, studies have shown that PLK1 serves as an important prognostic factor in cancers such as medul-

loblastomas. Our collaborative studies illustrated that JA was more active against a high expressing PLK1 cell line like DAOY. Hence, it was necessary to identify if JA has an affinity to PLK1 as well AURKs. Data obtained from this kinase screen revealed dose-dependent inhibition of PLK1 activity in the presence of JA. Aurora kinase B was only slightly, but significantly inhibited at low concentrations of JA. Initial cell viability studies clearly demonstrated potent growth inhibitory activities of JA in V-R HCT-116 cells. Hence, a more detailed investigation that probed mechanisms of resistance was carried out. Pgp expression has played a huge role in drug resistance faced in the clinic, especially seen in cases that involve vincristine-resistance. However, this does not appear to hinder the activity of JA as our data illustrates that Pgp expression in V-R HCT-116 cells remain unchanged for all treatment exposures. Increased levels of ROS have also contributed to mechanisms driving evolution of acquired resistance - through upregulation of many enzymes responsible for neutralising ROS. Indeed, ROS levels were higher in cells treated with JA compared to vincristine. JA-HCT-116 cells also inherently possessed 2.09 times the levels of ROS than V-R HCT-116 cells which may indicate differences in the way that these agents are metabolised in cells. Based on previous literature and crystal structures provided by our collaborators, one of the most important findings in this study was determining with a degree of confidence that the jerantinine family binds to the colchicine site on microtubules. This could explain why V-R HCT-116 cells are more sensitive to JA as it binds to a different site than vincristine.

Chapter 4

Genomic and Proteomic Studies in Cells Treated with Jerantinine A

4.1 Introduction

Investigating signal transduction pathways associated with JA's mechanism(s) of action through the use of genomics and proteomics can help elucidate key biological processes involved in evoking a growth inhibitory response. Both genomics and proteomics studies were conducted on the premise of corroborating phenotypes made evident in chapters 2 and 3. An additional aim within this chapter was identification and biological validation of genes that are needed for cell sensitivity towards JA. For this study, a genome-wide RNAi screen was carried out in collaboration with colleagues at the International Medical University (Malaysia). RNAi loss of function screening using complex lentiviral-based short hairpin RNAs (shRNA) expression libraries provides a unique and powerful approach to identify genes required for defined cell responses in a single assay. The pooled genome-wide shRNA libraries contain approximately 80,000 shRNA

constructs targeting 15,000+ genes. The pooled virus is added to the cell population at a predetermined multiplicity of infection (ratio of virus to the ratio of target cells within a defined space). Cells are then incubated and exposed to a selective pressure such as the test agent and selected based on desired phenotype or flow sorting. After selection, cells are then isolated and the integrated shRNA constructs are identified *via* "Next Generation" sequencing. The identification of potential "hits" can then be used to develop hypotheses regarding biological role(s) of the corresponding gene(s).

To identify genes functionally required for cell sensitivity to a treatment or compound, the most straightforward approach is to conduct a RNAi rescue screen, where the selection is a treatment, such as a drug, that kills almost all cells and is applied to a population that is infected with a heterogeneous lentiviral shRNA expression library. Briefly, the process first involves infecting cells (MCF-7) with this library, and then treating them with the test agent (JA) at a concentration that under normal conditions kills virtually 100% of cells, then determining which shRNA are present in the surviving cell population. Presumably, the genes targeted by the shRNA in the surviving cell population are essential for eliciting the killing response caused by the compound, factor, or small molecule since silencing the gene prevents the cell-death signal from propagating. Thus, analysis of the "rescued" survivors indicates which genes are necessary for lethal activity of the compound or factor.

The second section in this chapter explores temporal changes in protein expression of cells after an 8 h, 16 h, and 24 h exposure to JA using

Multidimensional Protein Identification Technology (MudPIT). This technique combines 2-dimensional (2D) liquid chromatography with tandem mass spectrometry. The figure below summarises the workflow associated with this technique.
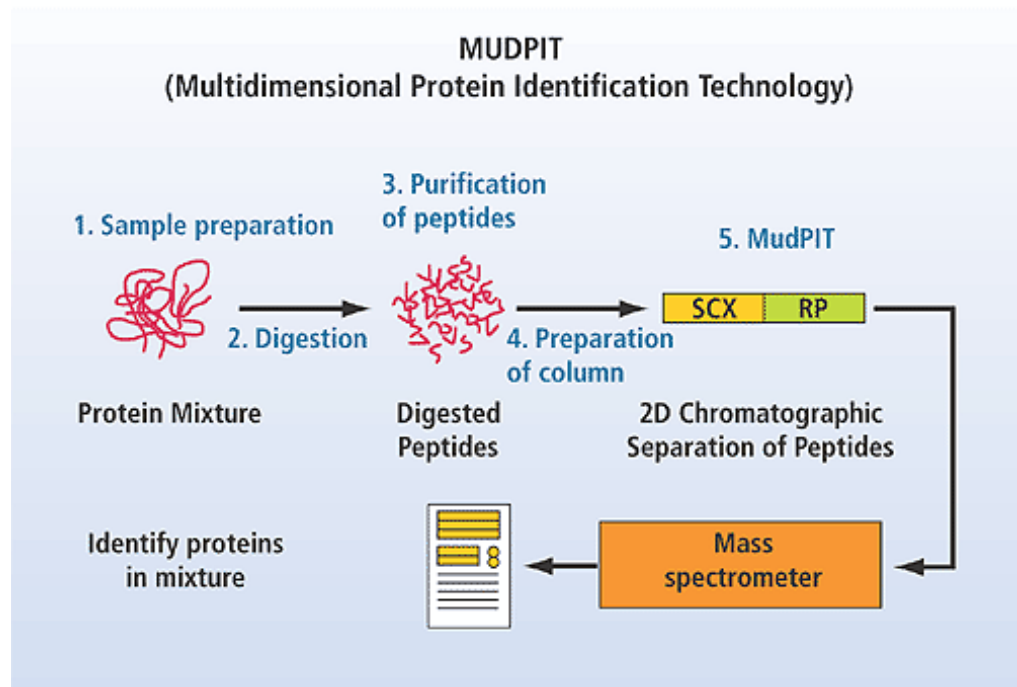
Figure 4.1: General illustration showing the workflow for MudPIT.

Proteins are extracted from samples, prepared, and digested into constituent peptides which are then subjected to separation *via* 2D liquid chromatography and analysed *via* tandem mass spectrometry. SCX=strong cationic exchange; RP=reversed-phase [191].

MudPIT specifically combines both strong cation exchange (SCX) prefractionations and reverse phase high-performance liquid chromatography (RP-HPLC). The SCX resin initially binds all peptides before they pass through to the octadecyl carbon chain (C18) bonded silica material which is frequently used in reversed-phase chromatography. As seen in the above figure, the SCX resin and C18 material are packed in tandem. Peptides

are eluted in a stepwise manner using ammonium salts starting with low concentrations and ending with high concentrations. This is followed by a cycle of organic gradients that are used to elute the peptides from the C18 and into the mass spectrometer for sequencing. Spectra are then generated and uploaded into databases that match peptide sequences to their corresponding protein (refer to 6.2.13 for more details).

4.2   Results and Discussion

4.2.1   Genome-wide RNAi screen in MCF-7 cells

Upon generating a stable pool of MCF-7 cells that were transduced with the shRNA library, cells were treated with JA for 72 h. As seen in fig.4.2, JA induced significant morphological changes in MCF-7 cells transduced with non-targeting shRNA, similar to changes observed in parental MCF-7 cells. However, cells transduced with the genome-wide shRNAs were more resistant to JA based on morphological characteristics. Genomic DNA was obtained from these samples, amplified *via* polymererase chain reaction (PCR), and lastly subjected to high throughput sequencing. The sequences were then queried against The RNAi Consortium shRNA Library (TRC) to identify targets with corresponding shRNA sequence(s) that match the sequencing data. Analyses of data revealed 381 candidate genes mediating sensitisation and 121 genes mediating resistance to JA and are listed in tables 4.1 and 4.2 (refer to appendix C.1 for more details on data analysis).
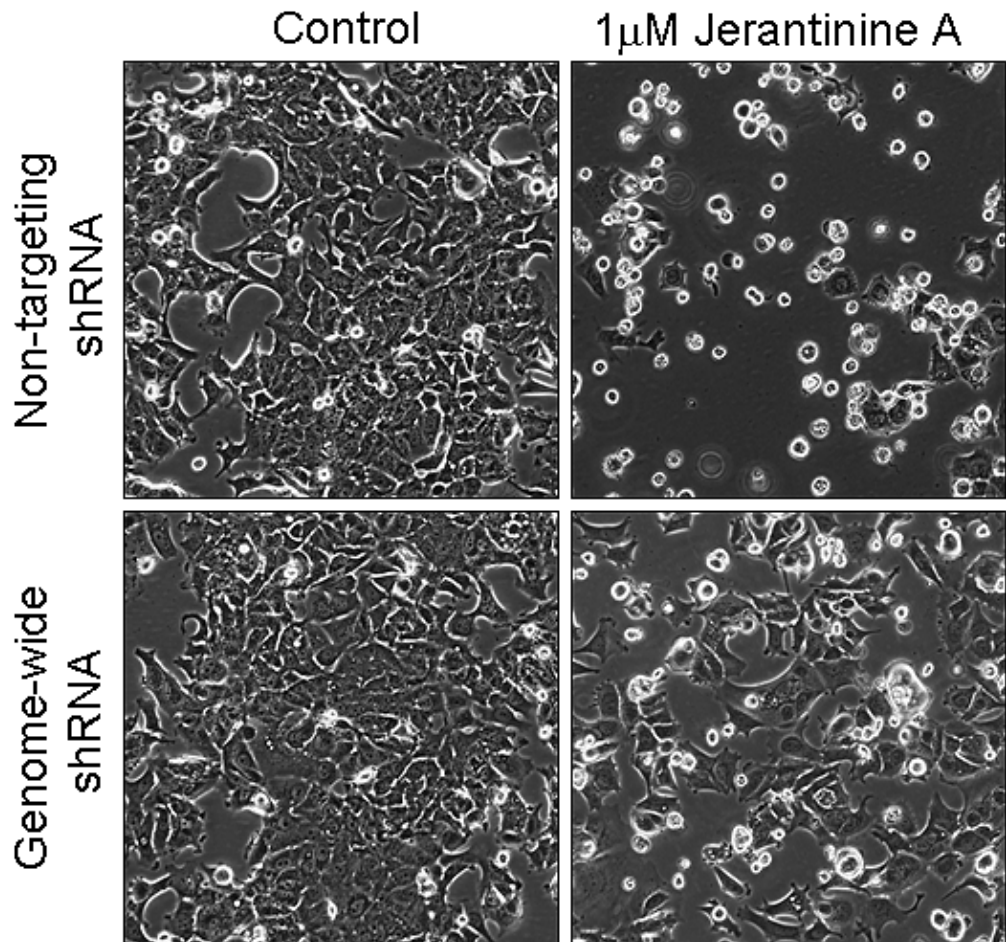
Figure 4.2: MCF-7 transduced with a pooled genome-wide shRNA confers resistance to JA.

MCF-7 cells transduced with a non-targeting shRNA (Top) or a pooled genome-wide shRNA (Bottom) were treatedwith 1μM of JA for 72h and their morphological changes observed using inverted light microscopy. Note that some of the cells transduced with genome-wide shRNA were resistant to JA compared to the non-targeting control cells which retained sensitivity to JA. Images were provided in collaboration with Dr. Chee-Onn Leong (IMU, Malaysia).

A1CF	CPSF3	GRSF1	MARK1	PCBP3	RCOR3	SNIP1	USP54
ABCB9	CSNK1G1	GSG2	MARK3	PCCA	RDH11	SNRNP40	USP6
ABCC1	CSNK2A1	GSK3B	MASTL	PCCB	RDH5	SNRPA	VANGL1
ABP1	CTNNB1	GSPT1	MBIP	PDE5A	REL	SNRPD2	VPS29
ACAD9	CWC22	GSTA3	MCCC1	PDHA2	REXO1	SNRPD3	WBP11
ACIN1	CYTL1	GUCY1B2	MCCC2	PDILT	RIC8B	SNRPE	WDR33
ACMSD	DDR2	HADHB	MCTP1	PGD	RNF180	SNRPF	WNK2
ACY1	DDX17	HAT1	MCTP2	PGK1	ROCK1	SNRPG	WNK3
ADC	DDX6	HMGCS1	ME1	PGR	RPE	SNW1	WSB2
ADCK1	DERA	HNRNPA3	ME2	PHF5A	RPL12	SRRT	XAB2
ADH4	DISC1	HNRNPH3	MELK	PIK3C2A	RPL13	STK31	ZC3HC1
ADH6	DLST	HNRNPUL1	MET	PIK3C2B	RPL18A	STK33	ZFC3H1
AGMAT	DNAJC17	HSD17B7	MFSD11	PIM2	RPL21	STRADB	ZIM2
AK4	DSPP	HSPA1L	MICALL1	PLCB2	RPL22	SUGP1	ZNF10
AKAP11	DUOX1	HUNK	MKI67IP	PLCG2	RPL23A	SUZ12	ZNF331
ALDH1A3	DUSP19	IFT46	MMP27	PLCL1	RPL39	SYT16	ZNF568
ALDH3A1	DYRK1B	IGF2BP3	MSH5	PLCL2	RPL4	SYTL5	ZNF658
ALDH3A2	EEF2K	IL1F8	MST1R	PLCXD2	RPL5	TAAR8	
AMD1	EFHA1	IL31	MST4	PLCZ1	RPLP0	TAF1	
ANKRD40	EFTUD2	INSRR	MTHFD2L	PLOD3	RPS10	TALDO1	
ANO6	EGR2	IRAK4	MXRA8	PLXNC1	RPS11	TAOK1	
AP1S2	EIF2AK3	IRS1	MYO3A	PPAT	RPS17	TARS2	
AQR	EIF2S2	ITCH	NAA15	PPM1J	RPS18	TAS1R2	
ARHGEF25	EIF3I	ITGB3	NAA38	PRCC	RPS25	TAS2R19	
ATF7IP2	EIF4A3	JAK1	NCOR1	PRKAA2	RPS27	TBX5	
BLMH	EMP1	JMJD7-PLA2G4B	NDST2	PRKACB	RPS3A	TCEB1	
BRDT	EPHA6	KAT2A	NDUFA4	PRKAR1B	RPS4X	TEK	
C11orf46	ERI2	KDM6A	NDUFAF1	PRKCG	RPS4Y1	TENC1	
C19orf43	EXT1	KHDRBS1	NDUFB6	PRLR	RPS4Y2	TET1	
C1orf55	FADD	KIAA1429	NDUFB9	PRMT3	RPS6KA4	THOC5	
C20orf158	FAM122B	KIAA1958	NEK1	PRODH2	RPS6KC1	TIA1	
C9orf11	FAM26D	KIF16B	NEK10	PROM1	RPS7	TJP2	
CALR3	FAM32A	KLK5	NINL	PRPF3	RPS8	TKT	
CAMKK2	FAM81A	KLKB1	NNT	PRPF4	RSL24D1	TKTL1	
CAP2	FASTK	KRT23	NPR1	PRPF6	RWDD3	TLK1	
CCDC68	FER	LACTB	NR3C2	PSAP	RYK	TMEM20	
CCR2	FGF5	LDHAL6B	NT5C2	PSIP1	SAFB2	TNNI3K	
CDC42BPA	FGFR2	LOC391513	NTF3	PTGR2	SAT1	TP53BP1	
CDC7	FIP1L1	LOC401313	NTRK2	PTK6	SCYL3	TRAF6	
CDK15	FLJ16124	LOC402677	NTRK3	RAB9B	SEC14L1	TSPAN1	
CDKL4	FYCO1	LRP6	ODC1	RAC1	SF3B1	TTBK1	
CDS2	GABRA6	LRRK2	OR10X1	RAF1	SF3B3	TUBB	
CELF2	GAD1	LSM11	P4HA2	RALA	SF3B5	TYK2	
CELF4	GAD2	LSM5	P4HA3	RALYL	SGK2	UGT8	
CENPA	GAPDH	LSM6	PABPC1	RASA2	SGK3	UHMK1	
CHDH	GLS	MAOA	PABPC4	RASSF3	SIK2	UNC13B	
CLK1	GLS2	MAP3K1	PAK1	RASSF6	SLC16A6	UROD	
CMPK1	GLUD1	MAP3K7	PAK3	RBL1	SLC1A5	USP11	
COL4A3BP	GLUD2	MAP4K2	PAN3	RBM10	SLC5A9	USP17L6P	
COPS2	GPATCH1	MAP4K5	PAPOLG	RBM12	SMPDL3B	USP38	
CPM	GPD2	MAPK10	PC	RBM15	SMS	USP47	
CPSF2	GPR113	MAPKAPK2	PCBP2	RBM8A	SMU1	USP50	

Table 4.2: List of resistance-causing genes (these genes when knocked-down confer sensitivity to JA)

ABCD3	CYP51A1	KRTAP10-6	PDE1C	SRPX
AGXT2L1	DECR1	LAPTM5	PES1	SSX7
ARHGAP15	DOPEY2	LCT	PIGU	SSX9
ATG4A	DUSP27	LEP	PLEKHA5	STX7
ATG4C	E2F6	LGSN	PPFIA2	TACR1
ATP9B	ENTPD2	LHPP	RAB36	TAS2R42
ATRNL1	EPB41L4B	LIG1	RAB39B	TFG
ATXN7	FAM169B	LOC401198	RASGRP3	TMEM120A
BTG3	FEZ2	LRP10	RHOBTB2	TNFRSF11B
BTG4	GALT	M6PR	RNF150	TOM1L2
C10orf12	GDF5	MAN2B2	ROBO1	TRIT1
C16orf5	GFRA1	METAP1	RUFY3	UBE2E4P
C1orf124	GK	MEX3B	SAMD9	UBLCP1
C3orf19	GMNN	MOCS3	SDHDP7	VPS36
C4orf43	GPR174	MSN	SERPIND1	WDR45L
C6orf10	GPS2	NAMPT	SH2B3	WFDC3
CCNT2	GRIK3	NCRNA00288	SLC16A14	WIF1
CD40	H1FOO	NKX3-1	SLC17A8	ZFP42
CDH20	HDHD2	NOS3	SLC2A2	ZNF441
CHD9	HOXA11	NPHP3	SLC4A5	ZNF510
CIR1	HUS1	NPSR1	SMARCA1	ZNF620
CLCA4	IL1B	NRL	SMOC1	
CLPTM1	IL1F5	OR51D1	SOS2	
CREB3L2	IMPDH2	P2RX1	SPINK14	
CXADR	ITPR2	PDE12	SREBF2	

4.2.1.1   shRNA target validation in MCF-7 and MDA-468 cells treated with JA

We chose to select a suitable candidate based on characteristics of JA treatment made evident in chapters 2 and 3 and was additionally present on the list of genes that when knocked down would confer resistance to JA. Pathway analyses from DAVID (Database for Annotation, Visualisation and Integrated Discovery) led to multiple hits in various pathways, however, the MAPK and Toll-like receptor pathways had several components that were identified in this shRNA screen as seen below in fig.4.3. C-Jun-N-terminal

kinase (JNK) is integral to both pathways and was thus selected as an ideal candidate for target validation. JNKs belong to the MAPK family and are involved in important physiological processes such as stress responses, inflammation, apoptosis, cell proliferation, differentiation, and survival. For the purposes of this study, we chose to knockdown JNK1/JNK2 in MCF-7 and MDA-468 cells, treat them with JA, and assess growth inhibition using the MTT assay. Interestingly, studies have shown that inhibiting JNK2 and subsequent treatments with cytoskeletal-interfering substances such as colchicine or taxol can actually promote tumour cell growth while simultaneously inducing apoptosis even under the influence of the same stimulus [192]. Microtubule-interfering agents such as paclitaxel, docetaxel, vinblastine, vincristine, nocodazole, and colchicine have all been reported to activate proteins such as RAS and apoptosis signal-regulating kinase 1 (ASK-1) which in turn activate JNK/stress-activated protein kinase (SAPK) [193]. The JNK pathway is also intriguingly tied to ROS production. Studies have shown that activation of JNK in conjunction with ROS production in breast cancer is capable of inducing apoptosis *via* the mitochondrial/caspase pathway [194]. It could therefore be hypothesised that ROS production and concurrent activation in the JNK pathway may mediate apoptosis to some extent in cells treated with JA.

Figure 4.3: Pathway analyses using DAVID revealed possible involvement of the JNK pathway in conferring sensitivity to JA.

JNK is an integral component that is shared between the MAPK and Toll-like receptor pathways identified by DAVID and was therefore selected for subsequent target validation studies.

Results obtained from experiments conducted in collaboration with Dr. Chee-Onn Leong revealed that knockdown of JNK1(M1a/M9 shRNA variants) and JNK 2 (J21/J22 shRNA variants) in MCF-7 and MDA-468 cells did indeed confer some resistance to JA when compared to vector controls (pLKO) suggesting that the JNK pathway may play a role in mediating sensitivity of these cell lines to JA (refer to figs. C.3 and C.4). Mean IC_{50} values are tabulated below (see tables 4.3 and 4.4). Blots confirming knock down are illustrated in fig. C.2.

Table 4.3: Mean IC_{50} values of MCF-7 cells transduced with JNK1/2 shRNA variants and subsequently treated with JA $1\mu M$ for 72 h.

MCF-7

	pLKO	M1A	M9	J21	J22
Log IC_{50}	3.865	3.881	4.406	4.15	5.801
IC_{50} (nM)	7320	7602	>10000	>10000	>10000

Mean IC_{50} values were obtained from at least 2 independent trials where n >4. Experiments were done in collaboration with Dr.Chee-Onn Leong (IMU, Malaysia).

Table 4.4: Mean IC_{50} values of MDA-468 cells transduced with JNK1/2 shRNA variants and subsequently treated with JA $1\mu M$ for 72 h.

MDA-468

	pLKO	M1A	M9	J21	J22
Log IC_{50}	3.079	3.529	3.399	3.155	3.038
IC_{50} (nM)	1199	3377	2509	1429	1091

Mean IC_{50} values were obtained from at least 2 independent trials where n >4. Experiments were done in collaboration with Dr.Chee-Onn Leong (IMU, Malaysia).

4.2.2 Proteome profiling in JA-treated MCF-7 cells

Examining temporal changes in protein expression may help elucidate other mechanisms that contribute to the apoptotic destiny of cells treated with JA (1μM). We chose to look at protein expression in MCF-7 cells treated with vehicle (medium) alone in conjunction with cells treated with JA for 8 h, 16 h, and 24 h. Protein samples were collected and prepared in the manner described in 6.2.13. Each of the 4 treatment samples were subjected to 6 SCX fractions which would allow for greater depth in the identification of protein groups. Figures. 4.4 and 4.5 were compiled from the entire dataset obtained which showed that proteins affecting cytoskeletal architecture and cell cycle were among the top 25 upregulated and downregulated biological processes. The wealth of data obtained from these proteomic profiles can be overwhelming and as such we chose to validate hits based on biological processes that resembled the phenotype of JA-treated cells as demonstrated in previous experiments; i.e. cell cycle perturbations and confocal images showing abnormal changes in cytoskeletal architecture. First and foremost, filtering data and ranking proteins by fold change and trends (high to low R^2 values) in temporal protein expression for all four samples may help unravel mechanisms more closely linked to biological processes affected by JA treatment. Data were therefore clustered into five categories: proteins that were expressed exclusively in the control (control >8 h $= 16$ h $= 24$ h $= 0$; see 4.6), proteins that were not present in the control, but gradually increased over time (control $= 0 <8$ h <16 h <24 h; see fig.4.7), proteins present in the control that increased over time (control <8 h <16

h <24 h; see fig.4.8), proteins present in the control that decreased over time (control >8 h >16 h >24 h), and lastly proteins that decreased to a fold change of 0 by 24 h (control >8 h >16 h >24 h = 0). Information in all GO figures were obtained from DAVID, a bioinformatics tool which is available online [195]. Some common terms that appeared across all applied filters were RNA splicing, RNA processing, protein transport and localisation, and more importantly the cytoskeleton, which corroborates images from confocal microscopy studies. As seen from the progression of applied filtering parameters, we were finally able to attain enriched terms covering biological processes such as those pertaining to microtubules and spindle organisation, which are relevant to JA's mechanism of action and its primary target.
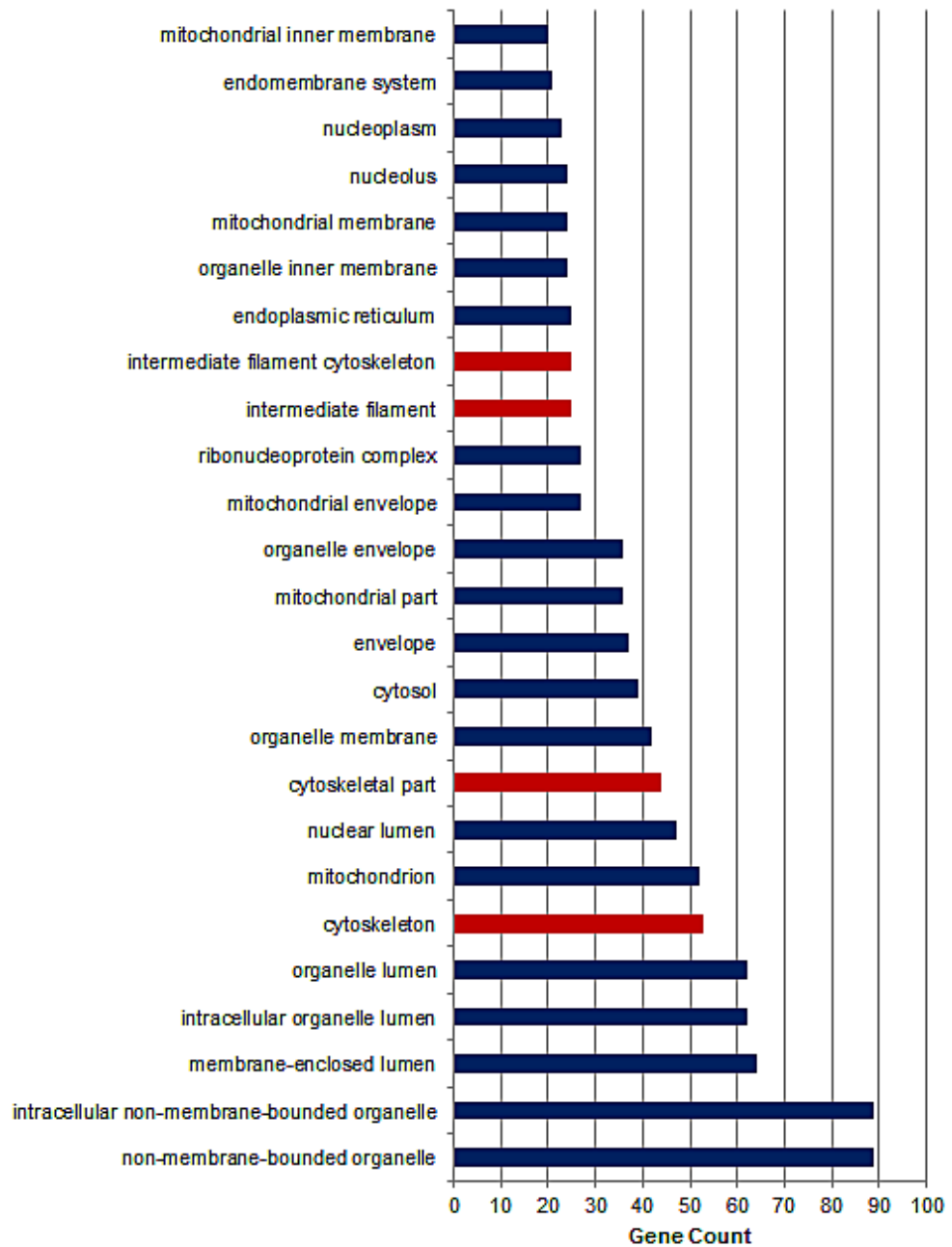
Figure 4.4: Top 25 enriched gene ontology (GO) terms from the entire dataset representing upregulated biological processes in MCF-7 cells as a consequence of JA treatment (1 μM).

Upregulation in biological processes involving components of the cytoskeleton corroborates data obtained from confocal microscopy showing dramatic changes in cell morphology. It is possible that cells increase proteins that maintain the cytoskeleton in an effort to oppose the effects exerted by JA. Bars in red represent processes associated with JA.
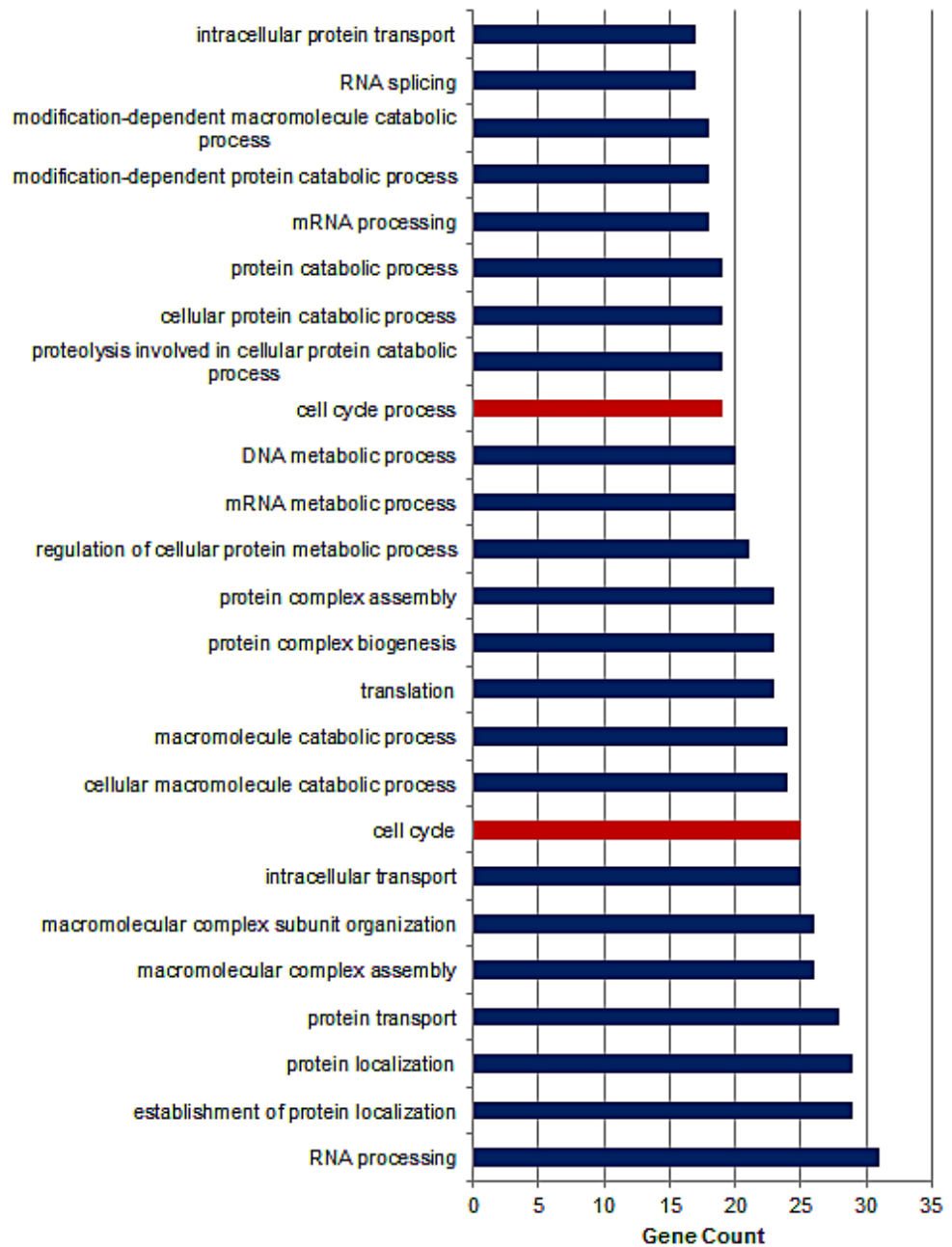
Figure 4.5: Top 25 enriched GO terms from the entire dataset representing downregulated biological processes in MCF-7 cells as a consequence of JA treatment (1 μM).

mRNA splicing, protein transport/localisation, and cell cycle were among the the list of downregulated biological processes. Decreased expression in proteins that facilitate the cell cycle were prioritised for further validation.
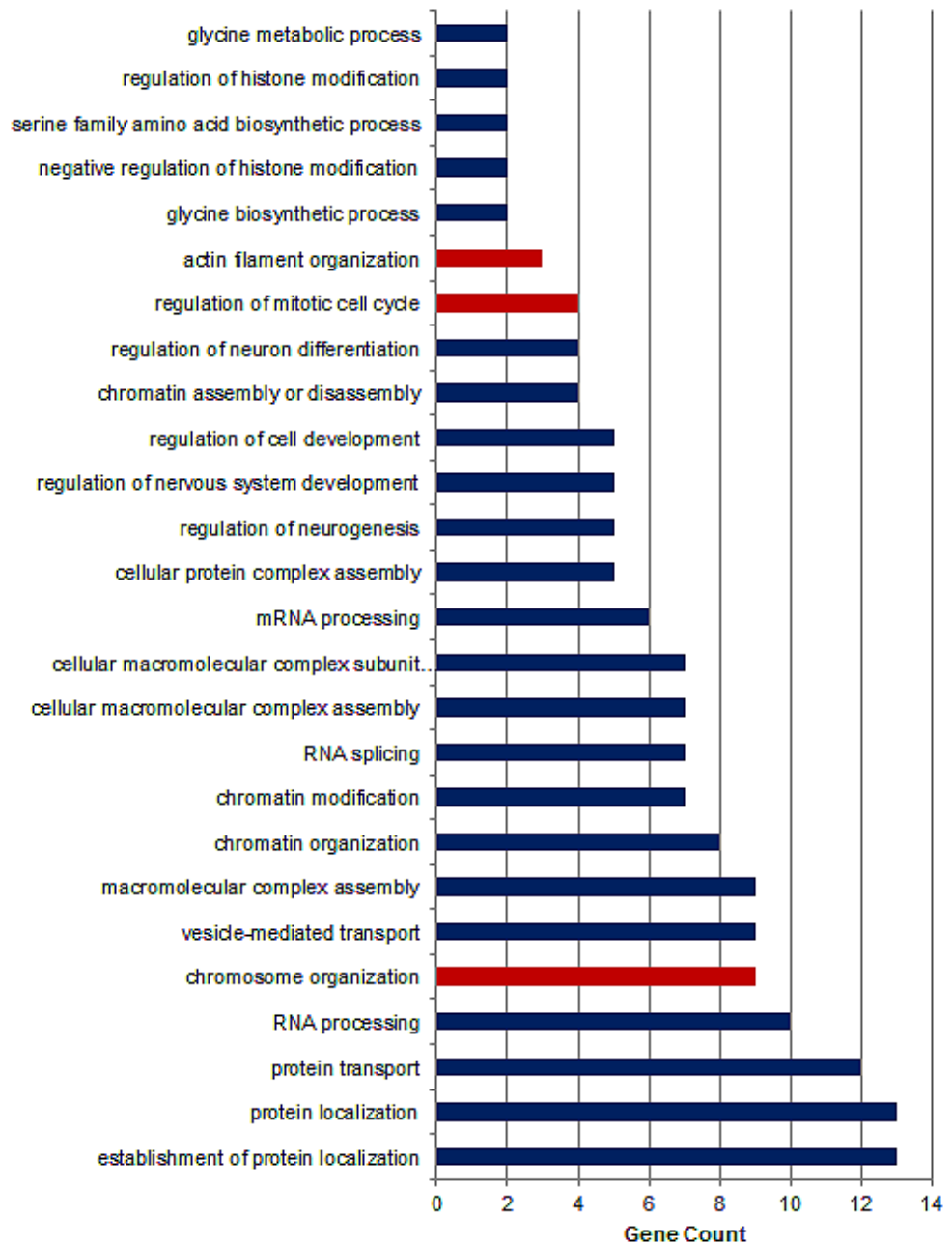
Figure 4.6: GO terms representative of biological processes comprising of proteins present exclusively in the control and absent in treatment samples (control >8 h = 16 h = 24 h = 0).

Proteins involved in chromosome organisation were among the top hits in this category. As seen in fig.3.8, chromosome misalignment due to microtubule disruption caused by JA, does indeed correspond with this set of filtered data. Proteins involved in RNA processing/splicing and protein transport and localisation were also among the most downregulated biological processes.
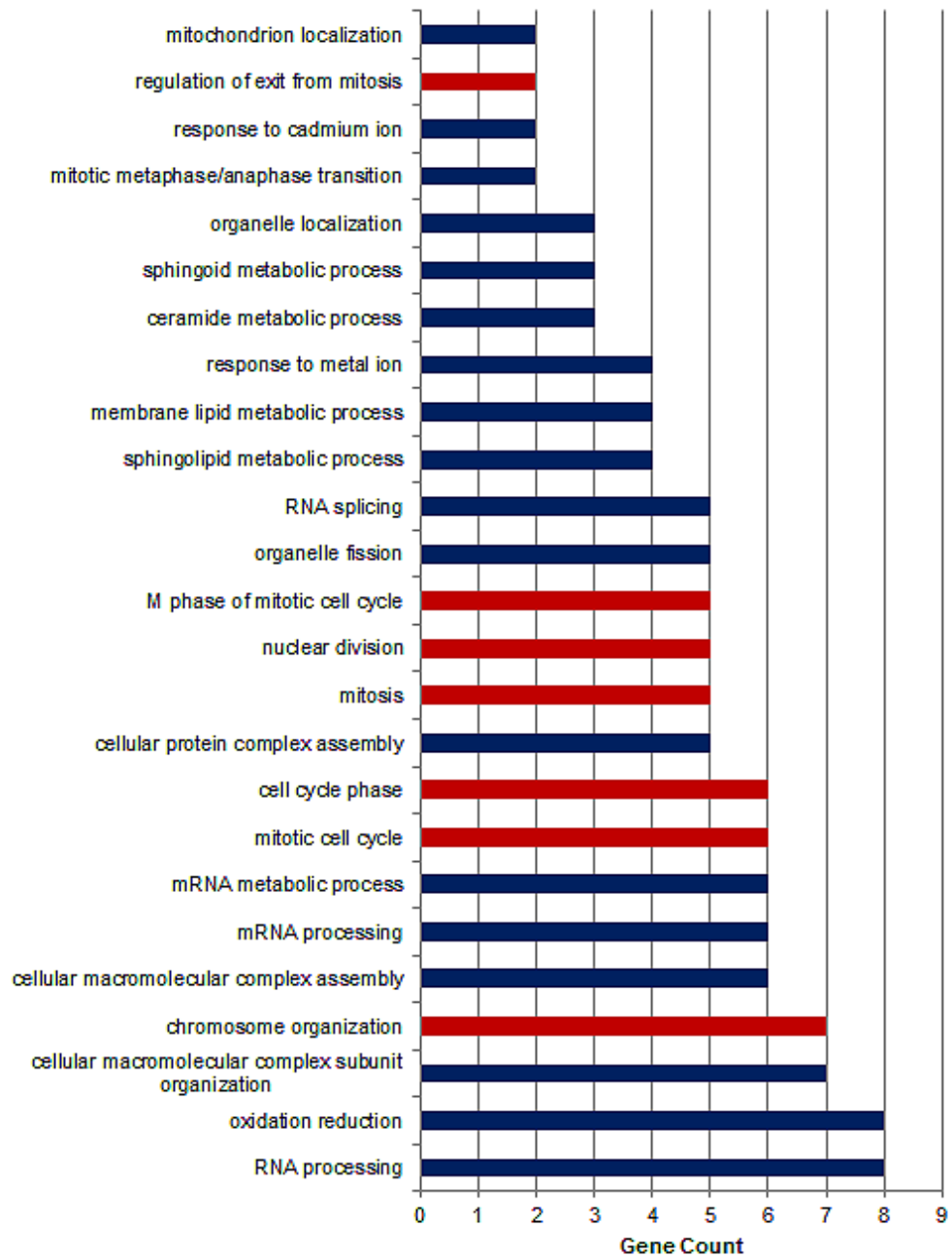
Figure 4.7: GO terms representative of biological processes comprising proteins absent in the control but increase in a time-dependent manner (control = 0 <8 h <16 h <24 h).

Increased gene counts in biological processes pertaining to cell cycle and mitosis were even more evident in this filter. RNA processing and splicing were also among upregulated processes.
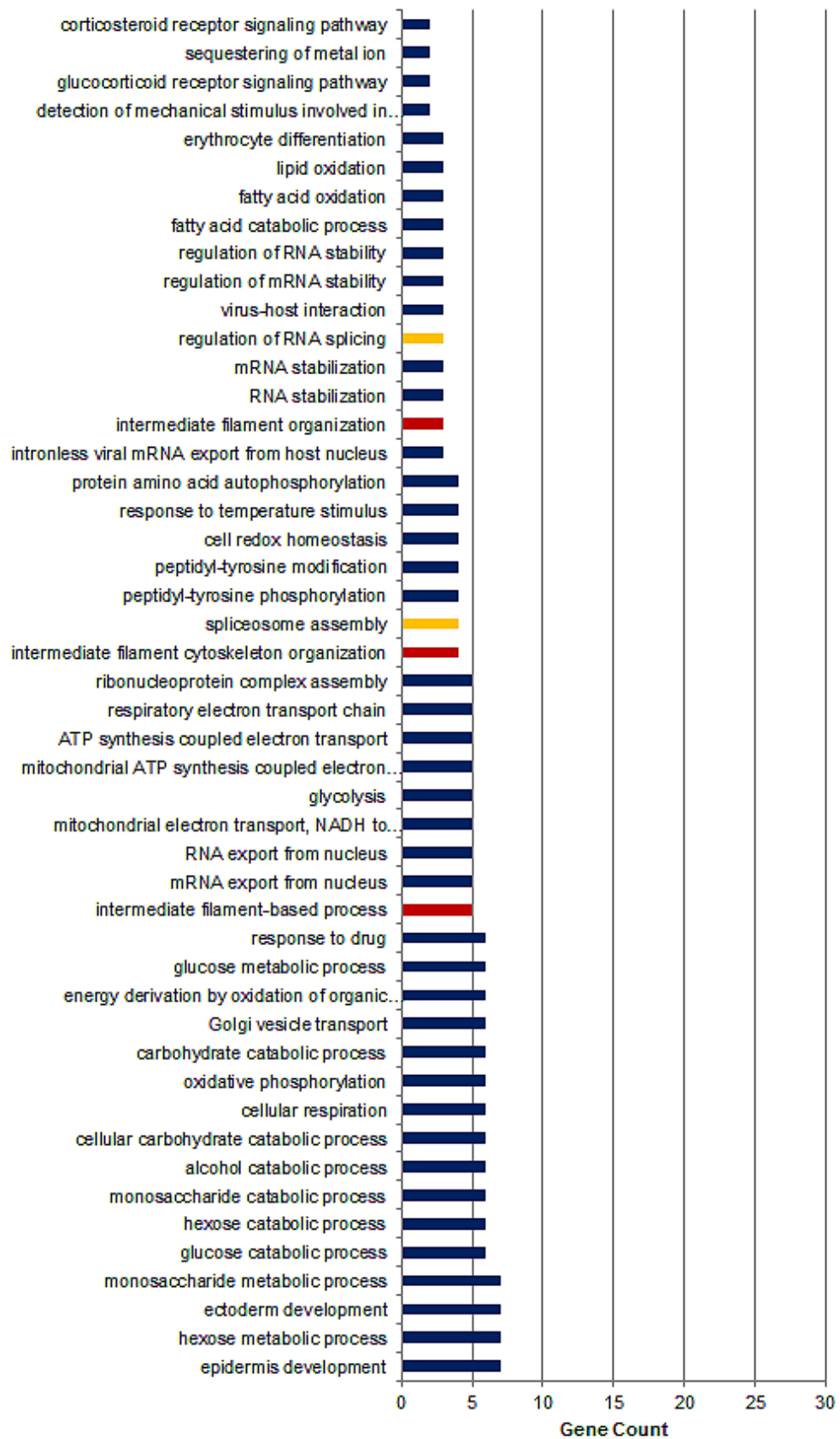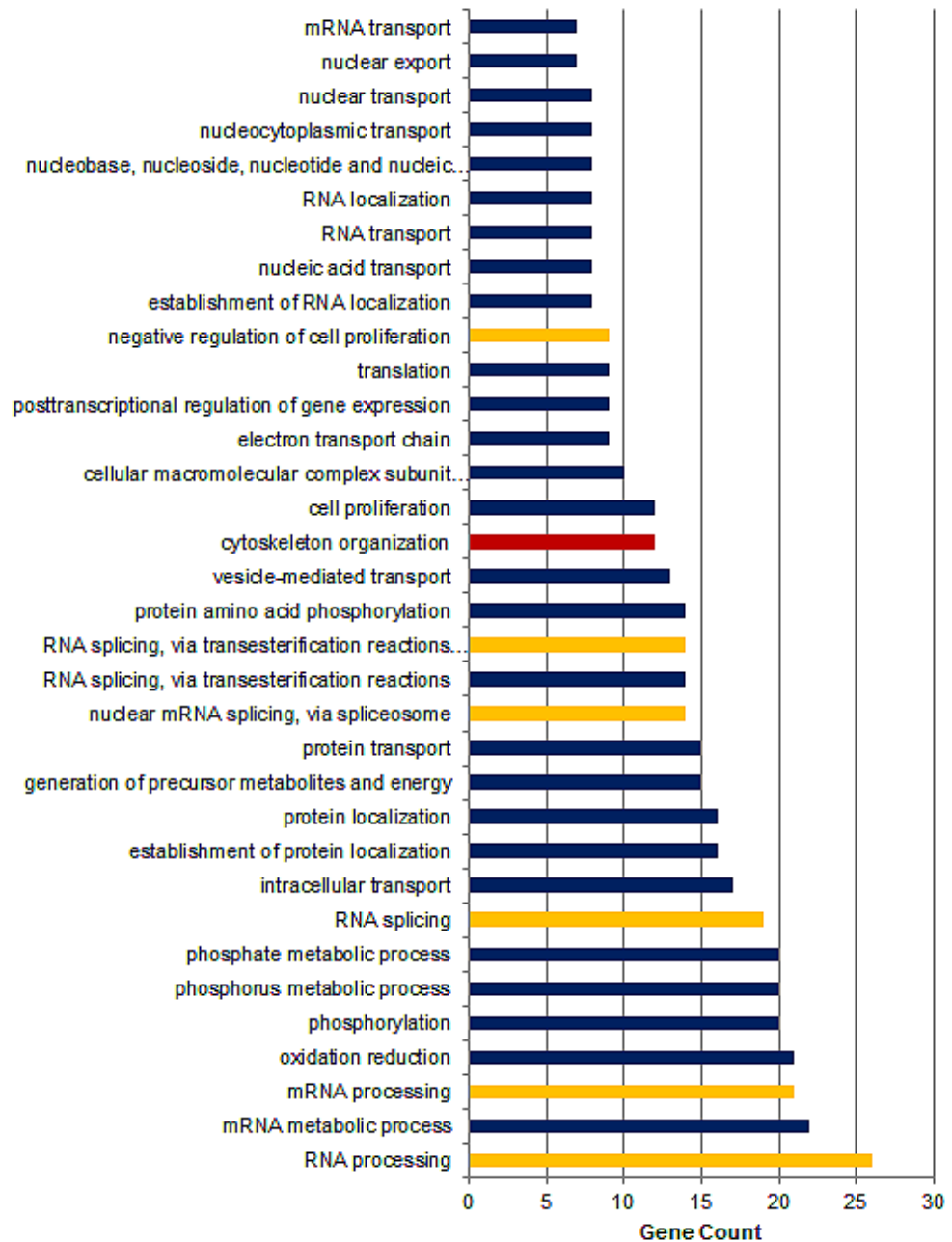
Figure 4.8: GO terms representative of biological processes comprising proteins present in the control that increase in a time-dependent manner (control <8 h <16 h <24 h).

Biological processes pertaining to the cytoskeleton (red bars) were not particularly prevalent in this filter. However, RNA processing and splicing (yellow bars) had higher gene counts and were more prevalent at this level.
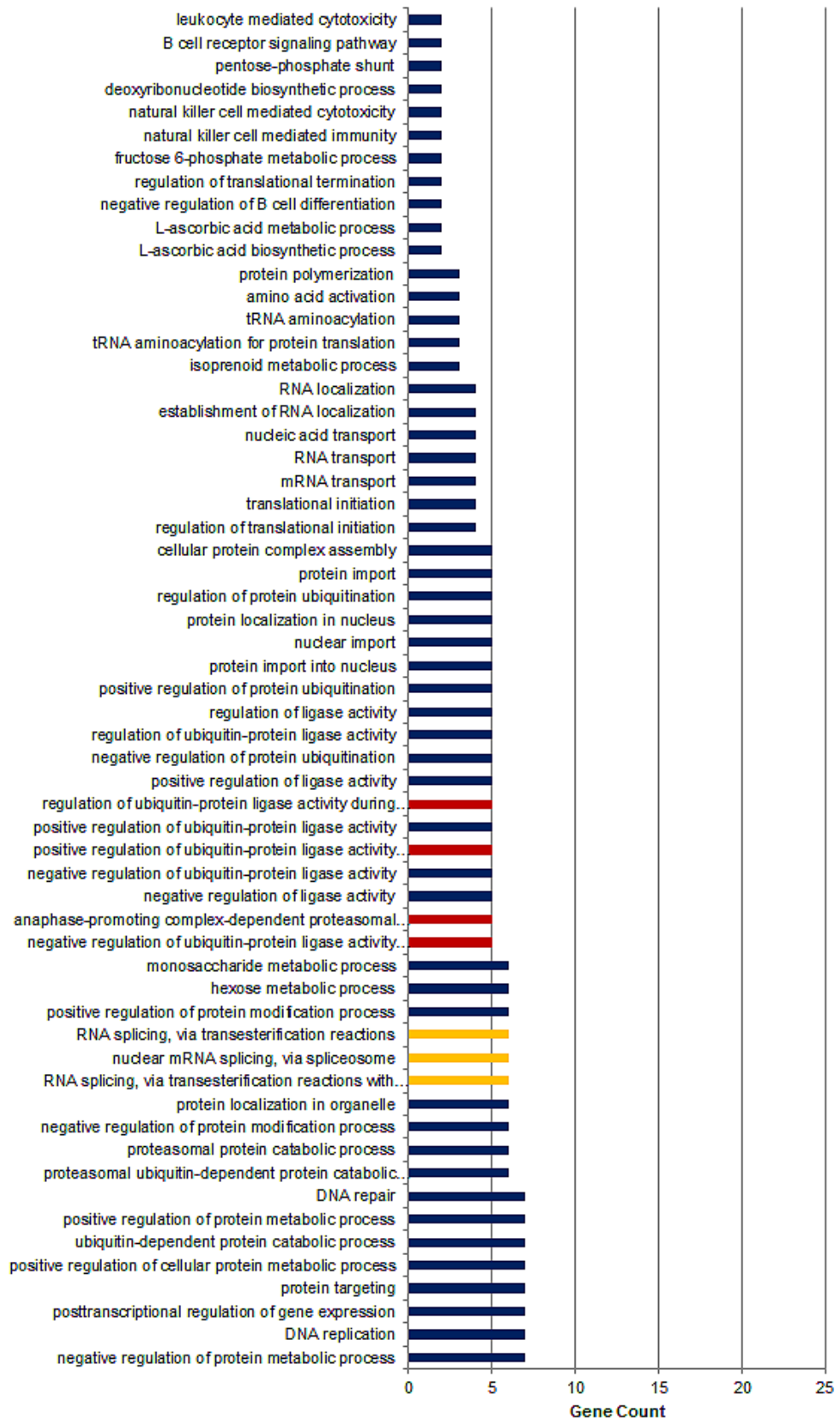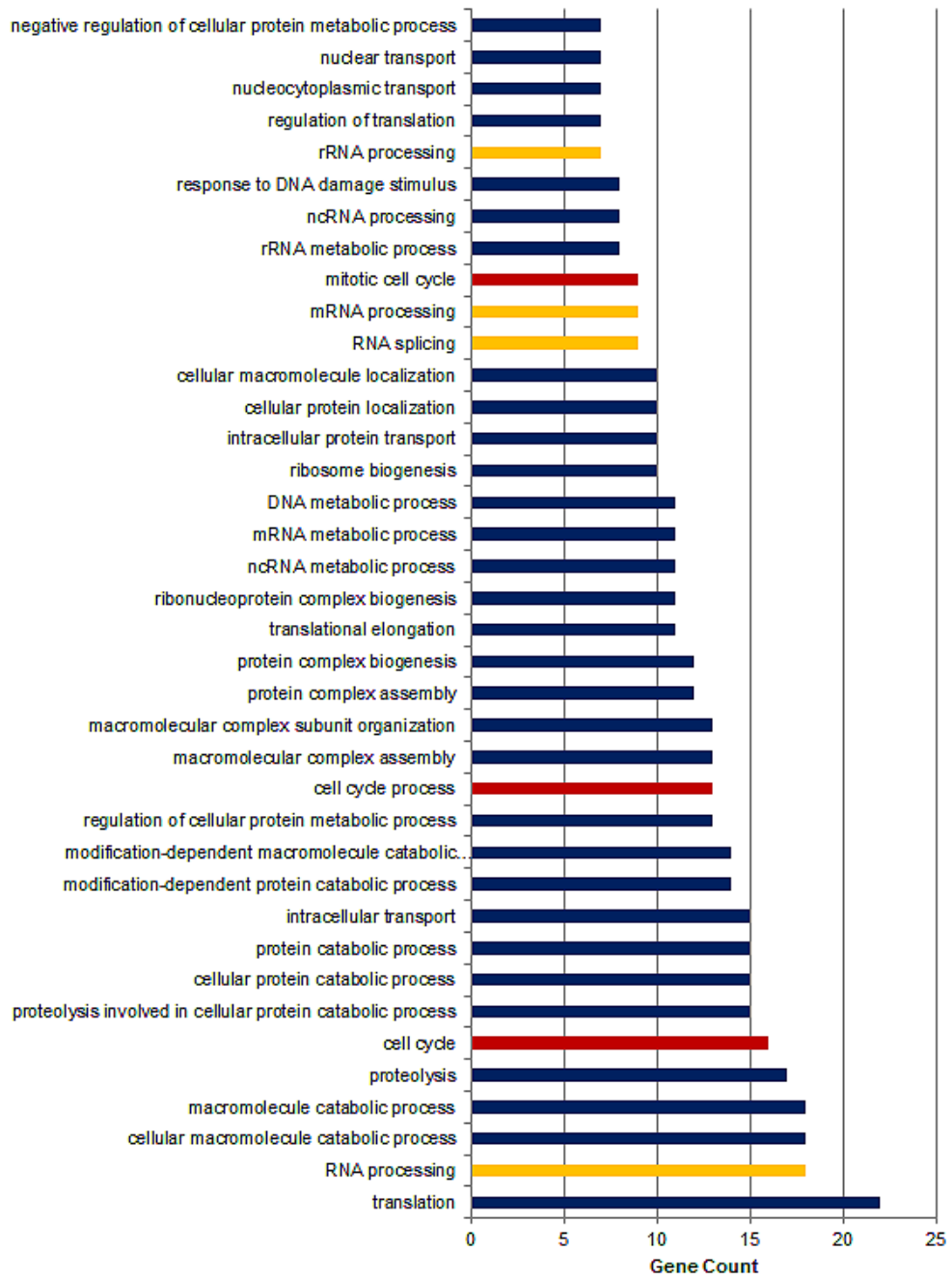
Figure 4.9: GO terms representative of biological processes comprising proteins present in the control that decrease in a time-dependent manner (control >8 h >16 h >24 h).

Processes related to the cell cycle (red bars) have increased gene counts in this particular filter. Yet again, RNA processing/splicing (yellow bars) have consistently been among the top enriched terms in both upregulated and downregulated processes for all filters applied thus far, suggesting that JA treatment may ultimately affect protein synthesis due to perturbations in the processing of their precursors.
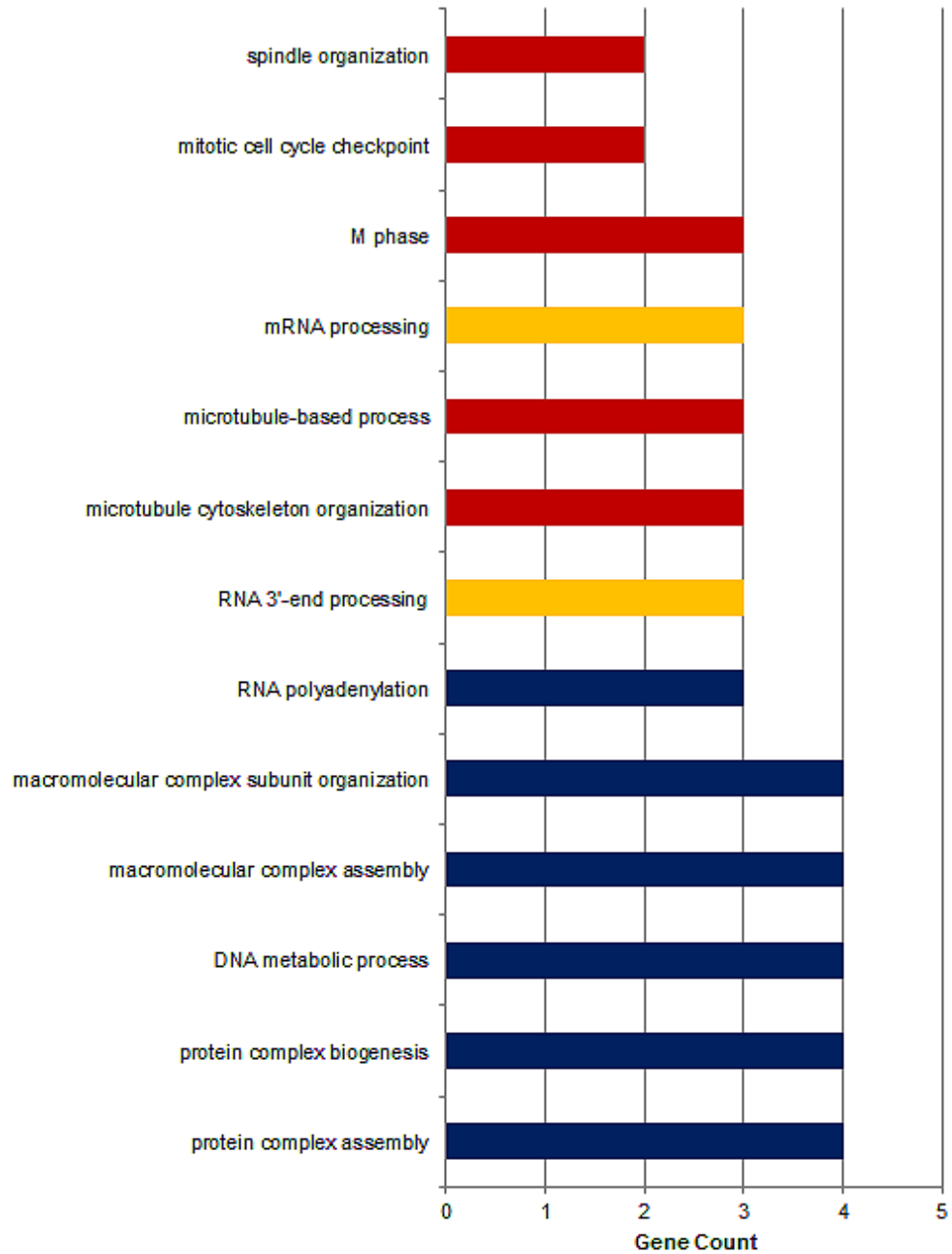
Figure 4.10: GO terms representative of biological processes consisting of proteins present in the control that decrease in a time-dependent manner (control >8 h >16 h >24 h = 0)

The last filter applied strongly corresponds with our target of interest. This is the only filter that consisted of enriched terms such as microtubule-based processes and spindle organisation (red bars) which is in line with JA's mechanism of action. We therefore pursued possible protein candidates and pathways for validation using this filter as a starting point.

Proteins comprising biological processes represented in fig.4.10 are tabulated below with fold-changes of MCF-7 cells treated with JA for 8 h, 16 h, and 24 h relative to untreated control cells. R^2 values obtained from linear regression analyses are also displayed in order of strength. As seen in 4.5, all proteins had strong linear trends (over 85%) showing downregulation at 24 h post JA treatment.

Table 4.5: List of proteins associated with biological processes represented in fig.4.10.

Protein Name	Gene	Fold-change relative to control			R^2 value
		8 h	16 h	24 h	
Ensconsin	MAP7	0.70	0.30	0	0.99
Equilibrative nucleoside transporter 1	SLC29A1	0.62	0.23	0	0.99
Zinc finger protein 277	ZNF277	0.57	0.34	0	0.99
Tumor protein p53-inducible protein 11	TP53I11	0.80	0.48	0	0.97
Syntaxin-16	STX16	0.83	0.49	0	0.96
TAF6-like RNA polymerase II p300/CBP-associated factor-65 kDa subunit 6L	TAF6L	0.84	0.49	0	0.95
60S ribosomal protein L22-like 1	RPL22L1	0.66	0.56	0	0.93
Lysosome-associated membrane glycoprotein 1	LAMP1	0.50	0.45	0	0.93
Tight junction protein ZO-3	TJP3	0.72	0.58	0	0.92
Nitric oxide synthase-interacting protein	NOSIP	0.42	0.35	0	0.91
Phosphopantothenate-cysteine ligase	PPCS	0.67	0.58	0	0.91
Thymidine kinase, cytosolic	TK1	0.56	0.53	0	0.91
Fanconi anemia group A protein	FANCA	0.56	0.53	0	0.91
Poly(A) polymerase alpha; Poly(A) polymerase beta	PAPOLA;PAPOLB	0.82	0.60	0	0.91
Ribonucleoside-diphosphate reductase subunit M2	RRM2	0.42	0.11	0	0.91
Protein FAM208A	FAM208A	0.39	0.26	0	0.91
5-AMP-activated protein kinase subunit gamma-1	PRKAG1	0.80	0.61	0	0.91
UV excision repair protein RAD23 homolog A	RAD23A	0.71	0.61	0	0.90
Mitochondrial import receptor subunit TOM34	TOMM34	0.52	0.54	0	0.89
Serine/threonine-protein kinase N1	PKN1	0.34	0.21	0	0.88
ZW10 interactor	**ZWINT**	0.90	0.63	0	0.88
Mitotic checkpoint serine/threonine-protein kinase BUB1 beta	**BUB1B**	0.79	0.67	0	0.87
ADP-ribosylation factor 4	ARF4	1.04	0.53	0	0.86

We were able to identify two proteins (in bold) that were part of the mitotic process from table 4.5. ZWINT has been shown to play an essential role in mitotic checkpoint signaling [196]. It is specifically required for kine-tochore localisation which is involved in crucial interactions with spindle microtubles that orchestrate proper chromosomal segregation [196]. Unfortunately, the exact role of ZWINT in kinetochore localisation and function is unknown leaving BUB1B as an ideal protein candidate for MudPIT validation.

4.2.2.1 Validating the spindle assembly checkpoint

BUB1B, also known as BUBR1, is a serine/threonine protein kinase and an integral component of the spindle assembly checkpoint (SAC). As discussed previously, the cell cycle is governed by specific checkpoints that ensure proper progression of each phase. The SAC is needed for appropriate segregation of chromosomes during mitosis or meiosis, specifically at the metaphase-anaphase transition [197, 198]. Interestingly, the very first studies that identified checkpoints such as the SAC that govern mitosis were done so with the use of microtubule depolymerising agents [198]. Figure 4.11 briefly illustrates central components of the SAC [199].

The main function of the SAC is to delay anaphase during mitosis to ensure that all chromosomes are attached to the mitotic spindle and aligned along the metaphase plate. Prolonged mitotic arrest occurs if requirements of the SAC are not met, which often leads to cell death. The SAC however, can be overcome by the release of CDC20 from the mitotic checkpoint com-
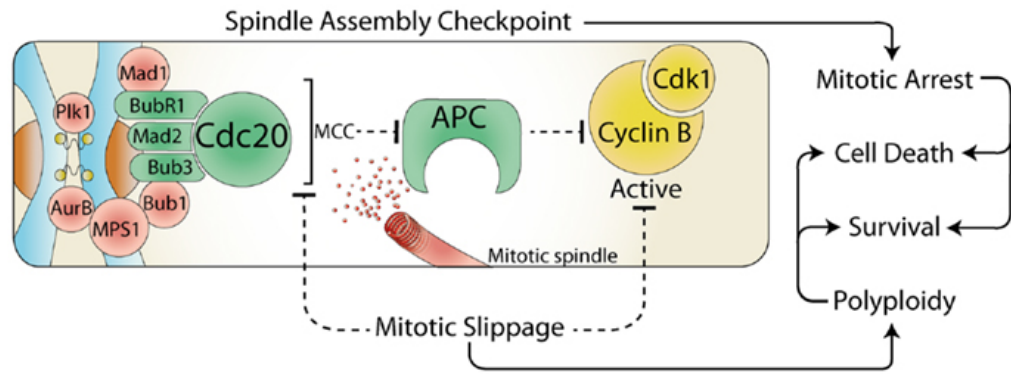
Figure 4.11: The spindle assembly checkpoint and cell fate.
[199]

plex (MCC) which consists of MAD2-BUBR1-BUB3-CDC20 or by direct inhibition of Cdk1. This mitotic slippage can result in polyploidy, increased cell survival, and provide a potential mechanism for escaping mitotic cell death [199]. In summary, when the SAC is not satisfied, MCC is formed and inactivates CDC20, which in turn prevents the APC/C from degrading cyclin B, a signal for metaphase, ultimately arresting cells in metaphase until rectification. On the other hand, if the SAC is satisfied, the MCC does not form, leaving CDC20 in an active state, which then directs the APC/C to degrade cyclin B and once degraded allows cells to progress to anaphase (refer to 2.12).

Results from MudPIT showing a decrease in BUB1B levels over time was corroborated by Western blots illustrated in fig.4.13. Several components of the APC (ANAPC1, 2, 4, 7) were also identified by MudPIT analyses. APC is a large ubiquitin E3 ligase that consists of at least 13 proteins [200]. Trends showed that levels of APC components increased at 24 h relative to 16 h.
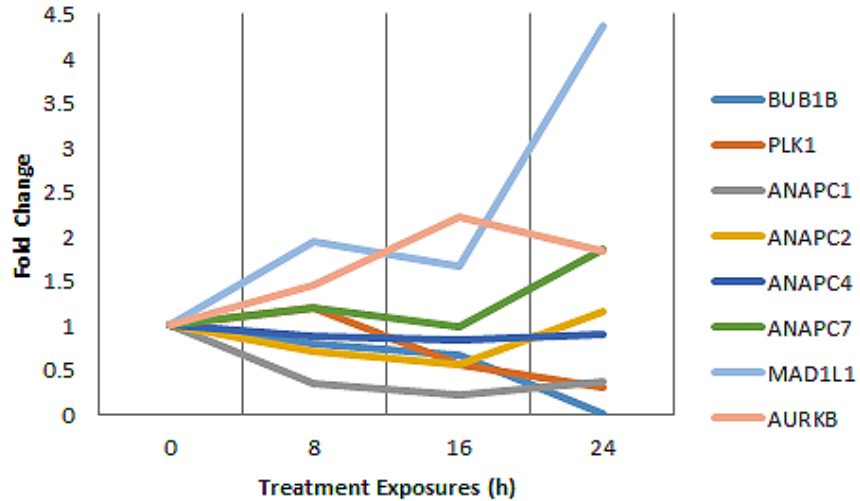
Figure 4.12: MudPIT results illustrating temporal protein expression of key components in the spindle assembly checkpoint in MCF-7 cells after JA treatment for 8, 16, and 24 hours.

All treatment samples are expressed in fold change relative to the control which is set to 1.

Another key protein integral to the SAC is CDC20. CDC20 was not indentified in our MudPIT studies, but was validated based on its association with the MCC. CDC20 levels decreased in MCF-7 and HCT-116 cell lines post 8 h treatment with JA. Interestingly, levels of CDC20 did not decrease in V-R HCT-116 cells even after 72 h exposure. This concurs with the idea that CDC20 is constantly active in V-R HCT-116 cells, which allows APC/C to degrade cyclin B, thus permitting cells to progress to anaphase. This defect in the SAC may paradoxically contribute to vincristine resistance and JA sensitivity as well.

MAD1L1 is one of the main proteins that is responsible for recruiting components of the MCC, specifically MAD2 to unattached kinetochores. As seen in fig.4.12, MAD1L1 levels quadrupled at 24 h. It may be that the number of unattached kinetochores cause increased levels of MAD1L1

132
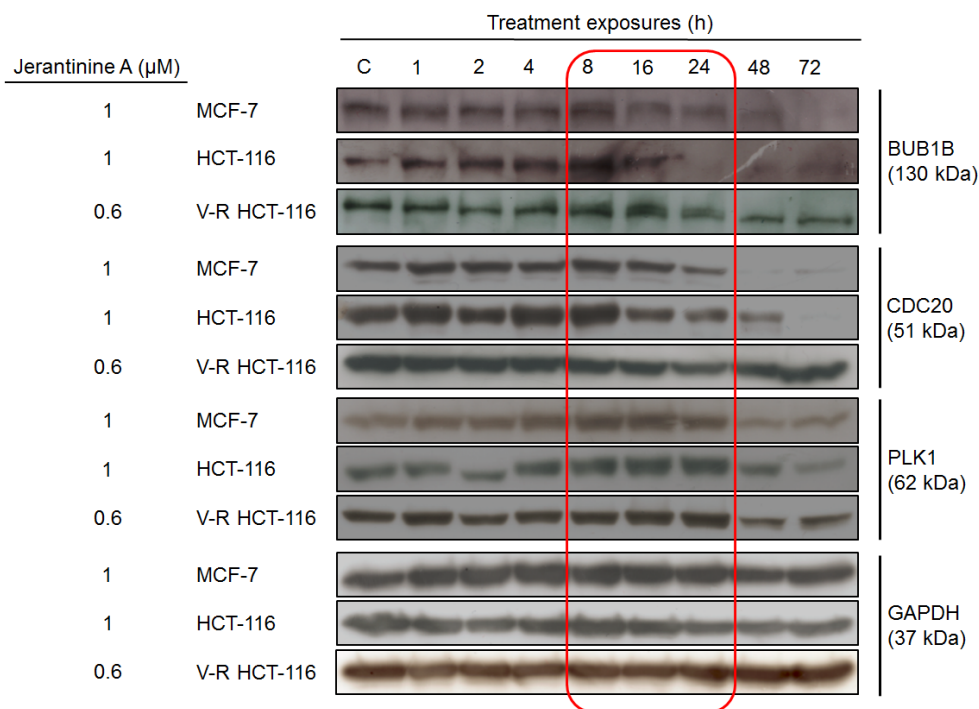
Figure 4.13: Western blots validating temporal protein expression observed in MudPIT of key components of the spindle assembly checkpoint in MCF-7, HCT-116 and V-R HCT-116 cells after JA treatment.

The red box indicates time exposures that were investigated in MudPIT studies.

at this time point, where the G2/M arrest was at its highest following JA treatment as observed from cell cycle analyses. Some studies have shown that upregulation of MAD1 leads to chromosomal instability and more importantly resistance to microtubule poisons [201].

PLK1 is another protein that we validated in reference to the SAC pathway. A very recent study showing that PLK1 is indeed needed to strengthen SAC signaling and acts cooperatively with Monopolar spindle 1 (MPS1) to regulate checkpoint establishment and maintenance. MPS1 is a protein kinase that establishes and maintains the MCC inhibitory signal, which accumulates and autoactivates unattached or misaligned kinetochores [202]. MudPIT studies revealed a decrease in PLK1 expression by

24 h which concurs with blots showing the same in MCF-7 cells. However, PLK1 expression relative to the control in MudPIT did not match Western blot data as levels at 24 h seemed higher. Levels of PLK1 did decrease in MCF-7, HCT-116, and V-R HCT-116 cells after 48 h exposure to JA.

4.2.2.2 Increased expression of ROS scavengers is indicative of ROS production

As discussed in 3.2.6.1, JA induces ROS in HCT-116, V-R HCT-116, and JA-R HCT-116 cells. MudPIT studies confirmed significant fold changes in key ROS scavengers such as glutathione S-transferase (GST) and catalase at 24 h (see fig.4.14). GSTs represent a major group of detoxification enzymes. There is evidence suggesting that the level of GST is an important factor in determining cell sensitivity to a broad spectrum of chemicals which include antitumour agents and products of oxidative stress [203]. Furthermore, induction of GST by ROS may represent an adaptive response as these enzymes detoxify some toxic metabolites containing epoxides (present in JB), peroxides, and carbonyls that are produced within the cell by oxidative stress [203]. Catalases and peroxiredoxins catalyse the decomposition or reduction of hydrogen peroxide into its constituents, water and oxygen. Some studies have found that migration and proliferative capacities of MCF-7 cells are impaired by the overexpression of catalases [204]. Peroxiredoxins come from a family of highly conserved antioxidant enzymes [205]. As seen in fig.4.14, levels of peroxiredoxin enzymes remain relatively stable compared to the control. Increased expression of thioredoxin reductase 1 (TXNRD1) was evident by 24 h post JA treatment. TXNRD1 reduces and activates thioredoxin, an oxidoreductase containing a dithiol-disulfide active site, which in turn reduces oxidized cysteine residues on cellular proteins and scavenges peroxides by peroxiredoxins [206].
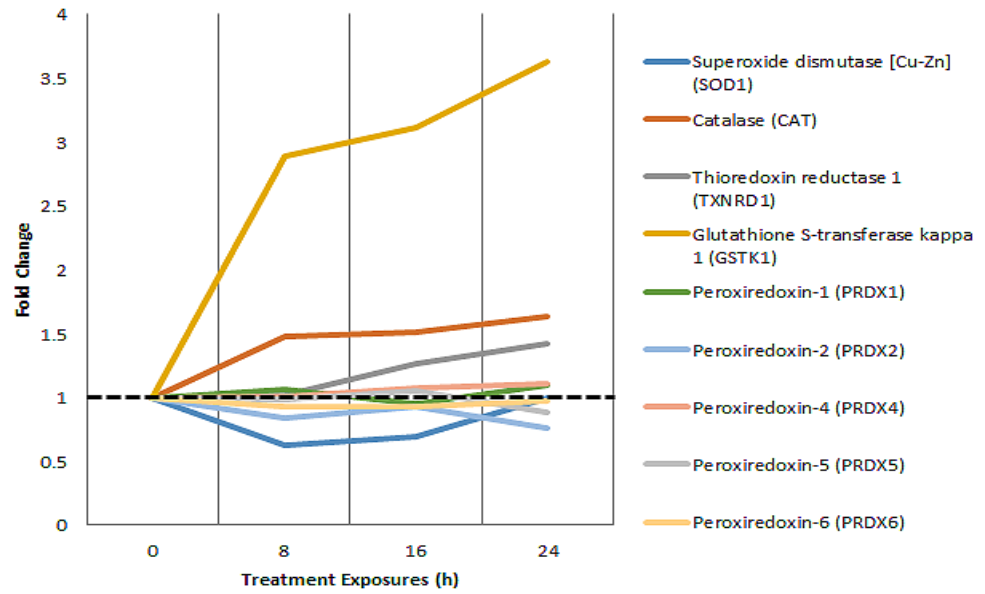
Figure 4.14: JA induces expression of key enzymes involved in detoxification in MCF-7 cells after treatment.

All treatment samples are expressed in fold change relative to control which is set to 1.
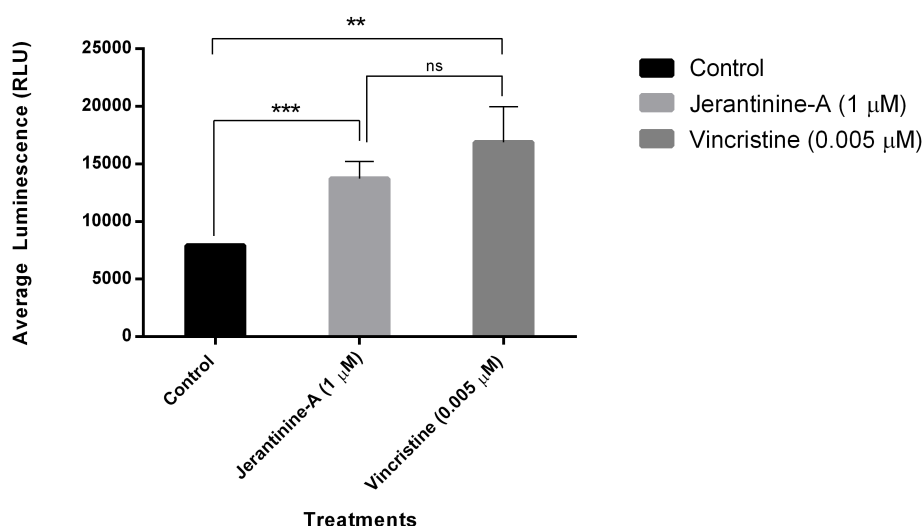
Figure 4.15: JA induces significant levels of ROS production in MCF-7 cells.

Cells treated with JA (1 μM) and vincristine (5 nM) also induced significant ROS in MCF-7 cells compared to the control (***p<0.001 and **p<0.01). However, differences in ROS levels between JA and vincristine treatment were not significant (ns). Experiments were repeated at least 2 times (n=4). Refer to 6.2.12 for experimental methodology.

This reducing environment mediated by thioredoxin is conducive to DNA binding of redox-sensitive transcription factors such as p53 and NF-κB [206]. Its main role is to bind ROS before they can harm cells, protecting them from oxidative stress [206]. Increase in ROS production in MCF-7 cells after JA treatment may have caused TXNRD1 levels to increase over time. Taken together, ROS assays and increased expression of ROS scavengers confirm ROS generation.

4.2.2.3 JA treatment causes reduced levels of differentially expressed tubulin types in MCF-7 cells

As seen in fig.3.7, β-tubulin is a target for clinically used antimitotic agents. Western blots confirmed reduction in TUBB levels observed in MudPIT af-

ter treatment with 1 μM JA. However, levels of TUBB remain unchanged in HCT-116 and V-R HCT-116 cells after 8 h, 16 h, and 24 h of JA exposure. However, decreases were seen at 72 h in HCT-116 cells. V-R HCT-116 clearly expressed higher levels of TUBB at 72 h in comparison to HCT-116 and MCF-7 cells which showed decreased expression of TUBB at that same time point (see figs.4.16) and 4.17. An interesting study showing that treatment with vincristine, a depolymerising agent, decreased tubulin levels in cancer cell lines [207]. This decrease was suggested to be a result of proteasome-mediated degradation of tubulin, albeit the process was significantly enhanced in neural cells [207]. Other studies have shown that novel peroxisome proliferator-activated receptor gamma (PPAR-γ) inhibitors induced tubulin degredation *via* proteasomal-dependent pathway without affecting polymerisation [208].
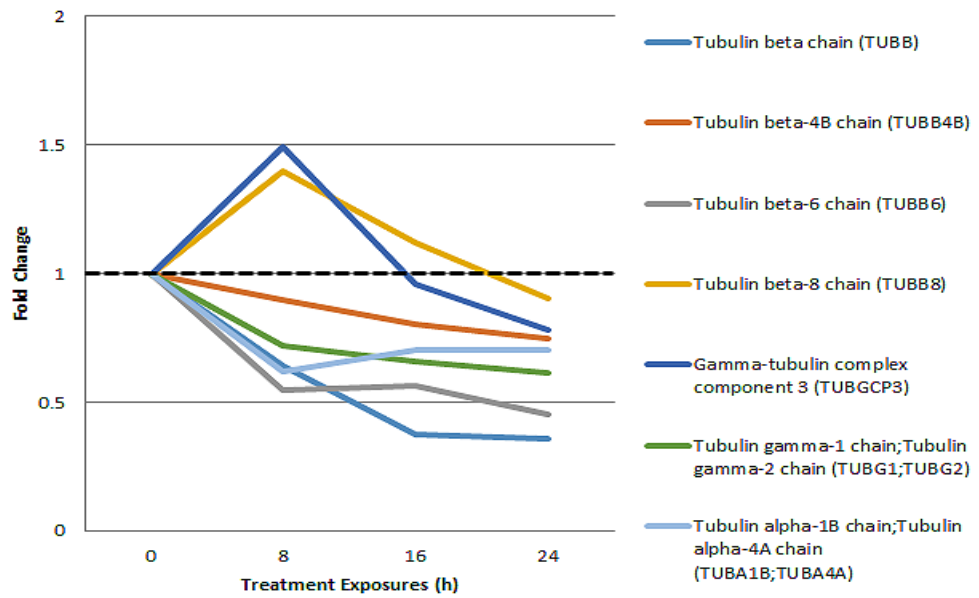
Figure 4.16: Jerantinine A (1 μM) reduced levels of various tubulin components in MCF-7 cells after treatment.

Control levels are normalised to 1 and any changes observed in treatment samples are displayed as fold changes relative to the control.
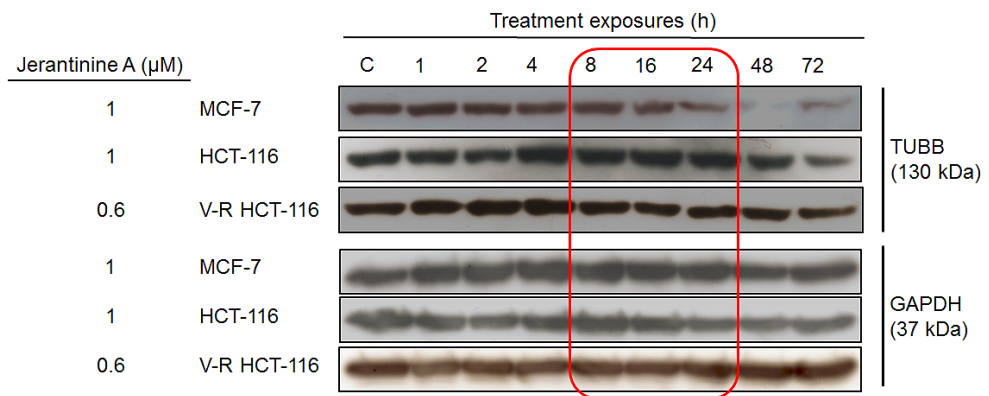
Figure 4.17: Blots showing reduction in TUBB in MCF-7 cells correspond to TUBB levels obtained in MudPIT after 8 h, 16 h, and 24 h exposure to JA (1 μM).

4.2.2.4 Short-term exposure to jerantinine A potently inhibits growth

In order to validate the use of an 8 h time exposure in our investigations of the proteome after JA treatment, it was necessary to determine if this short treatment was enough to inhibit growth in cells. We therefore conducted assays that were identical to MTTs with the exception of cells that were treated for 8 h instead of a continuous 72 h exposure, washed with PBS, replenished with medium, and incubated for 64 h alongside continuous exposure (72 h) as an appropriate control for agent activity. If cell growth was inhibited, we can deduce that this short term exposure was enough to cause changes in the proteome that ultimately lead to cell death. As seen in a representative graph (fig.4.18), HCT-116 cells were unable to recover from the short treatment yielding a mean GI_{50} value of 0.546 ± 0.140 μM. These results suggest that JA is able to permeate the cell membrane and inhibit cell proliferation within a short span of time. However, JA was not able to inhibit growth of MCF-7 cells by 50% at 1 μM after an 8 h exposure. A mean GI_{50} value of 4.362 ± 0.935 μM was obtained from three experimental trials. This is nearly 4.5 times the concentration used for our MudPIT studies. We know that 1μM is enough to evoke a significant G2/M block in MCF-7 cells after 24 h exposure to JA and perhaps proteins reflective of that phenotype appear closer to or at that particular time point. This is evident from the last filter (proteins that gradually and completely disappeared by 24 h i.e. 100% depletion) applied to MudPIT data showing spindle and microtubule-based organisation as possible hits

for pathway validation.
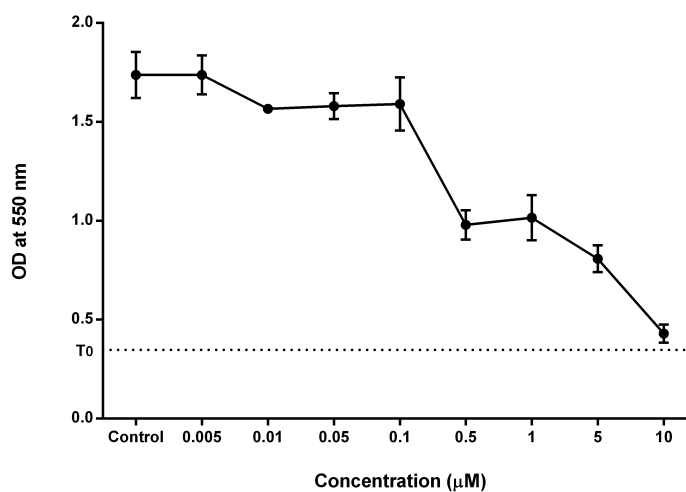
Figure 4.18: JA inhibits growth of HCT-116 cells after only 8 h exposure.

GI_{50} values were determined by MTT assays following an 8 h exposure in addition to a 64 h recovery period and expressed as a mean $\pm$ standard deviation of 3 independent trials (n=4).
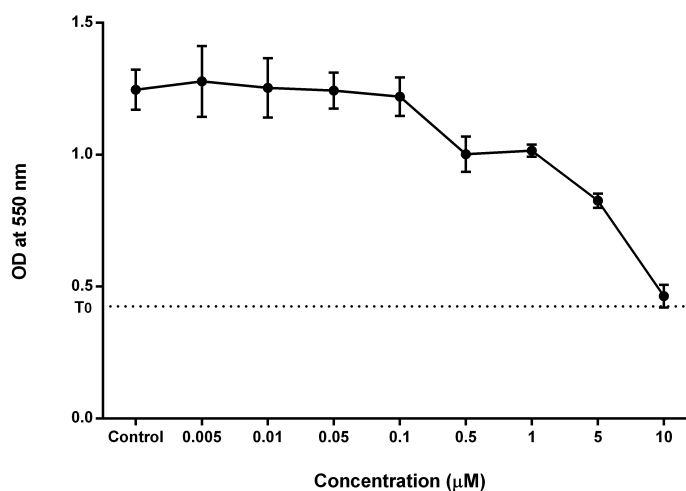
Figure 4.19: JA does not inhibit growth of MCF-7 cells by 50% at $1\mu M$ after 8 h exposure.

GI_{50} values were determined by MTT assays following an 8 h exposure in addition to a 64 h recovery period and expressed as a mean $\pm$ standard deviation of 3 independent trials (n=4).

Early changes in proteins representing the phenotype of JA-treated cells may be masked after only an 8 h exposure due to the fact that a lower than optimal JA concentration was used. However, as seen in fig. 4.20, differences in expression profiles between control and 8 h treatment samples were distinct enough to be clustered under different branches (i.e. all treatment samples were more similar to each other than the control).
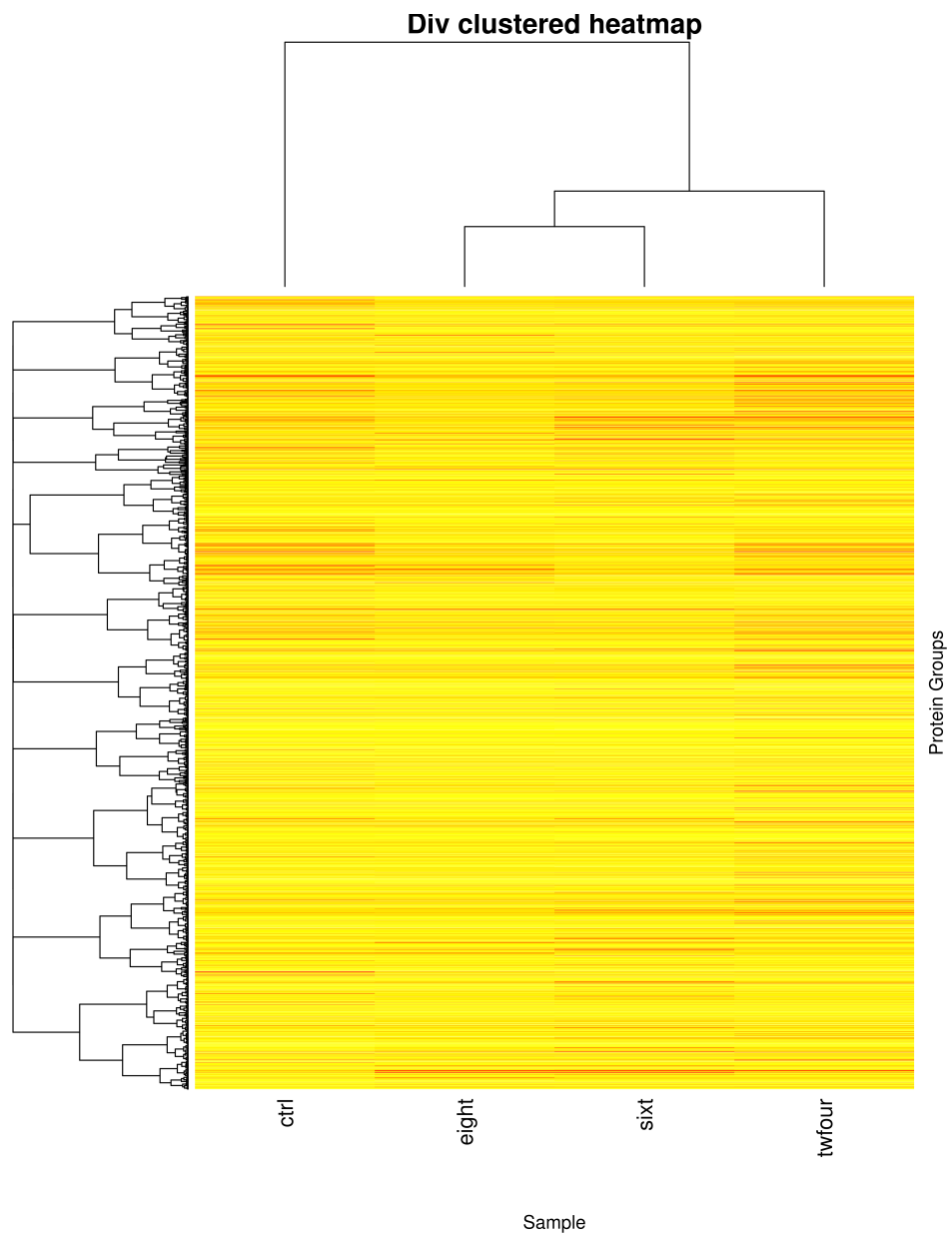
Figure 4.20: Clustered heatmap showing distribution of perturbed proteins across samples

Clustering protein expression profiles from all four samples revealed that the profile from the control sample was distinct from all three treatment samples (8, 16, 24 h) and that each treatment sample shared some similarity in expression profiles.

4.3 Conclusion

The genome-wide RNAi screen revealed several candidate genes of interest thought to mediate cell resistance or sensitivity to JA. Our investigations were narrowed to genes controlling JNK1/2 expression because of its involvement in multiple pathways identified by DAVID such as those related to MAPK and TLR. These targets were obtained from the list consisting of genes that when knocked down confer resistance to JA (table 4.1). JNK1/2 and variants were knocked down in MCF-7 and MDA-468 cells and then treated with JA (1 μM) for 72 h. Results showed that knocking down JNK1 or JNK2 made cells more resistant to JA relative to controls (up to 1.5 times in MCF-7 cells and 3 times more resistant in MDA-468 cells). Considering the important roles that JNKs play in cell proliferation, apoptosis, ROS production, and stress responses, it is possible that these proteins do in fact contribute to the phenotype observed in cells after JA treatment.

Analysis of the proteome using MudPIT in JA-treated cells also corroborated phenotypes observed throughout this study. Data analyses by way of filtering and using bioinformatics resources such as DAVID aided identification of BUB1B as a suitable candidate for validation. BUB1B is a key player in the SAC and is essential to mitotic integrity. Western blots showing protein expression of specific SAC components were in agreement with levels obtained in MudPIT trials. Increased expression of proteins involved in scavenging ROS were also identified by MudPIT suggesting

that this process may be involved in apoptotic events resulting from JA treatment. As discussed in chapter 3, JA is a potent inhibitor of tubulin polymerisation. Interestingly, MudPIT analysis of MCF-7 treated cells revealed decreased expression in α, β, and γ-tubulin. However, decreases in β-tubulin were not observed in HCT-116 or V-R HCT-116 cells at 8, 16, and 24 h post treatment with JA. It is possible that altered expression of tubulin isotypes and modulation of β-tubulin levels may impact the response of MCF-7 cells to JA as some studies have shown this to be the case in docetaxel-resistant MCF-7 and MDA-MB-231 cells [209].

Chapter 5

Concluding Remarks and Future Studies

5.1 Concluding Remarks

The contribution of natural product drug discovery to the field of medicine has been invaluable throughout human history. The impact of natural products in cancer chemotherapy alone has been significant by way of providing lead structures that can be used as templates for the construction of novel compounds that possess enhanced biological properties. The investigations carried out in this study serve as a testament to the untapped potential of natural products. In 2008, Lim et al. reported the isolation of seven novel indole alklaoids, jerantinines A-G, from a leaf ethanolic extract of the Malayan *Tabernaemontana corymbosa*. JA was the major constituent of the leaf extract and was thus used for the biological studies detailed here. Preliminary antiproliferative screens revealed potent growth inhibition of JA on multiple human-derived cancer cell lines (A549, HCT-116, HT-29, MCF-7, MDA-468, MiaPaCa-2, DAOY, MED1, and UW228-3). GI_{50} values obtained from MTT assays were $\leq 4\ \mu$M for all jerantinines (JA, JAA,

JB, JBA) tested. V-R HCT-116 cells were generated and shown to express Pgp. These cells were found to retain sensitivity to JA, being slightly more sensitive than parent HCT-116 cells, which is indicative of JA's ability to overcome vincristine resistance. A NCI60 cell line panel screen against JAA yielded GI_{50} values of less than 2 μM across all cell lines. JA was also able to potently inhibit colony formation in A549, HCT-116, HT-29, and MCF-7 cells after a brief 24 h exposure. Further assays were carried out in order to determine the nature of cell death in response to JA. Annexin V assays revealed dose- and time-dependent increases in apoptosis in treated cells. This was corroborated by upregulation and downregulation of pro- and anti-apoptotic proteins respectively.

Cell cycle analyses revealed potent G2/M arrests in A549, HCT-116, HT-29, MCF-7, and MDA-468 cells. Considering that JA shares a degree of structural similarity with vincristine and its ability to cause potent G2/M arrests typically seen in cells after treatment with taxanes and vinca alkaloids, it was hypothesised that JA may target microtubules. Indeed, tubulin polymerisation assays convincingly demonstrated that JA inhibited tubulin polymerisation and is thus similar to the vinca alkaloids. Phenotypes of JA-treated cells were determined using confocal microscopy. Images showed severe perturbations in cytoskeletal architecture such as membrane blebbing, multipolar spindle formation, DNA fragmentation, and aneupolidy. The integrity of DNA in JA-treated cells was investigated by measuring phophorylated γH2AX levels which is indicative of DNA DSBs. JA induced significant levels of phophorylated γH2AX after only a 24 h ex-

posure. As mentioned earlier, JA demonstrated potent growth inhibition in V-R HCT-116 cells. This was consistent with Western blots showing that expression of Pgp did not hinder the activity of JA. Increased levels of ROS have also been reported to play a role in acquired resistance. JA induced more significant levels of ROS than vincristine in HCT-116 and MCF-7 cells. Our collaborative studies revealed that JBA binds to the colchicine binding site on microtubules, suggesting the same may be true for the jerantinine family of compounds. Modelling studies exploring differences in JA and JB binding are currently under way.

Analyses of data from the genome-wide shRNA screen revealed involvement of JNK1/2 in mediating sensitivity of MCF-7 cells to JA. Validation of this data entailed knocking down JNK1/2 in MCF-7 and MDA-468 cells, treating them with JA, and measuring growth inhibition after 72 h exposure using MTT assays. Results showed that depletion in JNK1/2 conferred resistance to JA. Global proteome analysis was carried out using MudPIT. Data analyses and validation using Western blots revealed abberations in the SAC, increased expression in key ROS scavengers, and decreased expression in α, β, and γ-tubulin.

As studies that probe the mechanistic nature of JA continue, it should be taken into consideration that its effects *in vivo* are presently unknown. One of the most common problems associated with MTAs is the issue of neurotoxicity. Our assumption that JA may be neurotoxic stems from the fact that other clinically available MTAs like paclitaxel and vincristine cause neurotoxicity. Even though JA fulfils Lipinski's rule of 5, by no

means does it indicate suitability as a lead compound. On the other hand, both paclitaxel and vincristine violate Lipinski's rule of 5, but are still approved for use in the clinic. Additionally, our studies have confirmed that JA is not a Pgp substrate unlike paclitaxel and vincristine, which could potentiate neurotoxicity if it passes the blood-brain barrier. Further studies of JA's effects *in vivo* as it pertains to absorption, distribution, metabolism, and excretion need to be thoroughly explored in order to fully discern its potential as a chemotherapeutic agent.

5.2 Future Studies

Having identified the mechanism of action for JA *in vitro*, a more thorough understanding of its properties and suitability for *in vivo* testing needs to be achieved. Based on our observations throughout this study, JA appears to be more unstable than JB. Therefore, it is necessary to investigate how this compound breaks down in conditions similar to those subjected in cells after treatment. For instance, measuring stability and biproducts of JA at various time points when treated cells are incubated in 37℃ using LC/MS may give an indication of extracellular and intracellular concentrations of the agent. Another alternative is to use dialysis tubing as a model for the semi-permeable cell membrane which may provide a crude estimation of how much of the agent gets into the cell at various time points. This also can be measured using LC/MS, however, the model does not take other modes of cellular transportation (influx and efflux) into account i.e. active transport systems such as drug efflux pumps etc. One approach that is currently being explored by collaborators is the use of a fluorophore that is tagged on to JA. This would not only aid in measuring extracellular and intracellular concentrations, but also help in visualising possible localisation of the compound within the cell post-treatment.

The revelation that the jerantinines most likely bind to the colchicine binding site on microtubules allows for further investigations into the nature of binding between these compounds and tubulin. For instance, competitive binding assays with radio-labelled colchicine may be employed to determine

the affinity of the jerantinines to this particular site. This can be carried out using a scintillation proximity assay (SPA) constituting biotinylated tubulin, SPA streptavidin beads, tritiated colchicine and a competitor, which in this case is JA. SPA technology requires a close association between a solid phase scintillant (the beads) and a radio-ligand for signal emission and detection. The medium that brings the tritiated colchicine and SPA beads in close association is the biotinylated tubulin. If the radio-ligand occupies the binding sites on tubulin and is in close range of the SPA beads, the signal detected would be proportional to the number of sites occupied by this ligand. On the other hand, if an unlabelled competitor occupied these binding sites on tubulin, the decrease in signal would be proportional to the concentration of said competitor (see fig.5.1).

An additional advantage of this assay is that it allows identification of reversible or irreversible binding to the colchicine site over a long period of time. Colchicine was a failure in the clinic partly due to the fact that it binds to tubulin in an irreversible manner which contributed to severe toxicities. If JA binds reversibly to tubulin, it may be easier to liberate or metabolise the agent more readily.

It may be interesting to explore differential expression of proteins involved in metabolising colchicine and JA using LC-MS/MS (metabolomics) as this technique can provide a good indication of bioactivation and drug-induced cytoxicity in both *in vitro* and *in vivo* settings.
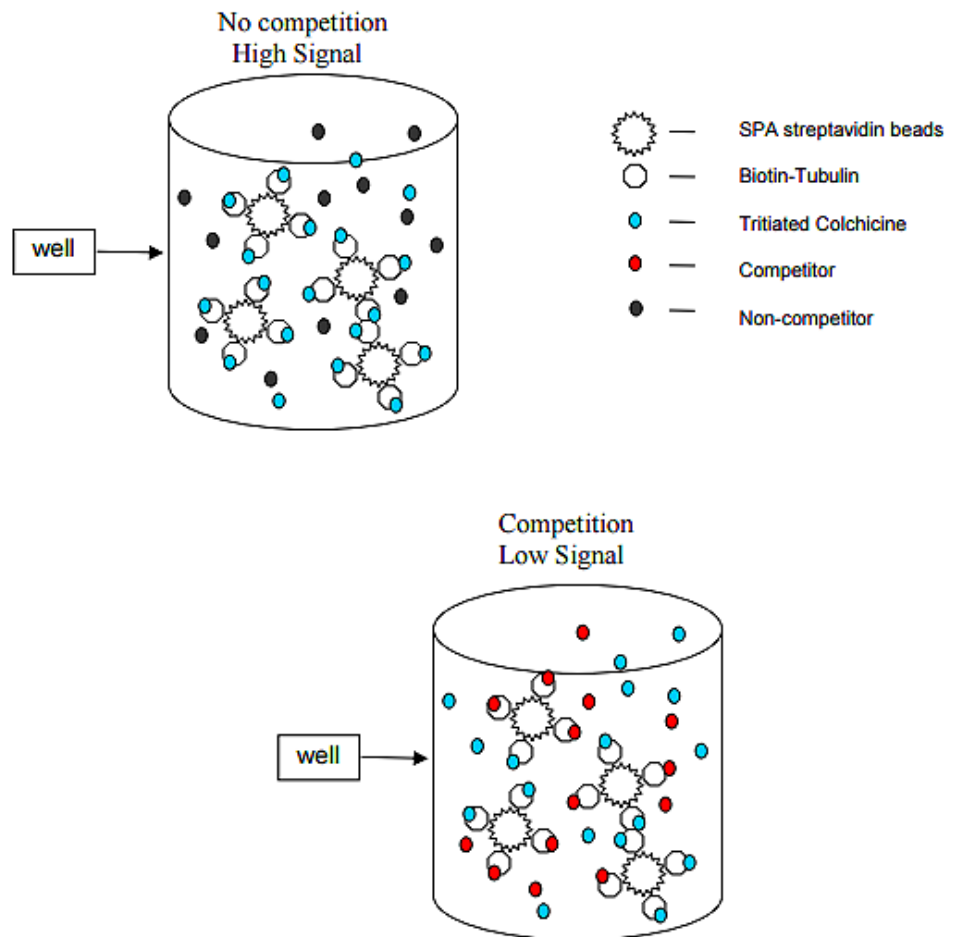
Figure 5.1: SPA assay with biotin-tubulin and streptavidin beads

Chapter 6

Materials and Methods

6.1 Materials

6.1.1 Cell Lines

The A549 cell line was first developed in 1972 from the culturing of an explanted tumour of a 58-year-old male [210]. They are alveolar basal epithelial cells that have an adherent mode of growth and have a doubling time of approximately 22 hours [210]. These cells are particularly unique because of their ability to produce lecithin, a phospholipid, and constitute high levels of desaturated fatty acids that are crucial to maintaining the integrity of the phospholipid bilayer forming the cell membrane [211]. It has been suggested that these changes in the cell membrane can be attributed to this cell line's increased resistance to chemotherapeutic agents [211].

The HCT-116 (wildtype p53; mutant RAS) cell line is one of three malignant cell lines (HCT-116a and HCT-116b) isolated from a male with colonic carcinoma. These cells are adherent and have a short doubling time of 17.4 hours in addition to possessing a modal chromosome number of 46 [212]. They are also reported to have higher levels of colony formation

capability [212].

The HT-29 (mutant p53) cell line was isolated from a woman with colon adenocarcinoma in 1964 [213].This cell line also has an adherent mode of growth with a doubling time of approximately 19.5 hours and is considered to be more invasive than the HCT-116 cell line [213]. HT-29 cells grow *in vitro* as discrete semispheroid clusters and have a rounded appearance [214].

MCF-7 (wildtype p53)is an ER+ breast cancer cell line derived from the pleural effusion of a 69-year-old woman who had invasive breast ductal carcinoma in 1970 [215].These cells form tightly cohesive structures thereby illustrating robust cell to cell adhesions and display a luminal epithelial phenotype [216].

The MDA-MB 468 is a triple negative (ER-, PR-, and Her2/neu-) p53 mutant cell line derived from the pleural effusion of a 51-year-old female who had metastatic breast adenocarcinoma and possesses an epithelial morphology that resembles loosely cohesive grape-like structures which is consistent with a more invasive phenotype [216].

The MRC-5 cell line was first derived from normal lung tissue of a 14-week-old male foetus in 1966 [217]. These cells are capable of 40-42 population doublings before the onset of senescence [217].

The cell lines used in this project were originally obtained from the ATCC and subsequently stored in the CBS cell bank for experimental use (see 6.2.1).

6.1.2 Cell Culture Media

MRC-5 fibroblasts were cultured in minimum essential medium (MEM) (Sigma-Aldrich UK, Catalogue No.: M2279) supplemented with 10% v/v foetal bovine serum (FBS) (Sigma-Aldrich UK, Catalogue No.: F9665), 7.5% sodium bicarbonate (Sigma-Aldrich UK, Catalogue No.: S8761), 1% 0.1 mM non-essential amino acids (Sigma-Aldrich UK, Catalogue No. M71 45), 1% 1 M HEPES (Sigma-Aldrich UK, Catalogue No. H0887), 1% 200 mM L-glutamine (Sigma-Aldrich UK, Catalogue No.: G7513), and 1% penicillin-streptomycin (Sigma-Aldrich UK, Catalogue No.: P4333). All other cell lines were maintained in RPMI-1640 (Sigma-Aldrich UK, Catalogue No.: R8758) growth medium supplemented with 10% FBS.

6.1.3 Compounds

Jerantinine A, B, and their acetate derivatives were kindly provided by Dr. Kam Toh Seok (University of Malaya) and Dr. Kuan Hon Lim (University of Nottingham Malaysia Campus).

6.1.4 Chemicals and Reagents

The chemicals used in this study are of analytical, biological or molecular biology grade. Trypsin 10x (Sigma-Aldrich UK, Catalogue No.: T1763); 3-(4,5-dimethylthiazol-2-yl)-2,5-diphenyltetrazolium bromide (MTT) (Alfa Aesar UK, Catalogue No.: L11939); DMSO (Sigma-Aldrich UK, Catalogue No.: D5879); FBS-heat inactivated (Sigma-Aldrich UK, Catalogue No.:

F9665); methylene blue solution (Sigma-Aldrich UK, Catalogue No.: 7220-79-3); ethanol/IMS (Sigma-Aldrich UK, Catalogue No.: 458600-2.5L); methanol HPLC grade (Fisher Scientific UK, Catalogue No.: M/4056/17); formaldehyde solution (Sigma-Aldrich UK, Catalogue No.: 252549); 16% formaldehyde solution (w/v), methanol-free (Thermo Scientific UK, Catalogue No.: 28908); propidium iodide(PI) (Sigma-Aldrich UK, Catalogue No.: P4170); Triton-X100 (Sigma-Aldrich UK, Catalogue No.: X100); RNAse A (Sigma-Aldrich UK, Catalogue No.: R6513); annexin V-FITC, PI and annexin binding buffer (0.1 M HEPES/NaOH, pH 7.4, 1.4 M NaCl, 25 mM $CaCl_2$); hypotonic fluorochrome solution (0.1% sodium citrate; 0.1% Triton X-100; 50μg/ml PI; 100μg/ml RNAseA); ammonium persulfate (AMPS) (Sigma-Aldrich UK, Catalogue No.: A3678); N,N,N,'N'-tetramethylethylenediamine (Sigma-Aldrich UK, Catalogue No.: T9281); β mercapto ethanol (Sigma-Aldrich, Catalogue No.: M3148); bromophenol blue (Sigma-Aldrich UK, Catalogue No.: B0126); Glycerol (Sigma-Aldrich UK, Catalogue No.: G5516); Tween-20 (Sigma-Aldrich UK, Catalogue No.: P9416); acrylamide/

bis-acrylamide (30%) (Sigma-Aldrich UK, Catalogue No.: A3574); Protease inhibitor cocktail tablets (Roche diagnostics UK), Catalogue No.: 11836153001); PhosStop inhibitor (Roche diagnostics UK), Catalogue No.: 04906837001), Bradford reagent (Sigma-Aldrich UK, Catalogue No.: B6916), Developer (Sigma-Aldrich UK, Catalogue No.: P7042); Fixer (Sigma-Aldrich UK, Catalogue No.: P7167); sodium dodecyl sulphate (SDS) (Melford UK, Catalogue No.: B2008); PageRuler plus prestained protein ladder (10-

250 kDa) (Thermo Scientific UK, Catalogue No.: 26619); Colour-coded prestained protein marker, High range (43-315 kDa) (New England Biolabs Ltd. UK, Catalogue No.: 12949S); cassettes 1.5 mm (Invitrogen UK, Catalogue No.: NC2015); bovine serum albumin (BSA) (VWR International Ltd. UK, Catalogue No.: 421501J); Bradford reagent (Sigma-Aldrich UK, Catalogue No.: B6916); Amersham^{TM} ECL^{TM} Western blotting detection reagents (GE Healthcare UK, Catalogue No.: RPN2106); Amersham Hyperfilm ^{TM} ECL high performance chemi-luminescence film (GE Healthcare UK, Catalogue No.: 28906837); Apo-one homogeneous caspase 3/7 assay kit (Promega USA, Catalogue No.: G7790) containing caspase substrate Z-DEVD-R110, 100x apo-one homogeneous caspase 3/7 buffer; ROS-Glo^{TM} H$_2$O$_2$ Assay (Promega USA, Catalogue No.: G8820) containing H$_2$O$_2$ substrate (10 mM), signal enhancer solution, H$_2$O$_2$ substrate dilution buffer, D-Cysteine (100x), luciferin detection reagent, and reconstitution buffer; tubulin polymerisation assay kit (Cytoskeleton USA, Catalogue No.: BK006P) containing tubulin protein, GTP stock, general tubulin buffer, tubulin glycerol buffer, paclitaxel, DMSO, and a half-area 96-well plate; vincristine (sulfate) (Cayman Chemical USA; Catalogue No.: 11764); 2,2,2-Trifluoroethanol (Sigma-Aldrich Canada, Catalogue No.: T63002); DL-Dithiothreitol (DTT) (Sigma-Aldrich Canada, Catalogue No.: D0632); Iodoacetamide (IAA) (Sigma-Aldrich Canada, Catalogue No.: I1149); Ammonium bicarbonate (Sigma-Aldrich Canada, Catalogue No.: A6141); trypsin gold, mass spectrometry grade (Promega USA, Catalogue No.: V5280); STAGE Tips [Built in-lab using P200 tips

stuffed with SCX teflon disc (Millipore) and C18 reverse phase teflon disc (Millipore)]; ammonium acetate (Sigma-Aldrich Canada, Catalogue No.: A1542); ammonium hydroxide solution (Sigma-Aldrich Canada, Catalogue No.: 338818).

6.1.5   Buffers

Phosphate buffered saline tablet (Sigma-Aldrich Catalogue No.: P4417; 1 tablet /200 ml of deionised water yields 0.01 M phosphate buffer, 0.0027 M potassium chloride and 0.137 sodium chloride, pH 7.4); Resolving gel buffer (1.5 M Tris-Cl, pH 8.8, 0.4% SDS); Stacking gel buffer [1 M Tris-Cl, pH 6.8, 0.8% SDS); resolving gel 7.5% per 10 mL (30% acrylamide (2.5 ml), resolving buffer (2.51 ml), dH_2O (4.99 ml)]; resolving gel 10% per 10 ml [30% acrylamide (3.33 ml), resolving buffer (2.51 ml), dH_2O (4.16 ml)]; Lysis buffer /10ml (1.5 ml of Nacl, 100 μL of NP-40, 0.5 ml of Tris pH 8.0, filled to a total volume of 10 ml ddH_2O, 1 tablet each of protease and phosphatase inhibitor).

6.1.6   Antibodies

The antibodies used in this project are summarised below along with supplementary information detailing blocking, dilution, and storage conditions in addition to suppliers and catalogue numbers:

Antibody	Blocking	Dilution	Storage	Supplier	Cat. No.
p53	10% milk	1:1000	4℃	Dako	M7001

158

HDM2	10% milk	1:1000	-20℃	Thermo Scientific	MA1-2331B
Cyclin B1	10% milk	1:1000	-20℃	Cell Signaling	4135
Caspase 3	10% milk	1:1000	-20℃	Cell Signaling	9668
PARP	10% milk	1:1000	-20℃	Cell Signaling	9532
Mcl-1	10% milk	1:1000	-20℃	Cell Signaling	4572
P-Glycoprotein	5% milk	1:1000	-20℃	GeneTex	GTX23364
BUB1B	5% milk	1:1000	-20℃	Thermo scientific	MA1-16577
CLASP1	5% milk	1:1000	-20℃	GeneTex	GTX62531
GEF-H1	5% BSA	1:1000	-20℃	Cell Signaling	4076
MARK2	5% BSA	1:1000	-20℃	Cell Signaling	9118
CDC20	5% BSA	1:1000	-20℃	Cell Signaling	4823
CLIP1/-CLIP170	5% BSA	1:1000	-20℃	Cell Signaling	8977
CRMP-2	5% BSA	1:1000	-20℃	Cell Signaling	9393
Rac1/Cdc42	5% BSA	1:1000	-20℃	Cell Signaling	4651
Diap2	5% BSA	1:1000	-20℃	Cell Signaling	5474
APC	5% BSA	1:1000	-20℃	Cell Signaling	2504
EB-1	5% BSA	1:1000	-20℃	Cell Signaling	2164
GSK-3β	5% BSA	1:1000	-20℃	Cell Signaling	9832
GAPDH	5% milk	1:1000	-20℃	Cell Signaling	5174

β-actin	5% milk	1:1000	-20℃	Cell Signaling	4970
p-Histone H2A.X	1% FBS	1:3333	4℃	EMD-Millipore	05-636
TUBB1	5% milk	1:1000	-20℃	Source Bio-science	SBS403514
Goat Anti-Mouse IgG/HRP	5% milk	1:4000	4℃	Dako	PO447
Goat Anti-Rabbit IgG/HRP	5% milk	1:4000	4℃	Dako	PO448
Alexa Flour® 488 F(ab')$_2$ fragment goat anti-mouse IgG	1% BSA	1:400	4℃	Invitrogen	A-11017

6.1.7 Software

All statistical analysis were conducted using GraphPad Prism 6. The DAVID bioinformatics resources 6.7 database was used to visualise functionally annotated MudPIT data. The Reactome database and Thermo Scientific's ProteinCenter software were also used for functional annotation. All visual statistics for the proteomics section (graphs, plots, etc.) were done using R statistics. Zeiss LSM 510 image browser was used to add appropriate scale bars to all confocal images obtained. FACS data were analysed using Beckman Coulter's Expo^{TM} 32 software.

6.2 Methods

6.2.1 Cell Culture

Cell culture was carried out aseptically in a BioMat^2 MDH Class II microbiological safety cabinet constituting a laminar flow system. The safety cabinet was swabbed with 70% IMS in dH_2O. All cell lines were passaged twice weekly upon reaching 80% confluency in order to maintain logarithmic cell proliferation. Cells were sub-cultured in 25 cm^2 and 75 cm^2 Corning and Costar tissue culture flasks with RPMI 1640 medium containing 0.3 g/L L-glutamine and 2 g/L sodium bicarbonate supplemented with 10% heat-inactivated FBS. The FBS was heat-inactivated by heating to approximately 56℃ for 1 h and either added immediately to RPMI 1640 medium or frozen in 50 ml aliquots. Upon sub-culturing, the medium was aspirated from the flask containing the cells and washed with 1 mL of PBS. Cells were then trypsinised with 1 mL of trypsin – EDTA 1X solution to detach the cells from the flask which was placed in the incubator for approximately 2 min. Fresh medium (5 ml) was added to neutralise the trypsin and re-suspend the cells. Cells were split at a 1:5 ratio in new flasks containing 7 ml of medium and placed in a Sanyo LEEC incubator at 37℃ in an atmosphere constituting 5% CO_2. The incubator also contained a tray of dH_2O to provide a humidified environment. All cells were initially taken from the cell bank containing liquid nitrogen and briefly incubated in 37℃ to thaw. Cells were then transferred from the cryovial into 25 cm^2 flasks with 10 ml of growth medium to allow growth. The newly revived cells were passaged

at least three times before experiemntal use. For long-term storage, cells were sub-cultured in 75 cm² flasks and allowed to reach approximately 80% confluence. They were detached using trypsin - EDTA 1X solution and suspended in sterile cryovials with 8% DMSO in FBS and subject to gradual cooling from -20℃ initially to -80℃ for 1-2 days and finally into the liquid nitrogen storage bank.

6.2.2   Compound Stock Solutions

Jerantinine A and B were provided in powdered form in bottled vials and reconstituted with the appropriate amount of DMSO to yield a concentration of 10 mM. Jerantinine A and B acetate were provided in oil form, bottled and reconstituted in the same manner as above. These vials were used as top stocks for subsequent experiments where dilutions were freshly prepared. Stocks were stored at -80℃ and protected from light in 10 μL aliquots to minimise freeze/thaw cycles. Vincristine (sulfate) was purchased and prepared in the same manner described above.

6.2.3   MTT Assay

The method used for this assay was adapted from Mosmann [218]. The MTT assay is colorimetric in nature and can be used to assess cell growth and viability, following treatment with therapeutic agents or toxic compounds. MTT (yellow) is reduced to a purple formazan in living cells by the activity of cellular enzymes, specifically mitochondrial dehydrogenases, and the intensity of the dye can be quantified by a spectrophotometer [218].

The assay is rapid, economical, and reproducible [219]. Cells harvested from cell culture were syringed through a 23 g (gauge) needle to attain a single cell suspension. The cells were counted and seeded at a density of 3 x 10^3 cells per well in a 96-well plate. The cells were suspended in 180 μl of RPMI 1640 tissue culture medium per well. The outer columns of the plate were filled with 300 μl of medium to minimise evaporation from experimental wells in addition to providing blank readings for the plate reader. Cells were additionally seeded in a time zero (t0) plate in the same manner as the experimental treatment plate. The cells were incubated overnight at 37℃ in a 5% CO_2 environment to allow for attachment. Cells were then treated with serial dilutions of various concentrations the following day. A volume of 20 μl of each dilution was added to respective treatment wells (total volume 200 μl) to yield final concentrations of 0.005 μM, 0.01 μM, 0.05 μM, 0.1 μM, 0.5 μM, 1 μM, and 5 μM. A separate DMSO control trial was done to ensure that it did not affect any of the results obtained. A volume of 20 μl from DMSO serial dilutions was added to two columns containing cells without any treatment. A t0 measurement was taken to obtain a measurement of cell viability at the time of treatment. Treated cells were incubated for 72 h at 37℃. After the treatment exposure period, 50 μl of MTT (concentration of 2 mg/mL in PBS) was added to each well and cells were incubated at 37℃ for 3-4 h. After incubation, all wells were carefully aspirated and 150 μl of DMSO was added to each well to solubilise formazan crystals. The plate was then placed in an orbital plate shaker for 2-3 min to aid formazan dissolution before obtaining the

absorbance reading at 555 nm on a Perkin Elmer Envision plate reader. All readings were recorded on an Excel spreadsheet supplied by the Wallac Envision® software. Resultant curves and GI_{50} calculations were obtained from GraphPad Prism.

6.2.4 Generating Vincristine and Jerantinine A-resistant HCT-116 cells

Vincristine- and jerantinine A-resistant HCT-116 cell lines were generated in the Centre for Biomolecular Sciences (CBS) using the aforementioned parent HCT-116 cells. HCT-116 cells were initially subbed into 25 cm^2 flasks and allowed to grow to approximately 80% confluence. Cells were then treated with GI_{50} values obtained from the MTT assay. Media were frequently changed every 3-4 days with the addition of compounds. Subsequently increasing concentrations from 5 nM up to 2 μM were used once cells were observed to have grown back to approximately 80-90% confluence. Cells were maintained at a final concentration of 2 μM thereafter.

6.2.5 Clonogenic Assay

The clonogenic assay was once considered the "gold standard" of cell sensitivity assays and originated from the evaluation of radiosensitivities of tumour cells *in vitro* [220]. It was thought that only a clonogenic assay was sensitive enough to detect cell kill at low percentage survivals (<1%). More specifically, it measures the ability of a single cell to survive a brief exposure to the test agent and maintain proliferative potential to form

colonies. The duration it takes for the cells to form colonies is comparable to recovery time. Furthermore, cytotoxic and cytostatic effects can be distinguished from each other after only a brief exposure to the test agent. This assay was used in addition to the MTT assay as an initial screen in this study.

Cells were counted using a haemocytometer and approximately 250-350 cells (depending on the cell line) were seeded per well in 6-well plates with 2 ml of medium. Cells were allowed to attach for 24 h. The cells were then treated using the GI_{50} values obtained from the MTT assays i.e. 1 x GI_{50} and 2 x GI_{50}. Cells in control wells were treated with vehicle (medium) alone. Following 24 h exposure to Jerantinine A, medium was aspirated along with the compound. Wells were washed 2 x with 1 ml of PBS and 2 ml of fresh medium was added to each well. Plates were placed in the incubator at 37℃ and inspected daily until cells in control wells formed colonies of $\geq$ 50 cells. The cells were washed with PBS before fixation with 100% methanol (0.5 ml) for 15 min and then stained with 0.7 ml of 0.5% methylene blue (1:1 water:methanol) for an additional 10 min. Colonies were counted and recorded graphically using GraphPad Prism.

6.2.6 Flow Cytometry

Flow cytometry is a powerful tool primarily used to measure properties of individual particles. Cells are analysed one at a time made possible through hydrodynamic focusing. Beams of light pass through each cell and are scattered in two distinct ways: forward scatter and side scatter. Forward

scatter (FSC) is an indication of the size of the cell and side scatter (SSC) depicts the granularity of the cell. Cumulatively, this data is represented as a dot plot of FSC versus SSC and allows for the estimation of viable cell fractions. Appropriate gates are set up and dependent upon the type of assay performed.

6.2.6.1   Cell Cycle Analysis

Cell cycle analysis was carried out using a method based on Nicoletti *et al* (1991) [221]. PI is an intercalating DNA dye that fluoresces strongly when bound to DNA. The DNA content of an individual cell is proportional to the fluorescence intensity of exited PI (excited by an argon laser at 488 nm). A histogram of DNA content of cells in a population can be used to derive the percentage of cells in each phase (pre-G1, G_1/G_0, S, and G_2/M) of the cell cycle and any perturbations caused by the tests compounds. PI is normally excluded by intact cells that need to be permeabilised via the use of a gentle detergent/hypotonic solution to allow PI entry into these cells.

Cells were seeded in 6-well plates at the following densities in 2 ml of medium and treated for the respective time exposures: A seeding density of 1×10^5 cells was used for 24 h and 48 h treatment exposures in all cell lines, whereas a lower seeding density of 5×10^4 cells in all cell lines for 72 h treatments was optimal to maintain logarithmic growth.

Following treatment, medium containing any floating cells was pipetted into labelled FACS tubes and kept on ice. Cells were trypsinised and once

detached pooled together with medium and then pelleted in a Beckman Coulter Allegro centrifuge at 1200 rpm for 5 min at 4℃. The supernatant was discarded and the pellet broken up by gently flicking the tube. The cells were re-suspended in 0.3-0.5 ml of fluorochrome solution and stored overnight in the dark at 4℃. A single cell suspension was achieved by gently passing the cells through a 23 g needle immediately prior to analysis on a Coulter Epics XL-MCL^{TM} flow cytometer. Appropriate gates were set up relative to the control and data stored for further statistical analyses.

6.2.6.2 Annexin V-FITC and Propidium Iodide Apoptosis Assays

One of the events triggered in early stage apoptosis involves the "flipping" of phosphatidyl serine (PS) from the inner to the outer leaflet of the cell membrane. At this stage, cells still retain membrane integrity, a fact that can be exploited to distinguish between early and late apoptosis/necrosis, where membranes have become compromised [150]. Annexin V is a small protein that binds to PS with high affinity. PI is also used to stain DNA and can be used as an indicator of cell membrane integrity. Combining fluorescently labelled Annexin V with PI allows discrimination of healthy cells (annexin V – FITC negative, PI negative) from early apoptotic cells (annexin V – FITC positive, PI negative) or late apoptotic/necrotic cells (annexin V- FITC positive, PI positive) [151].

Cells were seeded and harvested in the same manner described in section 7.2.5.1. After pelleting the cells, the supernatant was discarded, pellets

gently broken up by agitation and re-suspended in 2 ml of cold medium and kept on ice for 10 min to recover from any damage caused by trypsin. PBS (1 ml) was added to each tube and pelleted again at 1200 rpm for 5 min at 4℃. The supernatant was discarded, ensuring all the PBS had been removed and the pellet broken up by gentle flicking of the tube. Annexin binding buffer (100 μL; 1 x) was added to each tube followed by addition of 5 μl of Annexin V-FITC. Tubes were briefly vortexed and left at room temperature in the dark for approximately 15 min. Annexin binding buffer (400 μL; 1 x) and 10 μl of PI solution were added to each tube. Tubes were vortexed and kept on ice in the dark for 10 min prior to analysis on the flow cytometer. Samples were analysed within 1 h of completion of the above protocol to avoid deterioration of cells. Gates were set up on a dual colour plot for vehicle treated samples and the percentages of early apoptotic cells (annexin V – FITC positive, PI negative) or late apoptotic/necrotic cells (annexin V – FITC positive, PI positive) recorded.

6.2.6.3 Assessing DNA Damage using Flow Cytometry

DNA double-strand breaks (DSBs) are lesions that contribute to genomic instability and can lead to cancer. Paradoxically, DSBs can also cause cancer cell death [222]. H2AX is a key histone protein involved in recognition of DNA DSBs [223]. As DSBs occur, H2AX undergoes rapid phosphorylation to form γH2AX which in turn recruits and localises DNA repair proteins. The appearance of γH2AX foci represent DSBs in a 1:1 manner and can be used as a biomarker for DNA damage [223]. These foci are quantified by

fluorescence using primary γH2AX and fluorescently conjugated secondary antibodies [223].

Cells were seeded at a density of $1\text{-}1.5\text{x}10^6$ in 10 cm^2 dishes and allowed to adhere for 24 h at 37℃. Test agents were added along with fresh medium at desired concentrations. Following treatment, media/floating cells were decanted into labelled FACS tubes (12x75 mm). A ml of trypsin (1x) was added after washing cells with 1 ml of PBS, and incubated at 37℃ until detached. Cells were flushed from the bottom of the petri dish, added to respective FACS tubes, and pelleted in a centrifuge at 1300 rpm for 10 min at room temperature. Supernatant was aspirated leaving a small amount at the bottom of the tube to avoid disturbing the pellet. Pellets were resuspended by gently flicking the tubes.

Note: Repetitions of the above three steps will be referred to SAR (**S**pin - **A**spirate - **R**esuspend) when required again.

This process was then repeated after adding 1 ml of PBS. Cells were fixed in a vented class II cabinet by adding 500 μl of 1% methanol-free formaldehyde in PBS and pipetted up and down several times to ensure a single cell suspension. Following a 5 min incubation at room temperature, cells were permeabilised by adding 500 μl of Triton-X-100 in PBS and mixed gently. Cells were allowed to sit at room temperature for 1 min and subjected to a SAR cycle. Cells were resuspended with 1 ml of 1% FBS in PBS, gently mixed, and incubated at room temperature for 30 min (same day analysis) or stored at 4℃ for up to 1 week for convenient analysis. Cells were then subjected to a SAR cycle. Primary antibody (γH2AX

antibody was prepared using a 1:3333 dilution in 1% FBS in PBS) was added to each sample (200 μl), mixed gently, and allowed to incubate for 1.5 h at room temperature. Following incubation, cells were once again subjected to a SAR cycle after addition of 1 ml of PBS to each sample. Secondary antibody (goat anti-mouse Alexa Fluor 488, prepared using a 1:1750 dilution in 1% FBS in PBS to a final concentration of 1 μg/ml) was added to each sample, were mixed gently, and incubated for 1 h at room temperature in the dark. A last SAR cycle was carried out after addition of 1 ml of PBS. For concurrent cell cycle analysis, cells were resuspended in 300 μl of 50 μg/ml propidium iodide/ 0.1 mg/ml RNAse A in PBS and incubated for at least 10 min at room temperature before analysis on a Beckman Coulter Cytomics FC 500 MCL flow cytometer.

6.2.7   Tubulin Polymerisation Assay

The tubulin polymerisation assay is based on an adaptation of the original method of Shelanski et al. and Lee et al , which demonstrated that there is a proportional relationship between light scatter and concentration of microtubule polymer [224, 225]. Absorption spectral data in the form of polymerisation curves reveal three distinct phases of microtubule polymerisation: nucleation, growth, and steady state equilibrium. Compounds that interfere with tubulin polymerisation will affect one or more of these phases. Therefore, this assay can be used to identify novel antimitotic (or antimicrotubule) agents. Instructions for reconstituting the general tubulin buffer (PEM), guanosine triphosphate (GTP) were followed prior to begin-

ning the assay. The appropriate absorbance (340 nm) and temperature (37 ℃) settings for the Perkin Elmer Vision plate reader were also set prior to beginning the assay in order to maximise polymerisation activity. The plate reader was set to kinetic mode measuring 61 cycles of 1 reading per minute.

PEM (500 μl; required for tubulin ligand dilutions) was warmed to room temperature. The test compounds (paclitaxel and jerantinine A) were then diluted with PEM to yield final concentrations of 5 μM and 10 μM. Cold G-PEM minus glycerol buffer was made to re-suspend the tubulin and kept on ice for approximately 3 min. Paclitaxel and jerantinine A (10 μl) concentrations in addition to G-PEM buffer (control) were pipetted into their respective wells on a microtiter plate and placed in the incubator for 2 min at 37 ℃. Tubulin (100 μl) was added and pipetted into the wells containing the test compounds and immediately placed into the plate reader to obtain absorbance data. Data were recorded in an excel spreadsheet supplied by the Wallac Envision software and graphed using GraphPad Prism 6.

6.2.8 Confocal Microscopy

HCT-116 cells were seeded eight-well μ-slides (Ibidi Germany, Catalogue No.: 80826) and were allowed to adhere for 24 h at 37℃ before treatment with test agents for an additional 24 h. Cells were then fixed with formaldehyde (3.7% in PBS) and incubated at room temperature for 10-15 min before permeabilisation using PBT (PBS + 0.1% Triton-X-100).

Following incubation for 2-3 min at room temperature, cells were blocked using PBT + 1% BSA for 1 h to prevent non-specific binding of labelled antibodies. Cells were then incubated with 1° Ab (monoclonal anti α-tubulin antibody; 1:200 dilution; excited by the 488 nm blue laser) for 2 h at room temperature before being washed with PBT and incubated with the appropriate fluorescent 2° Ab (1:400 dilution) at room temperature in the dark for 1 h. After washing with PBT, cells were incubated with DRAQ5 (1:3000 dilution; excited by the 633 nm far red laser), a cell permeant DNA binding dye, at room temperature for 5 min in the dark. Images were captured on a Zeiss LSM510 Meta confocal microscope.

6.2.9 Kinase Assay

In vitro kinase inhibition assay for compounds was examined using a radiometric assay employed by Millipore kinaseProfiler service. Kinases (5-20 mU diluted in 50 mM Tris pH 7.5, 0.1 mM EGTA, 0.1% β-mercaptoethanol, 1 mg/ml BSA, 100 μM vanadate) were assayed against appropriate substrate peptide in a final volume of 25.5 μl containing 50 mM Tris pH 7.5,0.05% β-mercaptoethanol, 10 μM vanadate, 300 μM substrate peptide, 10 mM magnesium acetate and 0.005 mM [33P-γ-ATP] (50-1000 cpm/pmole) and incubated for 30 min at room temperature. 1 μM of JA was used to test for the presence of inhibitory activity. Assays were stopped by addition of 5 μl of 0.5 M (3%) orthophosphoric acid and then harvested onto P81 Unifilter plates with a wash buffer of 50 mM orthophosphoric acid.

6.2.10 Western Blotting Analysis

6.2.10.1 Preparation of cell lysates

Cells were seeded at a density of 1×10^6 and allowed to grow for 24 h. Test agents were then added for the desired duration. Following treatment, growth medium was collected in universal tubes and placed on ice. All plates were washed with ice cold PBS (10 ml). After aspiration, 300 μl of ice-cold lysis buffer was added to each plate. Cells were then scraped using a cell scraper and pooled into labelled 1.5 ml eppendorf tubes and placed on ice for 25 min. Universals containing media/floating cells were centrifuged at 1200 rpm for 5 min at 4 ℃. Supernatant was aspirated and cells were resuspended with ice cold PBS (5 ml) and centrifuged as before. PBS was aspirated, and cells were resuspended with 100 μl of lysis buffer and added to their respective eppendorf tubes. After centrifugation (13300 rpm for 10 min at 4 ℃) supernatant was collected in new labelled eppendorf tubes and the pellets were discarded. Cell lysates were stored at -20 ℃.

6.2.10.2 Determining protein concentration

Protein concentrations were determined using the Bradford reagent first described by M. Bradford [226]. It is a colourimetric assay based on an absorbance shift of the Coomassie Brilliant Blue G-250 dye from 465 nm to 595 nm. The amount of complexes that form between the protein's tertiary structure and the dye is proportional to the intensity of the dye which can be measured by obtaining an absorbance reading, thus yielding

an estimation of protein concentration.

Lysate (10 μl) sample was added to three wells containing 150 μl of Bradford reagent. After a 15 min development time, the absorbances were read at 595 nm. A standardised curve was constructed using BSA at concentrations ranging from 0-1 mg/ml and subsequently used to obtain estimated protein concentrations from acquired absorbances.

6.2.10.3   SDS-PAGE

Sodium dodecyl sulphate polyacrylamide gel electrophoresis (SDS-PAGE) was used to separate proteins in lysates acording to size. Polyacrylamide gels of different percentages (7.5-15%) were prepared depending on the molecular weight of the protein to be detected. Protein gels consisted of two phases: the lower resolving gel for separation and the upper stacking gel for loading. Appropriate volumes of acrylamide/bis-acrylamide, resolving buffer, and distilled water were mixed together depending on gel percentage. Polymerisation was initiated by adding 1 μl of TEMED and 4.5 μl of 10% AMPS per ml of gel and were allowed 30 min to polymerise. Isopropanol was immediately added to avoid any air bubbles after pouring the resolving gel into the cassette. The stacking gel was poured after washing off isopropanol with dH_2O. The stacking gel percentage was 4% and was formed by mixing 0.67 ml acrylamide stock, 0.63 ml of stacking buffer, and 3.7 ml of dH_2O. 3 μl of TEMED and 6 μl of 10% AMPS per ml of gel was added to initiate polymerisation. A comb was immediately inserted to create loading wells. Cell lysates containing a total of 50 μg was

mixed with loading buffer and denatured at 95 ℃ for 5 mins. Cassettes were inserted into an electrophoretic tank filled with running buffer during this time. After heating, samples were then loaded into wells along with a PageRuler Plus Prestained Protein Ladder (5 μl) to serve as a molecular marker and proteins were separated at a voltage of between 60-150 V. Electrophoresis was run for 1.5 h and the gel containing the separated proteins was removed and immersed in transfer buffer.

6.2.10.4   Immunoblotting

The proteins separated by SDS-PAGE were then electro-blotted onto nitrocellulose membranes previously soaked in transfer buffer. The membrane and the gel were sandwiched between 8 blot papers that were also previously soaked in transfer buffer before commencing with semi-dry transfer at 25 V for 1.5 h in a transfer machine. Gels were later discarded and the membranes were blocked in 5% dried non-fat milk in TBST for 1 h at room temperature with gentle shaking to prevent non-specific protein binding. After blocking, membranes were incubated with the primary antibody at 4 ℃ overnight. Membranes were washed with TBST the following day for 30 min to remove residual primary antibody (TBST was discarded and replaced with fresh TBST every 10 min for a total of 30 min). Membranes were then incubated with the appropriate horseradish peroxidase (HRP) conjugated secondary antibody (depending on the source of the primary antibody) for 1 h at room temperature. After incubation, membranes were washed for 30 min with TBST replaced every 10 min.

6.2.10.5 Enhanced chemiluminescence detection

The protein of interest on the membrane was detected by applying Amersham ^{TM} ECL ^{TM} Western blotting detection reagents following manufacturer's instructions. After removal of excess reagent, the membrane was exposed to high performance chemiluminescence film in the dark room for appropriate exposure time. The film was then developed by insertion into developer solution until bands were observed under red light. Following a quick wash (in running water), the film was fixed in fixer solution for approximately 2 min and air-dried after an additional wash to remove excess solution.

6.2.11 Caspase 3/7 Assay

Caspase 3/7 activity was assayed according to the Apo-ONE homogeneous Caspase 3/7 kit instructions supplied by Promega. Cells were seeded at a density of 1 x 10^4 in 96-well plates and incubated at 37 ℃, 5% CO_2 before introduction of test agents. Compound concentrations of GI_{50} were used for a 48 h exposure. After treatment, Apo-ONE caspase 3/7 reagent (caspase substrate + Apo-ONE caspase 3/7 buffer) was added to each well (100 μl) and mixed on a plate shaker for 1 min. Fluorescence was measured following a 30 min incubation at room temperature at an excitation wavelength of 485 nm and an emission wavelength of 530 nm using EnVision multilabel plate reader (Perkin Elmer). The amount of fluorescent product generated is proportional to the amount of caspase 3/7 present in the well.

6.2.12   ROS-Glo^{TM} H$_2$O$_2$ Assay

Levels of reactive oxygen species (ROS) were measured as per the kit instructions supplied by Promega. ROS generated in cells can act as signalling molecules and in excess can cause cell damage or death [227]. H$_2$O$_2$ is one of many ROS that can be generated in cell cultures or enzyme reactions and is convenient to use as it possesses the longest half-life of all ROS in cultured cells. Additionally various ROS can be converted to H$_2$O$_2$ within cells. Therefore, changes in H$_2$O$_2$ reflect a general change in ROS levels. The assay utilises a luciferin precursor which is produced as a biproduct from the reaction of the H$_2$O$_2$ substrate and H$_2$O$_2$ itself. The precursor is converted to luciferin after addition of a detection agent containing D-cysteine generating a luminescent signal proportional to H$_2$O$_2$ concentration.

Cells were seeded at a density of 5 x 10^3 in 70 μl of medium per well and allowed to attach overnight for 24 h in white-walled 96-well plates. Test agent or vehicle (10 μl) was added to respective wells for an additional 24 h. The H$_2$O$_2$ substrate was added for the final 6 h of the treatment. Upon terminating treatment, a 100 μl of ROS-Glo^{TM} Detection solution was added to each well and samples were incubated for 20 min at room temperature. Relative luminescence units (RLU) were recorded using a Perkin Elmer plate reader.

6.2.13 Proteomics

Liquid Chromatography-tandem mass spectrometry (LC-MS/MS) has been subject to exponential growth in clinical laboratories during the last 10-15 years [228]. Furthermore, it has become a powerful technology in proteomics studies in drug discovery, including target protein characterization and discovery of biomarkers [229]. Proteome analysis was conducted using Multidimensional Protein Identification Technology (MudPIT). MudPIT separates peptides in 2D liquid chromatography and allows greater separation of peptides that can be directly interfaced with the ion source of a mass spectrometer, which maximizes sensitivity. Mass spectra of fragmented ions from peptides can then be used to identify proteins from online databases.

Cells were seeded at a density of 5 x 10^6 and treated with test agent for desired time exposures. Upon termination of treatment, cells were scraped in ice-cold PBS and centrifuged at 2000 g for 10 min at 4℃. The pellet was resuspended in 50% (v/v) trifluoroethanol (TFE) in PBS (pH 7.4). Cells were subjected to 5 freeze/thaw cycles followed by 7 cycles of sonication lasting 30 seconds each to aid lysis. Proteins in cellular lysates were denatured by heat via incubation at 60 ℃ for 2 h. Subsequently, cysteines were reduced by addition of DTT to a final concentration of 5 mM and incubated for an additional 30 min at 60 ℃. Reduced cysteines were alkylated using IAA (final concentration of 25 mM) by incubating in the dark for 30 min at room temperature. Upon completion, samples were diluted 5x using 100 mM ammonium bicarbonate (pH 8.0). Proteins in the lysate were digested

into peptides using mass spectrometry grade trypsin and proteolysis was allowed overnight at 37 ℃.

Following digestion, samples were centrifuged at 12,000 relative centrifugal force (rcf) for 10 min at room temperature. The supernatant was enriched for peptides using C18 based reverse phase STAGE tips. Peptides were eluted from the reverse phase using 80% acetonitrile and captured on a SCX based stage tip. Bound peptides were eluted in six steps, with each step increasing in pH. Buffers for the six steps were: steps 1-5 (50, 75, 125, 200, 300 mM) ammonium acetate, 20% (v/v) acetonitrile with 0.5% (v/v) formic (methanoic) acid. The last step consisted of elution with 5% (v/v) ammonium hydroxide in 80% (v/v) acetonitrile.

Peptides from all fractions were dried using vacuum centrifugation and resuspended in 10 μl of HPLC grade water with 0.1% formic acid. Hence, six SCX based fractions were produced for each fraction. All 10 μl of peptides for each fraction were injected using an Easy LC 1000 nano flow, liquid chromatography system. Peptides were separated on a 50 cm C18 based reverse phase EasySpray column and analysed on a Thermo Scientific Orbitrap XL to obtain tandem mass spectrometry data.

The collected data were searched using MaxQuant (Version 1.5.2.8) and uniprot human fasta was used for protein sequences. Target-decoy was used for controlling false discovery of peptides and set to 1%. All protein groups were filtered to contain two peptides or more for further analysis.

6.2.14 Statistical Analysis

All experiments were repeated at least three times with representative experiments being selected for figures. Statistical differences between groups were assessed using a two-way ANOVA unless stated otherwise and expressed as mean or mean $\pm$ SD. Dunnett's multiple comparisons test was used to assess significance, defined in this study as a p-value < 0.05.

Bibliography

[1] The Mayo Clinic. Diseases and conditions: Cancer. *URL: http://www.mayoclinic.org/diseases-conditions/cancer/basics /definition/con-20032378*, Accessed: March 23, 2015.

[2] Cancer Research UK. World cancer factsheet. *Cancer Research UK*, 2014.

[3] R.A. Weinberg. *The Biology of Cancer*. 2007.

[4] World Health Orgnisation. Cancer. *URL: http://www.who.int/ mediacentre/factsheets/fs297/en/*, Accessed: March 29, 2015.

[5] National Cancer Institute. Cancer causes and risk factors. *URL: http://www.cancer.gov/cancertopics/causes*, Accessed March 29, 2015.

[6] C.M. Croce. Oncogenes and cancer. *The New England Journal of Medicine*, 358(5):502–11.

[7] L.R. Finger, R.C. Harvey, R.C.A. Moore, L.C. Showe, and C.M. Croce. A common mechanism of chromosomal translocation in t- and b-cell neoplasia. *Science*, 234:982–985, 1986.

[8] M.J. Berardi and V.R Fantin. Survival of the fittest: metabolic adaptations in cancer. *Current Opinion in Genetics & Development*, 21:59–66, 2011.

[9] H. Chial. Proto-oncogenes to oncogenes to cancer. *Nature Education*, 1(1):33, 2008.

[10] D. Hanahan and R.A. Weinberg. The hallmarks of cancer. *Cell*, 100:57–70, 2000.

[11] D. Hanahan and R.A. Weinberg. Hallmarks of cancer: The next generation. *Cell*, 144:646–674, 2011.

[12] N. Cheng, A. Chytil, Y. Shyr, A Joly, and H.L. Moses. Transforming growth factor-beta signaling-deficient fibroblasts enhance hepatocyte growth factor signaling in mammary carcinoma cells to promote scattering and invasion. *Molecular Cancer Research*, 6:1521–1533, 2008.

[13] N.A. Bhowmick, E.G. Neilson, and H.L. Moses. Stromal fibroblasts in cancer initiation and progression. *Nature*, 432(7015):332–337, 2004.

[14] N. Bardeesy and N.E. Sharpless. Ras unplugged: Negative feedback and oncogene-induced senescence. *Cancer Cell*, 10(6):451–453, 2006.

[15] M.A. Davies and Y. Samuels. Analysis of the genome to personalize therapy for melanoma. *Oncogene*, 29(41):5545–5555, 2010.

[16] I.A. Prior, P.D. Lewis, and C. Mattos. A comprehensive survey of ras mutations in cancer. *Cancer Research*, 72(10):2457–2467, 2012.

[17] M. Collado and M. Serrano. Senescence in tumours: evidence from mice and humans. *Nature Review Cancer*, 10(1):51–57, 2010.

[18] C.J. Sherr and F. McCormick. The rb and p53 pathways in cancer. *Cancer Cell*, 2(2):103–112, 2002.

[19] Eric Wong. Introduction to neoplasia. *McMaster Pathophysiology Review. URL: http://www.pathophys.org/introneoplasia/*, Accessed March 31, 2015.

[20] S.K. Das, T. Hashimoto, K. Shimizu, T. Yoshida, T. Sakai, Y. Sowa, A. Komoto, and K. Kanazawa. Fucoxanthin induces cell cycle arrest at g0/g1 phase in human colon carcinoma cells through up-regulation of p21waf1/cip1. *Biochimica et Biophysica Acta*, 1726(3):328–335, 2005.

[21] S. Polager and D. Ginsberg. p53 and e2f: Partners in life and death. *Nature Review Cancer*, 9(10):738–748, 2009.

[22] B. Vogelstein, S. Sur, and C. Prives. p53 : The most frequently altered gene in human cancers. *Nature Education*, 3(9):6, 2010.

[23] J.M. Adams and S. Cory. The bcl-2 apoptotic switch in cancer development and therapy. *Oncogene*, 26(9):1324–1337, 2007.

[24] S.W. Lowe, E. Cepero, and E. Gerard. Intrinsic tumour suppression. *Nature*, 432:307–315, 2004.

[25] A. Almasan and A. Ashkenazi. Apo2l/trail: apoptosis signaling, biology, and potential for cancer therapy. *Cytokine & Growth Factor Reviews*, 14(3-4):337–348.

[26] SABiosciences. Cellular apoptosis pathway. *URL: http://www.sabiosciences.com/images/Cellular_Apoptosis_Pathway_680.gif*, Accessed April 1, 2015.

[27] D.L. Burkhart and J. Sage. Cellular mechanisms of tumour suppresion by the retinoblastoma gene. *Nature Review Cancer*, 8:671–682, 2008.

[28] T.R. Wilson, P.G. Johnston, and D.B. Longley. Anti-apoptotic mechanisms of drug resistance in cancer. *Current Cancer Drug Targets*, 9(3):307–319, 2009.

[29] N. Ghebranious and L.A. Donehower. Mouse models in tumour suppression. *Oncogene*, 17:3385–3400, 1998.

[30] A.B. Maria. Telomeres and human disease: ageing, cancer and beyond. *Nature Reviews Genetics*, 6(8):611–622, 2005.

[31] J.W. Shay and W.E. Wright. Hayflick, his limit, and cellular ageing. *Nature Reviews Molecular and Cellular Biology*, 1(1):72–76, 2000.

[32] J.W. Shay, Y. Zou, E. Hiyama, and W.E. Wright. Telomerase and cancer. *Human Molecular Genetics*, 10(7):677–685, 2001.

[33] S.E. Artandi and R.A. DePinho. Telomeres and telomerase in cancer. *Carcinogenesis*, 31:9–18, 2010.

[34] A. Hoeben, B. Landuyt, M.S. Highley, H. Wildiers, A.T. Van Oosterom, and E.A. De Bruijn. Vascular endothelial growth factor and angiogenesis. *Pharmacological Reviews*, 56(4):549–580, 2004.

[35] D. Hanahan and J. Folkman. Patterns and emerging mechanisms of angiogenic switch during tumourigenesis. *Cell*, 86(3):353–364, 1996.

[36] J.A. Nagy, S.H. Chang, S.C. Shih, A.M. Dvorak, and H.F. Dvorak. Heterogeneity of the tumor vasculature. *Seminars in Thrombosis and Hemostasis*, 36(3):321–331, 2010.

[37] P. Baluk, H. Hashizume, and D.M. McDonald. Cellular abnormalities of blood vessels as targets in cancer. *Current Opinion in Genetics and Development*, 15(1):102–111, 2005.

[38] J. Rak, Y. Mitsuhashi, L. Bayko, J. Filmus, S. Shirasawa, T. Sasazuki, and R.S. Kerbel. Mutant ras oncogenes upregulate vegf/vpf expression: implications for induction and inhibition of tumor angiogenesis. *Cancer Research*, 55(20):4575–4580, October 1995.

[39] T.A. Baudino, C. McKay, H. Pendeville-Samain, J.A. Nilsson, K.H. Maclean, E.L. White, A.C. Davis, J.N. Ihle, and J.L. Cleveland. c-myc is essential for vasculogenesis and angiogenesis during development and tumor progression. *Genes and Development*, 16(19):2530–2543, October 2002.

[40] SABiosciences. Vegf pathway. *URL: http://www.sabiosciences.com/ images/VEGF_Pathway_680.gif*, Accessed April 7, 2015.

[41] G. Berx and F. van Roy. Involvement of members of the cadherin superfamily in cancer. *Cold Spring Harb. Perspect Biol.*, 1(6):a003129, December 2009.

185

[42] U. Cavallaro and G. Christofori. Cell adhesion and signalling by cadherins and ig-cams in cancer. *Nature Review Cancer*, 4(2):118–32, 2004.

[43] M.W. Klymkowsky and P. Savagner. Epithelial-mesenchymal transition: a cancer researcher's conceptual friend and foe. *American Journal of Pathology*, 174(5):1588–93, 2009.

[44] I. Stamenkovic. Matrix metalloproteinases in tumor invasion and metastasis. *Semin Cancer Biol.*, 10(6):415–33, 2000.

[45] K. Kessenbrock, V. Plaks, and Z. Werb. Matrix metalloproteinases: regulators of the tumor microenvironment. *Cell*, 141(1):52–67, 2010.

[46] L. Wan, K. Pantel, and Y. Kang. Tumor metastasis: moving new biological insights into the clinic. *Nature Medicine*, 19:1450–1464, 2013.

[47] L.M. Coussens and Z. Werb. Inflammation and cancer. *Nature*, 420(6917):860–867, December 2002.

[48] S. Rakoff-Nahoum. Why cancer and inflammation? *Yale Journal of Biological Medicine*, 79(3-4):123–130, December 2006.

[49] C.M. Ulrich, J. Bigler, and J.D. Potter. Non-steroidal anti-inflammatory drugs for cancer prevention: promise, perils and pharmacogenetics. *Nature Review Cancer*, 6(2):130–140, 2006.

[50] H.F. Dvorak. Tumors: wounds that do not heal. similarities between tumor stroma generation and wound healing. *New England Journal of Medicine*, 315:1650–1659, 1986.

[51] S. Ohnishi, N. Ma, R. Thanan, S. Pinlaor, O. Hammam, M. Murata, and S. Kawanishi. Dna damage in inflammation-related carcinogenesis and cancer stem cells. *Oxidative Medicine and Cellular Longevity*, 2013(Article ID 387014):1–9, 2013.

[52] N. Azad, Y. Rojanasakul, and V. Vallyathan. Inflammation and lung cancer: roles of reactive oxygen/nitrogen species. *J Toxicol Environ Health B Crit Rev.*, 11(1):1–15, 2008.

[53] M Karin. Nf-κb as a critical link between inflammation and cancer. *Cold Spring Harb Perspect Biol.*, 1(5):a000141, November 2009.

[54] B. Hoesel and J.A. Schmid. The complexity of nf-κb signaling in inflammation and cancer. *Molecular Cancer*, 12(86):1–15, 2013.

[55] S. Keerthivasan, K. Aghajani, M. Dose, L. Molinero, M.W. Khan, V. Venkateswaran, C. Weber, A.O. Emmanuel, T. Sun, D.J. Bentrem, M. Mulcahy, A. Keshavarzian, E.M. Ramos, N. Blatner, K. Khazaie, and F. Gounari. β-catenin promotes colitis and colon cancer through imprinting of proinflammatory properties in t cells. *Sci Transl Med.*, 6(225):225ra28.

[56] G. Trinchieri. Where cancer and inflammation intersect. *URL: http://www.the-scientist.com/?articles.view/ articleNo/30710/title/Where-Cancer-and-Inflammation-Intersect/*, (30710), 2011.

[57] S. Negrini, V.G. Gorgoulis, and T.D. Halazonetis. Genomic instability — an evolving hallmark of cancer. *Nature Reviews: Molecular Cell Biology*, 11, March 2010.

[58] Z. Shen. Genomic instability and cancer: an introduction. *Journal of Molecular Cell Biology*, 3(1):1–3, 2011.

[59] J.R. Cantor and D.M. Sabatini. Cancer cell metabolism: One hallmark, many faces. *AACR: Cancer Discovery*, 2(10):881–898, 2012.

[60] R.A. Cairns, I.S. Harris, and T.W. Mak. Regulation of cancer cell metabolism. *Nature Reviews*, 11:85–95, February 2011.

[61] O. Warburg. On the origin of cancer cells. *Science*, 123:309–314, 1956.

[62] C. Barron, E. Tsiani, and T. Tsakiridis. Expression of the glucose transporters glut1, glut3, glut4 and glut12 in human cancer cells. *BMC Proceedings*, 6(3):4, 2012.

[63] R.A. Medina and G.I. Owen. Glucose transporters: expression, regulation and cancer. *Biological Research*, 35(1):9–26, 2002.

[64] R.L. Elstrom, D.E. Bauer, M. Buzzai, R. Karnauskas, M.H. Harris, D.R. Plas, H. Zhuang, R.M. Cinalli, A. Alavi, C.M. Rudin, and C.B. Thompson. Akt stimulates aerobic glycolysis in cancer cells. *Cancer Research*, 64(11):3892–9, June 2004.

[65] Y. Fan, K.G. Dickman, and W.X. Zong. Akt and c-myc differentially activate metabolic programs and prime cells to bioenergetic inhibition. *Journal of Biological Chemistry*, 285:7324–7333, 2010.

[66] L.B. Sullican and N.S. Chandel. Mitochondrial reactive oxygen species and cancer. *Cancer and Metabolism*, 2(17):1–12, 2014.

[67] M.R. Ramsey and N.E. Sharpless. Ros as a tumour suppressor? *Nature Cell Biology*, 8:1213–1215, 2006.

[68] O.J. Finn. Immuno-oncology: understanding the function and dysfunction of the immune system in cancer. *Annals of Oncology*, 23(8):viii6–viii9, 2012.

[69] G. Bindea, B. Mlecnik, W.H. Fridman, F. Pages, and J. Galon. Natural immunity to cancer in humans. *Curr. Opin. Immunol.*, 22:215–222, 2010.

[70] Genentech. The cancer immunity cycle: the body's natural protection against cancer. *URL: http://www.biooncology.com/research-education/cancer-immunotherapy*, Accessed April 16, 2015.

[71] The 'trojan horse' approach to tumor immunotherapy: targeting the tumor microenvironment. *Journal of Immunology Research.*, 2014(Article ID:789069):1–14, 2014.

[72] S. Ostrand-Rosenberg and P. Sinha. Myeloid-derived suppressor cells: linking inflammation and cancer. *Journal of Immunology*, 182:4499–4506, 2009.

[73] D. Mougiakakos, A. Choudhury, A. Lladser, R. Kiessling, and C.C. Johansson. Regulatory t cells in cancer. *Adv. Cancer Res.*, 107:57–117, 2010.

[74] A. Urruticoechea, R. Alemany, J. Balart, F. Villanueva, F. Vinals, and G. Capella. Recent advances in cancer therapy: An overview. *Current Pharmaceutical Design*, 16:3–10, 2010.

[75] R.E. Pollock and D.L. Morton. Principles of surgical oncology. *Holland-Frei Cancer Medicine*, (6th Edition):Chapter 38.

[76] J. Figueras, J. Torras, C. Valls, L. Llado, E. Ramos, J. Marti-Rague, T. Serrano, and J. Fabregat. Surgical resection of colorectal liver metastases in patients with expanded indications: a single-center experience with 501 patients. *Dis. Colon. Rectum*, 50(4):478–88, 2007.

[77] B. Ohlsson, U. Stenram, and K.G. Tranberg. Resection of colorectal liver metastases: 25-year experience. *World J. Surg.*, 22(3):268–76, 1998.

[78] T.S. Lawrence, R.K. Ten Haken, and A. Giaccia. Cancer: Principles and practice of oncology. 8th Edition(Publisher: Lippincott Williams and Wilkins, Philadelphia), 2008.

[79] G. Delaney, S. Jacob, C. Featherstone, and M. Barton. The role of radiotherapy in cancer treatment: estimating optimal utilization from a review of evidence-based clinical guidelines. *Cancer*, 104(6):1129–37, 2005.

[80] Y. Matsui, Y. Tsuchida, and P.C. Keng. Effects of p53 mutations on cellular sensitivity to ionizing radiation. *Am. J. Clin. Oncol.*, 24(5):486–490, 2001.

[81] A.R. Cuddihy and R.G. Bristow. The p53 protein family and radiation sensitivity: Yes or no? *Cancer Metastasis Review*, 23(3-4)::237–57, 2004.

[82] A.V. Gudkov and E.A. Komarova. The role of p53 in determining sensitivity to radiotherapy. *Nature Reviews Cancer*, 3:117–129, 2003.

[83] V.T.Jr. DeVita and E. Chu. A history of cancer chemotherapy. *Cancer Research 2008*, 68(21):8643–8653, November 2008.

[84] S. Farber, L.K. Diamond, R.D. Mercer, R.F.Jr. Sylvester, and J.A. Wolff. Temporary remissions in acute leukemia in children produced by folic acid antagonist, 4-aminopteroyl-glutamic acid (aminopterin). *New England Journal of Medicine*, 238:787–93, 1948.

[85] L.L. Brunton, J.S. Lazo, and K.L. Parker. Goodman and gilman's The Pharmalogical Basis of Therapeutics. *Eleventh Edition*, McGraw Hill Medical Publishing Division:1316–1318, 2005.

[86] D. Fu, J.A. Calvo, and L.D. Samson. Balancing repair and tolerance of DNA damage caused by alkylating agents. *Nature Reviews Cancer*, 12:104–120, February 2012.

[87] S. Puyo, D. Montaudon, and P. Pourquier. From old alkylating agents to new minor groove binders. *Crit. Rev. Oncol. Hematol.*, 89(1):43–61, 2014.

[88] S. Payne and D. Miles. Mechanism of anticancer drugs. *Scott-Brown's Otorhinolaryngology: Head and Neck Surgery 7Ed*, 3(CRC Press 2008):34–46, 2008.

[89] P.D. Cole, J.A. Zebala, and B.A. Kamen. Antimetabolites: A new perspective. *Drug Discovery Today: Therapeutic Strategies*, 2(4):337–342, 2005.

[90] D.B. Longley, D.P. Harkin, and P.G. Johnston. 5-fluorouracil: mechanisms of action and clinical strategies. *Nature Reviews Cancer*, 3:330–338, 2003.

[91] J.B. Johnston. Mechanism of action of pentostatin and cladribine in hairy cell leukemia. *Leuk. Lymphoma.*, 52(2):43–5, 2011.

[92] Smith D. Kinsella, A.R. Tumor resistance to antimetabolites. *Gen. Pharmacol.*, 30(5):623–6, 1998.

[93] E.R. Simpson. Sources of estrogen and their importance. *The Journal of Steroid Biochemistry and Molecular Biology*, 86(3-5):225–30, 2003.

[94] D.E. Gerber. Targeted therapies: A new generation of cancer treatments. *Am. Fam. Physician.*, 77(3):311–319, 2008.

[95] A.L. Hopkins and C.R. Groom. The druggable genome. *Nat. Rev. Drug Discov.*, 9(1):727–730, 2002.

[96] I. Melnikova and J. Golden. Targeting protein kinases. *Nature Reviews: Drug Discovery*, 3:993–994, December 2004.

[97] J. Zhang, P. Yang, and N.S. Gray. Targeting cancer with small molecule kinase inhibitors. *Nature Reviews Cancer*, 9:28–39, 2009.

[98] H-C Cheng, R.Z. Qi, H. Paudel, and H-J. Zhu. Regulation and function of protein kinases and phosphatases. *Enzyme Research*, 2011(Article ID 794089):1–3, 2011.

[99] I. Shchemelinen, L. Sefc, and E. Necas. Protein kinases, their function and implication in cancer and other diseases. *Folia Biologica*, 52:81–101, 2006.

[100] N. Iqbal and N. Iqbal. Imatinib: A breakthrough of targeted therapy in cancer. *Chemotherapy Research and Practice*, 2014(Article ID 357027):1–9, 2014.

[101] J.V. Melo. Bcr-abl gene variants. *Baillieres Clin. Haematol.*, 10(2):203–22, 1997.

[102] S. Salesse and C.M. Verfaillie. Bcr/abl: from molecular mechanisms of leukemia induction to treatment of chronic myelogenous leukemia. *Oncogene*, 21(56):8547–8559, December 2002.

191

[103] D. Milojkovic and J. Apperley. Mechanisms of resistance to imatinib and second-generation tyrosine inhibitors in chronic myeloid leukemia. *Clinical Cancer Research*, 15(24):7519–7527, 2009.

[104] S. Mealing, L. Barcena, N. Hawkins, J. Clark, V. Eaton, I. Hirji, and C. Davis. The relative efficacy of imatinib, dasatinib and nilotinib for newly diagnosed chronic myeloid leukemia: a systematic review and network meta-analysis. *Experimental Hematology and Oncology*, 2(5):1–9, 2013.

[105] Y-J. Wang, Y-K. Zhang, R.J. Kathawala, and Z-S. Chen. Repositioning of tyrosine kinase inhibitors as antagonists of atp-binding cassette transporters in anticancer drug resistance. *Cancers*, 6(4):1925–1952, 2014.

[106] C. Yewale, D. Baradia, I. Vhora, S. Patil, and A. Misra. Epidermal growth factor receptor targeting in cancer: A review of trends and strategies. *Biomaterials*, 34(2013):8690–8707, 2013.

[107] Z. Zhang, A.L. Stiegler, T.J. Boggon, S. Kobayashi, and B. Halmos. Egfr-mutated lung cancer: a paradigm of molecular oncology. *Oncotarget*, 1(7):497–514, 2010.

[108] M.K. Paul and A.K. Mukhopadhyay. Tyrosine kinase- role and significance in cancer. *Int. J. Med. Sci.*, 1:101–15, 2004.

[109] C. Le Tourneau, E. Raymond, and S. Faivre. Sunitinib: a novel tyrosine kinase inhibitor. a brief review of its therapeutic potential in the treatment of renal carcinoma and gastrointestinal stromal tumors (gist). *Therapeutics and Clinical Risk Management*, 3(2):341–348, 2007.

[110] M. Merlano and M. Occelli. Review of cetuximab in the treatment of squamous cell carcinoma of the head and neck. *Ther. Clin. Risk. Manag.*, 3(5):871–876, 2007.

[111] Z. Mitri, T. Constantine, and R. O'Regan. The her2 receptor in breast cancer: Pathophysiology, clinical use, and new advances in therapy. *Chemother. Res. Pract.*, 2012(743193):1–22, 2012.

[112] M. Peyressatre, C. Prevel, M. Pellerano, and M.C. Morris. Targeting cyclin-dependent kinases in human cancers: From small molecules to peptide inhibitors. *Cancers*, 7:179–237.

[113] M. Malumbres. Cyclin-dependent kinases. *Genome Biology*, 15(122):1–10, 2014.

[114] U. Asghar, A.K. Witkiewicz, N.C. Turner, and E.S. Knudsen. The history and future of targeting cyclin-dependent kinases in cancer therapy. *Nature Reviews Drug Discovery*, 14:130–146, 2015.

[115] S. Dhillon. Palbociclib: first global approval. *Drugs*, 75(5):543–51, 2015.

[116] W.D. Figg and D.R. Newell. Pharmacologic biomarkers in the development of stratified cancer medicine. *Clinical Cancer Research*, 20(10):2525–2529, 2014.

[117] G.L. Patrick. An introduction to medicinal chemistry. *Oxford University press, United Kingdom*, pages 519–522, 2009.

[118] D.A. Dias, S. Urban, and U. Roessner. A historical overview of natural products in drug discovery. *Metabolites*, 2(4):303–336, 2012.

[119] J. Mann. Natural products in cancer chemotherapy: past, present and future. *Nature reviews*, 2(2):143–148, 2002.

[120] F.N. Lamari and P. Cordopatis. Exploring the potential of natural products in cancer treatment. *Anticancer Therapeutics*, (Publisher: Wiley-Blackwell):3–13, 2008.

[121] C. Basmadjian, Q. Zhao, E. Bentouhami, A. Djehal, C.G. Nebigil, R.A. Johnson, M. Serova, A. de Gramont, S. Faivre, E. Raymond, and

L.G. Desaubry. Cancer wars: natural products strike back. *Frontiers in chemistry*, 2(20):1–18, May 2014.

[122] A.L. Harvey, Ru*A*ngelie Edrada-Ebel, and R.J. Quinn. The re-emergence of natural products for drug discovery in the genomics era. *Nature reviews: Drug Discovery*, 14:111–129, February 2015.

[123] M.D. Siegelin and A.C. Borczuk. Epidermal growth factor receptor mutations in lung adenocarcinoma. *Laboratory Investigation*, 94:129–137, 2014.

[124] D.J. Newman and G.M. Cragg. Natural products as sources of new drugs over the last 25 years. *Journal of Natural Products*, 70(3):461–77, 2007.

[125] J.D. McChesney and J.T. Venketaramans, S.K. Henri. Plant natural products: back to the future or into extinction? *Phytochemistry*, 68:2015–22, 2007.

[126] A.I. Gray, J.O. Igoli, and R. Edrada-Ebel. Natural products isolation in modern drug discovery programs. *Methods Mol. Bio*, 864:515–534, 2012.

[127] Z.B. Ujang, T. Subramaniam, M. Diah, H.B. Wahid, Rashid A.H.B.A Abdullah, B.B., and D. Appleton. Bioguided fractionation and purification of natural bioactives obtained from *Alpinia conchigera* water extract with melanin inhibition activity. *Journal of biomaterials and nanobiotechnology*, 4:265–272, 2013.

[128] R.H. Shoemaker. The nci60 human tumour cell line anticancer drug screen. *Nature Reviews Cancer*, 6:813–823, October 2006.

[129] T. May, D.P. Goldstein, and R.S. Berkowitz. Current chemotherapeutic management of patients with gestational trophoblastic neoplasia. *Chemotherapy Research and Practice*, 2011(Article ID 806256):1–12, 2011.

[130] D.A. Gewirtz. A critical evaluation of the mechanisms of action proposed for the antitumor effects of the anthracycline antibiotics adriamycin and daunorubicin. *Biochem. Pharmacol.*, 57:727–741, 1999.

[131] G.L. Beretta, P. Gatti, L. Perego, and N. Zaffaroni. Camptothecin resistance in cancer: Insights into the molecular mechanisms of a dna-damaging drug. *Current Medicinal Chemistry*, 20:1541–1565, 2013.

[132] K.R. Hande. Etoposide: four decades of development of a topoisomerase ii inhibitor. *Eur. J. Cancer*, 34(10):1514–21, 1998.

[133] D.J. Newman, G. Crag, and K. Sander. Natural products as sources of new drugs over the period of 1981-2002. *Journal of Natural Products*, 66(7):1022–1037, 2003.

[134] Y. Damayanthi and J.W. Lown. Podophyllotoxins: current status and recent developments. *Curr. Med. Chem.*, 5(3):205–52, June 1998.

[135] K. Priyadarshini and A.U. Keerthi. Paclitaxel against cancer: A short review. *Medicinal Chemistry*, 2(7):139–141, 2012.

[136] M.C. Wani and S.B. Horwitz. Nature as a remarkable chemist: A personal story of the discovery and development of taxol. *Anti-Cancer Drugs.*, 25(4):482–7, 2014.

[137] A. Montero, F. Fossella, G. Hortobagyi, and V. Valero. Docetaxel for treatment of solid tumours: a systematic review of clinical data. *The Lancet Onclogy*, 2(4):229–239, April 2005.

[138] K.E. Gascoigne and S.S. Taylor. How do anti-mitotic drugs kill cancer cells? *J. Cell Sci.*, 122(15):2579–85, 2009.

[139] S. Lobert, B. Vulevic, and J.J. Correia. Interaction of vinca alkaloids with tubulin: a comparison of vinblastine, vincristine, and vinorelbine. *Biochemistry*, 35(21):6806–14, 1996.

[140] M.A. Jordan and L. Wilson. Microtubules as a target of anticancer drugs. *Nature Reviews Cancer*, 4:253–265, April 2004.

[141] C. Dumontet and M.A. Jordan. Microtubule-binding agents: a dynamic field of cancer therapeutics. *Nature Review Drug Discovery*, 9(10):790–803, 2010.

[142] T.J. Mitchison. The proliferation rate paradox in antimitotic chemotherapy. *Mol. Bio. Cell.*, 23(1):1–6, 2012.

[143] E. Komlodi-Pasztor, D. Sackett, J. Wilkerson, and T. Fojo. Mitosis is not a key target of microtubule agents in patient tumors. *Nature Reviews Clinical Oncology*, 8:244–250, 2011.

[144] E. Pasquier and M Kavallaris. Microtubules: A dynamic target in cancer therapy. IUBMB *Life*, 60(3):165–170, March 2008.

[145] N. M. Verrills, S. T. Po'uha, M. L. Liu, T. Y. Liaw, M. R. Larsen, M. T. Ivery, G. M. Marshall, P. W. Gunning, and M. Kavallaris. Alterations in gamma-actin and tubulin-targeted drug resistance in childhood leukemia. *J. Natl. Cancer Inst.*, 98:1363–1374, 2006.

[146] K-H. Lim, O. Hiraku, K. Komiyama, and T-S. Kam. Jerantinines a to g, cytotoxic *Aspidosperma* alkaloids from *Tabernaemontana corymbosa*. *Journal of Natural Products*, 71(9):1591–1594, 2008.

[147] J. Rautio, H. Kumpulainen, T. Heimbach, R. Oliyai, D. Oh, T. Jarvinen, and J. Savolainen. Prodrugs: design and clinical applications. *Nature Reviews Drug Discovery*, 7:255–270, March 2008.

[148] S. Sharma, F. Salehi, B.W. Scheithauer, F. Rotondo, L.V. Syro, and K. Kovacs. Role of mgmt in tumor development, progression, diagnosis, treatment and prognosis. *Anticancer Research*, 29(10):3759–68, 2009.

[149] R.H. Shoemaker. The nci60 human tumour cell line anticancer drug screen. *Nature Reviews Cancer*, 6:813–823, 2006.

[150] B. Verhoven, R.A. Schlegel, and P. Williamson. Mechanisms of phosphatidylserine exposure, a phagocyte recognition signal, on apoptotic

t lymphocytes. *Journal of Experimental Medicine*, 185(5):1597–601, 1995.

[151] G. Koopman, C.P. Reutelingsperger, G.A. Kuijten, R.M. Keehnen, S.T. Pals, and M.H. van Oers. Annexin v for flow cytometric detection of phosphatidylserine expression on b cells undergoing apoptosis. *Blood*, 84(5):1415–20, 1994.

[152] F.J. Geske, A.C. Nelson, R. Lieberman, R. Strange, T. Sun, and L.E. Gerschenson. Dna repair is activated in early stages of p53-induced apoptosis. *Cell Death Differ.*, 7(4):393–401, 2000.

[153] J. Jin, G. Lin, H. Huang, D. Xu, H. Yu, X. Ma, L. Zhu, D. Ma, and H. Jiang. Capsaicin mediates cell cycle arrest and apoptosis in human colon cancer cells via stabilizing and activating p53. *Int.J.Biol.Sci.*, 10(3):285–95, 2014.

[154] M.L. Smith and Y.R. Seo. p53 regulation of dna excision repair pathways. *Mutagenesis*, 17(2):149–156, 2002.

[155] R.W. Craig. Mcl1 provides a window on the role of the bcl2 family in cell proliferation, differentiation and tumorigenesis. *Leukemia*, 16(4):444–54, April 2002.

[156] Z. Herceg and Z.Q. Wang. Functions of poly(adp-ribose) polymerase (parp) in dna repair, genomic integrity and cell death. *Mutat.Res.*, 477(1-2):97–110, 2001.

[157] D. Davar, J.H. Beumer, L. Hamieh, and H. Tawbi. Role of parp inhibitors in cancer biology and therapy. *Curr.Med.Chem.*, 19(23):3907–21, 2012.

[158] A. Hershko. Mechanisms and regulation of the degradation of cyclin b. *Philos.Trans.R.Soc.Lond.B.Biol.Sci.*, 354(1389):1571, 1999.

[159] N.N. Kreis, M. Sanhaji, A. Kramer, K. Sommer, F. Rodel, K. Strebhardt, and J. Yuan. Restoration of the tumor suppressor p53 by

downregulating cyclin b1 in human papillomavirus 16/18-infected cancer cells. *Oncogene*, 29(41):5591–603, October 2010.

[160] S. Elmore. Apoptosis: A review of programmed cell death. *Toxocologic Pathology*, 35(4):495–516, June 2007.

[161] A. Levine and M. Oren. The first 30 years of p53: growing ever more complex. *Nature Reviews Cancer*, 9(10):749–58., October 2009.

[162] K. Podar, S.L. Gouill, J. Zhang, J.T. Opferman, E. Zorn, Tai Y.T., T. Hideshima, M. Amiot, D. Chauhan, J.L. Harousseau, and K.C. Anderson. A pivotal role for mcl-1 in bortezomib-induced apoptosis. *Oncogene*, 27(6):721–731, 2008.

[163] J. Hu, N. Dang, T. Song, and K. Vanderkerken. Mcl-1 reduction due to caspase-dependent cleavage during endoplasmic reticulum stress-induced apoptosis. *Journal of Biological Chemistry*, 286(44):le24, 2011.

[164] Y. Liang, C. Yan, and N.F. Schor. Apoptosis in the absence of caspase 3. *Oncogene*, 20(45):6570–6578, October 2001.

[165] A.L. Blajeski, V.A. Phan, T. Kottke, and S.H. Kaufmann. G_1 and g_2.

[166] J. Zhou and P. Giannakakou. Targeting microtubules for cancer chemotherapy. *Curr. Med. Chem. Anticancer Agents*, 5(1):65–71, 2005.

[167] H. Lodish, A. Berk, S.L. Zipursky, P. Matsudaira, D. Baltimore, and J. Darnell. Molecular cell biology. (4th edition):Section 19.2, 2000.

[168] P.G. Morris and M.N. Fornier. Microtubule active agents: beyond the taxane frontier. *Clin. Cancer Res.*, 14(22):7167–72, 2008.

[169] G.T. Charras. A short history of blebbing. *Journal of Microscopy*, 231(3):466–478, 2008.

[170] A. Singh, M.C. Zapata, Y.S. Choi, and S.O. Yoon. Gsi promotes vincristine-induced apoptosis by enhancing multi-polar spindle formation. *Cell Cycle*, 13(1):157–66, 2014.

[171] K. Strebhardt and A. Ulrich. Targeting polo-like kinase 1 for cancer therapy. *Nature Reviews Cancer*, 6:321–330, 2006.

[172] F. Eckerdt, J. Yuan, and K. Strebhardt. Polo-like kinases and oncogenesis. *Oncogene*, 24:267–276, 2005.

[173] V.A. Smits, R. Klompmaker, L. Arnaud, G. Rijksen, E.A. Nigg, and R.H. Medema. Polo-like kinase-1 is a target of the dna damage checkpoint. *Nature Cell Biology*, 2:672–676, 2000.

[174] T. Kezoe, J. Yang, C. Nishoika, Y. Takezaki, T. Tasaka, K. Togitani, P. Koeffler, and A. Yokoyama. A novel treatment strategy targeting polo-like kinase 1 in hematological malignancies. *Nature*, 23(9):1564–1576, 2009.

[175] J. Triscott, C. Lee, B. Foster, B. Manoranjan, M.R. Pambid, A. Berns, A. Fotovati, C. Venugopal, K. O'Halloran, A. Narendran, C. Hawkins, V. Ramaswamy, E. Bouffet, M.D. Taylor, A. Singhal, J. Hukin, R. Rassekh, S. Yip, P. Northcott, S.K. Singh, C. Dunham, and S.E. Dunn. Personalizing the treatment of pediatric medulloblastoma: Polo-like kinase 1 as a molecular target in high-risk children. *Cancer Research*, 73(22):6734–44, 2013.

[176] A.A. Dar, L.W. Goff, S. Majid, J. Berlin, and W. El-Rifai. Aurora kinases' inhibitors – rising stars in cancer therapeutics? *Molecular Cancer Therapeutics*, 9(2):1–19, 2010.

[177] W.M. Bonner, C.E. Redon, J.S. Dickey, A.J. Nakamura, O.A. Sedelnikova, S. Solier, and Y. Pommier. γh2ax and cancer. *Nature Reviews Cancer*, 8(12):957–967, November 2008.

[178] M.S. Poruchynsky, E. Komlodi-Pasztor, S. Trostel, J. Wilkerson, M. Regairaz, Y. Pommier, X. Zhang, T.K. Maity, R. Robey,

M. Burotto, D. Sackett, U. Guha, and A.T. Fojo. Microtubule-targeting agents augment the toxicity of dna-damaging agents by disrupting intracellular trafficking of dna repair proteins. *PNAS*, 112(5):1571–1576, February 2015.

[179] S. Soues, F. Laval, and J.Y. Charcosset. Mechanisms of resistance to combinations of vincristine, etoposide and doxorubicin in chinese hamster ovary cells. *Br.J.Cancer*, 71(3):489–497, 1995.

[180] K. Katayama, K. Noguchi, and Y. Sugimoto. Regulations of p-glycoprotein/abcb1/mdr1 in human cancer cells. *New Journal of Science*, 2014(Article ID 476974):1–10, 2014.

[181] S.V. Ambudkar, C. Kimchi-Sarfaty, Z.E. Sauna, and M.M. Gottesman. P-glycoprotein: from genomics to mechanism. *Oncogene*, 22(47):7468–85, 2003.

[182] R. Kanagasabai, K. Krishnamurthy, L.J. Druhan, and G. Ilangovan. Forced expression of heat shock protein 27 (hsp27) reverses p-glycoprotein (abcb1)-mediated drug efflux and mdr1 gene expression in adriamycin-resistant human breast cancer cells. *J.Biol.Chem.*, 286(38):33289–300, 2011.

[183] G. Szacks, J.K. Paterson, J.A. Ludwig, C. Booth-Genthe, and M.M. Gottesman. Targeting multidrug resistance in cancer. *Nature Reviews Drug Discovery*, 5(3):219–234, 2006.

[184] A.K. Maiti. Overcoming drug resistance through elevation of ros in cancer. *Molecular Mechanisms of Tumor Cell Resistance to Chemotherapy Resistance to Targeted Anti-Cancer Therapeutics*, 1:pp 135–149, 2013.

[185] J. Chen. Reactive oxygen species and drug resistance in cancer chemotherapy. *Austin J.Clin.Pathol.*, 1(4):1017, 2014.

[186] S. Ledoux, R. Yang, G. Friedlander, and D. Laouari. Glucose depletion enhances p-glycoprotein expression in hepatoma cells: roleof en-

doplasmic reticulum stress response. *Cancer Research*, 63(21):7284–90, 2003.

[187] H. Hong, Y. Lu, Z.N. Ji, and G.Q. Liu. Up-regulation of p-glycoprotein expression by glutathione depletion-induced oxidative stress in rat brain microvessel endothelial cells. *J. Neurochem.*, 98(5):1465–73, 2006.

[188] M. Wartenberg, E. Hoffmann, H. Schwindt, F. Grünheck, Petros. J., J.R. Arnold, J. Hescheler, and H. Sauer. Reactive oxygen species-linked regulation of the multidrug resistance transporter p-glycoprotein in nox-1 overexpressing prostate tumor spheroids. *FEBS Lett.*, 579(20):4541–4549, 2005.

[189] Y. Lu, J. Chen, M. Xiao, W. Li, and D.D. Miller. An overview of tubulin inhibitors that interact with the colchicine binding site. *Pharm.Res.*, 29(11):2943–2971, 2012.

[190] R. Frei, D. Staedler, A. Raja, R. Franke, F. Sasse, S. Gerber-Lemaire, and J. Waser. Total synthesis and biological evaluation of jerantinine e. *Angewandte Chemie International Edition*, 52(50):13373–13376, 2013.

[191] Got MudPIT? Netterwald, j. *Drug Discovery and Development*, http://www.dddmag.com/ articles/2007/10/got-mudpit, 2007.

[192] V. Waetzig, U. Wacker, W. Haeusgen, B. Bjorkblom, M.J. Courtney, E.T. Coffey, and T. Herdegen. Concurrent protective and destructive signaling of jnk2 in neuroblastoma cells. *Cell Signal*, 21(6):873–880, June 2009.

[193] T.H. Wang, H.S. Wang, H. Ichijo, P. Giannakakou, J.S. Foster, T. Fojo, and J. Wimalasena. Microtubule-interfering agents activate c-jun n-terminal kinase/stress-activated protein kinase through both ras and apoptosis signal-regulating kinase pathways. *The Journal of Biological Chemistry*, 273:4928–4936, 1998.

[194] Reactive Oxygen Species Signaling in Cancer: Comparison with Aging. Afanas'ev, i. *Aging Dis.*, 2(3):219–230, June 2011.

[195] D.W. Huang, B.T. Sherman, Q. Tan, J. Kir, D. Liu, D. Bryant, Y. Guo, R. Stephens, M.W. Baseler, H.C. Lane, and R.A. Lempicki. David bioinformatics resources: expanded annotation database and novel algorithms to better extract biology from large gene lists. *Nucleic Acids Res.*, 35(Web Server Issue):W169–W175, 2007.

[196] H. Wang, X. Hu, Dou Z. Ding, X, Z. Yang, A.W. Shaw, M. Teng, Cleveland D.W., M.L. Goldberg, L. Niu, and X. Yao. Human zwint-1 specifies localization of zeste white 10 to kinetochores and is essential for mitotic checkpoint signaling. *J.Bio.Chem.*, 279(52):54590–8, 2004.

[197] P. Lara-Gonzalez, F.G. Westhorpe, and S.S. Taylor. The spindle assembly checkpoint. *Curr.Biol.*, 22(22):R966–80, 2012.

[198] N. Malmanche, A. Maia, and C.E. Sunkel. The spindle assembly checkpoint: Preventing chromosome mis-segregation during mitosis and meiosis. *FEBS Letters*, 580(12):2888–2895, 2006.

[199] A. Burgess, M. Rasouli, and S. Rogers. Stressing mitosis to death. *Front.Oncol.*, 4(140):1–7, 2014.

[200] J.A. Robbins and F.R. Cross. Regulated degradation of the apc coactivator cdc20. *Cell Division*, 5(23):1028–5–23, 2010.

[201] S.D. Ryan, E.M. Britigan, L.M. Zasadil, K. Witte, A. Audhya, A. Roopra, and B.A. Weaver. Up-regulation of the mitotic checkpoint component mad1 causes chromosomal instability and resistance to microtubule poisons. *Proc.Natl.Acad.Sci. USA*, 109(33):E2205–14, 2012.

[202] C. von Schubert, F. Cubizolles, J.M. Bracher, T. Sliedrecht, G.J.P.L. Kops, and E.A. Nigg. Plk1 and mps1 cooperatively regulate the spindle assembly checkpoint in human cells. *Cell Reports*, 12:1–13, 2015.

[203] J.D. Hayes and D.J. Pulford. The glutathione s-transferase supergene family: regulation of gst and the contribution of the isoenzymes to cancer chemoprotection and drug resistance. *Crit.Review.Biochem.Mol.Biol.*, 30(6):445–600, 1995.

[204] C. Glorieux, N. Dejeans, B. Sid, R. Beck, P.B. Calderon, and J. Verrax. Catalase overexpression in mammary cancer cells leads to a less aggressive phenotype and an altered response to chemotherapy. *Biochem.Pharmacol.*, 82(10):1384–90, 2011.

[205] L.H. Butterfield, A. Merino, S.H. Golub, and H. Shau. From cytoprotection to tumor suppression: the multifactorial role of peroxiredoxins. *Antioxid.Redox Signal*, 1(4):385–402, 1999.

[206] Cadenas C., D. Franckenstein, M. Schmidt, M. Gehrmann, M. Hermes, B. Geppert, W. Schormann, L.J. Maccoux, M. Schug, A. Schumann, C. Wilhelm, E. Freis, K. Ickstadt, J. Rahnenfuhrer, J.I. Baumbach, A. Sickmann, and J.G. Hengstler. Role of thioredoxin reductase 1 and thioredoxin interacting protein in prognosis of breast cancer. *Breast Cancer Research*, 12(3):R44, 2010.

[207] L.M. Huff, D.L. Sackett, M.S. Poruchynsky, and T. Fojo. Microtubule disrupting chemotherapeutics result in enhanced proteasome-mediated degradation and disappearance of tubulin in neural cells. *Cancer Research*, 70(14):5870–5879, 2010.

[208] K.L. Schaefer. Ppar-gamma inhibitors as novel tubulin-targeting agents. *Expert Opin.Investig.Drugs*, 16(7):923–926, 2007.

[209] K. Shalli, I. Brown, S.D. Heys, and A.C. Schofield. Alterations of beta-tubulin isotypes in breast cancer cells resistant to docetaxel. *FASEB J.*, 19(10):1299–301, 2005.

[210] D. J. Giard, S. A. Aaronson, G. J. Todaro, P. Arnstein, J. H. Kersey, H. Dosik, and W. P. Parks. In vitro cultivation of human tumors: establishment of cell lines derived from a series of solid tumors. *Journal of the National Cancer Institute*, 51(5):1417–23, 1973.

[211] D. Shi, G. Shi, G. Huang, J. Zhang, and E. and Lartigau. Chemosensitivity of radioresistant cells in the multicellular spheroids of a549 lung adenocarcinoma. *Journal of Experimental and Clinical Cancer Research*, 28:72, 2009.

[212] M. G. Brattain, W. D. Fine, F. M. Khaled, J. Thompson, and D. E. Brattain. Heterogeneity of malignant cells from a human colonic carcinoma. *Cancer Research*, 41(5):1751–6, 1981.

[213] J. Fogh and G. Trempe. New human tumour cells. human tumour *in Vitro. Plenum Press*, pages 115–141, 1975.

[214] P.M. Kimball and M.G. Brattain. Isolation of a cellular subpopulation from a human colonic carcinoma cell line. *Cancer Research*, 40:1574–1579, 1980.

[215] H. D. Soule, J. Vazguez, A. Long, S. Albert, and M. Brennan. A human cell line from a pleural effusion derived from a breast carcinoma. *Journal of the National Cancer Institute*, 51(5):1409–16, 1973.

[216] D.L. Holliday and V. Speirs. Choosing the right cell line for breast cancer research. *Breast Cancer Research*, 13(4):215, 2011.

[217] J.P. Jacobs, C.M. Jones, and J.P. Baille. Characteristics of a human diploid cell designated MRC-5. *Nature*, 227(5254):168–70, 1970.

[218] T Mossman. Rapid colorimetric assay for cellular growth and survival: application to proliferation and cytotoxicity assays. *Journal of Immunological Methods*, 65(1-2):55–63, 1983.

[219] J.A. Plumb. Cell sensitivity assays: the mtt assay. *Methods in Molecular Medicine*, 28:25–30, 1999.

[220] J.A. Plumb. Cell sensitivity assays: Clonogenic assays. *Cancer Cell Culture Methods and Protocols*, pages 159–164, 2004.

[221] I. Nicoletti, G. Migliorati, M.C. Pagliaccia, F. Grignani, and C. Riccardi. A rapid and simple method for measuring thymocyte apop-

tosis by propidium iodide staining and flow cytometry. *Journal of Immunological Methods*, 139(2):271–279, 1991.

[222] W.M. Bonner, C.E. Redon, J.S. Dickey, A.J. Nakamura, O.A. Sedelnikova, S. Solier, and Y. Pommier. γH2AX and cancer. *Nature Reviews Cancer*, 8:957–967, 2008.

[223] L.J. Kuo and L.X. Yang. Gamma-H2AX - a novel biomarker for dna double-strand breaks. *In Vivo*, 22(3):305–9, 2008.

[224] M.L. Shelanski, F. Gaskin, and C.R. Cantor. Microtubule assembly in the absence of added nucleotides. *Proceedings of the National Academy of Sciences*, 70(3):765–768, 1973.

[225] J.C. Lee and S.N. Timasheff. In vitro reconstitution of calf brain microtubules: effects of solution variable. *Biochemistry*, 16:1754–1762, 1977.

[226] M.M. Bradford. A rapid and sensitive method for the quantitation of microgram quantities of protein utilizing the principle of protein-dye binding. *Analytical Biochemistry*, 72:248–254, 1976.

[227] C. Wittmann, P. Chockley, S.K. Singh, L. Pase, G.J. Lieschke, and C. Grabher. Hydrogen peroxide in inflammation: Messenger, guide, and assassin. *Advances in Hematology*, 2012, 2012.

[228] S.K. Grebe and R.J. Singh. LC-MS/MS in the clinical laboratory - where to from here? *Clinical Biochemist Reviews*, 21(1):5–31, February 2011.

[229] G. Chen and B.N. Pramanik. Application of LC/MS to proteomics studies: current status and future prospects. *Drug Discovery Today*, 14(9-10):465–471.

Appendix A
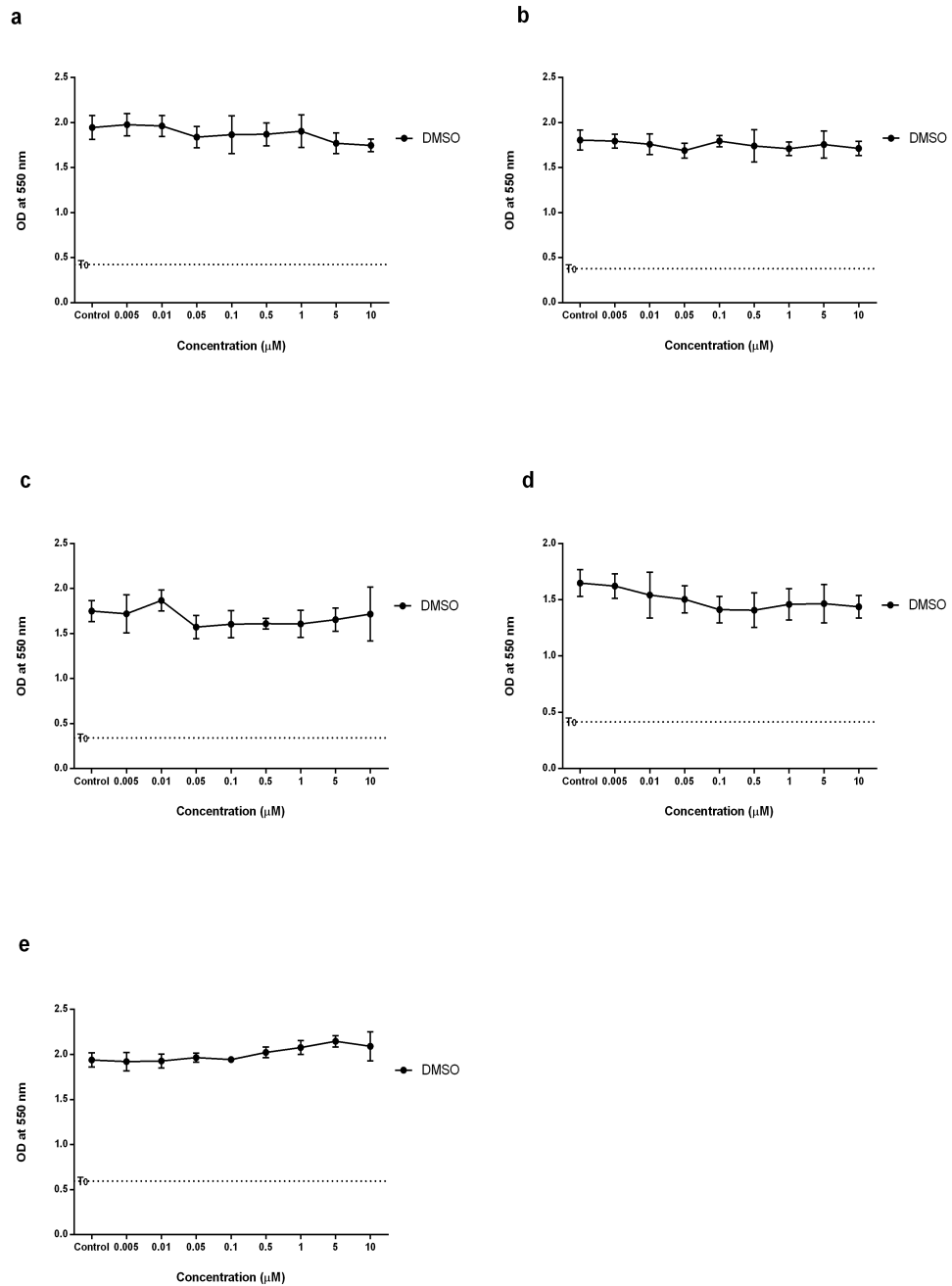
Figure A.1: Representative MTT graphs from a single trial displaying the effect of DMSO on all cell lines initially tested.

Effect of DMSO from one independent trial in A549 (a), HCT-116 (b), HT-29 (c), MCF-7 (d), MDA-468 (e), cells. Cells were seeded in 96-well plates at a density of 3 x 10^3 cells/well. After allowing to adhere (24 h), cells were treated with JA (n=4) and incubated for 72 h. MTT assays repeated $\geq$3 times.

Each *point* represents the mean±SEM of three determinations.
*** P<0.01 significantly different from control
** 0.01<P<0.5 significantly different from control.
ns= not significantly different from control.

Figure A.2: Representative MTT graph from a single trial displaying the growth inhibitory properties of JA and JAA against a pancreatic carcinoma cell line MIA PaCa-2.

Growth inhibitory effects of JA and JAA from one independent trial in MIA PaCa-2. Cells were seeded in 96-well plates at a density of 3×10^3 cells/well. After allowing to adhere (24 h), cells were treated with JA (n=4) and incubated for 72 h. MTT assays repeated ≥ 3 times. Both JA and JAA potently inhibited growth with a GI_{50} value of approximately 250 nM. This figure was kindly provided by Yan Lui (Undergraduate research student).
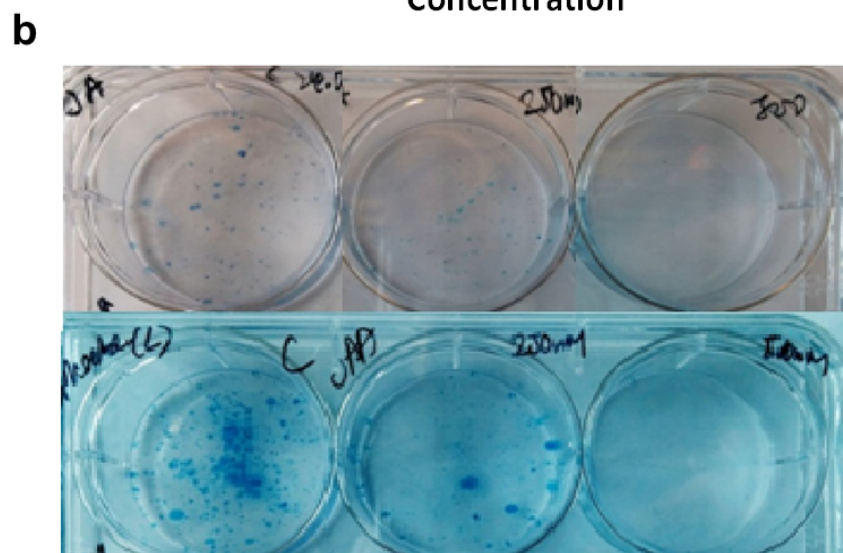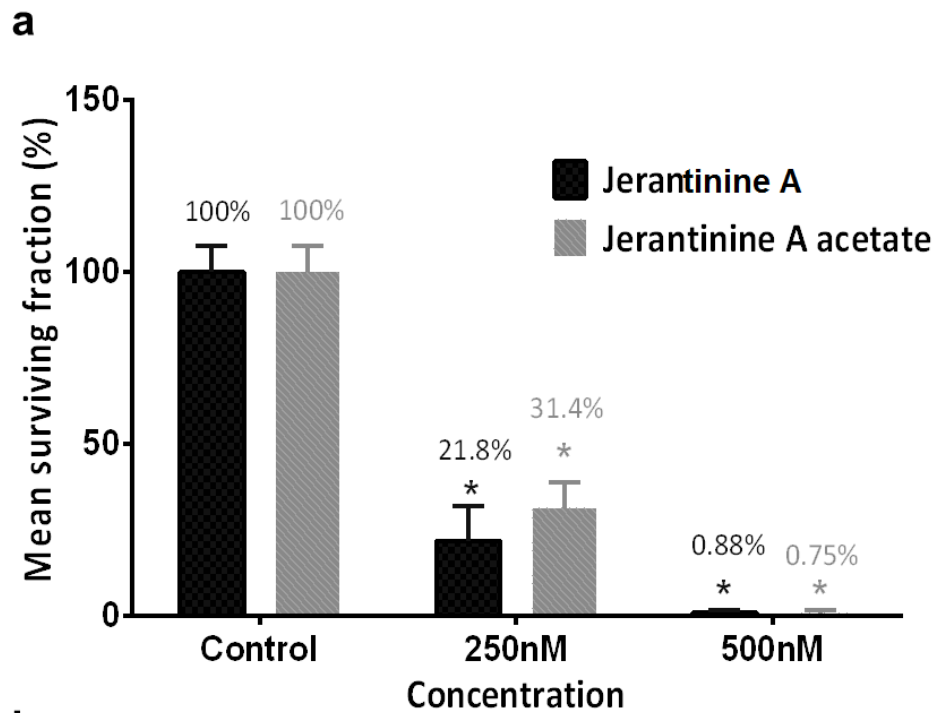
Figure A.3: Effect of jerantinine A and jerantinine A acetate on colony formation in MIA PaCa-2.

a) Mean graphs and SEMs showing potent inhibition of colony formation in MIA PaCa-2 cells after a 24 h exposure to JA and JAA (p<0.001; n=4 per trial) b) Representative photos taken from an individual trial clearly showing inhibition of colony formation (JA top; JAA bottom). Figures were kindly provided by Yan Lui (Undergraduate research student).

	Vincristine		Jerantinine A	
	Clonogenic Assay	MTT Assay	Clonogenic Assay	MTT Assay
DAOY	4.4nM	10nM	245nM	253nM
MED1	6.3nM	>20nM	277nM	557nM
UW228-3	2.4nM	2.9nM	773nM	587nM
FB83	/	9.9nM	/	>1000nM

Table A.1: IC_{50} values obtained from clonogenic assays and MTT assays for vincristine and jerantinine A in DAOY, MED1, UW228-3 and FB83 cell lines.

IC_{50} = concentration required to cause 50% of colony formation in clonogenic assays, and to cause 50% cell viability in MTT assays (both relative to vehicle treated controls). Table was provided by Amy Lloyd supervised by Dr. Beth Coyle (QMC, University of Nottingham)
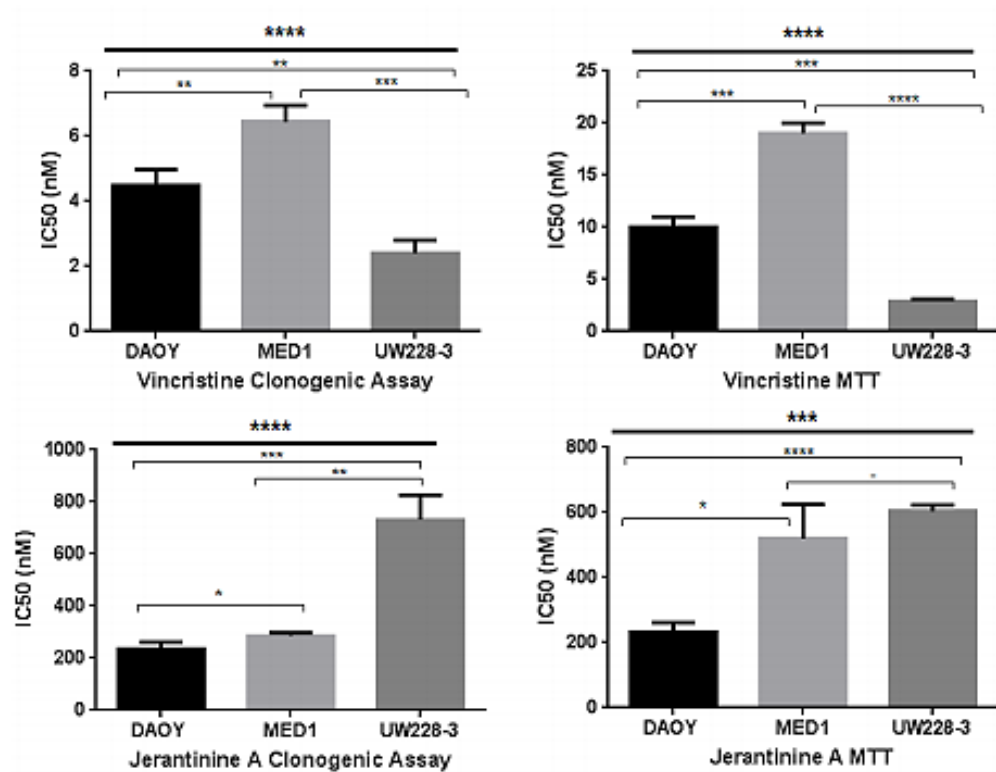
Figure A.4: Comparison of relative IC_{50} values from clonogenic and MTT assays for vincristine and jerantinine A in DAOY, MED1 and UW228-3 medulloblastoma cell lines.

One way ANOVA and unpaired t-tests were used to calculate significant differences. (**** $p<0.0001$, *** $p<0.001$, ** $p<0.01$, * $p<0.05$). Data represents mean $\pm$ SD. Figures were provided by Amy Lloyd supervised by Dr. Beth Coyle (QMC, University of Nottingham)

Appendix B
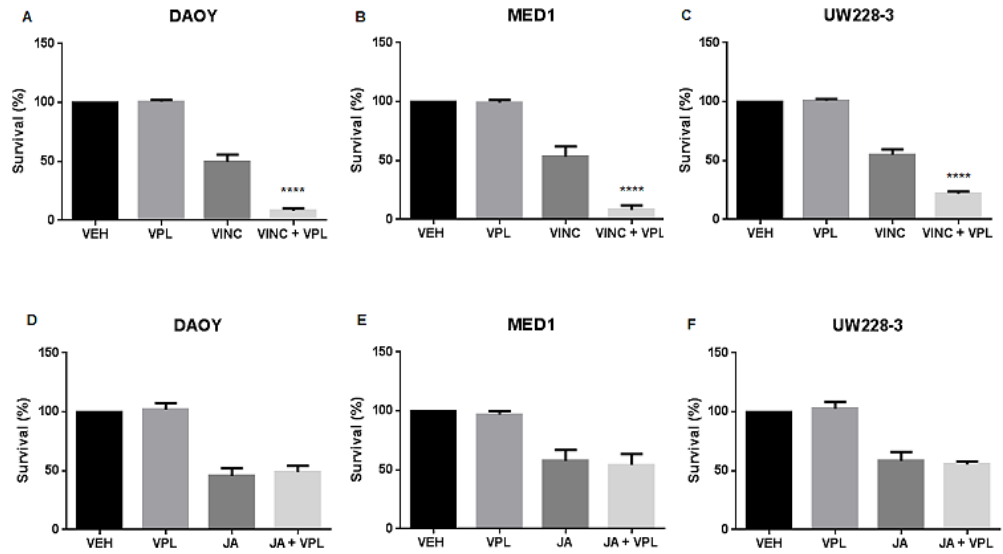
Figure B.1: The effects of Verapamil with Vincristine (A-C) and Jeranti-nine A (D-F) on the potentiation of inhibitory effects on colony formation using clonogenic assays.

DAOY, MED1, and UW228-3 cells were treated with JA or vincrsitine alone. JA and vincristine treatments along with verapamil were used to investigate if inhibition of ABCB1 enhanced the potency of JA. Verapamil clearly exhibited a synergistic effect with vincristine, but did not affect JA activity on all three cell lines. Experiments were repeated at least three times where n=2 (****= p<0.0001, one way ANOVA, paired T-test).
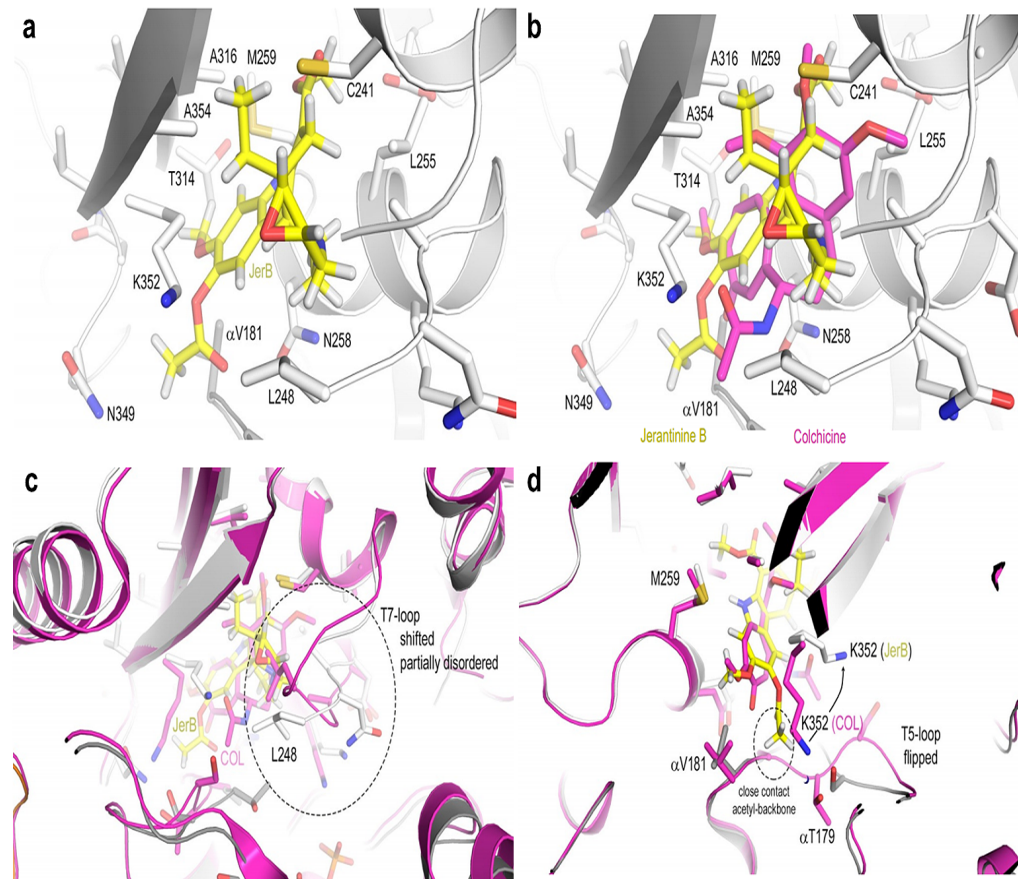
Figure B.2: Detailed crystal structures of jerantinine B acetate binding to the colchicine site on microtubules

(a) Detailed view of JBA binding to the colchicine site of microtubules. (b) Superimposed image comparing colchicine and JBA binding (c, d) Detailed interactions with amino acid residues within the colchicine binding site. Images (2.4Å) were provided by Natacha Olieric, Andrea E. Prota and Michel O. Steinmetz from the Paul Scherrer Institute (Switzerland).

Appendix C

C.1 Data Analysis of Genome-wide shRNA Screen

To define JA-modulating effects from the screen data, we used three parallel strategies previously used in RNA interference screens. In the first instance we selected significant effects according to the variance of the entire dataset. We calculated the median absolute deviation (MAD) to estimate the variance of the normalized data and defined resistance-causing hits as those shRNAs that gave DE scores <2 x MAD (Z score <2), a threshold approximately equal to 2 SDs from the median. Sensitization effects were defined as shRNAs that returned DE scores of $Z < -2$. In addition to this approach we also used RNAi Gene Enrichment Ranking (RIGER), as implemented in the Broad Institute's GENE-E software package. In brief, RIGER is derived from the weighted sum of the two top-ranked shRNAs for each gene on the basis of the log fold change for each condition, and provided a normalized enrichment score per gene. Finally, we also used RNAi Set Analysis (RSA), a modification of Gene Set Analysis (http://wwwstat.stanford.edu/~tibs/GSA/) that uses maximum–mean statistics to identify significantly enriched or depleted shRNA sets.

In total, Z score threshold identified 680 resistance-causing genes and 753 sensitization genes, RIGER generated a list of 821 resistance-causing and 790 sensitization genes with a P value of <0.05, and RSA generated a list of 651 resistance-causing genes and 339 sensitization genes with a false discovery rate approaching zero. Given the limitations of each method, we took a pragmatic approach and considered a subset of the genes identified by all three methods for further examination. This intersection approach identified 381 candidate genes mediating sensitization and 121 candidate genes mediating resistance to JA (see fig.C.1).
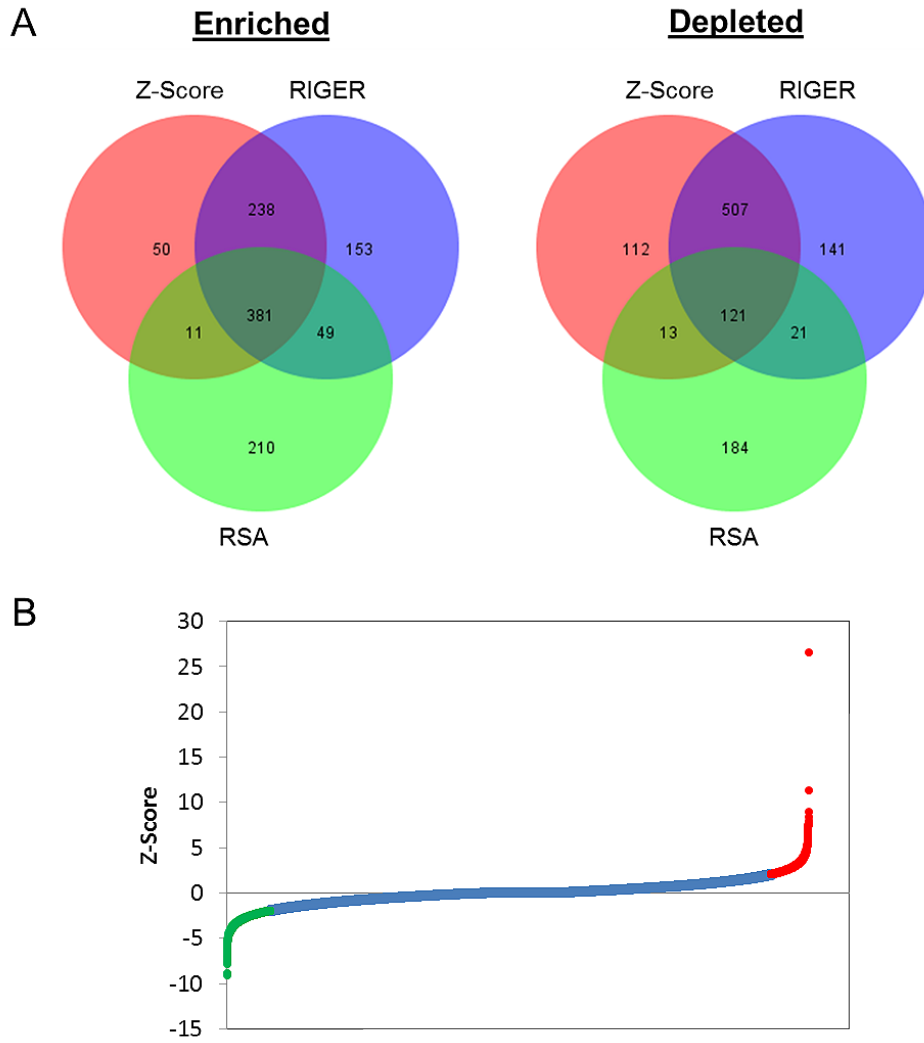
Figure C.1: Detection of JA sensitization and resistance-causing effects.

(A) Venn diagrams indicating the number of candidate hits defined by three parallel analysis methods. (B) Plot of shRNA DE Z scores ranked by size of effect.
Data analysis figures and procedure was kindly provided by Dr. Chee-Onn Leong (IMU, Malaysia).
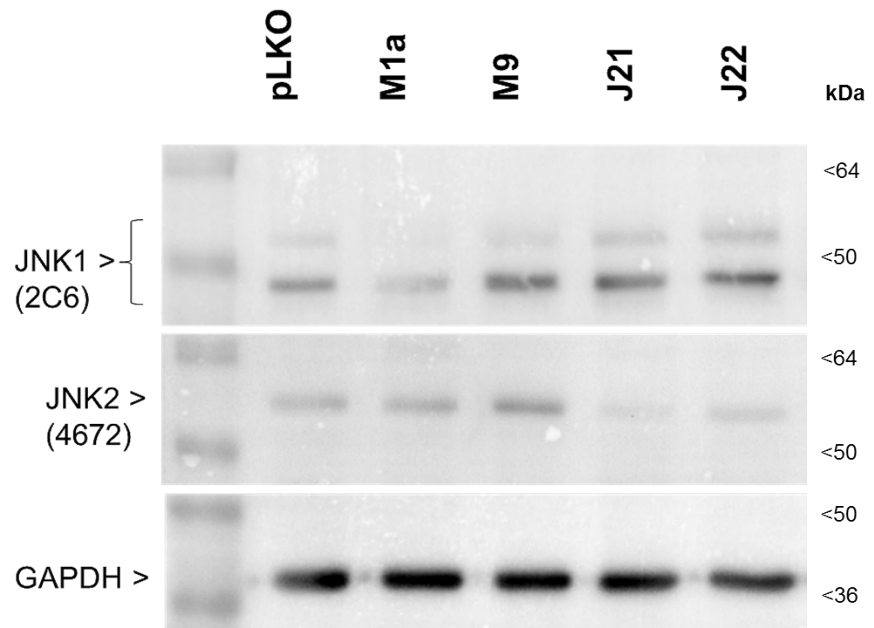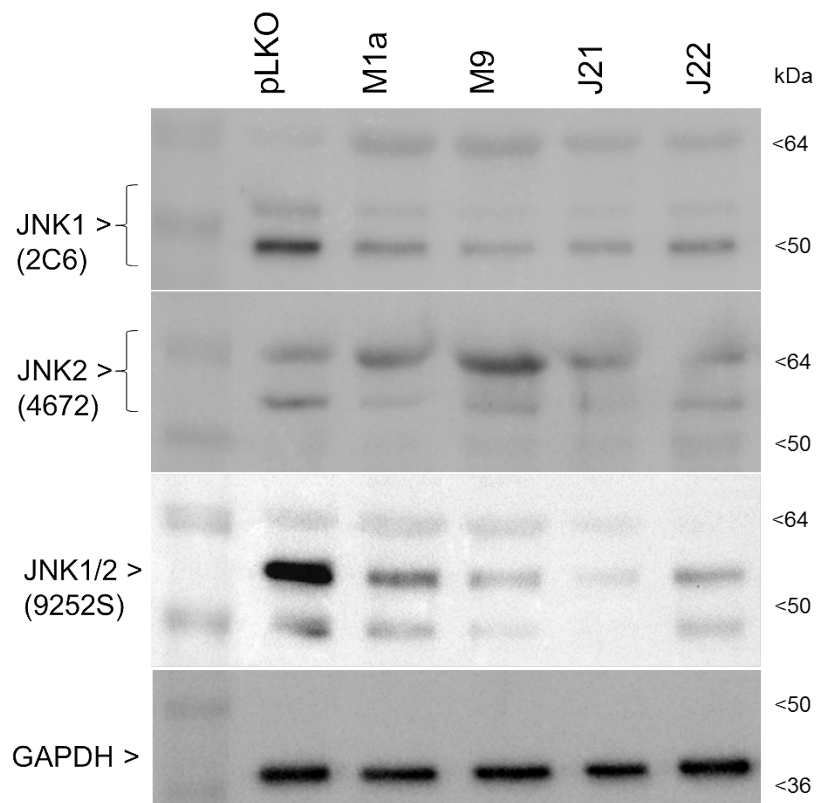
Figure C.2: Blots illustrating knockdown of JNK1/2 in MCF-7 and MDA-468 cells compared to their respective vector controls (pLKO).

M1a/M19 shRNA variants target JNK1 and J21/J22 shRNA variants target JNK2. MCF-7 cells transduced with the M9 variant did not appear to knock down JNK1 when compared to the vector control. Blots were kindly provided in collaboration with Dr. Chee-Onn Leong and Dr. Felicia Chung (IMU, Malaysia).
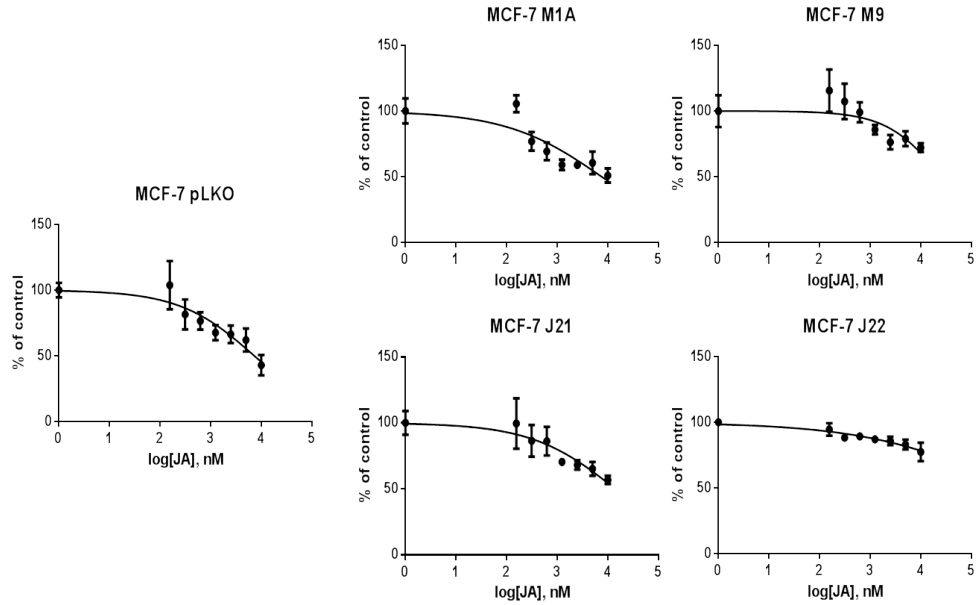
Figure C.3: Mean MTT graphs of JA-treated (1 μM) MCF-7 cells that are deficient in either JNK1 or JNK2.

Treatments were terminated after 72 h by addition of MTT and subsequently incubated for 4 hours. Absorbances were measured using a tecan microplate reader.
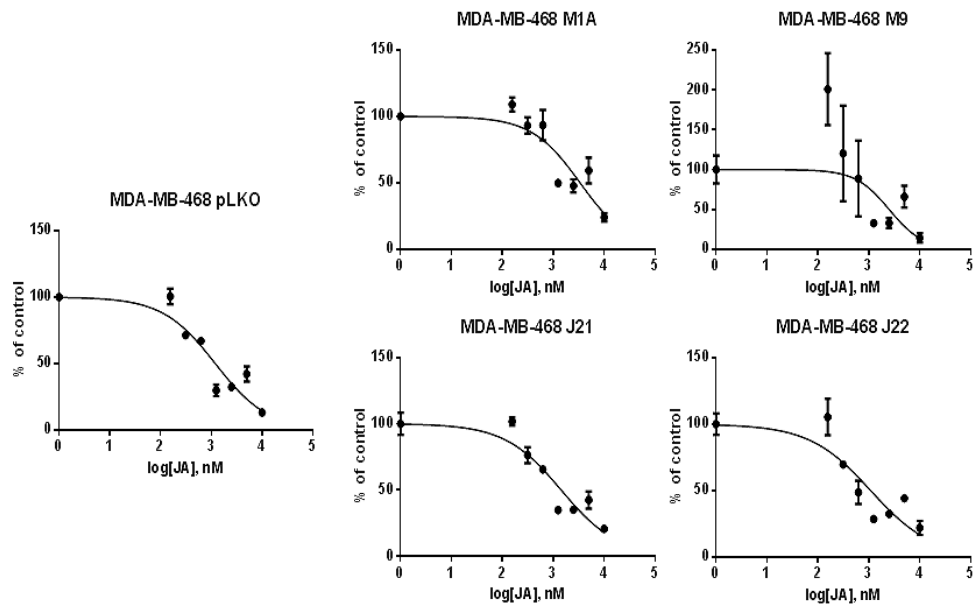
Figure C.4: Mean MTT graphs of JA-treated (1 μM) MDA-468 cells that are deficient in either JNK1 or JNK2.

Treatments were terminated after 72 h by addition of MTT and subsequently incubated for 4 hours. Absorbances were measured using a tecan microplate reader.